# Investigating the effects of oxidative stress on extracellular vesicle function and RNA cargo loading

**Elizabeth Ruth Dellar**




**Lincoln College**
**University of Oxford**

**A thesis submitted for the degree of Doctor of Philosophy in Interdisciplinary Bioscience**
**April 2021**

# Acknowledgements

This DPhil has been a journey, at times a very tough one, but with the support of my family, friends and colleagues I have come out the other side stronger and wiser for it. I would like to thank both my supervisors, Dave Carter and Alberto Baena-Lopez, for their guidance and belief in me during this project, but also for giving me the freedom to do my DPhil in a way that worked for me, enabling me to grow as a scientist. Thanks also the BBSRC and the Oxford Interdisciplinary Bioscience DTP through which my funding is provided, and without which this work would not have been possible. I would also like to thank the whole of the Carter-Pink lab, past and present, for their support and encouragement throughout the past four and a half years, in particular to Genevieve, Manu and Elise for helping to maintain my sanity. I am also very grateful to the rest of the community at Oxford Brookes for making it such a friendly place to work, with plenty of tea and cake and regular pub trips! To Claire, my thanks for working with me on this project from day one, and for her drive and commitment to yet more experiments to push this work forward. Finally, finishing a DPhil is hard enough, but doing it in the middle of a global pandemic has its own special challenges, so I cannot thank Oli, my housemates, and my family enough for their patience and continued encouragement to keeping me going through it.

# Abstract

**Investigating the effects of oxidative stress on extracellular vesicle function and RNA cargo loading**

**Elizabeth Dellar, Lincoln College**

Extracellular vesicles (EVs) are a heterogeneous group of membrane-enclosed structures which have been suggested to play a critical role in maintaining intracellular homeostasis through the elimination of unnecessary biological material from EV-producing cells, and as a delivery system enabling intercellular communication between distant cells. Although extensive study has revealed many RNA biotypes that are associated with EVs, and has begun to elucidate the mechanisms of their packaging and delivery, little is currently known about how these processes are conserved in different species and under different cellular conditions. In this thesis, an *in vitro Drosophila* model in S2R+ cells was set up to investigate EV biology under normal and stress conditions, as a complement to an *in vivo* system being set up in *Drosophila* larvae. Under hydrogen peroxide-induced oxidative stress, an increase to EV number was seen, whilst no changes to size or protein marker composition were evident. Preliminary work indicated that these stress-cell- derived EVs acted to induce cell death in recipient cells. Characterisation of the total RNA content of cells and EV samples under control and oxidative stress conditions revealed that EV RNA was not representative of parental cells, but was instead enriched for ribosomal RNA, *Copia* retrotransposon, snoRNA, and RNAs relating to cytoskeletal and developmental functions. Investigation of potential loading motifs in mRNA 3'UTRs found no sequences which could differentiate mRNA packaging under stress conditions. Further exploration of mRNA loading in EVs found no preference for short mRNA transcripts, but an enrichment of intronic and untranslated regions, and 3' end degradation, under stress. A striking increase in base mismatch in the RNA of EV preparations was seen under stress, possibly indicative of targeting of aberrant RNA to EVs, or of RNA modification. These results present strong evidence that the RNA content of *Drosophila* EVs is altered under oxidative stress and provides several avenues for further investigation of mechanisms by which it may occur. Furthermore, these data indicate the potential increased importance that EVs may play in metabolic and signalling functions under different cellular stress conditions, which has great relevance for disease pathology.

# Table of contents


**1 Introduction ..... 15**

1.1 EXTRACELLULAR VESICLES ..... 15

1.1.1 Cell homeostasis and intercellular communication ..... 15

1.1.2 History of extracellular vesicles ..... 15

1.1.3 Biogenesis and classification ..... 16

1.1.4 Mechanisms of extracellular vesicle function ..... 20

1.1.5 Extracellular vesicles and stress ..... 23

1.2 EXTRACELLULAR VESICLE RNA ..... 26

1.2.1 MicroRNA ..... 27

1.2.2 Transfer RNA ..... 28

1.2.3 Small nucleolar RNA ..... 29

1.2.4 Small nuclear RNA ..... 30

1.2.5 Non-coding RNA ..... 30

1.2.6 Ribosomal RNA ..... 31

1.2.7 Messenger RNA ..... 32

1.3 MECHANISMS OF RNA LOADING ..... 34

1.3.1 Passive loading/stability ..... 34

1.3.2 Sequence motifs ..... 34

1.3.3 Protein-based loading ..... 35

1.3.4 RNA-lipid interactions ..... 39

1.3.5 RNA modification ..... 39

1.4 *DROSOPHILA* AS A MODEL SYSTEM FOR EV BIOLOGY ..... 40

1.5 PROJECT AIMS AND OBJECTIVES ..... 41

**2 Materials and methods ..... 44**

2.1 CELL CULTURE ..... 44

2.1.1 Cell line maintenance ..... 44

2.1.2 Cell seeding for experiments ..... 44

2.1.3 Purification of EVs ..... 45

2.1.4 Induction of oxidative stress ..... 45

2.1.5 EV treatment of cells ..... 46

2.1.6 Transfection ..... 46

2.2 EV CHARACTERISATION ..... 46

2.2.1 Nanoparticle Tracking Analysis ..... 46

2.2.2 Transmission electron microscopy ..... 47

2.2.3 Protein extraction ..... 48

2.2.4 Western blotting ..... 48
2.2.5 Proteinase treatment of EVs ..... 49
2.3 CELL FUNCTIONAL ASSAYS ..... 50
2.3.1 MTT Assay ..... 50
2.3.2 Resazurin viability assay ..... 50
2.3.3 Annexin V and Propidium iodide Flow cytometry ..... 50
2.3.4 yH2Av immunocytochemistry ..... 51
2.3.5 Mitotracker orange staining ..... 51
2.3.6 CellROX staining ..... 52
2.4 RNA WORK ..... 52
2.4.1 RNA extraction and quantification. ..... 52
2.4.2 RNAse protection assay ..... 53
2.4.3 cDNA synthesis ..... 53
2.4.4 qPCR and primers ..... 53
2.4.5 RNA library preparation and sequencing ..... 54
2.5 RNA SEQUENCING ANALYSIS ..... 54
2.5.1 Initial RNA SEQ data analysis ..... 54
2.5.2 RNA Abundance estimates ..... 55
2.5.3 Differential expression analysis ..... 56
2.5.4 Gene ontology analysis ..... 56
2.5.5 Evolutionary conservation of differential expression ..... 56
2.5.6 Identification of unmapped reads ..... 57
2.5.7 Ribosomal RNA analysis ..... 58
2.6 mRNA LOADING ANALYSIS ..... 58
2.6.1 Junction saturation ..... 58
2.6.2 mRNA length and exon count ..... 59
2.6.3 Read type distribution ..... 59
2.6.4 Gene body coverage and base mismatch ..... 59
2.7 MOTIFS ..... 60
2.7.1 Defining EV and cell RNA groupings ..... 60
2.7.2 Motif searching ..... 60
2.7.3 Motif abundance ..... 61
2.7.4 Motif comparison ..... 61
2.7.5 RNA binding proteins ..... 61
2.7.6 Motif testing ..... 61
2.8 STATISTICAL ANALYSIS ..... 62

**3 Characterisation of purified EVs ..... 64**

3.1 BACKGROUND ..... 64
3.1.1 The effects of stress on EV-mediated cellular communication ..... 64
3.1.2 Methods for purifying EVs ..... 64
3.1.3 Best practice in characterisation of EVs ..... 65
3.2 AIMS AND OBJECTIVES ..... 66
3.3 RESULTS ..... 68
3.3.1 Size exclusion chromatography can be used to purify *Drosophila* cell EVs ..... 68
3.3.2 FBS contains non-EV particles which can be detected by NTA ..... 72
3.3.3 EVs eluted in PBS maintain their biophysical properties at 4°C for five days ..... 76
3.3.4 $H_2O_2$ induces dose-dependent oxidative stress in S2R+ cells ..... 77
3.3.5 $H_2O_2$ stress increases the number of EV produced per cell ..... 79
3.3.6 $H_2O_2$ stress does not alter the size of EVs produced ..... 82
3.4 DISCUSSION ..... 84
3.4.1 SEC for purification of EVs from *Drosophila* ..... 84
3.4.2 Quantification of EV release from stressed cells ..... 85
3.4.3 Measurement of EV size ..... 86
3.4.4 Storage of EVs at 4°C ..... 87
3.5 KEY FINDINGS ..... 88

**4 Functional effects on recipient cells ..... 90**
4.1 BACKGROUND ..... 90
4.1.1 Bystander effect ..... 90
4.1.2 Adaptive effect ..... 90
4.2 AIMS AND OBJECTIVES ..... 91
4.3 RESULTS ..... 91
4.3.1 Stress EVs induce an increase in resazurin reduction in recipient cells ..... 91
4.3.2 Three-hour EV treatment shows a trend towards reduced cell count ..... 92
4.3.3 EV treatment does not affect total mitotracker staining in recipient cells ..... 94
4.3.4 Stress EVs may increase necroptotic cell death in recipient cells ..... 95
4.3.5 Stress EVs increase the variability of DNA damage response in recipient cells ..... 97
4.4 DISCUSSION ..... 99
4.4.1 Use of resazurin reduction assay ..... 99
4.4.2 Investigating mitochondrial activity in EV-treated cells ..... 100
4.4.3 Investigating cell death in EV-treated cells ..... 100
4.4.4 Investigating DNA damage response in EV-treated cells ..... 101
4.4.5 Dosage and purity of EV preparations ..... 102
4.5 KEY FINDINGS ..... 103

**5 Profiling of EV and cell RNA ..... 105**
5.1 BACKGROUND ..... 105
5.1.1 RNA in EVs ..... 105
5.1.2 RNA loading into EVs ..... 106
5.1.3 Effect of stress on RNA in EVs ..... 106
5.2 AIMS AND OBJECTIVES ..... 107
5.3 RESULTS ..... 107
5.3.1 RNA in EV preparations is enriched over non-conditioned media ..... 107
5.3.2 EV-associated RNA is predominantly small RNA ..... 108
5.3.3 Ribosomal RNA is the predominant species in EV-associated RNA ..... 109
5.3.4 Ribosomal RNA maps almost exclusively to 28 and 18S subunits ..... 110
5.3.5 The Copia retrotransposon is abundant and enriched in EV-associated RNA ..... 111
5.3.6 EV-associated RNA contains minimal bovine contamination ..... 112
5.3.7 Viral RNAs are differentially enriched in EV-associated RNA relative to cell ..... 113
5.3.8 Altered gene expression confirms induction of stress in $H_2O_2$-treated cells ..... 114
5.3.9 Expression of EV biogenesis components are altered under stress ..... 115
5.3.10 RNA in EV preparations is partially enclosed within the vesicular membrane ..... 116
5.3.11 Biotype abundance in EV associated RNA is not representative of the cell ..... 118
5.3.12 RNAs involved in ribosomal functions are enriched in EVs ..... 119
5.3.13 EV-cell correlation of mRNA, snoRNA and snRNA is stress-dependent ..... 119
5.3.14 Cytoskeletal and developmental GO terms are common in all conditions ..... 122
5.3.15 Differential abundance affecting snoRNA and snRNA is lost under stress ..... 127
5.3.16 Dose-responsive changes are seen in stress EVs compared to control EVs ..... 127
5.3.17 Few specific gene changes in stress EVs are evolutionarily conserved ..... 131
5.4 DISCUSSION ..... 132
5.4.1 Ribosomal RNA in EV preparations ..... 132
5.4.2 Topology of EV-associated RNA ..... 133
5.4.3 Bovine RNA contamination ..... 134
5.4.4 Transposon content of EVs ..... 134
5.4.5 Similarities between viral RNA and EV RNA packaging ..... 136
5.4.6 Correlation of RNA types in EV and cell samples ..... 137
5.4.7 Enrichment of snoRNA ..... 139
5.5 KEY FINDINGS ..... 140

**6 Exploring mRNA loading in EVs ..... 142**
6.1 BACKGROUND ..... 142
6.1.1 Functionality of mRNA in EVs ..... 142
6.1.2 The role of sequence motifs in EV-mRNA loading ..... 143

6.1.3 Differential loading of mRNA under stress conditions ....143
6.2 AIMS AND OBJECTIVES ....144
6.3 RESULTS ....144
6.3.1 EVs are enriched for reads mapping to longer RNAs....144
6.3.2 Intronic reads become more abundant in EVs with increasing stress....147
6.3.3 Base mismatch is higher EV samples under stress conditions ....149
6.3.4 3' end gene coverage is lower in EV samples under stress conditions....150
6.3.5 Control EV enriched motifs are abundant in all stress conditions....152
6.3.6 3'UTR motifs do not specifically increase EV localisation of mRNA *in vitro* ....153
6.3.7 No high abundance stress-specific EV-enriched motifs can be identified....156
6.3.8 RNA binding proteins Smooth and PAPI may have a role in mRNA loading ....156
6.3.9 CAG trinucleotide repeats are enriched within the CDS of EV-mRNAs ....160
6.4 DISCUSSION ....162
6.4.1 No preference for shorter mRNAs in EV samples....162
6.4.2 Increased intronic and UTR reads in EVs under stress conditions....163
6.4.3 Presence of degraded mRNAs in EVs....164
6.4.4 Increased mismatch rate in stress EVs ....165
6.4.5 3'UTR motifs alone are not a strong determinant of mRNA loading....166
6.4.6 The RBP Smooth may link EV mRNA loading to mRNA degradation ....168
6.5 KEY FINDINGS ....169

**7 Discussion and future directions ....171**
7.1 SUMMARY OF KEY FINDINGS ....171
7.2 EFFECTS OF $H_2O_2$ ON EV PROPERTIES IN CELL CULTURE....173
7.3 UNDERSTANDING EV PACKAGING OF RNA ....174
7.4 FUNCTIONALITY OF EV-RNA ....178
7.5 FINAL CONCLUSIONS AND FUTURE DIRECTIONS....180

**8 Supplementary Materials ....184**

**9 References ....201**

# List of Figures

**Chapter 1**

Figure 1.1: Biogenesis of exosomes, microvesicles and apoptotic bodies ..... 17
Figure 1.2: Potential mechanisms of EV function in recipient cells ..... 21

**Chapter 3**

Figure 3.1: Size-exclusion chromatography for purification of *Drosophila* EVs ..... 69
Figure 3.2: Protein marker characterisation of mammalian and *Drosophila* EVs ..... 70
Figure 3.3: TEM of mammalian and *Drosophila* EVs. ..... 72
Figure 3.4 FBS depletion removes only larger particles ..... 73
Figure 3.5: Assessing approaches to minimising FBS contamination of EV samples ..... 75
Figure 3.6: Assessing EV stability ..... 76
Figure 3.7: MTT cell viability curves for three different inducers of oxidative stress ..... 78
Figure 3.8 Validating hydrogen peroxide concentrations for induction of stress ..... 80
Figure 3.9 Effect of $H_2O_2$ stress on EV production by S2R+ cells ..... 81
Figure 3.10: Effect of $H_2O_2$ stress on size of EVs produced by S2R+ cells ..... 82
Figure 3.11: Comparison of *Drosophila* EVs under control and stress conditions ..... 83

**Chapter 4**

Figure 4.1: Stress EVs increase signal in resazurin viability assay of recipient cells ..... 93
Figure 4.2: Three-hour EV treatment has no adaptive effect on recipient viability ..... 94
Figure 4.3: EVs have no effect on mitotracker orange staining in recipient cells ..... 95
Figure 4.4: EV treatment increases propidium iodide staining in recipient cells ..... 96
Figure 4.5: EV treatment increases variability of yH2Av staining in recipient cells ..... 98

**Chapter 5**

Figure 5.1: RNA is extracted from EV preparations with yield unaltered by stress ..... 108
Figure 5.2: Small and/or fragmented RNA are predominant in EV samples ..... 109
Figure 5.3: Alignment statistics for all EV samples ..... 110
Figure 5.4: Ribosomal RNA reads align to both 18S and 28S rRNAs ..... 111
Figure 5.5: Copia retrotransposon is enriched in EV samples ..... 112
Figure 5.6: Bovine-specific RNA contamination is low in EV samples ..... 113
Figure 5.7: RNA of viral species is differentially enriched in EVs ..... 114
Figure 5.8: Differential expression confirms stress induction in $H_2O_2$-treated cells ..... 115

Figure 5.9: Expression of several ESCRT components altered in cells under stress ..... 116
Figure 5.10: mRNAs in EV samples show partial sensitivity to RNAse treatment ..... 117
Figure 5.11: Relative abundance of EV RNA biotypes is not representative of cells..... 118
Figure 5.12: Gene ontology analysis for top 1000 most abundant RNAs in EVs ..... 119
Figure 5.13: EV and cell samples cluster distinctly in principal component analysis ..... 121
Figure 5.14: EV-Cell correlation decreases for mRNA and snoRNA under stress..... 122
Figure 5.15:Overlaps between EV-cell RNA differences are small ..... 123
Figure 5.16: EV enriched RNAs in common relate to cytoskeleton and development ..... 124
Figure 5.17: Gene ontology terms associated with RNAs of differential abundance in EV vs cell that are dose-dependently altered by stress ..... 126
Figure 5.18 Differential distribution of snoRNA and snRNA most affected by stress ..... 127
Figure 5.19 RNA upregulation in stress EVs is strongly stress-dose-dependent ..... 129
Figure 5.20 qPCR confirms up and downregulation in RNA sequencing data..... 130
Figure 5.21 Downregulated RNAs in stress EVs are cytoskeleton function related ..... 130
Figure 5.22 Conserved $H_2O_2$-induced changes in EV RNAs relate to mitochondria ..... 131

**Chapter 6**

Figure 6.1: EVs contain reads derived from both long and short mRNAs ..... 146
Figure 6.2: Significantly enriched EV mRNAs are longer than EV-depleted mRNAs..... 147
Figure 6.3: Intronic, 3'UTR and 5'UTR reads are enriched in EVs under stress ..... 148
Figure 6.4: Example genes showing region specific enrichment..... 149
Figure 6.5: Read alignment mismatch rate is increased in EVs under stress ..... 150
Figure 6.6: EV RNAs exhibit greater 3' end degradation under stress ..... 151
Figure 6.7: Outline of pipeline for grouping mRNAs for motif analysis..... 152
Figure 6.8: EV-enriched motifs from control conditions also abundant under stress..... 154
Figure 6.9: WT and shuffled Para 3'UTR show tendency to increased EV Cre ..... 155
Figure 6.10: No high abundance stress-specific EV motifs can be identified..... 157
Figure 6.11: EV-enriched motifs shown similarity to known RBP motifs ..... 158
Figure 6.12: Smooth and PAPI are RBP candidates for involvement in mRNA loading..... 159
Figure 6.13: EV-enriched motifs are present in all mRNA regions ..... 161

**Supplementary Figures**

Supplementary Figure 1: SKOV3 cells tolerate serum-free conditions for 72 hours..... 184
Supplementary Figure 2: Optimisation of minimal FBS culture conditions in S2R+ cells. ..... 185
Supplementary Figure 3: Testing of CellROX staining in MCF7 and S2R+ cells ..... 186

Supplementary Figure 4: Comparison of median particle size by Nanosight and Zetaview..... 187
Supplementary Figure 5: Agilent bioanalyser traces for all sequenced RNA samples ..... 189
Supplementary Figure 6: FastQC quality control data for all sequenced samples ..... 190
Supplementary Figure 7: Alignment statistics for all sequenced samples ..... 191
Supplementary Figure 8: Alignment statistics for all EV samples..... 192
Supplementary Figure 9: RNAs upregulated in both cells and EVs under stress..... 192
Supplementary Figure 10: Bovine-specific RNA contamination in all samples ..... 193
Supplementary Figure 11: Repeat sequences/transposons in all samples..... 193
Supplementary Figure 12: Viral RNA content of all samples..... 194
Supplementary Figure 13: Effect of viral infection on viable cell count..... 195
Supplementary Figure 14: Junction saturation analysis..... 197
Supplementary Figure 15: Validation of low stringency control motif set..... 198
Supplementary Figure 16: 3'UTR sequences for motif constructs ..... 198
Supplementary Figure 17: Comparison of cDNA motifs to $(CAG)_6$ ..... 199

# List of Tables

Table 1.1: Overview of classification of EVs and nanoparticles..... 16
Table 1.2: Proteins identified in literature as involved in EV RNA loading ..... 37
Table 2.1: Primary antibodies used in Western blotting ..... 49
Table 2.2: Secondary antibodies used in Western blotting..... 49
Table 2.3: qPCR primer sequences ..... 54
Table 3.1: Purification and characterisation used in study of *Drosophila* EVs ..... 67

# Abbreviations

| | |
|---|---|
| µg | Microgram |
| µl | Microlitre |
| 25nt | 25-nucleotide motif ACCCTGCCGCCTGGACTCCGCCTGT (Bolukbasi *et al*., 2012) |
| 3' UTR | 3' untranslated region |
| 5' UTR | 5' untranslated region |
| ABs | Apoptotic bodies |
| ag | Attogram |
| Alix | AlG-2 interacting protein X |
| BE | Bystander effect |
| BSA | Bovine serum albumin |
| CDS | Coding sequence |
| CRC | Colorectal cell |
| Cre | Cre recombinase |
| CTCF | Corrected total cell fluorescence |
| DAMP | Damage associated molecular pattern |
| DIOPT | DGRC Integrative Ortholog Prediction Tool |
| DTT | Dithiothreitol |
| DTV | *Drosophila* melanogaster totivirus |
| ESCRT | Endosomal sorting complexes required for transport |
| EMSA | Electrophoretic mobility shift assay |
| EVs | Extracellular vesicles |
| FBS | Foetal bovine serum |
| FHV | Flock House Virus |
| FIMO | Find Individual Motif Occurrences |
| FPKM | Fragments per million mapped reads |
| GEO | Gene Expression Omnibus |
| GO | Gene ontology |
| $H_2O_2$ | Hydrogen peroxide |

| | |
|---|---|
| HERV | Human endogenous retrovirus |
| IGV | Integrative Genome Viewer |
| ILVs | Intraluminal vesicles |
| ITS | Insulin-selenium-transferrin supplement |
| LDELS | LC3-dependent extracellular vesicle loading and secretion |
| LINE | Long interspersed nuclear element |
| LncRNA | Long non-coding RNA |
| LTR | Long terminal repeat |
| MEME | Multiple EM for Motif Elicitation |
| MFE | Minimum Free Energy |
| miRNA | MicroRNA |
| ml | Millilitre |
| MTT | 3(4,5–dimethylthiazol–2–yl)–2,5 diphenyl tetrazolium bromide |
| MV | Microvesicle |
| MVB | Multivesicular body |
| n.s. | Not significant |
| NAC | N-acetyl-cysteine |
| NCM | Non-conditioned media |
| ng | Nanogram |
| nm | Nanometre |
| nSMase | Neutral sphingomyelinase |
| nt | Nucleotide |
| NTA | Nanoparticle Tracking Analysis |
| PAMP | Pathogen associated molecular pattern |
| Para | Paralytic (gene) |
| PBS | Phosphate-buffered saline |
| PCA | Principal Component Analysis |
| PI | Propidium iodide |
| PRRs | Pattern recognition receptors |
| PTM | Post-translational modification |

| | |
|---|---|
| RBP | RNA binding protein |
| RISC | RNA-induced Silencing Complex |
| RNAi | RNA interference |
| ROCK1 | Rho-associated protein kinase 1 |
| ROS | Reactive Oxygen Species |
| rRNA | Ribosomal RNA |
| SEC | Size exclusion chromatography |
| SnoRNA | Small nucleolar RNA |
| SnRNA | Small nuclear RNA |
| SUMO | Small ubiquitin-like modification |
| tBHP | tertbutyl-hydroperoxide |
| TEM | Transmission electron microscopy |
| TLRs | Toll-like receptors |
| tRNA | Transfer RNA |
| TSG101 | Tumour susceptibility gene 101 |
| UC | Ultracentrifugation |
| VLPs | Virus-like particles |
| yH2Av | phosphorylated histone H2Av |

# Chapter 1

## Introduction

# 1 Introduction

## 1.1 EXTRACELLULAR VESICLES

### 1.1.1 Cell homeostasis and intercellular communication

Cell homeostasis is the maintenance of a stable internal environment to promote optimal cellular function, which is achieved by regulated activity of many different mechanisms. Disruptions to this homeostasis through exposure to harmful conditions may therefore lead to cellular damage and subsequent pathological processes of disease. In multicellular organisms, intercellular communication is also essential for coordinating cellular functions, and responses to these changes in internal and external environment. Accumulating evidence indicates that the release of small membrane-bound bodies into the extracellular environment, known as extracellular vesicles (EVs), is important for clearance of unwanted molecules, but also as a means by which cells can communicate with each other. Thus, there is a need to understand the mechanisms by which these EVs are produced and loaded with biological cargoes, and how they may be altered, in order to help determine both effective interventions in different pathological contexts, and to make use of the potential of EVs for delivering cargoes for therapeutic purposes.

### 1.1.2 History of extracellular vesicles

Extracellular vesicles (EVs) are small membrane-bound particles that are released by cells into the extracellular environment. They were first described by Peter Wolf as lipid-rich “platelet-dust” with pro-coagulant activity, that could be separated from blood plasma and serum by ultracentrifugation at 134,211g (Wolf, 1967). In the 1980s, the release of plasma-membrane derived vesicles that reflected parental cell ecto-enzyme were reported, with two populations at 500-1000nm and 40nm diameter respectively (Trams *et al*., 1981). The extracellular release of internally-derived vesicles was then described as a mechanism for shedding of the transferrin

receptor from reticulocytes, leading to the belief that EVs function primarily as a means of cellular waste disposal (Pan and Johnstone, 1983; Harding *et al*., 1984). However, later work on EVs suggested a signalling function, with the demonstration that they contribute to initiation or amplification of immune response via antigenic presentation (Raposo *et al*., 1996; Théry *et al*., 2002). More recent research has highlighted specific roles in various forms of signalling in complex organisms, including in neuronal communication (Holm *et al*., 2018), development (Gross *et al*., 2012; Beckett *et al*., 2013; Gradilla *et al*., 2014), cancer progression (Minciacchi *et al*., 2015; Xu *et al*., 2018) and inflammation (Buzas *et al*., 2014).

### 1.1.3 Biogenesis and classification

As the different discoveries suggest, EVs can be produced by multiple distinct biogenesis pathways, importantly whether they derive from the external plasma membrane or from intracellular pathways. EVs are typically classified into three major types depending on their biogenesis pathway; exosomes, microvesicles (MVs) and apoptotic bodies (ABs), although additional other overlapping EV-like nanoparticles have been discovered (Table 1.1 and Figure 1.1).

| Type | Size | Biogenesis | Reference |
|---|---|---|---|
| Exosome | 50-150nm | Multi-vesicular body | van Niel *et al*., 2018 |
| Microvesicle/ectosome | 100-1000nm | Membrane shedding | van Niel *et al*., 2018 |
| Apoptotic body | 50-5000nm | Apoptosis | Poon *et al*., 2014 |
| Oncosome | 1-10µm | Membrane shedding of cancer cells | Di Vizio *et al*., 2009, 2012 |
| Exomere | 35-50nm | Unknown | Zhang *et al*., 2018, 2019 |
| Ribonucleoprotein particle | Unknown | Unknown | Turchinovich *et al*., 2011<br>Wei *et al*., 2017 |

Table 1.1: Overview of classification of EVs and nanoparticles

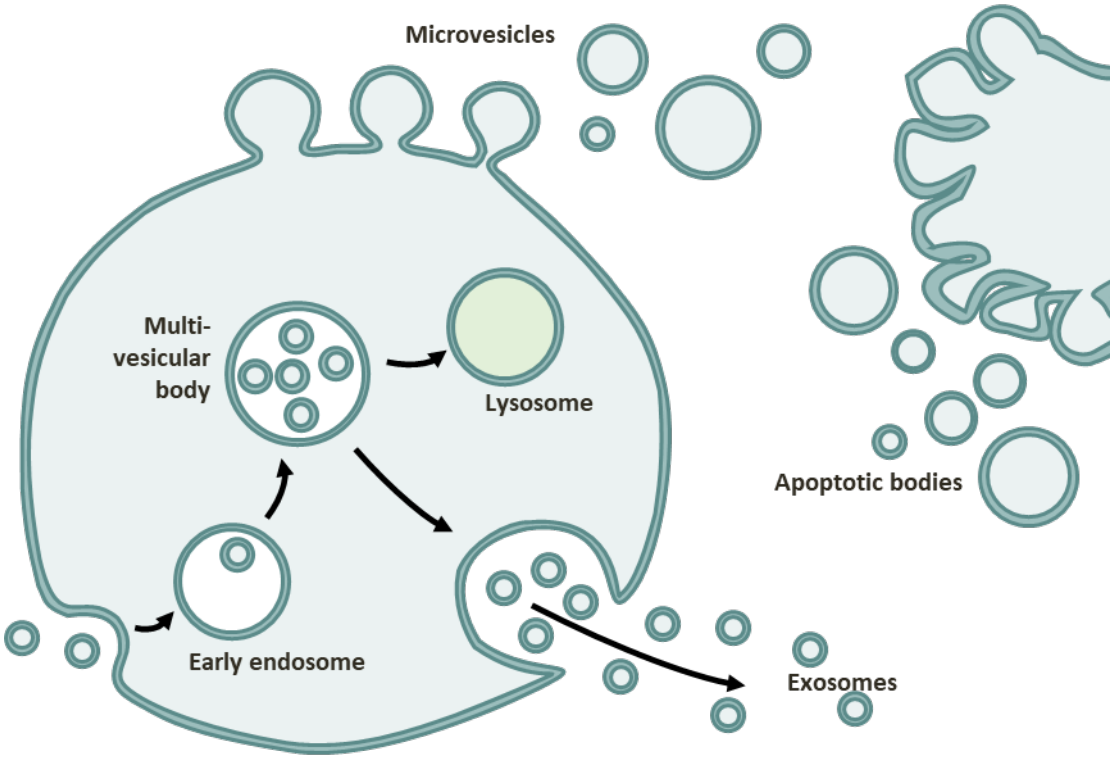


Figure 1.1: Biogenesis of exosomes, microvesicles and apoptotic bodies

**Exosomes**

Exosomes are 50-150nm vesicles which derive from intraluminal vesicles (ILVs) in multivesicular bodies (MVBs) of the endosomal system, requiring microtubular transport of the MVB to the plasma membrane to allow fusion and extracellular release of the ILVs. However, MVBs may instead fuse with the lysosome to enable degradation of ILV contents, so exosome biogenesis is likely also closely linked to lysosomal activity. In mammalian systems, typical marker proteins include tumour susceptibility gene 101 (TSG101) and AlG-2 interacting protein X (ALIX), part of the endosomal sorting complexes required for transport (ESCRT) machinery, pointing to their importance in biogenesis (Théry *et al*., 2018). ESCRT-dependent biogenesis is known to be one major pathway of exosome formation, and is responsible for the sorting of ubiquitinated protein cargo into MVBs (van Niel *et al*., 2018). However, the ESCRT machinery is also involved in an array of other cellular processes, including cytokinesis, nuclear envelope maintenance, viral

replication and budding, and plasma membrane budding and repair, the latter including MV formation (Vietri *et al*., 2020). Exosome formation also occurs via multiple other ESCRT-independent pathways, including the involvement of neutral sphingomyelinase (nSMase) and lipid rafts, hence the exosomal enrichment of cholesterol, sphingomyelin and ceramide lipids, and associated proteins such as flotillins and caveolins (Trajkovic *et al*., 2008). Biogenesis also involves tetraspanin-enriched microdomains, with tetraspanins CD63, CD81 and CD9 amongst the canonical EV markers in mammalian cells (van Niel *et al*., 2011; Andreu and Yáñez-Mó, 2014; Théry *et al*., 2018).

### Microvesicles

Microvesicles (MVs), also known as ectosomes, have a size range of around 100-1000nm diameter, so are more variable than, but overlap with, exosomes. In addition, they carry many of the same marker proteins, including tetraspanins. MVs bud directly from the cell plasma membrane, with formation dependent on localised changes in curvature and actin cytoskeletal dynamics (van Niel *et al*., 2018). MV shedding can firstly be driven by alterations in distribution of membrane phosopholipids. Phospatidylserine and phosphatidylethanolamine are normally located on the inner, cytosolic-facing leaflet of the plasma membrane, with this localisation dependent on ATP-dependent activity of flippase enzymes (Zwaal and Schroit, 1997). Calcium-induced activity of ATP-dependent floppase, or ATP-independent scramblase, enzymes move these phospholipids to the outer extracellular-facing leaflet, which promotes membrane curvature and cytoskeletal rearrangement to enable vesicle formation (Zwaal and Schroit, 1997; van Niel *et al*., 2018). Hydrolysis of sphingomyelin by acid sphingomyelinases may also trigger this membrane curvature (Bianco *et al*., 2009), whilst activation of small GTPases, including the RhoA family members ARF6 and ARF1, may also initiate the process (Muralidharan-Chari *et al*., 2009; Schlienger *et al*., 2014). Interaction of TSG101 with ALIX and ARDDC1 may also induce formation in a viral-like process (Nabhan *et al*., 2012). Finally, oncosomes, ranging between 1-

10um in size, are cancer cell-derived EVs which bud similarly from the plasma membrane, but with different trigger events, such as activation of the EGF receptor (Di Vizio *et al*., 2009, 2012).

### Apoptotic bodies

Apoptotic bodies (ABs) have an even broader size range than MVs, at 50-5000nm, and are formed during programmed cell death (Poon *et al*., 2014). As part of the apoptotic cascade, caspase-3 cleaves Rho-associated protein kinase (ROCK1) to remove an autoinhibitory region, which again results in actin and microtubule reorganisation to allow blebbing of the plasma membrane (Coleman *et al*., 2001). ABs contain a wide range of cargo, including fragmented DNA, RNA protein and lipids. They are typically considered to be large 1μm+ particles which are rapidly phagocytosed to avoid inflammation, however there is increasing investigation of smaller "ApoEVs", which, alongside exosomes and MVs, are thought to play important signalling functions (Caruso and Poon, 2018). Additionally, EVs produced during non-apoptotic forms of cell death, such as necrosis and pyroptosis are beginning to undergo greater investigation (Baxter *et al*., 2019).

### Overlap in EV sub-type definitions

Whilst these different biogenesis pathways for exosomes, MVs, and ABs exist, there is a high level of overlap and crosstalk between them. Additionally, although studies have attempted to define specific markers, there are currently none identified, and as such it is not possible to purify EVs formed from a single pathway. EVs are consequently typically defined by their size, with an understanding that the population is heterogenous, and that the cargo of any given purified sample is representative of this heterogeneity. Finally, alongside membrane-bound EVs, several groups have also described the existence of additional non-vesicular nanoparticles which have overlapping characteristics; 35-50nm "exomeres", notably enriched in Argonaute proteins (Zhang *et al*., 2018, 2019), and ribonucleoproteins containing components similar to those reported for EVs (Turchinovich *et al*., 2011; Wei *et al*., 2017).

### 1.1.4 Mechanisms of extracellular vesicle function

#### Intercellular communication via surface interaction

Although evidence suggests that EVs do play a role in an array of communication processes, they may do so by several different modes of action, as summarised in Figure 1.2 (Camussi *et al*., 2010; Mathieu *et al*., 2019; Roefs *et al*., 2020). EVs can function directly in surface-to-surface interactions, whereby ligands on the EV interact with receptors on the recipient cell surface (or *vice versa*) to induce signalling cascades, similarly to classical cell-cell juxtacrine signalling. In one of the first demonstrated functions for EVs, B-cell derived EVs were found to have the capability for antigenic presentation of MHC-II-bound peptides to T-cells for immune activation, with both MHC-I and MHC-II, and small and large EVs now known to function similarly (Raposo *et al*., 1996; Tkach *et al*., 2017). Another study found that Sw71 trophoblast EVs induced production of IL-1β in macrophages via fibronectin, even when recipient cells were treated with the actin polymerisation inhibitor cytochalasin D to block endocytic uptake (Atay *et al*., 2011). However, since there are several different pathways of EV uptake (discussed later), it possible that this inhibition was incomplete, and that the IL-1β production may be still attributed to internalised EVs (Mulcahy *et al*., 2014). EVs may also act to by transferring membrane constituents to the recipient cell membrane, including both transmembrane proteins and lipids (Del Conde *et al*., 2005; Camussi *et al*., 2010).

#### Maintenance of cellular homeostasis by removal of cellular waste

EVs are carriers of a wide range of biological cargos, including lipids, sugars, proteins, DNA, and many biotypes of RNA, on the membrane or within the EV lumen. One function of EVs may therefore be as a homeostatic mechanism for the producing cell, as a means for disposing of unwanted cellular material (Desdín-Micó and Mittelbrunn, 2017). Alongside their role in removal of reticulocyte transferrin receptor (Pan and Johnstone, 1983; Harding *et al*., 1984), EVs have been strongly implicated in neurodegenerative disease, with toxic misfolded proteins such

as alpha-synuclein (Parkinson's disease), beta-amyloid (Alzheimer's disease), and prion proteins (Creutzfeldt-Jakob disease) all shown to be packaged into EVs, possibly as a means for clearance (Emmanouilidou *et al*., 2010; Yuyama *et al*., 2012; Guo *et al*., 2015). EVs have also been suggested as a means for removal of cholesterol to relieve lysosomal dysfunction in Niemann-Pick type C1 disease (Strauss *et al*., 2010), of cytosolic-localised nuclear DNA fragments to avoid activation of DNA damage response (Takahashi *et al*., 2017), and of Y-RNA and mRNA fragments to remove aberrant RNA (Van Balkom *et al*., 2015). Whilst release of these molecules may have detrimental impacts to recipient cells, seen most prominently in the transmission of misfolded proteins through the brain in neurodegenerative disease, it may be that this is a means by which an overloaded cell outsources degradation to healthy neighbouring cells (Vidal, 2019). Thus, the ability to load EVs with cargo may be a function that is primarily of importance to the EV-producing cell.

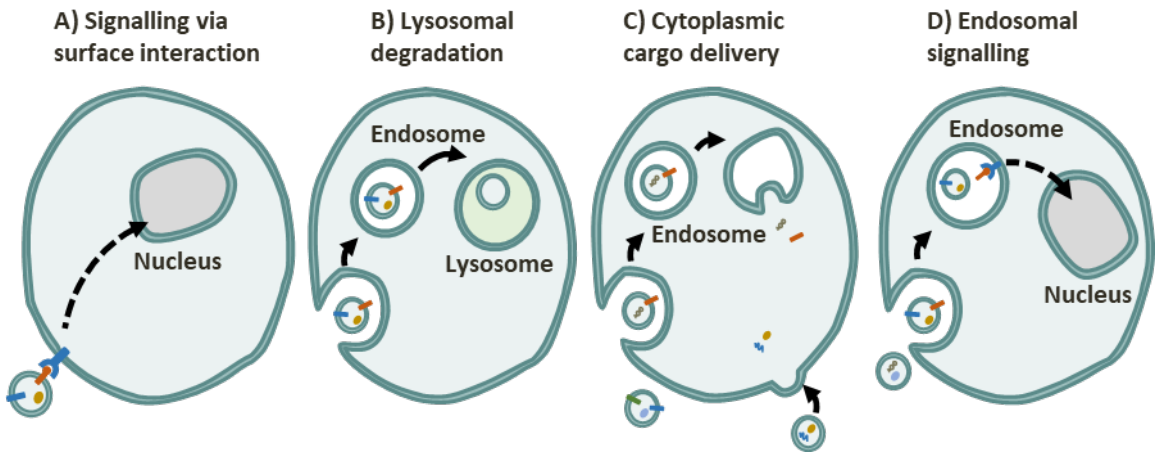


Figure 1.2: Potential mechanisms of EV function in recipient cells

*A) Ligands on the EV surface may interact with receptors in the recipient cell plasma membrane, stimulating downstream signalling events leading to changes in phenotype e.g. by altering gene expression. B) EVs are taken up by the recipient cells and trafficked to the lysosome where cargo molecules are degraded. C) Cargo molecules are delivered to the cytoplasm, either by direct fusion of EVs with the plasma membrane, or through endosomal escape. D) Ligands on the EV may interact with receptors from within the endosomal compartment, stimulating downstream signalling events.*

### EV uptake and cargo delivery

Although surface interaction and homeostatic waste disposal may be important mechanisms of EV function, what has driven the most excitement in the EV field is the potential for the delivery of both protein and RNA cargo to recipient cells, as a means of intercellular communication. The mechanisms by which EVs are targeted to recipient cells, enter, and deliver cargo, are an active area of investigation. Three main mechanisms for uptake have been suggested; firstly cell surface membrane fusion, which may be mechanistically similar to viral membrane fusion, and would imply direct delivery of cargo to the cytoplasm (Parolini *et al*., 2009; Montecalvo *et al*., 2012). Secondly, EVs may be transferred via cell-contact dependent mechanisms. In one study microRNA transfer between donor T-cells and recipient B-cells was observed only when synapse formation was induced, but was blocked by neutral sphingomyelinase inhibition or *Rab27a* knockdown, indicating a cell-contact dependent EV route (Mittelbrunn *et al*., 2011). Contact dependence of mRNA cargo transfer was seen in variety of cell lines in a second study, with the authors concluding that transfer occurred only via nanotube structures (Haimovich *et al*., 2017). However, the majority of EV uptake is believed to occur via endocytic pathways, which include clathrin-mediated, caveolin-dependent and receptor-mediated endocytosis, micropinocytosis, and phagocytosis (Mulcahy *et al*., 2014). These mechanisms imply that the cargo would be delivered to the late endosome, so would require endosomal escape to avoid lysosomal degradation and access cytoplasmic targets. Endosomal escape has been suggested to be a key limiting factor for effective cargo delivery (Kanada *et al*., 2015; Hung and Leonard, 2016; Heath *et al*., 2019; Bonsergent *et al*., 2021). Using membrane-bound GFP/NanoLuc tagged-CD63, or luminal NanoLuc-tagged Hsp70, to assess cytoplasmic delivery, 10-30% of internalised EVs released cargo to the cytoplasm, although with a higher rate at a longer timepoint (Joshi *et al*., 2020; Bonsergent *et al*., 2021). Protein delivery was also found to be increased when recipient cells were treated with chloroquine or UNC10217832A to promote endosomal lysis, or concanomycin A to inhibit lysosomal acidification, and reduced with Bafilomycin A1 to inhibit

endosomal acidification, indicating that the functioning of the recipient cell may be critical to cytoplasmic delivery (Kanada *et al*., 2015; Heath *et al*., 2019; Joshi *et al*., 2020; Bonsergent *et al*., 2021).

Nevertheless, it is also possible that EV cargo can be taken up and induce effects within recipient cells even without effective endosomal escape. In one study, EV-miRNAs miR-21 and miR-29a were found to stimulate the inflammatory response via activation of endosomal toll-like receptors (TLRs) TLR-7 and TLR-8 (Fabbri *et al*., 2012). Small EVs were also found to activate MYD88/TRIF-mediated immune activation through TLR-7 and TLR-9 in a second study, with the effect increased by knockout of LATS1/2, likely due to a dramatic increase in RNA cargo of the EVs (Moroishi *et al*., 2016). In a third study, the acidic environment of the endosome was found to enable release of glycoprotein-associated TGFβ-1 from the EV membrane, where it induced a migratory phenotype in primary mesenchymal stem cells via SMAD2 signalling (Shelke *et al*., 2019). Therefore, it is possible that a greater range of EV cargo may be able to trigger signalling pathways from within the endosomal compartment, with stimulation of pattern recognition receptors (PRRs), such as TLRs, providing a means for a relatively non-specific effect of cargo on recipient cells.

### 1.1.5 Extracellular vesicles and stress

#### Effects of stress-cell derived EVs on recipient cells

In addition to the function of EVs under normal conditions, attention has also extended towards understanding how exposure to different cellular stimuli affects EV production and subsequent function. There has been significant research in EV-mediated communication in the cancer field in order to understand the effects of radiotherapy and chemotherapy on non-targeted neighbouring cells. Alongside secreted agents such as cytokines and nitric oxide, EVs can induce DNA damage and apoptosis, a phenomenon termed the bystander effect (BE) (Hei *et al*., 2008; Kumar Jella *et al*., 2014; Al-Mayah *et al*., 2015; Xu *et al*., 2015; Szatmári *et al*., 2017). Further

work has found that such bystander effects can extend towards other stressors such as heatshock (Bewicke-Copley *et al*., 2017). However, in addition to damaging effects, these neighbouring cells have been suggested to be more resistant to damage from direct stress, indicating the potential role of EVs in mediating protective adaptive responses (Mutschelknaus *et al*., 2016; Bewicke-Copley *et al*., 2017). Indeed, other studies have suggested that EVs act primarily as proliferative or anti-apoptotic factors (Eldh *et al*., 2010; Kucharzewska and Belting, 2013; Wang *et al*., 2015; Atienzar-Aroca *et al*., 2016; Kore *et al*., 2018). It is therefore likely that these opposing results are due to differences in the type and degree of stress applied, or the specific cell lines studied, indicating that effects may be highly context specific.

### Alteration to EV biogenesis under stress conditions

Multiple studies appear to show an increase in the production of EVs as a response to endogenous or exogenous stressors; including x-rays (Arscott *et al*., 2013; Al-Mayah *et al*., 2015), Y-rays (Kumar Jella *et al*., 2014; Mutschelknaus *et al*., 2016), photodynamic chemotherapy (Aubertin *et al*., 2016), heat stress (Hedlund *et al*., 2011), hypoxia (King *et al*., 2012; Salomon *et al*., 2013) and oxidative stress (Hedlund *et al*., 2011; Atienzar-Aroca *et al*., 2016), although this is not detected by others in heat stress (Bewicke-Copley *et al*., 2017), hypoxia, TNF-alpha, high glucose or mannose (de Jong *et al*., 2012). In addition to changes in the number of EVs produced, several studies have also reported particles to be smaller in response to heat (Bewicke-Copley *et al*., 2017) and hypoxia (Kore *et al*., 2018), although no differences were seen in response to X-rays (Al-Mayah *et al*., 2015), Y-rays (Mutschelknaus *et al*., 2016), hypoxia, TNF-alpha, high glucose or mannose (de Jong *et al*., 2012). Such changes in EV size may be reflective of altered pathways of EV biogenesis; for example, the smaller EVs seen in response to heat and hypoxia may represent an increase in production of MVB-derived exosomes. These changes in EV biogenesis may signify that EVs are either of greater importance to the producing cell under

non-physiological conditions, such as in the removal of damaged cell contents, or of a greater need for intercellular communication to allow adaptation to these stress conditions.

### Alteration to EV uptake under stress conditions

Understanding the role of EVs in intercellular communication requires an understanding of uptake dynamics, and evidence suggests that this may also be altered under stress conditions. Assessment of the uptake of EVs by U87MG glioma cells by labelling with the lipid dye PKH26 showed that, at 24 hours after EV application, EVs derived from x-ray irradiated cells had higher uptake than non-irradiated controls (Arscott *et al*., 2013). This same increased uptake of EVs derived from irradiated cells was seen in oral squamous cell carcinoma BHY cells (Mutschelknaus *et al*., 2016). However, this latter study further showed that the irradiation of recipient cells, in addition to EV-producing cells, significantly increased uptake of EVs derived from either irradiated or non-irradiated cells. In co-culture systems, mRNA delivery was also found to be increased with stress treatment of either donor or recipient cells, but with recipient cell stress (heatshock, hydrogen peroxide, dithiothreitol or serum starvation) having the greatest effect (Haimovich *et al*., 2017). Therefore, it seems that the health state of both donor and recipient cells is a factor in determining the function of EVs under stress conditions.

### Alteration to EV cargo under stress conditions

Alongside biogenesis and uptake, changes to EV cargo in response to cellular stress have been widely studied, including protein (de Jong *et al*., 2012; Arscott *et al*., 2013; Kucharzewska *et al*., 2013), mRNA (Eldh *et al*., 2010; de Jong *et al*., 2012; Arscott *et al*., 2013; Kucharzewska *et al*., 2013; Atienzar-Aroca *et al*., 2016) and microRNA (Arscott *et al*., 2013; Xu *et al*., 2015; Lee *et al*., 2019). Since EVs are released into a range of biofluids, such as blood, cerebrospinal fluid and urine (Raposo and Stoorvogel, 2013), the contents of EVs isolated from these fluids can provide a snapshot of cell contents, and as such provide a novel source for disease diagnostics, with particular value for identifying pre-symptomatic changes, from cancer to neurodegenerative

disease (Thompson *et al*., 2016; Carollo *et al*., 2019). Additional interest, however, lies in whether these cargoes are altered in EVs only, which would imply that cellular stress may cause differences to cargo sorting pathways.

### Oxidative stress

Oxidative stress is defined as the state in which the level of reactive oxygen species (ROS) in the cell exceeds its antioxidant capacity, with these free radicals causing oxidative damage to DNA, proteins and lipids (Pizzino *et al*., 2017). Mechanisms of regulation include the detoxification enzymes superoxide dismutase and catalase, scavenging by glutathione (using peroxidases, NADPH and glutathione transferase to recycle), and iron sequestration. This form of stress is of specific interest because it is thought to play a dual role in aging, with high levels of ROS-induced damage thought to be a causative factor in age-associated diseases including neurodegenerative disorders (Ischiropoulos and Beckman, 2003), cardiovascular disease (Madamanchi *et al*., 2005), and cancers (Reuter *et al*., 2010), whilst low levels are suggested to induce an adaptive response that may promote longevity and healthy ageing (Ristow and Zarse, 2010; Pickering *et al*., 2013; Wong *et al*., 2016).

## 1.2 EXTRACELLULAR VESICLE RNA

In 2006-2008, the discovery that EVs appear to contain mRNAs and miRNAs contributed to an explosion in the study of EVs and their cargo (Baj-Krzyworzeka *et al*., 2006; Ratajczak *et al*., 2006; Valadi *et al*., 2007; Skog *et al*., 2008). Detection of mutated *EGFRvIII* within EVs purified from glioblastoma patient serum indicated that EVs could provide a novel source of disease biomarkers (Skog *et al*., 2008). In addition to this diagnostic use, these mRNAs were shown to be translatable, and thus likely functional, in cells treated with exogenous EVs (Valadi *et al*., 2007). Additional work suggested that the functional effects of EVs on cellular proliferation and viability were mediated specifically by the RNA, indicating a wider importance in intercellular communication in other contexts (Ratajczak *et al*., 2006; Eldh *et al*., 2010). RNA sequencing is

now widely employed to characterise the content of EVs and has provided a wealth of data. However, differences in individual studies; the cell lines used, EV subtypes studied, purification protocols, sequencing library preparation, sequencing type *etc.* means that data is often conflicting and makes effective comparison difficult. Nevertheless, the total body of evidence demonstrates that EVs contain all manner of RNAs, which will be discussed in this section.

### 1.2.1 MicroRNA

MicroRNAs (miRNAs) are small ~22nt single-stranded RNAs which are important in regulation of messenger RNA (mRNA) expression, largely through interaction with 3' untranslated regions (3'UTRs) to cause translational repression or degradation (Bartel, 2004). miRNAs have been one of the most heavily studied of RNA cargos in EVs, likely because they are easier to study (easier to identify and easier to delineate a mechanism of action) and have great biomedical interest, both as biomarkers of disease and from the perspective of RNA-mediated therapies (Pérez-Boza *et al*., 2018). In small RNA sequencing, miRNA has been reported to make up anywhere from <1% to 30% of total reads (Nolte-'t Hoen *et al*., 2012; Koppers-Lalic *et al*., 2014; Baglio *et al*., 2015; Tosar *et al*., 2015; Chiou *et al*., 2018). Such differences may be reflective of methodological artefacts, with both bovine serum contaminants (even when media is EV-depleted) and co-purified extracellular ribonucleoprotein particles, such as AGO2 and high-density lipoproteins, making significant contributions to total extracellular miRNA (Arroyo *et al*., 2011; Turchinovich *et al*., 2011; Vickers *et al*., 2011; Wei *et al*., 2016).

EVs have been proposed as a means to dispose of miRNAs present in excess to their target mRNAs, since overexpression of mRNAs resulted in EV depletion of their regulatory miRNAs, whilst overexpression of the miRNAs themselves resulted in enrichment in EVs (Squadrito *et al*., 2014). However, several studies additionally link the delivery of miRNA to phenotypic alterations in recipient cells, including both promotion and inhibition of angiogenesis, cell migration, immunosuppression and differentiation (reviewed in: O'Brien *et al*., 2020). However, if RNA

cargo delivery is a major function of EVs, an outstanding question to be answered within the field is how it can be delivered in sufficient quantities to elicit measurable effects in recipient cells. Alternative less miRNA-specific mechanisms may provide some explanation, such as through the activation of TLRs (Fabbri *et al*., 2012). Additionally, since shRNA expression is able to oversaturate endogenous small RNA pathways such that lower abundance regulatory miRNAs can no longer compete for binding to the RNA-induced Silencing Complex (RISC), it is possible that bulk miRNA delivery could act in a similar fashion (Grimm *et al*., 2006; Brown *et al*., 2007). Hence, whilst individual miRNAs are of low abundance within EVs, this does not exclude them from playing a role in intercellular communication, although does indicate that non-canonical functions may be involved.

### 1.2.2 Transfer RNA

Transfer RNAs (tRNA) are highly structured 76-90nt RNAs which function as adaptor molecules in translation, with a 3-nt anticodon loop for mRNA recognition and an amino acid attachment site (Goodenbour and Pan, 2006). In EVs, tRNAs have been reported to be both abundant as a percentage of total RNA, constituting up to 95% of small RNA in syncytiotrophoblast EVs, and enriched relative to cells, although again with a high abundance in free ribonucleoprotein particles (Baglio *et al*., 2015; Tosar *et al*., 2015; Cooke *et al*., 2019). In-depth study of tRNA has also demonstrated the presence of fragments, with a greater prevalence of 5’ regions relative to 3’ halves, (Nolte-’t Hoen *et al*., 2012; Wei *et al*., 2017; Chiou *et al*., 2018; Cooke *et al*., 2019). GlyGCC has been identified as an especially abundant or enriched tRNA, and has been the focus for functional studies (Baglio *et al*., 2015; Cooke *et al*., 2019; Gámbaro *et al*., 2019). In addition to high abundance in EVs, Cooke *et al*. show that treatment of fibroblasts with 500nM of the 5-tRNA-half-GlyGCC reduces global protein synthesis by 12.4% compared to scrambled control, indicating that it could induce significant effects if delivered via EVs in high enough quantities. Treatment of MCF-7 cells with EVs derived from cells transfected with synthetic 5’-tRNA-half-

GlyGCC showed significant alterations in gene expression that were not seen with non-EV fractions or scrambled control-tRNA, with delivery also demonstrated by fluorescence microscopy and stem-loop-RT-qPCR, indicating that functional delivery is possible (Gámbaro *et al*., 2019). EV loading of 5' tRNA halves has also been suggested to be of importance to producing cells, as a means of releasing fragments that would otherwise induce T-cell activation, thus providing further evidence of an RNA homeostatic function for EVs (Chiou *et al*., 2018).

### 1.2.3 Small nucleolar RNA

Small nucleolar RNAs (snoRNAs) are stable species of around 60-300nt in length which function in the modification or cleavage of ribosomal RNA and small nuclear RNA (Bratkovič *et al*., 2020). SnoRNAs can be separated into two major groups, box C/D which contain C (RUGAUGA) and D (CUGA) motifs, and box H/ACA which contain box H (ANANNA) and (ACA) motifs. These motifs form specific secondary structures, allowing the snoRNAs to function in 2'-O-methylribosylation (box C/D) and pseudouridylation (box H/ACA) (Bratkovič *et al*., 2020). SnoRNAs are commonly transcribed within introns of mRNAs and subsequently excised, although they may also be transcribed as mono or poly-transcriptional units. SnoRNAs have been identified in small RNA sequencing studies of EVs, although at low abundance and depleted in EVs relative to cells (Nolte-'t Hoen *et al*., 2012; Baglio *et al*., 2015; Tosar *et al*., 2015; Lässer *et al*., 2017; Wei *et al*., 2017; Chiou *et al*., 2018; Driedonks *et al*., 2018). In total RNA sequencing however, snoRNA abundance was similar in human HepG2 EVs and cells, whilst appearing enriched in *Drosophila* cells (Lefebvre *et al*., 2016). One study has investigated functionality of EV snoRNAs, studying *Rpl13a*-intron derived snoRNA U33*,* which was present in EVs from bone-marrow derived macrophages (Rimer *et al*., 2018). In transwell co-cultures (in which cell types are separated by a 1µm pore membrane), U33 labelling could be seen in the nucleus of knockout cells co-cultured with wildtype, whilst significant differences in ribosomal RNA 2'-O-methylribosylation were seen in a long-range transfer model utilising shared circulation of wildtype and *Rpl13a* knockout mice.

Whilst indicating that snoRNAs can be functionally transferred via EVs, as for miRNAs, the underlying question of sufficient delivery quantities still stands.

### 1.2.4 Small nuclear RNA

Small nuclear RNAs (snRNAs) are ~150nt nuclear RNAs which associate with Sm proteins to form small nuclear ribonucleoproteins, together forming the spliceosome complex which, in concert with other protein factors, functions in mRNA splicing (Matera *et al*., 2007). SnRNAs have also been identified in small RNA sequencing of EVs, although reported in different studies to be of similar abundance, enriched, or depleted in EVs relative to cells (Nolte-'t Hoen *et al*., 2012; Lässer *et al*., 2017; Chiou *et al*., 2018; Driedonks *et al*., 2018). In total RNA sequencing, snRNA appears to be enriched in both human and *Drosophila* cell line EVs (Lefebvre *et al*., 2016). Functional activity of EV snRNAs has not at this time been investigated.

### 1.2.5 Non-coding RNA

Long non-coding RNAs (lncRNAs) are >200nt RNAs which do not code for protein, but are instead associated with a range of regulatory functions, including direct or indirect transcriptional regulation, binding of miRNAs, and mRNA stability (Fatica and Bozzoni, 2014). Enrichment of lncRNAs in EVs has been investigated by several groups, which have demonstrated their involvement in mediating cell proliferation, angiogenesis and resistance to chemotherapeutic drugs in recipient cells (Kogure *et al*., 2013; Gezer *et al*., 2014; Takahashi *et al*., 2014; Hewson *et al*., 2016; Hinger *et al*., 2018). The study by Hinger *et al.* demonstrated, using a CRISPR-Display luciferase reporter system, that the oncogenic lncRNA *CRNDE* was taken up into the nuclei of recipient cells (Hinger *et al*., 2018). Other non-coding RNAs of a range of lengths have also been found to be enriched in EVs, including *7SL*, Y-RNAs and vault RNAs. *7SL* is a 300nt RNA which forms a ribonucleoprotein complex that is involved in targeting proteins to the endoplasmic reticulum (Nolte-'t Hoen *et al*., 2012; Nabet *et al*., 2017; Tosar *et al*., 2020). Y-RNAs are ~100nt

RNAs that form a ribonucleoprotein complex with the Ro60 autoantigen, functioning in the recognition, refolding and decay of variant and misfolded RNAs, such as U2 snRNA and pre-5S ribosomal RNA (Chen *et al*., 2003; Fuchs *et al*., 2006; Nolte-'t Hoen *et al*., 2012; Tosar *et al*., 2015; Van Balkom *et al*., 2015; Cambier *et al*., 2017; Wei *et al*., 2017). Vault RNAs, 86-140nt RNAs that associate with ribonucleoprotein complexes containing major vault protein, play a role in nucleocytoplasmic and cytoskeleton transport, although their function has been poorly characterised (Nolte-'t Hoen *et al*., 2012; Van Balkom *et al*., 2015). However, alternative studies have reported vault RNAs to be absent in mammalian EVs (Jeppesen *et al*., 2019), whilst it has been suggested that only specific fragments of *7SL*, Y-RNA and vault RNAs are found in EVs (Nolte-'t Hoen *et al*., 2012).

### 1.2.6 Ribosomal RNA

Ribosomal RNA (rRNA) is formed of two subunits, large and small, which in *Drosophila* are made up of five RNAs, 28S, 18S, 5.8S, and 2S transcribed as a single unit, and 5S independently (Stage and Eickbush, 2007; Richard *et al.*, 2008). Ribosomal genes are present within the genome as multiple tandem repeats, along with many rRNA pseudogenes, whilst some rRNA is also encoded in the mitochondrial genome. Since rRNA is generally considered to make up approximately 80% of total cell RNA, many studies opt for either small RNA sequencing, or preparation of poly(A)-selected or ribo-depleted total RNA libraries, in order to achieve high sequencing depth (Chen et al., 2017; Statello et al., 2018; Cherlin et al., 2020). ABs and large MVs, on the basis of bioanalyser profiles, appear to contain some intact rRNA (Crescitelli *et al*., 2013; Lässer *et al*., 2017; Wei *et al*., 2017) which is absent in small EVs (Valadi *et al*., 2007; Lässer *et al*., 2011; Bellingham *et al*., 2012; Nolte-'t Hoen *et al*., 2012). However, many RNA sequencing studies have shown that, even in small EVs, ribosomal fragments are highly abundant (Jenjaroenpun *et al*., 2013; Wei *et al*., 2017). Whilst functional roles for these rRNA fragments have been suggested elsewhere, nothing has yet been investigated with regards to EVs (Lee *et al*., 2009b; Wang *et al*.,

2016; Chen *et al*., 2017; Zhu *et al*., 2018). However, since these fragments make up such as a high proportion of EV-RNA, it seems highly plausible that they could have signalling functions.

### 1.2.7 Messenger RNA

Intact mRNAs are long RNAs of between ~150 and 60,000nt in length that code for protein production. Within their DNA-encoded sequence they contain coding exons (CDS) interspersed within non-coding introns, preceded by a 5' untranslated region (5' UTR) and followed by a 3'untranslated region (3'UTR), both of which are involved in regulating stability, localisation and translation of the mRNA. Some studies have detected full-length long mRNAs in EVs, of up to 5000bp in length, using qPCR (Enderle *et al*., 2015; Matsuno *et al*., 2019), whilst others have been unable to detect full-length RNAs longer than 1000bp (Wei *et al*., 2017; Hinger *et al*., 2018). The presence of intact mRNA may also be inferred, but not proved, from full-length coverage in RNA sequencing studies. However, since the majority of RNA in EV samples lies between 25-700nt in bioanalyser traces, this indicates the predominance of smaller RNAs, or fragments of longer ones. Therefore, although initial work by Valadi *et al.* did show the potential for translation of EV-mRNAs, questions remain as to the extent of this functionality *in vivo*.

Multiple elegant reporter systems have now been developed to study EV-mRNA function, both *in vitro* and *in vivo.* Several groups have made use of Cre-Lox reporter systems in which Cre mRNA is expressed in one cell line, organism, or tissue, and subsequently transferred via EVs to a recipient, where it is translated and results in the excision of LoxP sites in a reporter construct, thus permitting the expression of a detectable protein such as gfp, rfp, luciferase or beta-galactosidase. Such a system was first used to demonstrate that haemopoietic-derived, RNAse treated EVs, injected into the cerebellum, could mediate beta-galactosidase reporter activation in a range of cell types including Purkinje neurons and microglial cells, which was not induced by the injection of purified protein or cell lysate (Ridder *et al*., 2014). Further work by the same group demonstrated that transplanted TU2449 astrocytic or LLC2 cells, or purified EVs, could

also mediate reporter activation (Ridder *et al*., 2015). A similar reporter, with Cre inducing a switch from dsRed to eGFP expression, showed activation both *in vitro*, in co-culture and transwell experiments, and *in vivo*, with injected EVs, in a range of tissues including lymph nodes, lungs and spleen (Zomer *et al*., 2015). However, since the efficiency of reporter activation was low, ranging from 0.005% in Purkinje neurons to 2.4% in cardiomyocytes, and the Western blotting or ELISA techniques used to demonstrate absence of Cre protein have lower sensitivity than the qPCR used to detect mRNA, this activity cannot be unequivocally attributed to Cre mRNA (Ridder et al., 2014; Zomer et al., 2015, 2016; Das et al., 2019). In a luciferase-based reporter in HEK-293F cells, the presence of full-length mRNA in both small and large EVs was also demonstrated. However, through the use of transcriptional and translational inhibitors, they found that no reporter activation could be attributed specifically to the mRNA (Kanada *et al*., 2015). Evidence on the functionality of mRNA carried within EVs therefore seems mixed; whilst it appears that some is present and intact, delivery appears to be highly variable, and perhaps dependent on the specific cell types investigated.

Intact mRNA aside, it seems clear that at least some EV-mRNA is fragmented, with intronic or exonic mRNA fragments suggested to be present at 1 per EV, compared to 1 per 10 EVs for any intact mRNA (Wei *et al*., 2017). Furthermore, several studies have indicated that UTR regions, particularly 3' UTRs, are overrepresented in EVs relative to the CDS (Nolte-'t Hoen *et al*., 2012; Batagov and Kurochkin, 2013; Wei *et al*., 2017; Pérez-Boza *et al*., 2018). Differential expression of 3'UTRs relative to the CDS has been documented in several studies in cells, so these isolated 3'UTRs may have important, likely regulatory, roles (Mercer *et al*., 2011; Kocabas *et al*., 2015; Sudmant *et al*., 2018). Equally so, it is possible that these fragments are preferentially stable products of the degradation of full-length mRNAs. Single-stranded RNA is able to activate toll-like receptors in endosomes (Diebold *et al*., 2004; Karikó *et al*., 2004), so these fragments could induce inflammation in recipient cells in a manner analogous to that demonstrated for EV miRNAs and non-coding *7SL* RNA (Fabbri *et al*., 2012; Nabet *et al*., 2017).

## 1.3 MECHANISMS OF RNA LOADING

Since many studies have identified differences in the relative RNA abundance in cells and EVs, it has been argued that this evidences specific, active mechanism(s) by which the RNA is packaged into EVs (Ekström *et al*., 2012; Villarroya-Beltri *et al*., 2013; Baglio *et al*., 2015; Cha *et al*., 2015; Chiou *et al*., 2018). As such, a variety of processes, including RNA sequence motifs, RNA binding proteins, lipid interactions and RNA modifications, are under study as candidates for these mechanisms, with study primarily relating to miRNAs to date.

### 1.3.1 Passive loading/stability

Although differences in EV and cell RNA abundance may indicate that some species are actively loaded, in a study of miRNAs Tosar *et al*. (2015) argue for a passive secretion model, as 95% of 182 detected miRNAs were unaltered in EV relative to cell. In further support of this model, the same group suggest that the stability of RNA is a key factor to maintaining high concentrations, which increase the chance of incorporation (Gámbaro *et al*., 2019). On the other hand, in the microRNA study, it must be noted that a strict 4-fold threshold for determining differential abundance was applied, but even at this high stringency, 5% of the miRNAs were altered (Tosar *et al*., 2015). It is therefore suggested that, whilst intracellular RNA concentration is a major determinant of EV-RNA abundance, specific secretion mechanisms likely also co-exist.

### 1.3.2 Sequence motifs

One possibility for the determination of RNA packaging is the sequence composition of each molecule. The existence of specific sequence motifs was first suggested in 2011, with identification of three motifs, ACCAGCCT, CAGTGAGC and TAATCCCA, enriched in mRNA of glioblastoma cell EVs (Skog *et al*., 2008; Batagov *et al*., 2011). Similar work identified a 25nt "zipcode" motif (ACCCTGCCGCCTGGACTCCGCCTGT), present in the twenty most EV-enriched transcripts in primary glioblastoma and melanoma cell lines, which was further shown to

mediate an increase in the level of eGFP in EVs of HEK293T cells (Bolukbasi *et al*., 2012). Both studies find these motifs to be present as part of predicted loop regions, which may be important in the loading. Bolukbasi *et al.* further suggest the binding of miR-1289 to be involved in this process. However, this same zipcode sequence was not found to be enriched in EVs of the hepatic cell line MLP29, instead C[TA]G[GC][AGT]G[CT]C[AT]GG[GA] was identified, leading the authors to propose that motif-based systems are likely involved, but highly tissue-specific (Szostak *et al*., 2014).

Studies of miRNA in EVs have also revealed enriched motifs. In miRNAs whose enrichment was common to both primary T-cells and the Jurkat T-cell line, in both resting and activated conditions, [GU]G[ACG][GC] (GGAG) and [CUG]CC[UGA] were found to be overrepresented in EV miRNAs, whilst several longer motifs were identified in cell miRNAs, one containing the 4nt sequence UGCA (Villarroya-Beltri *et al*., 2013). Mutation of these GAGG or UGCA motifs to the opposing motif in candidate miRNAs was then found to induce the expected change in EV/cell localisation. Several other studies have identified additional motifs in other contexts, GGCU in murine hepatocyte 3A cells (Santangelo *et al*., 2016), UGGA in breast cancer MDA-MB-231 cells (Temoche-Diaz *et al*., 2019), and AAUGC in miRNAs upregulated after inflammatory activation of monocytic THP-1 cells (Wozniak *et al*., 2020). No specific enriched motifs however, could be detected in HEK293 cells (Shurtleff *et al*., 2016) or colorectal cancer cell lines (Cha *et al*., 2015), although the latter study did find a tendency for C-rich motifs when comparing more highly enriched miRNAs.

### 1.3.3 Protein-based loading

#### RNA binding proteins associated with specific motifs

Following on from the identification of sequence motifs that promote EV loading, several studies have gone on to highlight specific RNA-binding proteins (RBPs) that bind to these motifs, and likely mediate the packaging process. After discovery of the GGAG motif, Villarroya-Beltri *et al*.

(2013) used biotin-miR pull-down with mass spectrometry to identify the RBPs hnRNPA2B1, hnRNPA1, hnRNPC and RS4X, which bound to EV-enriched miR-198 but not cell-enriched miR-17. Electrophoretic mobility shift assays (EMSA) then confirmed the binding of hnRNPA2B1 to miR-198 and a second EV-miRNA, miR-601. Additional miRNA motifs from other studies are also believed to act via RBPs, Syncrip for GGCU (Santangelo *et al*., 2016), Lupus La for UGGA (Temoche-Diaz *et al*., 2019), and FMR1 for AAUGC (Wozniak *et al*., 2020). Less follow-up study has focused on mRNAs, although motifs identified by Batagov *et al*. (2011) were later shown by the same group to bind the methyltransferase NSUN2 and RBP YBX-1 (Kossinova *et al*., 2017).

### Other protein involvement

In order to carry out an unbiased assessment of RBPs involved in packaging of RNA, one study carried out EMSAs of EV protein incubated with either total EV RNA, cellular mRNA or cellular microRNA (Statello *et al*., 2018). Of 90 interacting proteins in total, one (MVP) was functionally validated, and five others (HNRNPA2B1, HNRNPK, HNRNPU, NSUN2 and VAPA) demonstrated to have involvement in independent works (Villarroya-Beltri *et al*., 2013; Kossinova *et al*., 2017; Barman *et al*., 2020; Leidal *et al*., 2020; Zietzer *et al*., 2020). Additional studies have identified KRAS (Cha *et al*., 2015), HuR (Mukherjee *et al*., 2016), MEX3C (Lu *et al*., 2017), Ago2 (Gibbings *et al*., 2009; McKenzie *et al*., 2016) and IGFBP2 (Ghoshal *et al*., 2019) as having some effect on EV miRNA. Other biotypes of RNA have remained largely uninvestigated, although recent work has shown that VAPA has an effect on snoRNA and tRNA loading as well as miRNA (Barman *et al*., 2020). Of notable interest, YBX-1 is the only RBP implicated in both short (miRNA, tRNA, vault RNA, Y-RNA) and long (mRNA) RNA loading (Shurtleff *et al*., 2016, 2017; Kossinova *et al*., 2017). Contrastingly, the effect of KRAS was seen in miRNA but not long RNA (Cha et al., 2015; Hinger et al., 2018). Therefore, it seems that whilst protein-mediated loading is a common process for multiple RNA biotypes, there may be little overlap in the specific proteins involved.

| Protein | RNA biotype | Reference |
|---|---|---|
| hnRNPA2B1 | miRNA | Villarroya-Beltri et al. (2013)<br>Pérez-Boza et al. (2020) |
| SYNCRIP | miRNA | Santangelo et al. (2016) |
| YBX-1 | mRNA, miRNA, tRNA,vRNA, YRNA | Batagov et al. (2011)<br>Kossinova et al. (2017)<br>Shurtleff et al. (2016)<br>Shurtleff et al. (2017)<br>Yanshina et al. (2018) |
| HuR | miRNA | Mukherjee et al. (2016) |
| Ago2 | miRNA | Gibbings et al (2009)<br>McKenzie. (2016) |
| MEX3C | miRNA | Lu et al. (2017) |
| AnxA2 | miRNA | Hagiwara et al. (2015)<br>Pérez-Boza et al. (2020) |
| Alix | miRNA | Iavello et al (2016) |
| MVP | miRNA | Teng et al. (2017)<br>Statello et al. (2018) |
| Lupus La | miRNA | Temoche-Diaz et al. (2019) |
| NSUN2 | mRNA | Batagov et al. (2011)<br>Kossinova et al. (2017) |
| KRAS | miRNA | Cha et al. (2015) |
| FMR1 | miRNA | Wozniak et al. (2020) |
| VAPA | miRNA, snoRNA, tRNA | Barman et al. (2020) |
| hnRNPU | miRNA | Zietzer et al. (2020)<br>Villarroya-Beltri et al. (2013) |

Table 1.2: Proteins identified in literature as involved in EV RNA loading

Although proteins have clear involvement in the packaging of RNA into EVs, there are many possible pathways by which this could occur. It is possible that they directly transport the RNA to sites of EV-biogenesis, to the plasma membrane for MVs or to the MVB for exosomes, or they may indirectly alter RNA sub-cellular localisation (Tosar *et al*., 2021). In primary lymphoblast-derived cells, an assessment of the role of tetraspanin-enriched microdomains in protein cargo loading was carried out, using pull-down of the EV tetraspanin marker CD81 and its associated receptors; ICAM-1 and EWI-2 (Perez-Hernandez *et al*., 2013). Several of the RBPs later identified as involved in RNA packaging were found to interact; HnRNPA2B1 and HnRNPA1 with CD81, and YBX-1, SYNCRIP and HnRNPU with EWI-2 and ICAM-1. Recent work to assess the protein

interactome of an autophagy component, phospholipid-conjugated LC3, identified a striking similarity with the EV proteome, with 81% overlap and a heavy enrichment for RBPs (Leidal *et al*., 2020). Knockout of *ATG7* and *ATG12*, essential for LC3 conjugation, but not degradative autophagy, had significant impact on both EV protein and EV RNA content, although the effect on RNA was on small RNA (miRNA and snoRNA) only (Leidal *et al*., 2020). This led the authors to propose LC3-dependent extracellular vesicle loading and secretion (LDELS) as a mechanism for cargo loading, strengthening the regulatory linkage between EV biogenesis and lysosomal autophagy. Also noted in the study is the presence of a large number of RBPs which are known to be present in stress granules and P-bodies, therefore there may be a connection between these RNA granules and the EV-loaded RNA (Leidal and Debnath, 2020).

### Post-translational modification of RBPs

Proteins, including RBPs, may undergo a vast array of chemical post-translational modifications (PTMs), the most well-known of which include phosphorylation, glycosylation, methylation and ubiquitination, and is one possible mechanism by which their interaction with EV biogenesis components could be regulated (Carnino *et al*., 2020). Phosphorylation of YBX-1 was seen to be higher in HEK293 cell extract but not EVs, suggesting that dephosphorylation may be a mechanism by which the protein, and bound mRNAs, may be directed towards EVs (Kossinova *et al*., 2017). SUMOylation (small ubiquitin-like modification) of hnRNPA2B1 has also been shown to be specific to EV-localised protein, whilst anacardic acid inhibition of SUMOylation decreased miR-198 levels in the EV (Villarroya-Beltri *et al*., 2013). O-GlcNAc glycosylation of hnRNPA2B1 has also been found to alter EV miRNA content, a modification which is regulated by oxidative stress–induced phosphorylation of Caveolin-1 (Lee *et al*., 2019). Since many of these PTMs, such as phosphorylation, are rapidly reversible, they likely play a wider role in regulating RNA loading of EVs under different cellular conditions.

### 1.3.4 RNA-lipid interactions

An alternative determinant proposed for the loading of RNA into EVs is via direct interaction with lipid membranes during biogenesis (Janas *et al*., 2015). A key factor may be the differential lipid content, since binding of tRNASec to HeLa cell liposomes was increased by addition of sphingomyelin/cholesterol to the membrane (Janas *et al*., 2012). Given the enrichment of these lipids in raft regions in EVs, such interactions could drive specific loading *in vivo*. This group have also suggested that RNA-lipid raft binding, whilst weaker than in non-raft regions, was more structure dependent, and may be altered by hydrophobic modifications to the RNA (Janas *et al*., 2006, 2012). Most recently, the group selected for RNA aptamers that bound liposomes containing lipid-raft regions, interactions which were not seen in controls (Janas *et al*., 2020). Furthermore, comparison of the bound sequences identified a set of motifs; UUGU, UCCC, CUCC and CCCU, which were common to both the enriched aptamers and to a set of 4-nt motifs over-represented in EV-enriched pro-tumoral miRNAs. It is therefore possible that motifs in miRNA and mRNA of EVs, and any structured regions formed by these motifs, act directly to promote association with the MVB or plasma membrane, and subsequently increase loading into EVs.

### 1.3.5 RNA modification

A final potential mechanism for the control of EV RNA incorporation is specific modifications, or additions, to the RNA itself. Despite an overall underrepresentation of miRNA in EVs, one study found poly-uridylated miRNAs to be significantly enriched, and poly-adenylated miRNAs depleted, indicating that non-templated additions may be an important determinant of specific secretion (Koppers-Lalic *et al*., 2014). An RNA modification, although not identified, has also been proposed as a mechanism for specific incorporation of tRNA (Shurtleff *et al*., 2017). Increase in non-templated RNA base modification/addition has also been suggested as an explanation for the low mapping rate in EV RNA sequencing samples, raising the question of whether such modifications have a role in loading of other RNA biotypes (Hinger *et al*., 2018).

## 1.4 *DROSOPHILA* AS A MODEL SYSTEM FOR EV BIOLOGY

Although the predominant focus for EV research has been in mammalian systems, EVs can be produced by a diverse range of organisms including bacteria (reviewed in Kulp and Kuehn, 2010), fungi (Oliveira *et al*., 2010), protozoa (Bayer-Santos *et al*., 2013), invertebrates (Liégeois *et al*., 2006) and plants (Rutter and Innes, 2017). Much study of EVs has been carried out in cell culture systems, but understanding their physiological relevance relies on the use of *in vivo* systems. EV biogenesis, uptake and cargo transfer have been begun to be studied in murine models, and in a vertebrate model, the zebrafish (Ridder *et al*., 2014; Hoshino *et al*., 2015; Lai *et al.*, 2015; Morishita *et al.*, 2015; Zomer *et al.*, 2015; Hyenne *et al*., 2019). However, use of mouse models is highly specialised, time-consuming, and expensive. Historically, invertebrate models such as *Drosophila melanogaster and Caenorhabditis elegans* have provided a means through which to elucidate key aspects of basic biology that are conserved across evolutionarily diverse organisms, with 75% of humans disease-causing genes having a functional homolog in *Drosophila* (Bier, 2005). Indeed, these invertebrate models have already contributed to an understanding of the formation, release and function of EVs (reviewed Beer and Wehman, 2017).

As a well-established model organism, *Drosophila* provides many advantages, not least its well-characterised genome (Larkin *et al.*, 2021). The existence of a wide array of genetic tools for specific control of gene expression, such as the Gal4-UAS system, and the accessibility of distinct tissues such as the imaginal wing disc, also make it an ideal system for studies of intercellular communication (Brand and Perrimon, 1993; Beira and Paro, 2016). The availability of *Drosophila* cell lines such as S2R+ allows for initial *in vitro* studies to be made in a simple system that can be translated to an *in vivo* system that maintains the same genetics. In addition, *Drosophila* has frequently been used in the study of ageing and disease contexts relevant to oxidative stress,

such as neurodegeneration, whilst showing a high level of similarity to vertebrates in regulation of antioxidant response pathways (Loboda *et al.*, 2016).

Although extensive study has revealed many types of RNA that are associated with EVs in mammalian systems, the cargo content of non-mammalian EVs has been little studied. In the case of *Drosophila* this has focused primarily on the protein morphogens Wnt and Hedgehog, their regulation, and role in development (Gross *et al*., 2012; Gradilla *et al*., 2014; Matusek *et al*., 2014; González-Méndez *et al*., 2020). Some work has been carried out in *Drosophila* cell lines to characterise cargo more broadly, with proteomic analysis of Kc167 and S2 cells establishing similarity in contents to mammalian EVs (Koppen *et al*., 2011). Small RNA sequencing (Van den Brande *et al*., 2018), poly(A) mRNA sequencing (Ashley *et al*., 2018) and total RNA sequencing (Lefebvre *et al*., 2016) have also been carried out in a mixture of S2, S2R+, D17 and Cl8 cell lines. In the latter work by Lefebvre *et al.*, a direct comparison is made with human HepG2 and A431 lines, establishing further similarity in cargo content, and thus suitability as an appropriate model system.

## 1.5 PROJECT AIMS AND OBJECTIVES

Given the need for a transition towards *in vivo* models to aid in unravelling of the biological significance of this EV cargo, the mechanisms by which it is packaged, and how it is modulated in different cellular conditions, *Drosophila* makes for a powerful model system. This thesis work was therefore carried out in a *Drosophila* cell line, alongside the work of Claire Hill in *Drosophila* larvae, working in tandem to establish a system in which novel mechanisms of biogenesis, cargo loading, and functional transfer can be more easily identified and validated in complex tissues. The aims of this thesis were therefore to a) investigate the effect of oxidative stress on EV properties and function and b) to investigate how RNA cargo is packaged into EVs. The specific objectives were to:

1. Establish a *Drosophila* cell culture model to investigate EV-biology.
2. Analyse how oxidative stress affects EV properties in cell culture conditions.
3. Test the functional effects of oxidative stress-cell derived EVs on recipient cells.
4. Characterise RNA of normal and stress EVs and parental cells by RNA sequencing.
5. Identify candidate RNAs in EVs which may mediate stress responses in recipient cells.
6. Identify potential sequence motifs that promote mRNA loading into EVs.
7. Explore alternative mechanisms of RNA loading, and alterations under oxidative stress.

# Chapter 2

## Materials and Methods

# 2 Materials and methods

## 2.1 CELL CULTURE

### 2.1.1 Cell line maintenance

The *Drosophila* S2 cell line is an immortalised cell line isolate of type-I haemocyte lineage, of which the S2R+ line is a semi-adherent derivative. Predominantly S2R+ cells were used in this work, with some experiments also tested in S2 cells. Both cell types were maintained in Schneider's medium (Thermofisher, 21720024) supplemented with 100 IU/ml penicillin, 100 µg/ml streptomycin (Fisher, 15140-122) and 10% (v/v) heat-inactivated foetal bovine serum (FBS) (Fisher, 10500064) in T75 flasks at 25°C and ambient $CO_2$. Cells were passaged twice a week, first removing media, washing with 3ml fresh media, and detaching in 6-10ml media by vigorous pipetting or using a cell scraper if required. Cells were seeded into new flasks at either 1:3-1:5 dilution.

On occasions MCF7 or MCF7-CD81-emGFP stably transfected cells (latter produced by Dr Paschalia Pantazi) were used for testing of methods. MCF7 cells were maintained in DMEM F-12 (Sigma, D8062) supplemented with 10% (v/v) heat-inactivated FBS (Fisher, 10500064) at 37°C and 5% $CO_2$ in a humidified environment. Cells were passaged at ~80% confluence, washing twice in PBS, then incubating with 3ml trypsin-EDTA solution. Once detached, 9 ml whole cell media was added to cell solution and cells pelleted by centrifuging at 300g for 5 minutes. Cell were then resuspended in fresh media and seeded as required.

### 2.1.2 Cell seeding for experiments

For experiments, cells were seeded at set densities, with cell counts carried out either manually using a haemocytometer, or using an automated cell counter, both 1:2 cell suspension with trypan blue (Biorad 1450021). During EV isolation experiments S2R+ cells were first seeded in normal media at either $1.5x10^7$ or $1x10^7$ cells in T75 flasks, then after one or two days

respectively, switched to media with 10% (v/v) FBS pre-depleted of bovine EVs, for 48 hours of conditioning. EV-depletion of FBS was carried out by ultracentrifugation in open-topped tubes (Beckman Coulter, 344058) in a SW32Ti swing–bucket rotor (Beckman Coulter κ-factor 204) at 120,000g for 16 h at 4°C. Supernatant was removed and filter sterilised with a 0.22µm filter and aliquoted for storage at -20˚C. For testing of alternatives to FBS, cells were supplemented with Insulin-Transferrin-Selenium (Thermo Fisher Scientific, 41400045), diluted to 5µg/µl in PBS, in combination with EV-depleted FBS or bovine serum albumin (BSA) (Sigma, A7906).

### 2.1.3 Purification of EVs

EVs were enriched from conditioned media using size-exclusion chromatography (SEC). Columns (Biorad, 7321010) were filled with 14ml Sepharose CL-2B (Fisher, 10217754), topped up with phosphate buffered saline containing $MgCl_2$ (0.1 $gL^{-1}$) and $CaCl_2$ (0.133 $gL^{-1}$) (PBS) (Sigma, D86626), and left to settle for at least three hours to give a 10ml column bed. After placing column bed support above resin, column was washed three times in PBS. Conditioned media was cleared of cells (10 minutes at 300g), then cell debris and large vesicles (16,500g for 20 minutes at 4°C) before filtering through 0.22µm filters pre-blocked with 0.01% BSA (Sigma, A7906). Conditioned media was then reduced to a volume of 0.5ml in a 100kDa MWCO vivaspin concentrator (Fisher, 10774797) by centrifuging at 3000g in a swing bucket rotor. Samples were loaded onto the columns and eluted in sterile PBS, with 20 0.5ml fractions collected for initial validation experiments. For later experiments, 2.5ml volume (fraction 1-5) was voided and 2.5ml (fractions 6-10) EV fractions collected together. Where required, columns were reused for multiple runs of the same sample, washing three times in 10ml PBS between uses.

### 2.1.4 Induction of oxidative stress

Stress treatments were carried out one day after seeding. Hydrogen peroxide ($H_2O_2$) (Sigma, 216763), menadione sodium bisulphite (Sigma, M5750) or tert-butyl hydroperoxide (tBHP) (Sigma, 458139) were serially diluted in media containing 10% pre-depleted FBS and placed onto

cells for one hour, before changing to fresh media (containing 10% EV-depleted FBS) and incubating for 48 hours prior to EV extraction.

### 2.1.5 EV treatment of cells

All EVs were isolated from S2R+ donor cells treated with $H_2O_2$ (0mM, 0.5mM or 2mM) and counted by Nanoparticle Tracking Analysis to allow dilution to final doses of $6.4x10^4$, $3.2x10^4$,$1.6x10^4$, or $8x10^3$ particles per seeded cell, in pre-depleted media. No EV control contained a volume of PBS equal to the largest required for these EV doses.

### 2.1.6 Transfection

Transfection was carried out using effectene non-liposomal lipid reagent (Qiagen, 301425), approximately eight hours after seeding. 1900ng DNA was diluted in RNase-free water, to which 150ul EC buffer and 15.2ul enhancer were added, then each tube vortexed for 30 seconds and incubated at room temperature for 5 minutes. Following incubation, 19µl effectene was added to each tube, vortexed for 30 seconds and incubated for 10 minutes at room temperature. DNA complexes were added dropwise to 3ml serum-free media and then added onto cells. Plates were shaken gently before overnight incubation, in preparation for change to EV-depleted media the following day.

## 2.2 EV CHARACTERISATION

### 2.2.1 Nanoparticle Tracking Analysis

Quantification and sizing of EVs was carried out by Nanoparticle Tracking Analysis (NTA), a method which allows detection of nanoparticles in suspension, based on Brownian motion. Laser light scatter is used to track individual particles, within the known cell volume, to determine particle concentration. Application of the Stokes-Einstein equation allows size determination of each particle. NTA here was initially carried out using NanoSight NS500 (NanoSight, Malvern Instruments), facilitated by Dr Rebecca Dragovic at the Nuffield

Department of Obstetrics & Gynaecology, University of Oxford. The machine was calibrated with polystyrene beads, then loaded, using a syringe pump at speed 15AU, with EV samples diluted 1:4 to 1:10 such that the concentration was within the recommended range ($1\times10^8$ - $8\times10^8$ particles/ml). Data was acquired at 25°C with sCMOS camera with settings as follows. Viscosity: 0.89cP, camera level: 13, Slider Shutter: 1232, Slider Gain: 219, Shutter: 30.8ms, Camera Histogram Upper Limit: 8235, Camera Histogram Lower Limit: 0 Frame rate: 25fps, Max Jump Mode: auto, Blur: Auto, Min Track Length: Auto. For each measurement, 3-5 one-minute videos were captured and analysed by NanoSight Software NTA 3.2 Build 3.2.16, with a detection threshold of 5.

The majority of NTA was carried out using ZetaView 110 (Particle Metrix, GmbH). The machine was first calibrated with 100nm polystyrene beads (Applied Microspheres) at a concentration of 1:25,000, and visually checked for cleanliness before loading samples. Samples were diluted to between 1:1000 and 1:250,000 in PBS such that the average number of counted particles per frame for all conditioned media was between 100 and 500. Where triplicate measurements are indicated, independent dilutions of sample were carried out. PBS washes were performed between each measurement. Data was acquired at room temperature with settings: sensitivity 80, shutter 100, frame rate 30, 2 cycle, minimum brightness 25, maximum size 1000, minimum size 5, tracelength 15, at all 11 positions and analysed using ZetaView software version 8.04.12.

### 2.2.2 Transmission electron microscopy

10µl EV samples of ~$2x10^{10}$ – $3x10^{11}$ particles (as measured by zetaview NTA) were pipetted onto carbon 300 mesh copper grids (TAAB, C267), previously glow discharged for 20s at 15mA, and incubated for 2 minutes. Grids were then dabbed against filter paper and placed onto a 20ul drop of 2% uranyl acetate for 10 seconds, then left to airdry before storage. Grids were visualised using a Hitachi H7650 Transmission Electron Microscope at 100 kV, or Jeol JEM-1400 Flash transmission electron microscope with Gatan OneView 16 Megapixel camera at 100kV.

### 2.2.3 Protein extraction

For cellular protein extraction, the cells were washed in PBS, pelleted and snap frozen at -80°C. EV samples were concentrated to 40-200ul in 5kDa MWCO vivaspin 2 concentrators (Fisher 10723837). Lysis was carried out with ice-cold RIPA buffer (Sigma 20-188) supplemented with 1:100 protease inhibitor cocktail III (Fisher P2202-1), 1x for cell pellets and 2x for EV samples. Samples were incubated on ice for 40 minutes, vortexing every 10 minutes. Lysates were then centrifuged at 14,000g for 15 minutes at 4°C. Protein content of the supernatant was quantified using Pierce BCA Protein Assay Kit (Thermofisher, 23225) according to the manufacturer's protocol, but modified to use minimal sample volume, loading 5ul of samples and standards and 45ul of working reagent. Absorbance was measured on a platereader (Molecular Devices, Spectramax i3x) using Softmax Pro 7 software at 562nm.

### 2.2.4 Western blotting

Western blots were run using the Invitrogen NuPAGE system. 6-40ug total protein sample was prepared in LDS sample buffer (Thermofisher NP0007), with or without 0.4mM dithiothreitol (DTT) (Sigma 10708984001), then boiled at 95°C for 5 minutes. 20µl samples and 5µl ladder (Biorad, 1610374) were run on precast 4-12% polyacrylamide Bis-Tris gels (Thermofisher, NP0322) in MES SDS buffer (Thermofisher, NP0002) for 90 minutes at 125V. Protein was wet-transferred onto nitrocellulose membrane in NuPAGE transfer buffer with 15% methanol (Thermofisher, NP0006) for 2 hours at 150V at 4°C. After confirming protein transfer with ponceau staining (Sigma P7170), membranes were cut as required and blocked in 5% milk in 0.1%-PBS-Tween for one hour. Membranes were incubated with primary antibodies (Table 2.1) overnight at 4°C, then washed four times in 0.1% PBS-Tween, before incubating in secondary antibodies (Table 2.2) for 1 hour. After four PBS-Tween washes, membranes were incubated with ECL (Millipore Sigma, GERPN2232) for 5 minutes and imaged using ChemiDoc MP (BioRad) for up to 5 minutes as required.

| Antibody | Target species | Species raised in | Source | Dilution | DTT |
|---|---|---|---|---|---|
| Anti-TSG101 | Human/*Drosophila*/ Bovine | Mouse | Abcam ab83 | 1:500 | NO |
| Anti-CD9 | Human | Rabbit | Cambridge Biosciences EXOAB-CD9A-1 | 1:1000 | NO |
| Anti-CD63 | Human | Mouse | Novus Biologicals NBP2-42225 | 1:1000 | NO |
| Anti-CD81 | Human | Mouse | Abcam ab79559 | 1:1000 | NO |
| Anti-Alix | Human | Mouse | Abcam ab117600 | 1:2500 | NO |
| Anti-GM130 | Human/*Drosophila* | Rabbit | Abcam ab52649 | 1:1000 | YES |
| Anti-cytochrome C | Human/*Drosophila* | Rabbit | Abcam 79559 | 1:1000 | YES |
| Anti-actin | Human/*Drosophila* | Mouse | Proteintech 66009-1-Ig | 1:5000 | YES |
| Anti-HSP70 | Human/*Drosophila* | Mouse | Abcam ab5439 | 1:1000 | NO |
| Anti-Alix | *Drosophila* | Guinea pig | Gift from Kaisa Haglund | 1:1000 | NO |
| Anti-TSG101 | Human/*Drosophila* | Rabbit | Abcam ab30871 | 1:1000 | NO |
| Anti-Lbm | *Drosophila* | Mouse | DSHB 10C9 | 1:500 | NO |
| Anti-Histone H3 | Human/*Drosophila* | Rabbit | Cell signalling 4499 | 1:1000 | NO |
| Anti-Golgin84 | *Drosophila* | Mouse | DSHB 12-1 | 1:500 | NO |

Table 2.1: Primary antibodies used in Western blotting

| Antibody | Species raised in | Source | Dilution |
|---|---|---|---|
| Anti-mouse | Goat | Promega W4021 | 1:20,000 |
| Anti-rabbit | Goat | Promega W4011 | 1:5000 |
| Anti-guinea pig | Goat | Thermofisher A18769 | 1:5000 |

Table 2.2: Secondary antibodies used in Western blotting

### 2.2.5 Proteinase treatment of EVs

EV samples were treated with Proteinase K (VWR, E195), diluted in PBS with $MgCl_2$ (0.1 $gL^{-1}$) and $CaCl_2$ (0.133 $gL^{-1}$) (Sigma, D86626), at a final concentration of 50µg/ml. Samples were heated to 37°C for 30 minutes, then inhibited by heating the sample to 90°C for 10 minutes.

## 2.3 CELL FUNCTIONAL ASSAYS

### 2.3.1 MTT Assay

For initial cell viability assays, 3(4,5–dimethylthiazol–2–yl)–2,5 diphenyl tetrazolium bromide (MTT) (Sigma, M5655) was made up at 2mg/ml in PBS and filtered through a 0.22µm filter. 100µl solution was added directly to growing cells to give working concentration of 1mg/ml and incubated for either one or two hours. Media was pipetted out and replaced with 100µl MTT solvent (4mM HCl, 0.1% IGEPAL CA-630, all in isopropanol) to dissolve formazan salt. Plate was shaken on low setting for 20 seconds before reading absorbance on a platereader (Molecular Devices, Spectramax i3x) using Softmax Pro 7 software at 595nm.

### 2.3.2 Resazurin viability assay

A resazurin reduction assay was used to test the effect of treatments on cell viability. Cells were seeded in clear bottomed 96-well plates, with at least 5 technical replicates per condition. After stress or EV treatments, 0.15mg/ml resazurin dye, filter sterilised with a 0.22µm filter (Sigma R7017), was added directly to culture media at 10% volume and incubated for 1.5 hours before reading on a fluorescence platereader (Molecular Devices, Spectramax i3x) using Softmax Pro 7 software (bottom read, 5 point well scan with 560nm excitation / 590nm emission).

### 2.3.3 Annexin V and Propidium iodide Flow cytometry

Viability of cells was analysed using Annexin V-FITC and Propidium Iodide Apoptosis Detection Kit (eBioscience™ Thermofisher, BMS500FI-100CE). Cells in 24-well plates were detached in PBS using cell scrapers, then processed according to the manufacturer's protocol. Flow cytometry was carried out on Cytoflex S flow cytometer (Beckman Coulter) and analysed using CytExpert software. All events were analysed.

### 2.3.4 yH2Av immunocytochemistry

Cells were seeded onto 13mm sterile coverslips in 24-well plates. Immediately after stress treatment, cells were fixed for 20 minutes in 4% paraformaldehyde and washed three times in PBS before storing at 4°C. For EV treatment, cells were treated with $1.6x10^4$ EVs/ seeded cell and incubated for 3 hours before fixing. Cells were briefly permeabilised in 2% Tween-20 and blocked in 1% BSA, 0.2% Tween-20 for 30 minutes before overnight incubation at 4°C with yH2Av primary antibody (Histone H2A.vS137phos, Genetex, GTX48733) at 2µg/ml made up in blocking buffer. Cells were washed three times in PBS then incubated with secondary goat anti-Rabbit IgG (H+L) Alexa Fluor 568 (Thermofisher, A11036) at 2µg/ml for 1 hour at room temperature. Cells were stained with Hoechst 33342 for 10 minutes and washed three times in PBS, before mounting on slides in Fluoromount (SLS, F4680). Slides were imaged on ZEISS Axio Imager 2 with 40x objective, with 10 images taken per coverslip, 3 biological replicates per condition, and 3 technical replicates per biological replicate. Images were analysed using FIJI software, segmenting cells in Hoechst channel using IsoData method and watershed function, then calculating corrected total cell fluorescence (CTCF) by:

CTCF = Integrated Density – (Cell area x Mean fluorescence of background)

### 2.3.5 Mitotracker orange staining

Cells were seeded onto 13mm sterile coverslips in 24-well plates. The following day cells were treated with $1.6x10^4$ EVs/ seeded cell and incubated for 24 hours. Cells were then stained with mitotracker orange (Thermofisher, M7510) at 50-200nM and Hoechst 33342 (Sigma B2261) at 1:2000 for 30 minutes, then washed twice in media before fixing for 20 minutes in 4% PFA. After washing 3 times in PBS, coverslips were mounted on slides in Fluoromount. Slides were then imaged on ZEISS 800 confocal microscope with 100x objective, taking z-stacks. Images were analysed using FIJI software, manually defining the cell area regions of interesting, then quantifying total fluorescence in the mitotracker channel to calculate CTCF as in section 2.3.4.

### 2.3.6 CellROX staining

Induction of ROS was tested using CellROX Deep Red Reagent (Fisher, 15744212). MCF-7 mammalian breast cancer cells or *Drosophila* S2R+ cells were stressed with $H_2O_2$ or tBHP for one hour, with controls pre-treated with 1mg/ml N-acetylcysteine antioxidant (NAC) (Sigma, A7250) for two hours. 5µM CellROX was added to cells for 30 minutes, and Hoechst 33342 (Sigma B2261) for 10 minutes, before live cell imaging on ZEISS 880 confocal microscope, or fixation and imaging on ZEISS 800 confocal as in section 2.3.5.

## 2.4 RNA WORK

### 2.4.1 RNA extraction and quantification

For RNA extraction, 2.5ml EV preparations from SEC were further concentrated to 100ul using 5kDa MWCO vivaspin concentrators (Fisher, 10723837). Total RNA was isolated using Qiagen miRNeasy kit according to the manufacturer's protocol with some modifications. Quizol was added to 100µl concentrated EV sample and parental cell pellets (snap-frozen at -80°C) (700µl for EV samples, and 700µl per $7x10^7$ cells). 70µl 1-bromo-3-chloropropane per 700µl Qiazol was added and processed with on-column DNase I treatment (Qiagen, 79254) using buffers prepared with isopropanol in place of ethanol. One additional centrifugation step was included (5 minutes at 16,000 × g) to ensure complete removal of the washing buffer. RNA samples were eluted in 30µl of RNAse-free water. Absorbance distributions were immediately quantified using a NanoDrop 2000c spectrophotometer for cellular and EV RNA, and Qubit RNA HS kit (Thermofisher Q32852) for EV RNA. Aliquots were submitted to capillary electrophoresis on a Bioanalyser 2100 machine (Agilent) using RNA Nano chip, according to the manufacturer's instructions. Sequenced samples were analysed by Bioanalyser with Nano chip for cell samples and Pico chip for EV samples by Liverpool Centre for Genomic Research.

### 2.4.2 RNAse protection assay

EV samples were concentrated to ~60ul in 5kDa MWCO vivaspin concentrators (Fisher, 10723837) immediately after extraction. After overnight storage at 4°C, samples were split into three aliquots of 15µl. 15µl of 2% Triton X-100 detergent (Sigma X100, diluted in PBS) or PBS was added to relevant tubes, vortexed briefly and incubated on ice for 30 minutes. 2µl RNase A (Fisher Scientific, 10546881) was added to relevant tubes and incubated for 20 minutes at 37°C (final concentration 0.31µg/µl), before adding 300µl of Qiazol and continuing with RNA extraction as described in section 2.4.1.

### 2.4.3 cDNA synthesis

cDNA synthesis was carried out on 15-40ng of RNA. RNA was diluted in RNase-free water to a total volume of 8µl in PCR strip tubes, then DNase-treated (Sigma, AMPD1-1KT) according to the manufacturer's instructions. Tubes were incubated for 15 minutes at room temperature before addition of 1µl stop solution and incubation for 10 minutes at 70$^{o}$C to denature DNAse and RNA. After incubation on ice, cDNA synthesis was carried out with Maxima First Strand cDNA Synthesis Kit for RT-qPCR (Thermo Scientific, K1641). Reagents were added directly to the treated RNA as described by the manufacturer. Samples were placed in a thermal cycler and incubated for 10 minutes at 25$^{o}$C, 30 minutes at 65$^{o}$C, and 5 minutes at 85$^{o}$C before placing on ice.

### 2.4.4 qPCR and primers

Real-time quantitative PCR was carried out using iTaq Universal SYBR Green Supermix (Bio-Rad, 1725121). Stock solutions of each primer pair (Table 2.3) were prepared at 500nM; then master mixes prepared for 1.1 times the necessary number of reactions for each primer set, containing 105µl SYBR Green, 6.5µl nuclease-free water and 1.55µl primer mix per reaction. 20µl reactions were run in duplicate where sample quantities permitted, with 18µl master mix and 2µl cDNA per well. Samples were incubated for 30 sec at 95$^{o}$C, before 40 cycles of 5 sec at 95$^{o}$C and 30 sec at 60$^{o}$C, followed by a melt curve from 65-95$^{o}$C, in a CFX96 Touch thermal-cycler (Bio-Rad).

| Gene | Forward | Reverse | Source |
|---|---|---|---|
| *Rpl32* | AAGCGGCGACGCACTCTGTT | GCCCAGCATACAGGCCCAAG | (Ling and Salvaterra, 2011) |
| *Arc1* | TAGAAGGTATCAGCGACGAG | GCCATACCGTAGAACAGCA | (Lefebvre et al., 2016) |
| *Cre* | CGGTCTGGCAGTAAAAACTAT | CAGGGTGTTATAAGCAATCCC | (Sanchez-Fernandez et al., 2012) |
| *Uba1* | GCCGAGTTAAACAACTATGTGCG | GGCAAACTTGGCGATCCTCT | Flyprimer bank (Hu et al., 2013) |
| *Akap200* | AAGTGGTCCTTCCGAAGCATT | TTGTAGCCACCGATGGTTCTG | Flyprimer bank (Hu et al., 2013) |

Table 2.3: qPCR primer sequences

For measurement of gene expression changes the ΔΔCq method was used, with Ribosomal protein L32 (*Rpl32*) used as a housekeeping gene. For RNase protection experiments, a dilution curve was carried out, and each sample expressed relative to no RNAse, no Triton sample.

### 2.4.5 RNA library preparation and sequencing

Library preparation, RNA sequencing and initial processing was carried out by Liverpool sequencing facility. Biological triplicates of dual-indexed, strand-specific sequencing libraries were prepared from DNase-treated RNA extracted from EV and parental cells from control, 0.5mM and 2mM $H_2O_2$ treatment conditions using NEBNext Ultra Directional RNA kit. 150bp paired end sequencing was carried out on an Illumina HiSeq 4000 machine. Raw Fastq files were trimmed for the presence of Illumina adapter sequences using Cutadapt version 1.2.1, using the option -O 3 to remove the 3' end of any reads which match the adapter sequence for 3 bp or more. Reads were further trimmed using Sickle version 1.200 with a minimum window quality score of 20 to remove reads shorter than 20 bp after trimming.

## 2.5 RNA SEQUENCING ANALYSIS

### 2.5.1 Initial RNA sequencing data analysis

The majority of RNA sequencing analysis was carried out using the public sever of the Galaxy Project (usegalaxy.org), a user-friendly interface for a variety of bioinformatics analyses (Afgan

*et al*., 2016). Sequencing quality control was carried out using FastQC (Galaxy Version 0.72) (Andrews, n.d.) and summarised with multiQC. For continuity with parallel analyses carried out by Claire Hill, the work on the *Drosophila* genome-mapped portion of the RNA was carried out on alignments generated by Jana Terenova. For this alignment, ribosomal RNA reads were first filtered out by mapping to a FASTA file of rRNA sequences using BBtools (v.38.42)((Bushnell). The FASTA file was generated from Ensembl via biomart, including all unspliced gene sequences annotated as rRNA in the BDGP6 genome of Ensembl Genes 95 (Yates *et al*., 2020). Read alignments were performed with RNA STAR (v.2.5.3a) (Dobin *et al*., 2013) on the *Drosophila melanogaster* r6.26_FB2019_01 genome downloaded from Flybase (Larkin *et al*., 2021). The index was first generated with genome file dmel-all-chromosomes-r6.26.fasta and GTF file dmel-all-r6.26.gtf, with length of genomic sequence around annotated junctions (sjdbOverhang) set to 149. Additional settings used were: maximum number of mismatches, plus 1 (outFilterMismatchNmax) at 1, Minimum alignment score normalized to read length (outFilterScoreMinOverLread) and Minimum number of matched bases, normalized to read length (outFilterMatchNminOverLread) at 0.3, and with output set to a BAM file sorted by co-ordinate. Aligned bam files were visualised using Integrative Genome Viewer (IGV) (Thorvaldsdottir *et al*., 2013). Read counting of the sorted BAM file was carried out with HTSeq-count (v0.9.1) (Anders *et al*., 2015), with mode set to union, strandedness to reverse, minimum alignment set to 10 and feature type set to exon.

### 2.5.2 RNA Abundance estimates

Fragment per kilobase of transcript per Million mapped reads (FPKM) values were generated using Cufflinks (v.2.2.1) (Trapnell *et al*., 2010) with library-type as fr-first strand. Of note, these values were generated via command-line in a Linux environment, as minor discrepancies with values generated via cufflinks on the Galaxy server could not be accounted for. In the case of ribosomal RNA, FPKM values were calculated manually as:

(Read count x $1x10^6$)/ (Σ Readcounts x Gene length).

The biotypes of mapped genes were determined using the vlookup table function in Microsoft Excel. The dictionary was generated from Ensembl via biomart from the BDGP6 genome of Ensembl Genes 95 (Yates *et al*., 2020). All gene identifiers in the Cufflinks file were input and 'Transcript type' identifiers output. Any unlabelled genes were then checked on Flybase (Larkin *et al*., 2021) and additional identifiers input manually.

### 2.5.3 Differential expression analysis

Differential expression of HTSeq-count files was determined using DESEQ2 (v.2.11.40.2) via Galaxy server (Love *et al*., 2014). A standard adjusted p-value of 0.05 was used as a cut-off for statistical significance unless otherwise stated. Principal component analysis (PCA) was carried out using normalised readcounts output from this tool. PCA at RNA biotype level, as defined in section 2.5.2, was carried out by Claire Hill using the Scikit-learn Python package (v.0.23.1). StandardScaler was used to standardise the data so that all datasets had a mean of 0 and a variance of 1.

### 2.5.4 Gene ontology analysis

Gene ontology analysis was carried out using g:profiler (Raudvere *et al*., 2019) as this tool could successfully identify all gene identifiers in lists. A custom background was defined by inputting all gene identifiers listed in the Cufflinks gene abundance file, with statistical scope set to annotated genes only. Unless otherwise stated, a significance cut-off of 0.001 with Benjamini-Hochberg False Discovery Rate was applied.

### 2.5.5 Evolutionary conservation of differential expression

Evolutionary conservation of stress-induced changes to EV content was tested using an existing microarray dataset of mouse MC/9 mast cells and EVs (Eldh *et al*., 2010). Data were accessed via NCBI Gene Expression Omnibus (GEO) under accession number: GSE24886. Analysis was

carried out using GEO2R tool linked to GEO (Barrett *et al*., 2013). Orthologs for all probes with $p<0.05$ and $Log_2(FC)$ of at least 1 were identified using DRSC Integrative Ortholog Prediction Tool (DIOPT) (Hu *et al*., 2011).

### 2.5.6 Identification of unmapped reads

RNA sequencing data were subsequently reanalysed in order to more comprehensively identify all read, iteratively aligning to different FASTA files using the Galaxy server (Afgan *et al*., 2016). Ribosomal reads were first mapped using Bowtie2 (v2.3.4.3) (Langmead and Salzberg, 2012) using default (sensitive end-to-end) settings and outputting unaligned and aligned reads separately. The rRNA FASTA file was generated from Flybase (Larkin *et al*., 2021), downloading entire gene sequences for all genes annotated as rRNA. Unaligned reads were sequentially mapped to transposon sequences downloaded from Flybase (dmel-all-transposon-r6.26.fasta.gz) and repeat masked sequences from UCSC Table Browser (Karolchik *et al*., 2004) with settings Clade: Insect, Genome: *D.melanogaster*, Assembly: Aug.2014 BDGP Release 6 + ISO1 MT/dm6, group: Variations and Repeats, Track: RepeatMasker, Table:rmsk, Region: Genome, Output format: Sequence. Subsequently, unaligned reads were mapped to the *Drosophila melanogaster* r6.26_FB2019_01 genome downloaded from Flybase using HISAT2 with stranded set to reverse, both aligned and unaligned reads written to separate files and otherwise default settings (Kim *et al*., 2015). Using bowtie, unaligned reads were then mapped to a built-in bovine genome (Bos.taurus_UMD_3.1.1/bosTau8) on the Galaxy server. Remaining reads were BLAST searched, which indicated reads mapped to viral species, so data was subjected to Kraken analysis via Galaxy server (v.1.3.1) (Wood and Salzberg, 2014). This identified *Drosophila melanogaster totivirus* and *alphanodavirus* species (highly related species such as *Flock house virus*, *Boolarra virus* and *Black beetle virus*) to account for large numbers of reads. The remaining unaligned reads were further sequentially mapped to these viral sequences (*totivirus* sequence NC_013499.1 and all *alphanodavirus* sequences taxid:143920)

downloaded from NCBI Virus (Brister *et al*., 2015), using Bowtie2 in end-to-end mode. Lower quality matches to *alphanodavirus,* rRNA, *Drosophila* genome and *totivirus* sequences were additionally identified by mapping with Bowtie2 in sensitive local mode. Reads aligned to the transposon sequences were then remapped to a fasta file of just sequences containing '*Copia*' within the sequence name in the dmel-all-transposon-r6.26.fasta.gz file from Flybase. Additional S2R+ EV RNA sequencing datasets from Lefebvre *et al*. (2016) were downloaded from the European Nucleotide Archive (EMBL-EBI) for direct comparison, using accession numbers SRX1492035 and SRX1492036.

### 2.5.7 Ribosomal RNA analysis

Reads aligning to the rRNA sequences (section 2.5.6) were further aligned to the *Drosophila* genome with STAR aligner (Dobin *et al*., 2013) with largely default settings, with the exception of outFilterMultimapNmax, which was set to 1000. Aligned bam files were visualised using Integrative Genome Viewer (IGV_2.7.2) (Thorvaldsdottir *et al*., 2013). Read counting was carried out with Feature counts (Liao *et al*., 2014), with a filtered gtf file containing only rRNA annotations, with the exclusion of pre-rRNA, with strandedness set to reverse, and reads not permitted to contribute to multiple features.

## 2.6 mRNA LOADING ANALYSIS

### 2.6.1 Junction saturation

Junction saturation determines whether read depth is sufficient for splice variant level differential expression analysis. This was determined via the Galaxy server using the RSeQC tool junction_satration.py 2.6.4 (Wang *et al*., 2012) with default settings: Minimum intron length 50, minimum number of supporting reads to call a junction 1, minimum mapping quality 30. The reference gene model in bed.12 format was generated from the *Drosophila melanogaster* r6.26_FB2019_01 genome gtf file downloaded from Flybase (Larkin *et al*., 2021). Annotations

for miRNAs and the trans-spliced gene mdg4 were removed (as these caused programme failure), then USC tools gtftoGenePred and GenePredtoBed were used to produce a bed.12 file.

### 2.6.2 mRNA length and exon count

In order to determine the number of exons per gene, all individual exons were downloaded from Ensembl via biomart from the BDGP6 genome of Ensembl Genes 95 (Yates *et al*., 2020). All gene identifiers in the Cufflinks file were input and 'Transcript stable ID', 'Exon stable ID', and 'gene length' identifiers output. The number of exons per gene was calculated using the countif function in Microsoft Excel, then normalised to gene length value to give number of exons per 1000nt. For transcript lengths the same inputs were used, but with 'Transcript length (including UTRs and CDS)' as output.

### 2.6.3 Read type distribution

Read type distribution (Coding exons, 3'UTR, 5'UTR or intron) of aligned bam files was determined using the RSeQC tool read_distribution.py 2.6.4.1 via Galaxy server (Wang *et al*., 2012), using reference gene model in bed.12 format (see section 2.6.1). Percentages for read types were calculated as tags/total tags.

### 2.6.4 Gene body coverage and base mismatch

Gene body coverage was determined using the RSeQC tool geneBody_coverage.py 2.6.4.3 via Galaxy server (Wang *et al*., 2012) with default settings: minimum mRNA length 100. A bed.12 file of mRNAs only was used as the reference gene model (see section 2.6.1). Quantification of coverage bias was determined using Picard tool CollectRNASeqMetrics (Picard Tools - By Broad Institute) which calculates the mean coverage of the 100 most 3' or 5' bases divided by the mean coverage of the whole transcript. Relative 5'/3' bias gives an indication of whether degradation has occurred. Base mismatch rate was determined using the Picard AlignmentSummaryMetrics tool on bam alignment files (Picard Tools - By Broad Institute).

## 2.7 MOTIFS

### 2.7.1 Defining EV and cell RNA groupings

To search for motifs enriched in EV samples, a shortlist of genes was first produced. zFPKM transformation was performed on mean FPKM values for each of the 6 sample type (EV and cell under each of the three stress conditions) with R studio (v.3.5.1), to separate biologically meaningful expression values (Hart *et al*., 2013). A cut-off of -3 was used to define active genes. These active genes were filtered by read counts (section 2.5.1) at either a low stringency threshold; minimum one read count in at least one of three replicates in EV samples, and minimum five read counts in at least one of three replicates in cell samples, or high stringency threshold, where all three replicates had to reach these cut-off values. For each stress condition, active genes were split into three groups, those found 'only in cell', those found 'only in EV', and those found in both 'cell and EV'. For genes in the 'cell and EV' group, all showing significant differential expression (see section 2.5.3) with log2 fold-change of 2 or higher were defined as 'enriched in EV' and combined with 'only in EV' to form an 'EV only plus EV enriched' group.

### 2.7.2 Motif searching

Motif searching was carried out using the MEME Suite tool "Multiple EM for Motif Elicitation" (MEME) (Bailey and Elkan, 1994; Bailey *et al*., 2009). Either full cDNA sequences or 3'UTR sequences for all transcript variants of genes defined as 'Cell only' or 'EV only plus EV enriched' (section 2.7.1) were downloaded from ensembl via biomart (Yates *et al*., 2020), and filtered to include only sequences longer than 30nt, using a custom python script written by Claire Hill. MEME was then used to detect motifs enriched in the 'EV only plus EV enriched' group with settings -dna, objective function: differential enrichment, model: zero or one occurrence per sequence, number of motifs to found:30, max width of motifs:25, and background set to the 'Cell only' group. This process was repeated with additional groupings as described in relevant chapter e.g. stress EVs vs control EVs with all other settings remaining the same.

### 2.7.3 Motif abundance

Each set of thirty identified motifs from MEME were then scanned for their presence in the full-length 3'UTRs (or CDS or 5'UTR in some cases) of all mRNA transcripts in a single file, using MEME Suite Tool "Find Individual Motif Occurrences" (FIMO) (Grant *et al*., 2011). The search was carried out using a zero-order background model i.e. normalised by nucleotide frequencies, with output of all hits with p-value less than $1x10^{-4}$. The fimo.tsv output file was then filtered to include hits only on the positive sense strand and with q-value less than 0.05. This file was used as dictionary for lookup of motif hits for all genes within 'EV only plus EV enriched' or 'Cell only' groups under each stress condition in Microsoft Excel.

### 2.7.4 Motif comparison

Motifs were compared to each other, and those from the literature, using MEME Suite Tool TOMTOM (Gupta *et al*., 2007). Comparison was carried out using Euclidian distance as the motif column comparison function, with q-value cut-off at 0.2 and complete scoring activated, and reverse complements of target motifs not scored.

### 2.7.5 RNA binding proteins

A database of 68 known motifs across 51 unique *Drosophila* RNA binding proteins (Ray *et al*., 2013), available within the MEME Suite programme,, were used in combination with FIMO or TOMTOM to identify occurrences of motifs, or compare to MEME outputs.

### 2.7.6 Motif testing

Motif constructs encoding for the Cre recombinase sequence, appended to a 25nt zipcode sequence (Bolukbasi et al., 2012), the 3'UTR of wild-type *Drosophila paralytic (para)* and shuffled 3'UTR of *para* were designed and produced by Claire Hill.

## 2.8 STATISTICAL ANALYSIS

Statistical analysis was carried out using GraphPad Prism (version 6), using parametric or non-parametric tests as appropriate, stated within each figure. P-values in figures are shown as p <0.05 *, p<0.01 **, p<0.001 *** and p<0.0001 ****. Correlation coefficients were also calculated with GraphPad Prism, generating two-tailed mon-parametric Spearman correlation matrices for Log transformed FPKM values.

# Chapter 3

## Characterisation of purified EVs

# 3 Characterisation of purified EVs

## 3.1 BACKGROUND

### 3.1.1 The effects of stress on EV-mediated cellular communication

EVs have been implicated in mediating cell-cell communication in response to a wide range of cellular stimuli, including various sources of cellular stress (section 1.1.5). Multiple studies appear to show an increase in production of EVs as a response to stress (Hedlund et al., 2011; King et al., 2012; Arscott et al., 2013; Salomon et al., 2013; Kumar Jella et al., 2014; Al-Mayah et al., 2015; Atienzar-Aroca et al., 2016; Aubertin et al., 2016; Mutschelknaus et al., 2016), indicating that they may be especially important under non-physiological conditions, whilst others show changes in size (Bewicke-Copley et al., 2017; Kore et al., 2018) cellular uptake (Arscott et al., 2013; Mutschelknaus et al., 2016), or cargo (Eldh et al., 2010; de Jong et al., 2012; Arscott et al., 2013; Kucharzewska et al., 2013; Atienzar-Aroca et al., 2016; Lee et al., 2019),The mechanistic pathway by which EVs can mediate a diversity of effects, such as increased proliferation, DNA damage or apoptosis, on neighbouring and distant cells is poorly understood, so characterising which of these biophysical factors are altered under cellular stress is important in understanding how EVs are formed, released, transported, taken up and degraded in all conditions. It also essential in understanding whether the specificity of the EV cargo is important for the donor cell or receiving cell, or indeed both, and thus its relevance as a form of cell communication *in vivo*.

### 3.1.2 Methods for purifying EVs

As the EV field is new and in rapid evolution, there is no single standard method for their purification. The most established technique, and most commonly used, has been differential ultracentrifugation (UC) (Gardiner *et al*., 2016), but other methods such as size-exclusion chromatography (SEC), precipitation-based methods, bead-based immunoaffinity capture, ultrafiltration, density gradients and microfluidic devices have been used alone or in

combination. Whilst high purity methods such as density gradients, are evidently preferable, purity frequently comes at the expense of yield, so may not always be appropriate. The method of choice is therefore a compromise based on several factors, including yield, purity, cost, and the specific EV subpopulation of interest. These factors will apply differently depending on the source of the EVs under study, such as conditioned cell culture medium or human biofluids, and the planned downstream assays, such as *in vitro* or *in vivo* functional assays, proteomics, lipidomics or RNA sequencing.

### 3.1.3 Best practice in characterisation of EVs

Since little is known about how different purification methods may impact upon the EV subpopulation obtained, it is particularly important to characterise preparations to ensure that downstream assay results can be put into appropriate context. The International Society for Extracellular Vesicles has published guidelines for EV characterisation (Théry *et al*., 2018) with three major recommendations.

- **Global Quantification***:* Total protein, total particles or total lipid, ideally in a ratio.
- **Protein markers:** Three positive protein markers, including at least one transmembrane/ lipid-bound, and one cytosolic, alongside at least one negative protein marker.
- **Single vesicle characterisation**: High-resolution images of single EVs e.g. electron microscopy, atomic-force microscopy or super-resolution microscopy), and single particle biophysical analysis e.g. resistive pulse sensing, nanoparticle tracking analysis, high resolution flow cytometry, Raman spectroscopy).
- **Assessment of topology of EV- associated components** e.g. Protease and nuclease digestions, detergent permeabilization, antibodies to outer epitopes or inner epitopes.

Protein markers typically used in mammalian systems include the tetraspanin proteins CD81, CD63, CD9 (transmembrane), TSG101, ALIX, flotillins, hsp70, actin (cytosolic) and negative

markers for nuclear histones, mitochondria or secretory pathway components. Whilst some have been validated in *Drosophila* (Table 3.1), the extent to which they are applicable to other organisms is not fully known.

## 3.2 AIMS AND OBJECTIVES

*Drosophila* makes a good model to study the role of EVs due to its well-established status as model organism, high level of characterisation, availability of genetic tools such as the Gal4-UAS system for specific control of gene expression, and accessibility of distinct tissues such as the imaginal wing disc (section 1.4). Some work has been carried out on *Drosophila* EVs *in vivo*, in the context of tissue patterning in development (Gross *et al*., 2012; Beckett *et al*., 2013; Gradilla *et al*., 2014; Matusek *et al*., 2014), synaptic growth at the neuromuscular junction (Korkut *et al*., 2009, 2013; Koles *et al*., 2012) and behavioural signalling (Corrigan *et al*., 2014). However, whilst some work has been carried out in *Drosophila* cell lines to validate this work, the EVs have been poorly characterised relative to those in mammalian cell culture systems. Combining these complementary *in vitro* and *in vivo* approaches in *Drosophila* gives a powerful system to dissect the mechanisms involved in EV-biogenesis, loading and transfer in complex tissues, and how these may be altered under a range of conditions, such as cellular stress. The aims of this chapter were therefore to:

1. Establish a *Drosophila* cell culture model to investigate EV-biology.
2. Analyse how oxidative stress affects EV properties in cell culture conditions.

| Paper | Cell line | Conditions | Purification | EM | Protein markers |
|---|---|---|---|---|---|
| Koppen et al, 2011 | Kc167 | Serum-free HyQ-CCM3 72H | UC at 100,000g + sucrose cushion | Yes | Rho1, Rop<br>Actin, tubulin in large EVs only |
| | S2 | Serum-free Express Five 72H | | | |
| Gross et al, 2012 | Kc167 | 10% (normal) FBS Schneider's | UC at 100,000g + sucrose gradient for MS of Kc167 | Yes | In Kc167: Wg |
| | S2 | 10% (normal) FBS Schneider's | | | |
| Koles et al, 2012 | S2 | Serum-free SFX | UC at 100,000g + sucrose cushion | Yes | Wg, Tub, Evi-GFP, Alix, Lbm |
| Korkut et al, 2013 | S2 | Serum-free SFX 24H | UC at 120,000g | Yes | Evi, Syt4 |
| Beckett et al, 2013 | S2 | 10% depleted FBS Schneider's, 72H | UC at 100,000g | Yes | Wg, Wnt3A, Flo2, Csp, Syntaxin 1A, Rab35, Hrs, Vps28, Evi |
| Gradilla et al, 2014 | S2 | 10% depleted FBS Schneider's 96H | UC at 100,000g<br>+sucrose gradient for some validation | No | In Cl8: Hsp70, Syntaxin 1A, Rab11, Rab8, TSG101<br>In S2::Hh-GFP:Hsp70, TSG101, Rab11<br>In S2: Hsp70, Rab11 |
| | S2::Hh-GFP | 10% depleted FBS Schneider's 96H | | | |
| | Cl8 | 2.5% depleted FBS, 2.5% fly extract M3 48H | | | |
| Matusek et al, 2014 | Cl8 | Serum-free Schneider's, overnight | UC at 120,000g | Yes | Hedgehog |
| Parchure et al, 2015 | S2R+ | 10% depleted FBS Schneider's | UC at 100,000g<br>+sucrose gradient for some validation | Yes | Hedgehog, Syntaxin 1A, Csp, Alix, Lbm, Vps28, Hrs, Transferrin receptor, Rab5, Rab27, Vps4, Shrub |
| Lefebvre et al, 2016 | S2R+ | 10% depleted FBS Schneider's 48H | UC at 110,000g | Yes | None |
| | D17 | 10% depleted FBS M3 48H | | | |
| Lauwers et al, 2018 | S2 | Serum-free Sf-900 II 72H | UC at 265,000g | Yes | Evi |
| Van den Brande et al, 2018 | S2 | 10% depleted FBS M3 | Qiagen precipitation kit | No | Rho1, Rop, Rab11 |
| | Cl8 | 2.5% depleted FBS, 2.5% fly extract M3 | | | |
| Kerr et al, 2018 | S2 | 10% depleted FBS M3 24H | UC at 100,000g + sucrose cushion | Yes | Syntaxin 1A |
| Ashley et al, 2018 | S2 | Serum-free SFX | UC at 100,000g + sucrose cushion | Yes | None |
| Thomas et al, 2018 | Haemolymph | / | Invitrogen precipitation kit | No | Rab11<br>Alix-HA |
| Tsai et al, 2019 | S2 | Details not provided | Systems Biosciences precipitation kit | No | TSG101, Syntaxin 1A, Rab11 |
| | Haemolymph | / | | | |
| González-Méndez et al, 2020 | Cl8 | 2.5% depleted FBS, M3, 144H | UC at 100,000g<br>+ sucrose gradient/ SEC for some validation | No | Ptc, Rab8, Syntaxin 1A, Lbm, Hsp70 |

Table 3.1: Purification and characterisation used in study of *Drosophila* EVs

*Note, only protein markers which were found to be present are included in the table.*

## 3.3 RESULTS

### 3.3.1 Size exclusion chromatography can be used to purify *Drosophila* cell EVs

The aim of this thesis was to investigate the RNA cargo of *Drosophila* cell EVs, so a purification method permitting high yield, in order to ensure sufficient material for RNA sequencing, was needed. A combination of ultrafiltration followed by size exclusion chromatography (SEC) was chosen, as this is thought to remove free protein, whilst retaining high yield (Böing *et al*., 2014). This method was applied to conditioned media of *Drosophila* S2R+ cells, an adherent cell line used widely in *Drosophila* research. Nanoparticle Tracking Analysis (NTA) using Nanosight showed a peak in particle number in SEC fraction 8 (although technical replicates indicated their presence in fractions 6-10), whilst protein concentration began to rise rapidly at fraction 11 (Figure 3.1A). Using zetaview NTA (used in all experiments from this point forward), a similar profile was seen, although peaking at fraction 7, and with the concentration several orders of magnitude higher than for Nanosight (Figure 3.1B). Since both technologies indicated particles in fractions 6-10 inclusive, these were pooled to maximise yield for future studies. These results for S2R+ cells paralleled those seen using the SEC method in mammalian cell line EVs, such as MCF7 and A2780 (Figure 3.1C), indicating successful purification of EVs in the *Drosophila* model.

With the purification method showing suitability for purification of *Drosophila* cell EVs, SEC fractions 6-10 were then pooled together to give a single EV sample and subjected to further characterisation. Although some work has been done on protein markers of *Drosophila* EVs, consensus is less established than for mammalian EVs, so a range of markers were tested by Western blot (Beckett *et al*., 2013; Gradilla *et al*., 2014; Gross *et al*., 2012; Koles *et al*., 2012; Matusek *et al*., 2014; Thomas *et al*., 2018). In the mammalian EVs, the classical transmembrane tetraspanin markers CD81 and CD9 were clearly detectable (the former enriched) (Figure 3.2A), whilst *Latebloomer* (the only *Drosophila* tetraspanin to which an antibody is available), was also clearly and consistently visible in *Drosophila* EV samples (Figure 3.2B). In both models, cytosolic

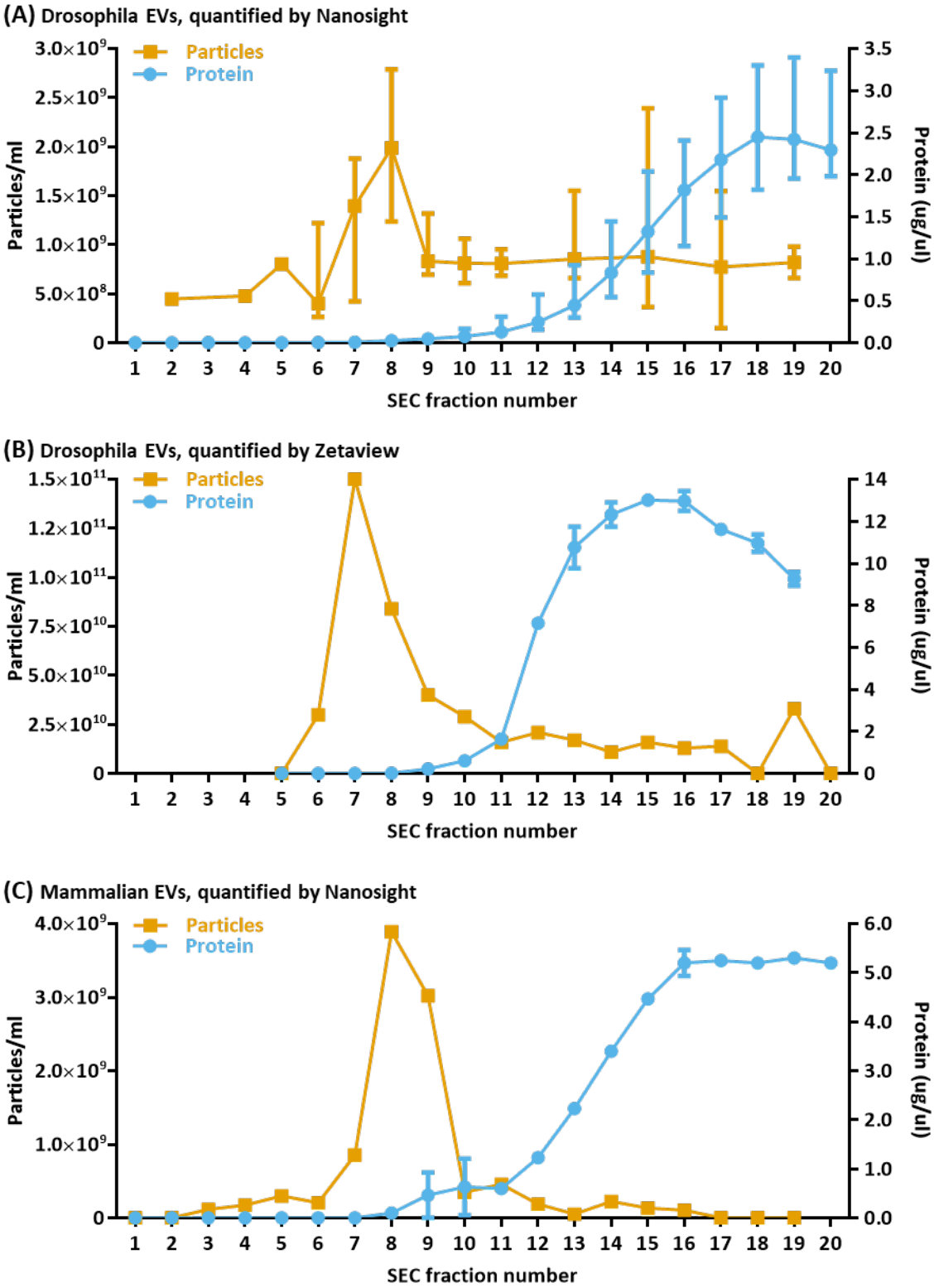


Figure 3.1: Size-exclusion chromatography for purification of *Drosophila* EVs

*Concentrated conditioned culture media was run on a sepharose SEC column and twenty 50µl fractions collected manually. Fractions were analysed for particle content by NTA (yellow) and free protein content by BCA assay (light blue). (A) NTA by Nanosight NS500 on four technical replicates of* Drosophila *S2R+ (single biological sample split between four SEC columns). Data shows median and interquartile range. Work was carried out together with Claire Hill. (B) NTA by Zetaview on one biological replicate. For protein quantification, mean and standard deviation of repeat measurements are shown. (C) NTA by Nanosight NS500 on mammalian A2780 cells. Data from one biological replicate, for protein quantification mean and standard deviation of repeat measurements are shown. Data was kindly provided by Priya Samuel.*

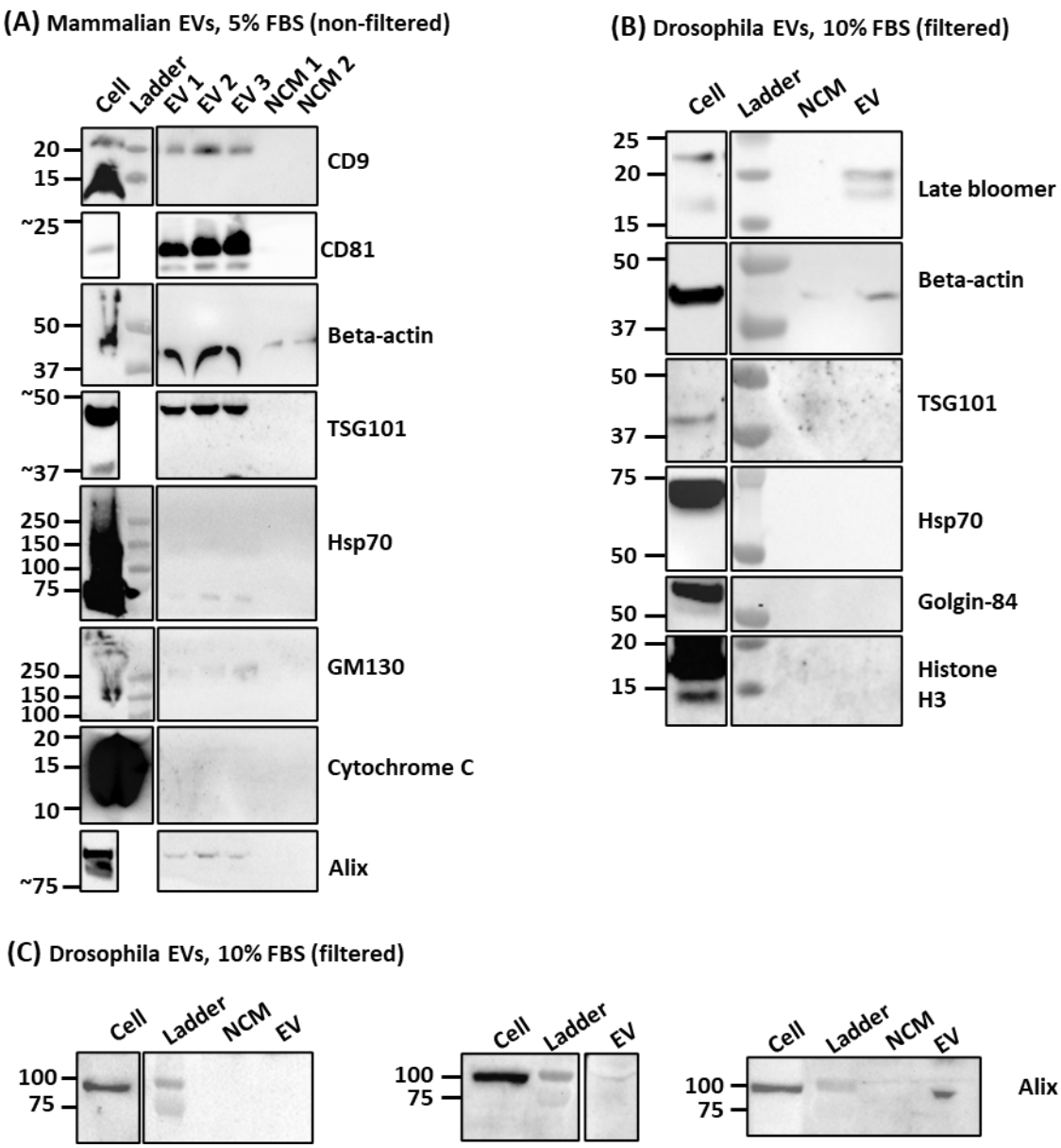


## Figure 3.2: Protein marker characterisation of mammalian and *Drosophila* EVs

*(A) Western blots of EV marker proteins and common contaminants in MCF7 pooled SEC fractions 7-9, with 0.22µm filtration step excluded. Cell culture media contained 5% depleted FBS and 20µg protein loaded for cell and EV samples, 6.67µg for non-conditioned media (NCM) controls. Beta-actin, GM130 and Cytochrome C carried out in reducing conditions, all others non-reducing. Data shows three technical replicates (single biological sample split between three SEC columns). Work was carried out together with Priya Samuel. (B) Representative Western blots for S2R+ pooled SEC fractions 6-10. Cell culture media contained 10% depleted FBS and 20µg protein loaded for all sample types, 8µg for actin and golgin-84 blots. (C) Blots for Alix from three different biological replicates. Blots for MCF-7 EVs were carried out together with Priya Samuel and are contained within submitted manuscript Melling et al (2021).*

beta-actin, recently suggested to be a pan-EV marker (Hoshino *et al*., 2020), was also clearly seen. However, the membrane associated cytosolic marker TSG101 could only be visualised in mammalian EV preparations, and was never seen in *Drosophila* EVs, whilst hsp70 was weakly present in mammalian EVs but absent in *Drosophila* EVs. ALIX, whilst weakly present in the single biological replicate tested in mammalian EVs, ranged from complete absence to clear band in *Drosophila* (Figure 3.2C). In both models Golgi markers (GM130 and Golgin-84 for mammalian and *Drosophila* respectively) were either very weak or completely undetected. In *Drosophila* EVs the nuclear marker Histone H3 was also not visible. These results indicated that the purification procedure produced EV samples with minimal contamination from other cellular components.

For beta-actin, TSG101 and hsp70, the same antibodies were used in human and *Drosophila* samples, highlighting that many of the antibodies show cross-species specificity, and may also react to bovine-derived EVs. In contrast, tetraspanin antibodies CD81 and CD9 showed no reactivity in *Drosophila* cells, indicating possible specificity to human over bovine EVs. However, since the cells were cultured in media containing FBS (although depleted of bovine EVs using standard protocols), it was particularly important to include a non-conditioned media (NCM) control. CD81 and CD9 showed no reactivity, whereas actin gave a visible, but weak, band. This indicated that some bovine EVs may remain after depletion of the FBS.

Finally, transmission electron microscopy (TEM) was used to for single vesicle characterisation. Structures with the typical cup-shaped morphology expected for EVs, in the size range 40-150nm, were seen in *Drosophila* EV samples, very similar to the structures seen in mammalian EV preparations (Figure 3.3). Although some protein was present in both cases, taken together with NTA and Western blotting data, this indicated that the SEC protocol effectively purified EVs from the conditioned media of S2R+ cells.

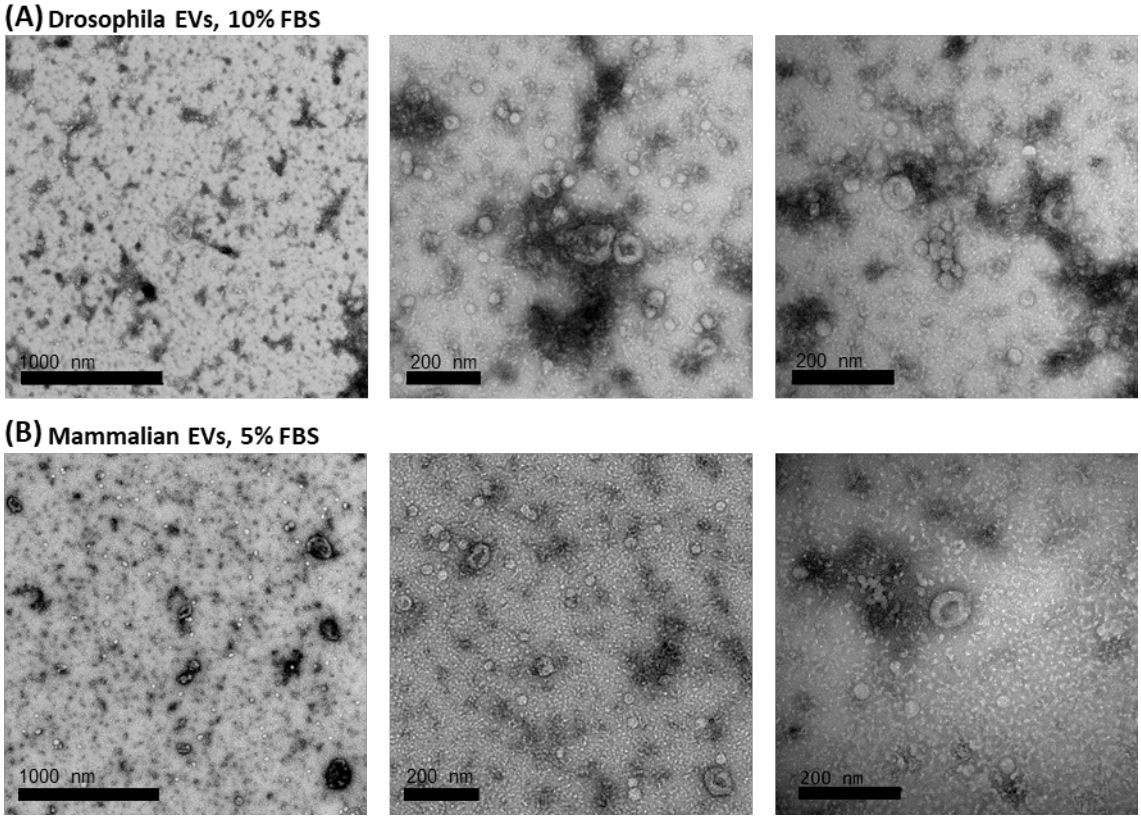


Figure 3.3: TEM of mammalian and *Drosophila* EVs.

*Representative transmission electron microscopy of negatively stained EVs for (A)* Drosophila *S2R+ EVs and (B) mammalian MCF7 EVs, purified in 10% and 5% FBS respectively. Preparation and imaging for* Drosophila *EVs carried out with Errin Johnson.*

### 3.3.2 FBS contains non-EV particles which can be detected by NTA

Although TEM clearly showed the presence of EVs in both mammalian and *Drosophila* samples, small circular structures were also visible, thought to be lipoprotein. In NCM, whilst cup-shaped EVs occurred rarely, these smaller lipoprotein structures were abundant (Figure 3.4A, B), but absent in serum-free media (Figure 3.4C), indicating likely bovine origin. Further characterisation of EV-depleted FBS was therefore carried out to understand the effects that it might have on future experiments. Using five different batches of FBS, the efficiency of the depletion protocol was tested by NTA. This showed that, whilst there was a 76% (±11%) reduction in the number of particles, $5.61 \times 10^{10} \pm 2.231 \times 10^{10}$ per ml of FBS were still present, a number within one order of magnitude of counts in EV samples (Figure 3.4D). Of note, NTA size analysis demonstrated that the median size of the particles was reduced in the depleted FBS (Figure 3.4E), consistent with removal of EVs but presence of lipoproteins, as seen in TEM.

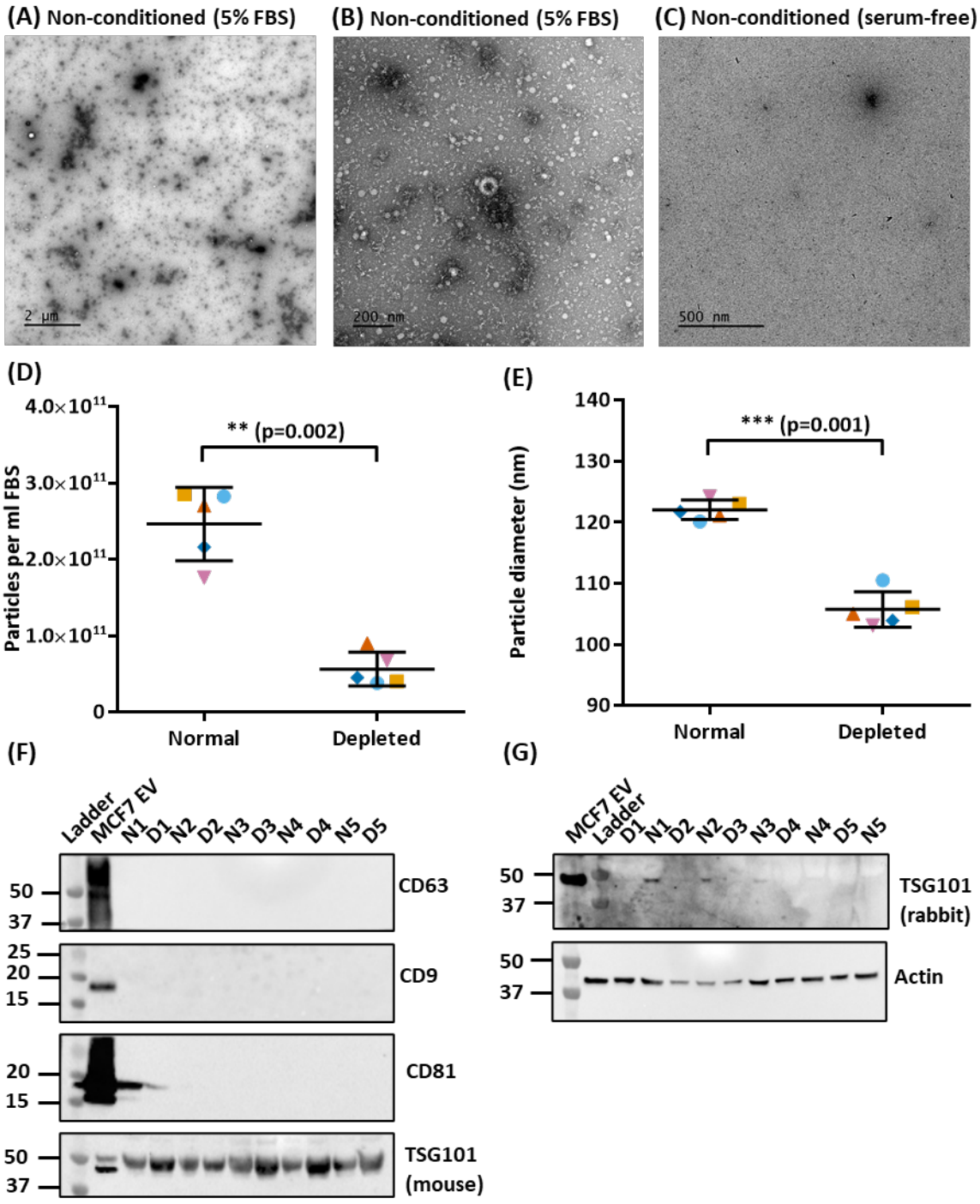


## Figure 3.4 FBS depletion removes only larger particles

*Transmission electron microscopy of negatively stained (A) and (B) non-conditioned media containing 5% depleted FBS, and (C) serum-free media control. (B) Shows the only EV-like structure that was observed. (A) - (G) Concentrated FBS was run through SEC and analysed for EV content by NTA for (A) particle number and (B) particle size. Five biological replicates, each data point representing mean of three replicate measurements. Statistical significance assessed with two-tailed Wilcoxon matched-pairs signed rank test. (F) and (G) Western blotting of EV markers in FBS. 20µg protein loaded and all carried out in non-reducing conditions, except for actin. N1-5 represent normal FBS, and D1-5 EV depleted. Work done together with Elise Padbury.*

Since some evidence of EV marker proteins was previously seen in NCM controls, the FBS itself was further tested. This showed the absence of bands for CD63, CD9 and CD81 tetraspanin proteins in both normal and depleted FBS, indicating that, whether due to the species specificity of antibodies or the absence of bovine EVs, detection of mammalian EVs was specific (Figure 3.4F). Probing with TSG101 gave two distinct bands for the positive control, and a single band in all FBS samples that was enriched in depleted FBS. The upper bands may be due to cross-reactivity with the heavy chain of IgG which also migrates at ~50kDa. Repeating with a different TSG101 antibody showed faint bands within the normal FBS that were absent in the depleted FBS, indicting successful bovine EV removal (Figure 3.4G). Actin however, showed high reactivity in all samples, regardless of EV depletion state, possibly indicating its presence in non-typical EV populations. These results together indicated that, whilst EVs could be specifically detected using protein markers, small particles present in FBS can be detected by NTA, and thus interfere with accurate EV quantification.

Knowing that particles in FBS could be detected by NTA, the signal-noise ratio was next tested in S2R+ EV samples. Analysis of SEC fractions indicated that particles eluted similarly, although peaking slightly later in fraction 9 (Figure 3.5A). Calculation of the total particle content showed a median enrichment of 2.6-fold over that of NCM (Figure 3.5B). A related cell line, S2, showed a higher 7.7-fold enrichment, but appeared to show high stress levels under normal conditions so was not pursued any further. Another alternative that many EV studies employ is to seed cells in normal media containing FBS, but to switch to serum-free media for the duration of the EV conditioning period, thus avoiding contamination with bovine EVs. However, serum-starvation alone is frequently used as an inducer of oxidative stress, and initial attempts to culture the S2R+ cells in serum-free media indicated that this cell line appeared to be highly stressed after just 24 hours (Figure 3.5C), whilst other cell lines appeared to tolerate it (Supplementary Figure 1). At a later date, further tests did attempt to optimise conditions further, using a combination of synthetic substitutes and reduced FBS concentrations, but, whilst FBS concentrations down to

0.625% were able to support cells much better than serum-free medium, increased stress was observed by just transmitted light images alone (Supplementary Figure 2). Choice of culture conditions is therefore a compromise between the level of interference from FBS, and induction of stress. However, for RNA extraction experiments in Chapter 5, conditioning continued to be carried out in media containing 10% depleted FBS.

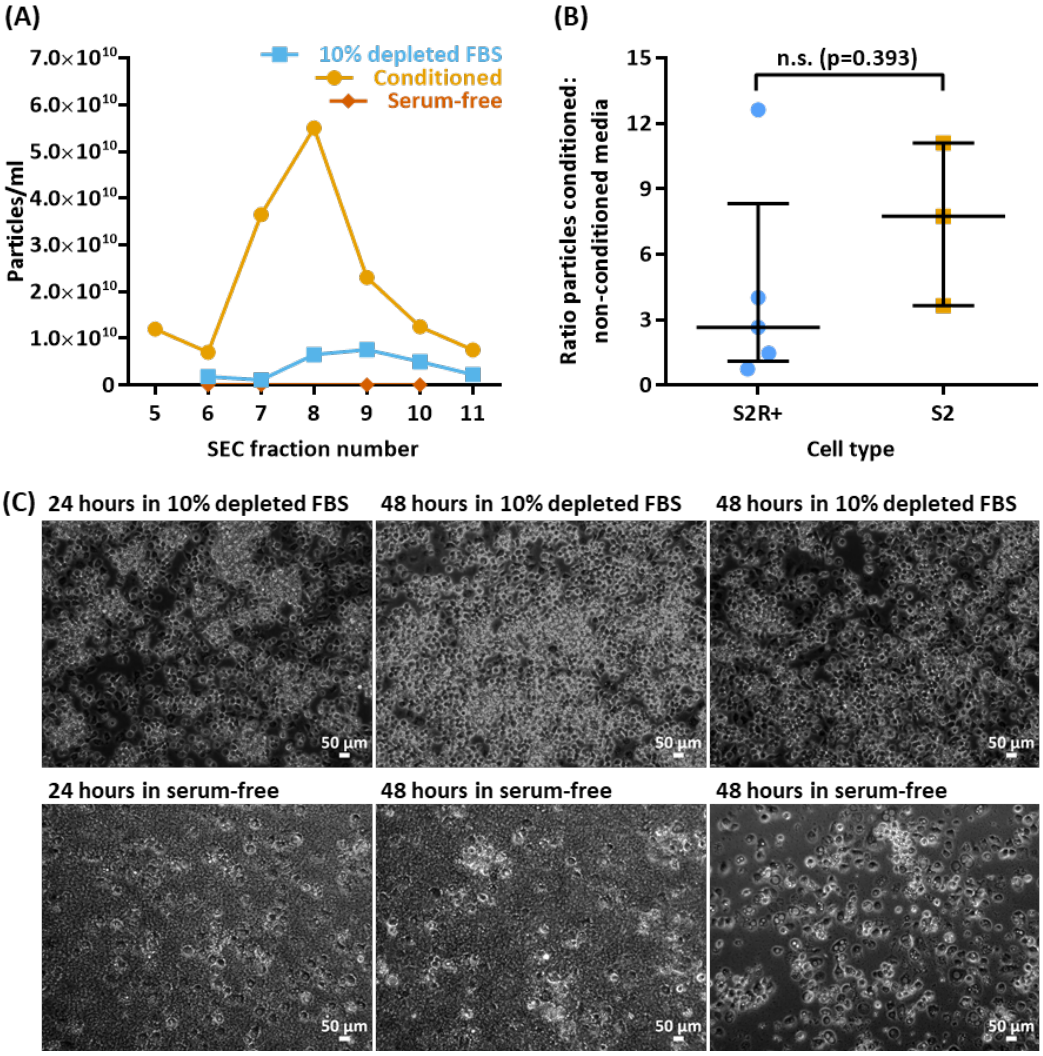


Figure 3.5: Assessing approaches to minimising FBS contamination of EV samples

*(A) NTA particle counts for EV SEC fractions in cell conditioned media (yellow), non-conditioned control containing 10% depleted FBS (light blue) and non-conditioned serum-free control (red). (B) Ratio of particle counts in conditioned to depleted FBS control in SEC fractions 6-10 for two cell lines. Median and interquartile range shown, for five and three biological replicates respectively. Statistical significance assessed with two-tailed Mann-Whitney test. (C) S2R+ cells cultured in 10% depleted FBS or serum-free media in 12-well (left, middle) or 96-well (right) plates.*

### 3.3.3 EVs eluted in PBS maintain their biophysical properties at 4˚C for five days

Whilst consensus guidelines recommend storage of EVs at -80°C, the effect of freeze-thaw on biological function of EVs is poorly understood (Witwer et al., 2013; Jeyaram and Jay, 2018). Since one of the aims of this work was to assess the functional effect of EVs on recipient cells, use of freshly prepared EVs has been recommended (Lorincz et al., 2014), but is not always practicable. To test the stability of the EVs over time at 4°C, the particle number of the same sample was measured over multiple days using NTA. Whilst only one replicate was tested, the results showed that there were minimal changes in particle number or size in EV fractions 6-10 between day 1 and day 5 (Figure 3.6A, B). In contrast, after 12 days, or with proteinase/heat-

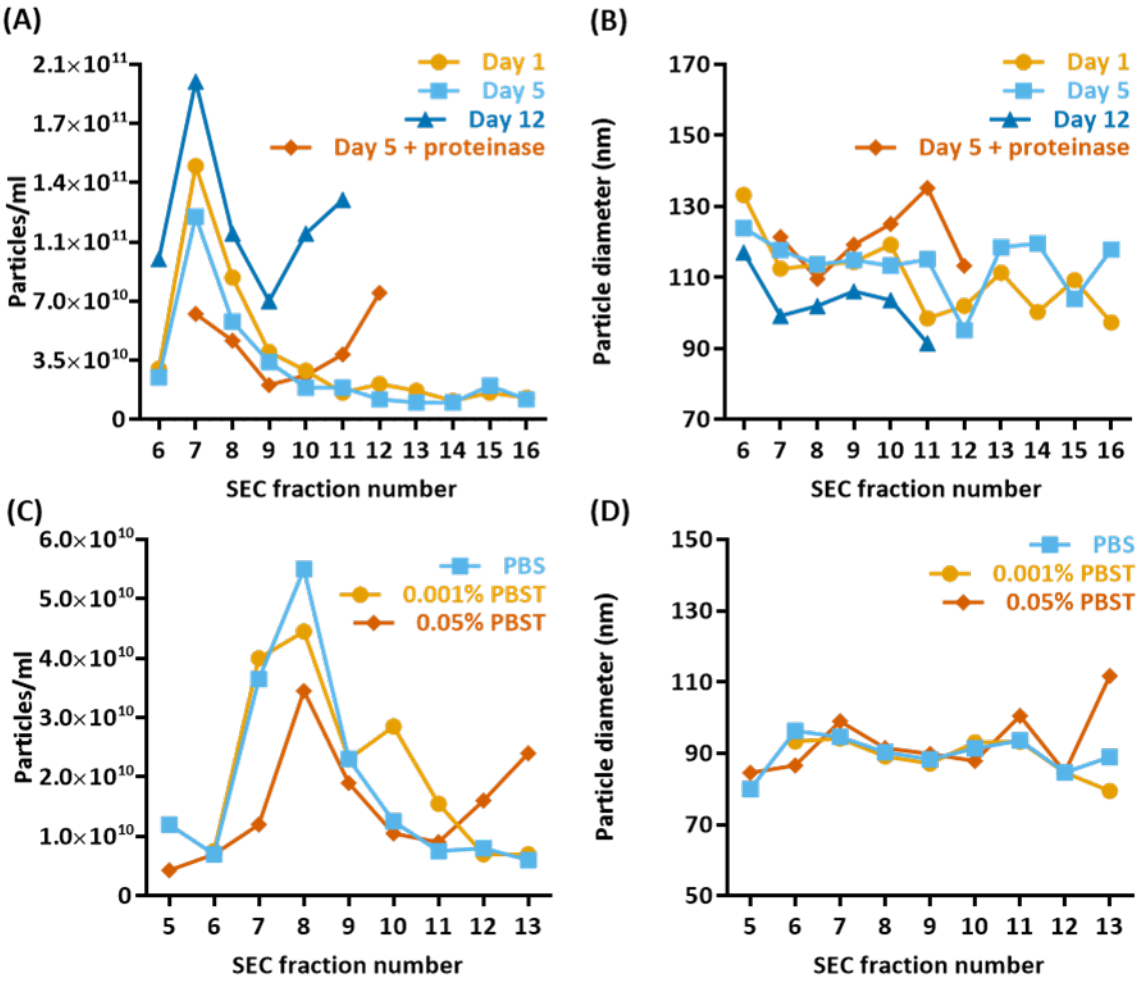


Figure 3.6: Assessing EV stability

*(A) and (B) SEC fractions of Drosophila S2R+ conditioned culture media for a single sample were analysed by NTA on day of purification (Day 1), after storage at 4℃ or after proteinase treatment as indicated. (A) Particle counts and (B) median particle size. (C) and (D) One biological replicate was split between three columns and eluted with 0.05% PBS-Tween as previously, PBS diluent alone or a reduced concentration. (C) Particle counts and (D) median particle size.*

treatment at day 5, both an increase in particle number and more variation in size were seen (Figure 3.6A, B). These changes were interpreted as possible degradation of the EVs over time. Since the SEC protocol used initially up to this point used 0.05% PBS-Tween as elution buffer, it was possible that this might also be causing some degradation effect. Although the profile of particle size seemed largely unaffected (Figure 3.6D), particle number at 0.05% Tween appeared to be similar to that of proteinase/heat-treated EVs, whilst PBS as a buffer produced a much cleaner profile (Figure 3.6C). From these combined results, it was concluded that a) Tween should be removed from the elution buffer, and b) EVs should be stored at 4°C for a maximum of 5 days.

### 3.3.4 $H_2O_2$ induces dose-dependent oxidative stress in S2R+ cells

Since the aim was to assess the effect of oxidative stress on EV production, cargo and biological function, the next objective was to optimise stress induction. A range of approaches were possible, including acute application of reactive oxygen species (ROS) such as hydrogen peroxide ($H_2O_2$), generation of ROS by redox cyclers (e.g. paraquat), mitochondrial complex I inhibitors e.g. rotenone), drug metabolism (e.g. tertbutyl-hydroperoxide (tBHP), direct electrophilic attack (e.g. menadione sodium bisulphite), or inhibition of cellular antioxidant response by chemicals (e.g. Butathione sulfoxamine). Three of these chemical inducers were initially trialled, tBHP, menadione bisulphite and $H_2O_2$, using MTT assays as an indicator of overall cell viability. Results indicated that $H_2O_2$ appeared to induce a relatively consistent dose-dependent effect on overall cell viability when diluted in either serum-free or serum-containing media, whereas tBHP and menadione showed high variability (Figure 3.7). Since $H_2O_2$ has been used previously in both studies on *Drosophila* cells (Radyuk *et al*., 2006) and EV studies (Eldh *et al*., 2010; Atienzar-Aroca *et al*., 2016), it was taken forward for future work.

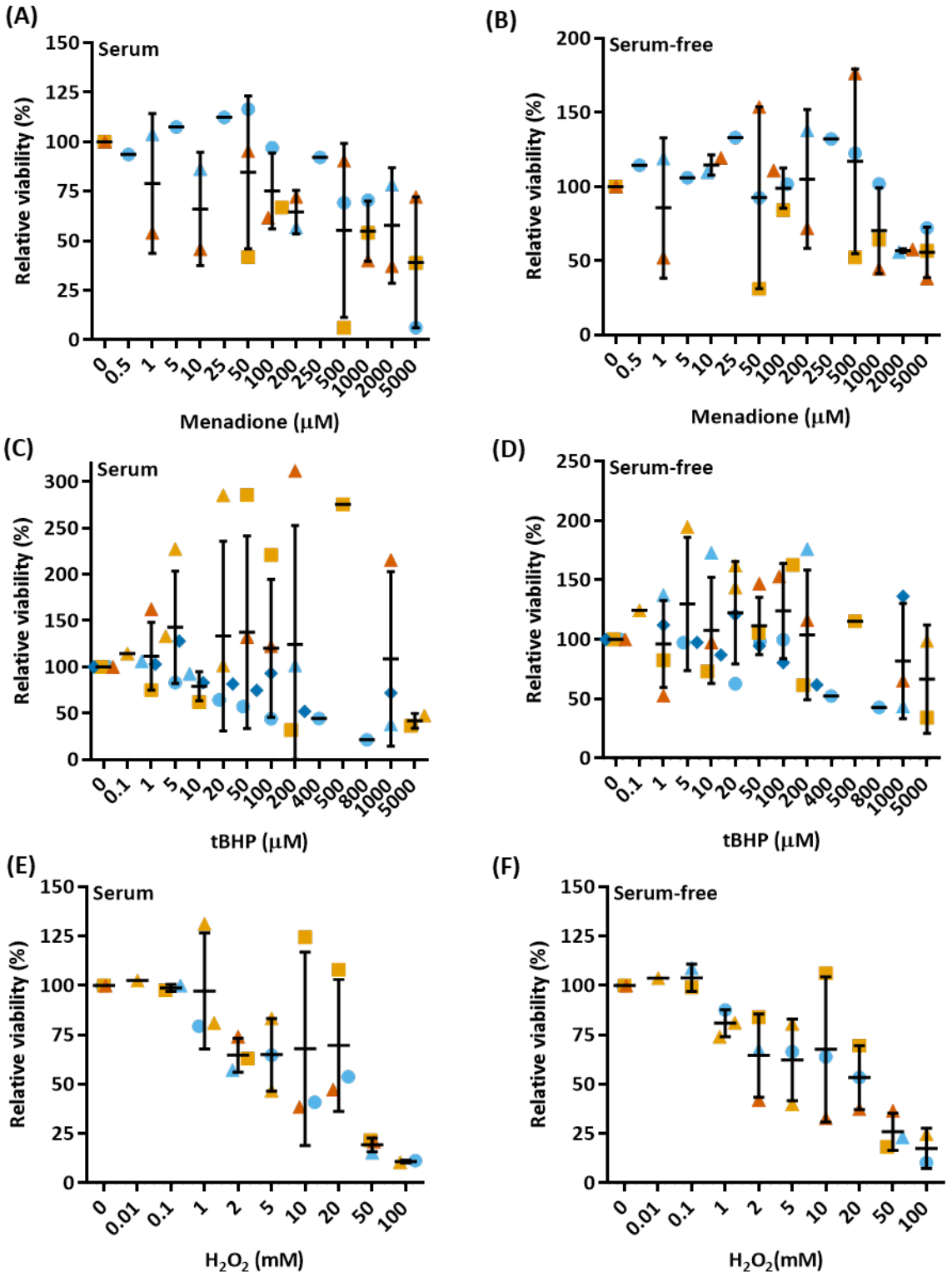


Figure 3.7: MTT cell viability curves for three different inducers of oxidative stress

*MTT assays for cell viability of S2R+ cells treated with different concentrations of tBHP, menadione sodium bisulphite, and $H_2O_2$. Drugs were diluted in either media containing 10% FBS (A, C, E) or serum-free media (B, D, F) and incubated for one hour before washing and returning to 10% serum for 48 hours, after which MTT carried out. Mean and standard deviation of three or four biological replicates shown, indicated by colour and shape. Each point represents the mean absorbance value of technical replicates, after normalisation to the no treatment control condition for that biological replicate.*

S2R+ cells are only semi-adherent, so the wash steps associated with MTT assay were causing inconsistent cell loss, thus cell viability assessment was changed to use of a resazurin-based assay. This indicated that 0.5mM and 2mM concentrations of $H_2O_2$ resulted in the reduction of viability to an average of 74% and 52% respectively (Figure 3.8A). This was confirmed using flow cytometric analysis with Annexin V and Propidium Iodide (PI) staining, which showed an equivalent reduction in live cell count to 68±26% and 48±19% (Figure 3.8B). Annexin V and PI staining indicated that this was due to an increase in the level of apoptosis and cell death, rather than just a decrease in proliferation alone. Assessment of direct induction of ROS was trialled with CellROX fluorogenic probe, but success was variable, and $H_2O_2$-induced stress incompatible, likely due to quenching of the probe (Supplementary Figure 3). However, phosphorylation of histone H2Av (yH2Av), widely used as stress marker (Li *et al*., 2006; Park *et al*., 2012) showed a dose dependent increase in staining between control, 0.5mM and 2mM $H_2O_2$ (Figure 3.8C,D), indicating suitability as conditions in future experiments.

### 3.3.5 $H_2O_2$ stress increases the number of EV produced per cell

The next objective was to assess whether the method used for purification of EVs was suitable under these oxidative stress conditions, and whether there was any alteration of the EV population purified. NTA again showed that EVs eluted in fractions 6-10 (Figure 3.9A), but the total number of particles in the pooled fractions in each condition did not significantly differ (Figure 3.9B). Since the total cell population differed in each condition (Figure 3.9C), the number of EVs produced per cell was also calculated, expressed as EVs per viable seeded cell (Figure 3.9D), and per viable cell counted at the end of the 48-hour conditioning period (Figure 3.9E). The results indicated a significant increase when expressed as per counted cell only, indicating that stress did increase the number of EVs produced to some extent.

Additional methodological validation was then carried out, as for future RNA extraction, further concentration of the 2.5ml EV preparation would be necessary, with the effect on EV

subpopulations unknown. These results showed that, although an estimated 50% of particles were lost as a result of concentration, there was no significant difference when comparing between stress conditions (Figure 3.9F). This confirmed that the purification protocol was yielding equivalent populations of EVs under each stress condition tested.

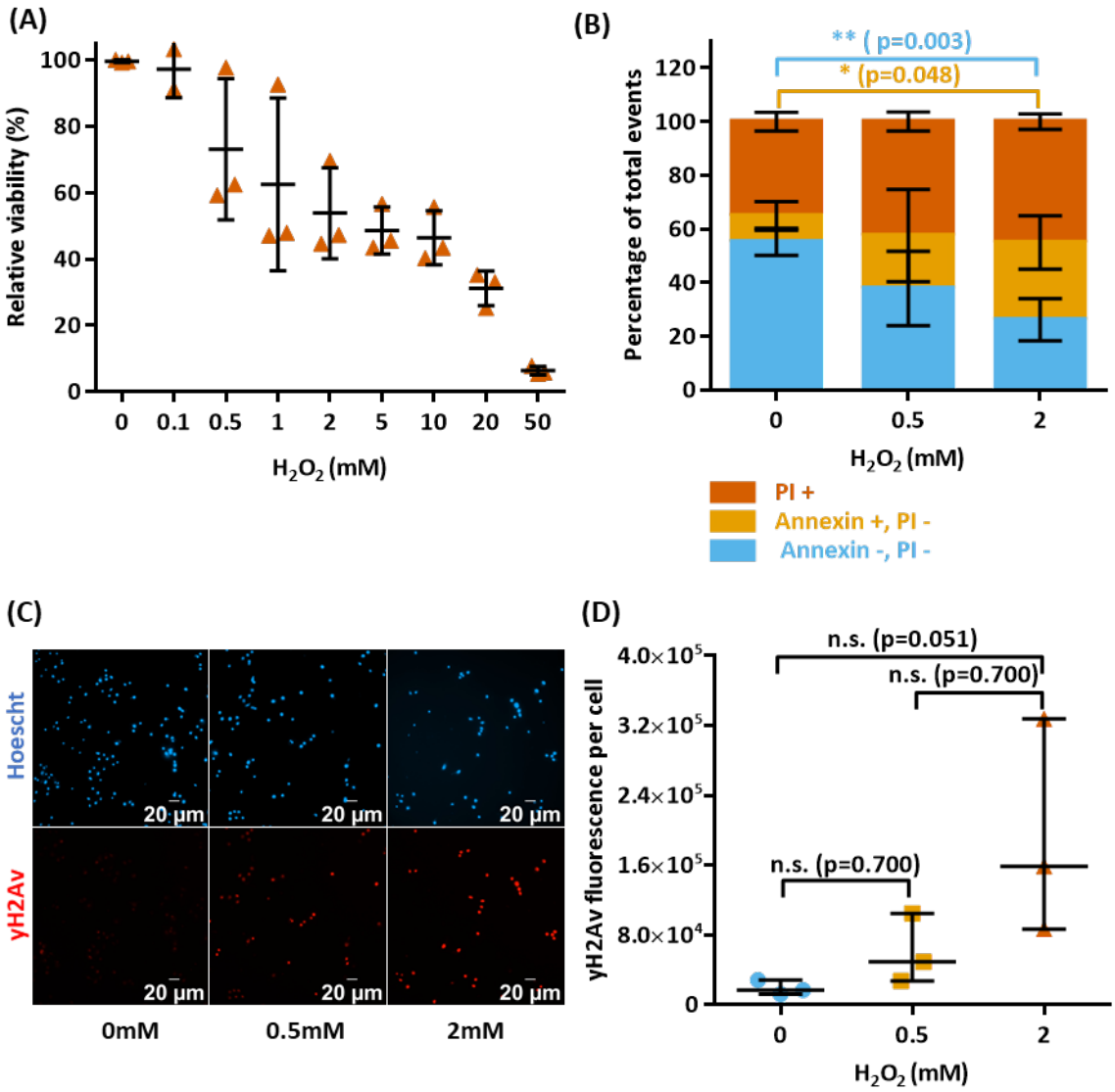


## Figure 3.8 Validating hydrogen peroxide concentrations for induction of stress

*(A) $H_2O_2$ viability curve for S2R+ cells using resazurin assay, after one-hour treatment with $H_2O_2$ diluted in media with 10% depleted FBS and 48-hour incubation. Median and interquartile range of three biological replicates shown. Each point the mean value of technical replicates, normalised to control condition for that biological replicate. (B) Flow cytometry of Annexin V and propidium iodide staining in live S2R+ cells. Results show percentages of total events across three biological replicates. Annexin - PI - represent viable cells, with increases in Annexin and PI staining indicating increases in apoptosis and cell death respectively. Statistical significance assessed with two-way ANOVA followed by Tukey's multiple comparisons test. Only p-values for significant differences shown. (C) yH2Av immunocytochemistry as indicator of DNA damage response in stressed cells, yH2Av in red and nuclei in blue. (D) Quantification of yH2Av. Three biological replicates per condition, each point median value for minimum 2000 cells. Statistical significance assessed with Kruskal-Wallis test followed by Dunn's multiple comparisons test.*

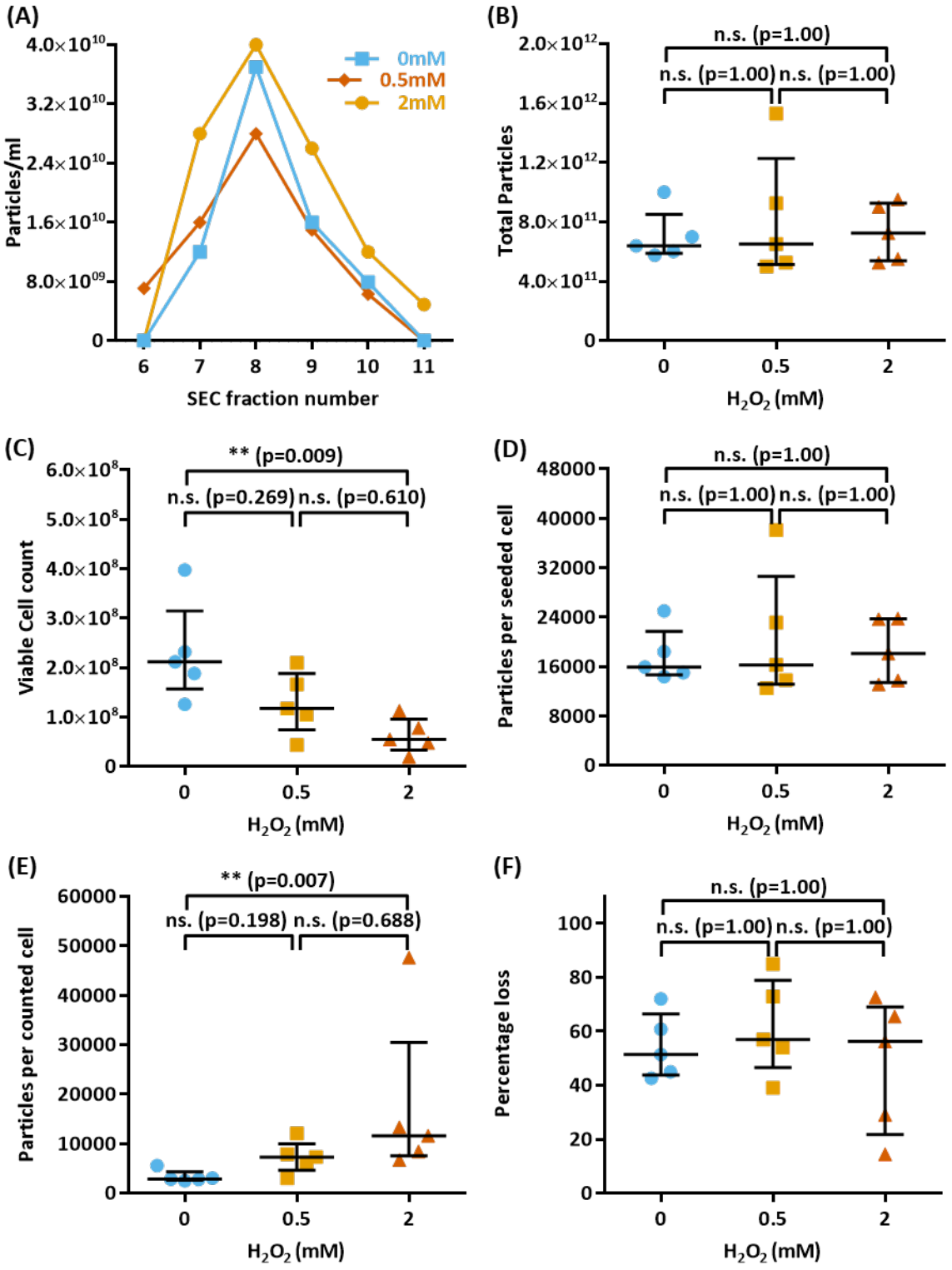


Figure 3.9 Effect of $H_2O_2$ stress on EV production by S2R+ cells

*(A) NTA particle counts of EV SEC fractions from S2R+ cells subjected to $H_2O_2$ stress. One biological replicate shown. (B) Total NTA particle counts under each stress condition (C) Total viable cell count at the point of conditioned media collection. (D) Particle count normalised to seeded cell number. (E) Particle count normalised to cell count from (C). (F) Estimated loss of particles due to concentration in vivaspin 2 concentrator. Median and interquartile range of five biological replicates shown, for cells between seven and twelve passages. Statistical significance for all data assessed with Kruskal-Wallis test followed by Dunn's multiple comparisons test.*

### 3.3.6 $H_2O_2$ stress does not alter the size of EVs produced

Knowing that comparable EV populations were being purified, the effect of stress on particle size was then tested. NTA size profiles were observed to be similar between each stress condition, all peaking between 70-120nm, with 10-15% of total particles above 150nm, the maximum size range for exosomes reported in the literature (Figure 3.10A). A comparison of the median sizes also showed no statistically significant differences, either between stress conditions or pre versus post concentration (Figure 3.10B). Together these results showed that the EV purification process did not introduce bias to any one condition.

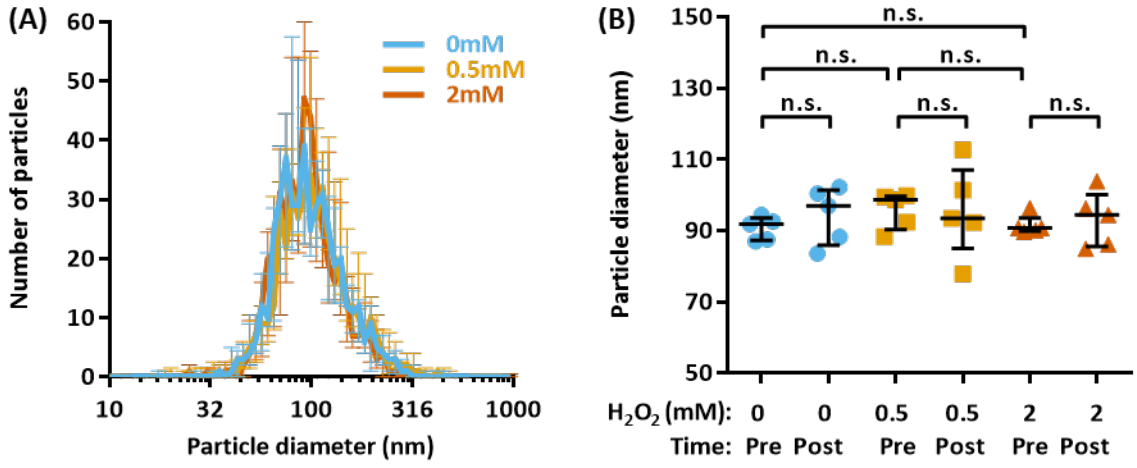


Figure 3.10: Effect of $H_2O_2$ stress on size of EVs produced by S2R+ cells

*(A) NTA size profiles for EVs purified from cells subjected to $H_2O_2$ stress. (B) Median particle size at each stress level, pre and post concentration in vivaspin 2 concentrator. For both (A) and (B) median and interquartile range of five biological replicates shown, for cells between at passage 7-12. Statistical significance for both assessed with Kruskal-Wallis test followed by Dunn's multiple comparisons test.*

Further characterisation by TEM did not reveal any notable differences in size, whilst Western blotting of protein markers indicated little difference under stress (Figure 3.11). Only actin showed any consistent difference, producing a weaker band in the stress EVs. However, since this marker also showed reactivity in NCM controls, it is difficult to determine whether this is due to true differences in the EV population. Nevertheless, taken together these results indicate that any differences in the EVs appear to be in the number produced by cells, rather than any differences in their size, morphology or protein composition.

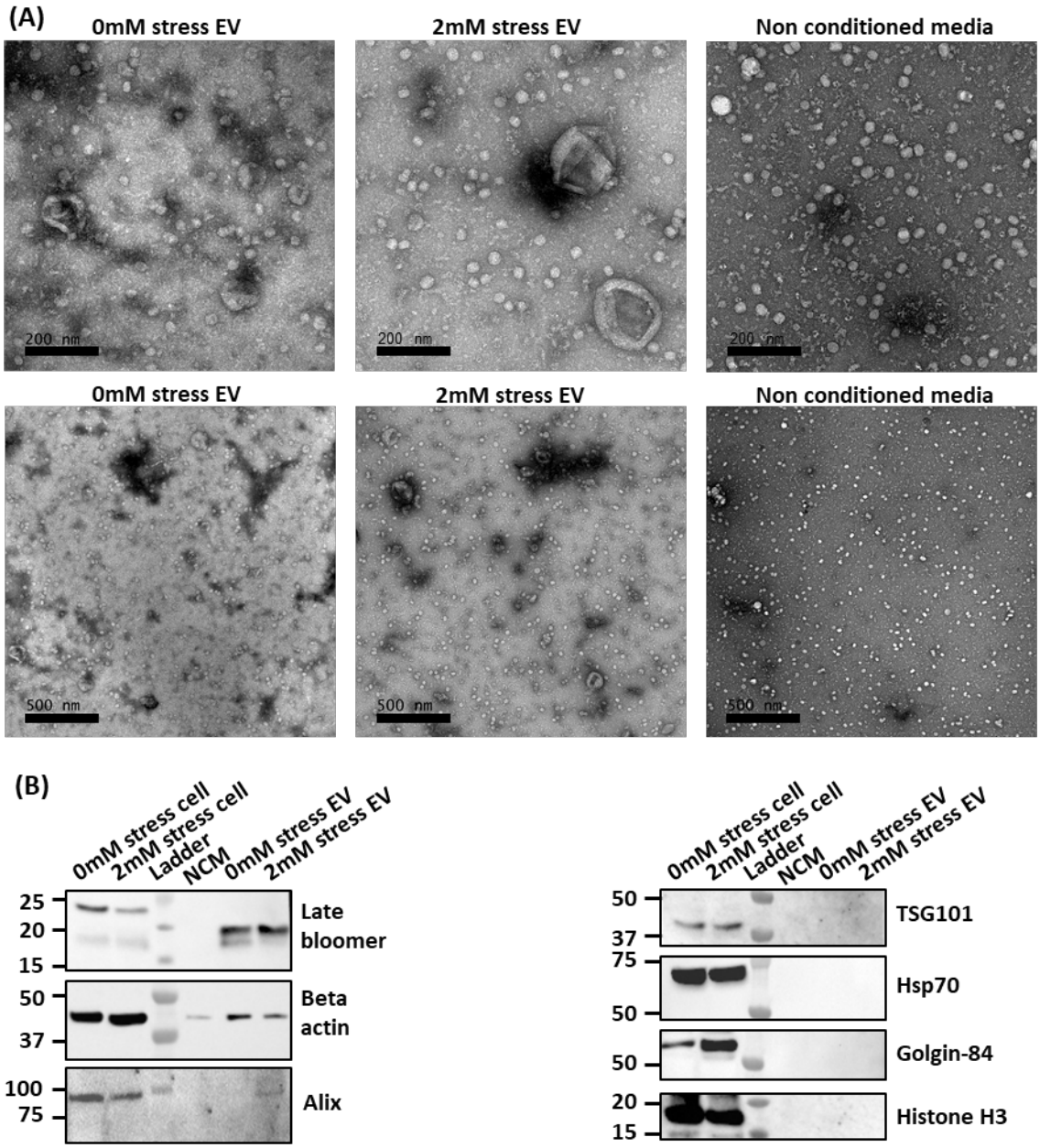


## Figure 3.11: Comparison of *Drosophila* EVs under control and stress conditions

*(A) Representative TEM of negatively stained EVs under each condition. Preparation of grids by Elise Padbury and imaging by Flavia Moreira-Leite (B) Representative Western blots for S2R+ pooled SEC fractions 6-10 purified from cells under control and 2mM $H_2O_2$ stress conditions. Cell culture media contained 10% depleted FBS and 20µg protein loaded for all sample types, 8µg for actin and golgin-84 blots. Beta-actin only under reducing conditions.*

## 3.4 DISCUSSION

### 3.4.1 SEC for purification of EVs from *Drosophila*

A growing number of studies have attempted to purify EVs from *Drosophila* cell lines and flies, with the majority using UC (Table 3.1). However, this protocol can be time-consuming and there are concerns as to contamination with protein complexes, and the effect of high speed spins on the integrity and aggregation of EVs (Jeppesen *et al*., 2014; Linares *et al*., 2015; Nordin *et al*., 2015). As an 'gentler' alternative, SEC has the potential to overcome some of these problems. Recent work has demonstrated that ultrafiltration followed by SEC performs very similarly to UC when considering particle size, morphology and proteome, with some indicating a higher particle/protein ratio as an indicator of purity (Jeppesen *et al*., 2014; Lobb *et al*., 2015; Nordin *et al*., 2015; Mol *et al*., 2017). Mol *et al*. also found that SEC EVs from cardiomyocyte progenitor cells were able to induce greater phosphorylation, indicating that this method may be more appropriate for testing of the functional activity of EVs in other areas. The current work has demonstrated that *Drosophila* cell EVs can also be effectively purified by SEC, as shown by particle/protein separation and TEM imaging.

This purification of *Drosophila* cell EVs by SEC was further validated by testing for EV marker proteins corresponding closely to the most common used in mammalian systems; Lbm, Alix, Hsp70, TSG101 and actin. In other studies of *Drosophila* EVs (Table 3.1), Alix (inconsistently present in this work) was present in three separate studies (Koles *et al*., 2012; Parchure *et al*., 2015; Thomas *et al*., 2018), whilst Hsp70 (absent in this work) was present in two cell lines, Cl8 and S2 (Gradilla *et al*., 2014; González-Méndez *et al*., 2020). Lbm was clearly present in the samples herein, conflicting with the absence identified by one previous study (Beckett *et al*., 2013) but in agreement with three others (Koles *et al*., 2012; Parchure *et al*., 2015; González-Méndez *et al*., 2020). Actin, recently suggested to be a pan-EV marker (Hoshino *et al*., 2020) has not been identified in *Drosophila* EVs before, but is clearly present in this work.

Although TSG101 was not visible in the *Drosophila* EVs here, this marker has been validated in one study in S2 cells (Tsai *et al*., 2019), but was absent in normal S2 cells in a second (Gradilla *et al*., 2014), although in the latter was identified in Cl8 cells and transfected S2 cells. TSG101 has been suggested to be predominantly associated with lower density EVs (Gradilla *et al*., 2014; Willms *et al*., 2016), so its absence may reflect the purification of primarily higher density EVs. However, in contrast, when analysing just very small EVs (UC at a higher speed of 250,000g or density gradient fraction 1.12g/ml), González-Méndez *et al.* identify a Cl8 cell EV population which is positive for Lbm and negative for hsp70, in line with the results seen in this work. Parchure *et al.* also find Alix to be absent when analysing just this smaller 250,000g EV population in S2R+, although Lbm was also not visible at this speed. The absence of hsp70 in González-Méndez *et al.* is also of interest as similar results have been seen using SEC in mammalian systems by one group, where tetraspanins CD81 and CD63 were seen in early particulate fractions and hsp70 in later protein fractions (Benedikter *et al*., 2017). This may indicate that hsp70 is a poor EV-specific marker protein. Together these results indicate the heterogeneity of proteins present in purified EVs depending on cell line, EV size and extraction method. Further work to assess whether protein markers associated with EVs of both high and low density, such as Vps28, Hrs and Csp (Parchure *et al*., 2015), would therefore be of interest to further and understand the specific EV population purified by the SEC method compared to UC in *Drosophila*. Nevertheless, in line with the majority of previous work, the tetraspanin Latebloomer has been shown to be a specific marker for small EVs in *Drosophila*.

### 3.4.2 Quantification of EV release from stressed cells

Increasingly, EV studies use serum-free media for the EV conditioning period to avoid contamination of samples with bovine EVs, RNA and other contaminants. However, serum-starvation alone is frequently used as an inducer of oxidative stress, and initial attempts to culture the S2R+ cells in serum-free media indicated that this cell line is particularly sensitive,

appearing highly stressed within 24 hours, whilst other cell lines tolerated it reasonably well; mammalian SKOV3 at least up to 72 hours (Supplementary Figure 1), and N2a neuroblastoma cells up to 48 hours (Li *et al*., 2015). The alternative, which was employed in this work, is to use FBS depleted of bovine EVs, which has been shown to support cell growth, albeit with a reduced rate of proliferation (Eitan *et al*., 2015). Since, comparison of the EVs purified from neuroblastoma under these two conditions showed differences in the proteome, particularly those relating to oxygen and reactive species metabolic processes and RNA binding (Li *et al*., 2015), the effect of cell culture conditions on EV cargo cannot be underestimated.

Although both FBS and NCM did not show detectable classical EV marker proteins in Western blots (aside from actin), high particle counts were observed with NTA. To allow accurate quantification of cell-derived EVs, one possibility considered was normalisation to particle content within NCM controls. However, since cells are able to take up FBS EVs (Eitan *et al*., 2015), it cannot be assumed that uptake will be the same under all conditions. One alternative would be to quantify EVs by an alternative method with higher specificity, such as imaging flow cytometry, which is becoming increasingly viable but at present limited to mammalian EVs (Görgens *et al*., 2019). However, within this quantification limitation, $H_2O_2$-treated cells did appear to produce more EVs per cell, in agreement with other studies on Jurkat T cells (Hedlund *et al*., 2011) and retinal pigment epithelium cells (Atienzar-Aroca *et al*., 2016), although the same was not seen in Raji B cells (Hedlund *et al*., 2011). With increased sensitivity of alternative approaches, it may also be possible to monitor EV release by stressed cells over shorter periods of time to identify when this increase occurs.

### 3.4.3 Measurement of EV size

Particle size is a key characteristic used in EV studies to define the subpopulation under study, since MVB-derived exosomes are believed to be of a smaller size than plasma membrane derived MVs and ABs. In particular, the loading of cargo is likely to differ by EV size, so is of additional

interest in this work. The most widely used methods for sizing of EVs are TEM, NTA and resistive pulse sensing, all of which have limitations to accurate sizing, such as assumptions of sphericity in NTA/resistive pulse sensing and lack of shrinkage in TEM (van der Pol *et al*., 2014). Whilst only a few TEM images were taken for validation, TEM EV sizes of S2R+ EVs in this work were in the range 40-180nm, as for mammalian EVs, and in good agreement with the median particle of 90nm determined by zetaview. This is in contrast to previous work which has suggested *Drosophila* EVs to be smaller than mammalian EVs, at 47.9±1.2nm versus 62.8±2.1nm when measured by TEM, and 151.9±2.9nm versus 219.3±3.2nm by Nanosight NTA (Lefebvre *et al*., 2016). The difference in *Drosophila* EV size as determined by NTA may be partially reflective of reduced numbers of aggregates in EV samples purified by SEC rather than UC, but likely primarily due to differences in NTA technology, as in the limited experiments with Nanosight in this work, particle sizes were also found to be larger than by zetaview (Supplementary Figure 4). With the lower limit of NTA size quantification estimated to be about 41nm, these differences highlight that NTA is a relatively poor method for EV size comparison (Kestens *et al*., 2017). Thus, although stress was not observed to influence EV size measured by NTA, further imaging using the higher resolution of TEM will be needed to confirm this finding.

### 3.4.4 Storage of EVs at 4°C

Little is known about the effect of storage on EV stability and function. Previous work has suggested that EVs derived from endothelial colony forming cells and mesenchymal stem cells are stable for two days at 4°C, and three days for HEK cells (Sokolova *et al*., 2011). A study of neutrophilic granulocyte EVs saw no significant reduction in particle number or functional anti-bacterial activity over 7 days at 4°C (Lorincz *et al*., 2014), whilst EVs from Kaposi's sarcoma-associated herpesvirus-infected human endothelial cells stored at 4°C show similar biophysical properties to those at − 70°C for at least 8 days, and in the short time showed slightly higher functional activation of the complement system (Park *et al*., 2018). In this work, at 4°C S2R+ EVs

appeared to be stable over five days, based on concentration and size change, lying within the 2-8-day range reported for other cell lines. However, since much of EV function has been attributed to their cargo, further assessment of the stability of EV-cargo is required, which has had limited study. Park *et al.* assess the effect of storage conditions on mammalian EV markers CD63 and CD81, with storage at 4°C having no impact over the 25-day period. Therefore, although no tests on functional activity over time were carried out, the results seen in these other studies suggest that this short-term storage at 4°C was the best approach to maximising the likelihood of detecting differences in functional activity of normal and stress EVs in the next chapter.

## 3.5 KEY FINDINGS

- EVs can be purified from *Drosophila* S2R+ cell conditioned media by SEC.
- The tetraspanin Latebloomer is a specific marker of small EVs in *Drosophila*.
- UC EV-depletion of FBS does not remove small non-EV particles.
- Actin is present in FBS from both normal and EV-depleted FBS.
- $H_2O_2$ stress may increase the number of EVs produced, but does not alter size.

# Chapter 4

## Functional effects on recipient cells

# 4 Functional effects on recipient cells

## 4.1 BACKGROUND

### 4.1.1 Bystander effect

Direct exposure to stressors such as radiation causes injury to cells, but in 1992 it was suggested that damage-causing agents could be transmitted from irradiated cells to non-irradiated neighbouring cells, via the bystander effect (BE) (Nagasawa and Little, 1992). More recently this BE has been observed in cells exposed to heat (DeVeaux *et al*., 2006; Purschke *et al*., 2010) or genotoxic drugs such as bleomycin, neocarzinostatin (Chinnadurai *et al*., 2011), paclitaxel and vincristine (Alexandre *et al*., 2007), indicating that it may have more broad relevance to a wider range of cellular stressors. Various mechanisms have been suggested as mediators of BE. Gap junctions have been shown to have a role in the response to radiation (Azzam *et al*., 2001) and cisplatin (Arora, 2012), but this mechanism is cell-contact dependent. Radiation-induced BE was also shown to be inducible by filtered media transferred from directly exposed cells (Mothersill and Seymour, 1997), indicating a possible role for secreted agents. Production of ROS has been strongly implicated in the process, either by direct secretion or indirectly via effects such as heatshock protein production or oxidized extracellular DNA (Havaki *et al*., 2015). Recent research has also highlighted a role for EVs, as EVs isolated from conditioned media of irradiated MCF-7 cells were particularly potent in inducing DNA damage (Al-Mayah *et al*., 2012, 2015).

### 4.1.2 Adaptive effect

Prior to the discovery of the BE, an opposing adaptive response had been proposed in 1971, whereby the transfer of cell-conditioned media from normal stationary phase cells to irradiated cells increased their survival (Little, 1971). EVs have been implicated in this adaptive effect, showing proliferative or anti-apoptotic effects on directly stressed recipient cells, including in the context of oxidative stress (Atienzar-Aroca *et al*., 2016; Chen *et al*., 2013; Kore *et al*., 2018; Kucharzewska and Belting, 2013; Wang *et al*., 2015). However EVs derived from stressed cells

have been found to induce such effects over and above EVs derived from normal cells, indicating it may be a means by which a cell communicates its stress to neighbouring cells to better protect them against possible future stress (Eldh *et al*., 2010; Mutschelknaus *et al*., 2016; Bewicke-Copley *et al*., 2017).

## 4.2 AIMS AND OBJECTIVES

Although BE has been heavily studied from perspective of radiation and cytotoxic drug treatments, in the context of oxidative stress most studies have focused on adaptive effects (Eldh *et al*., 2010; Chen *et al*., 2013; Wang *et al*., 2015). In addition, very little is known about bystander and adaptive effects outside the mammalian environment. The aim of this chapter was therefore to investigate whether EVs derived from oxidatively stressed *Drosophila* S2R+ cells induce functional effects in normal recipient cells. Specifically, the objectives were to assess effect of EVs on:

1. Total cell viability
2. Cell death
3. DNA damage response

## 4.3 RESULTS

### 4.3.1 Stress EVs induce an increase in resazurin reduction in recipient cells

Having characterised the effect of oxidative stress on the biophysical characteristics of EVs, the next aim was to investigate whether stress altered the functional impacts of EVs on recipient cells. Since many studies have implicated effects of EVs on cell proliferation and viability, this was first investigated using the resazurin reduction viability assay. Given that stressed cells appeared to show some increase in particle number (Figure 3.9), to exclude this and identify whether the specific nature of the EVs was important, a set number of EVs were applied to recipient cells. Approximately 2000-4000 particles per viable cell were counted after 48 hours of conditioning time (Chapter 3), so fresh recipient cells were dosed with 4000 particles per

seeded cell as a starting point. Testing first with EVs derived from normal, non-stressed cells showed an increase in signal relative to no EV control after 24 hours, an effect which appeared somewhat dose-dependent, plateauing in significance at 16,000 particles per recipient cells (Figure 4.1A). With an appropriate dose range validated, EVs from both normal and high stress (2mM $H_2O_2$) were tested together, showing a similar dose-responsive effect with the normal EVs, but with no dose-effect for the stress EVs (Figure 4.1B). The stress EVs, however, induced their effect at a lower dose than the normal EVs, indicating that they may be more bioactive. Both experiments demonstrated a significant effect on assay signal with a dose of 16,000 particles per cell, so this was then taken forward as the main treatment dose for subsequent experiments. Testing of normal, low stress (0.5mM $H_2O_2$) and high stress (2mM $H_2O_2$) cell derived EVs from multiple independent purifications showed that the high stress EV treatment resulted in a significant increase in assay signal compared to normal EVs, whilst low stress EVs resulted in a non-significant increase (Figure 4.1C). This therefore indicated that $H_2O_2$, independently of any effect on the number of EVs produced, induced changes to EVs which influence their activity in recipient cells.

### 4.3.2 Three-hour EV treatment shows a trend towards reduced cell count

Given some studies have suggested EVs to mediate an adaptive effect on recipient cells (Eldh *et al*., 2010; Mutschelknaus *et al*., 2016; Bewicke-Copley *et al*., 2017), the effect of EV treatment on viability of $H_2O_2$ -stressed recipient cells was investigated. S2R+ cells were pre-treated with EVs for three hours before stress induction and subsequent incubation for a further 20 hours. However, this demonstrated no effect of the EVs on altering viability of stressed cells (Figure 4.2A). Furthermore, in non-stressed recipient cells, no effect of EV donor source was seen, indicating that the three-hour treatment was either not of sufficient length to induce an effect, that the effect was transient, or smaller, such that the assay was not sensitive enough to detect it. In parallel cell counting experiments, in non-stressed recipient cells, there was a non-

significant but downward trend in the relative viable cell number in all three independent experiments, while again no effect in stressed recipients could be seen (Figure 4.2B). This indicated that, whilst some changes in recipient cells were occurring at this earlier timepoint, other assays were necessary to elucidate the nature of those changes.

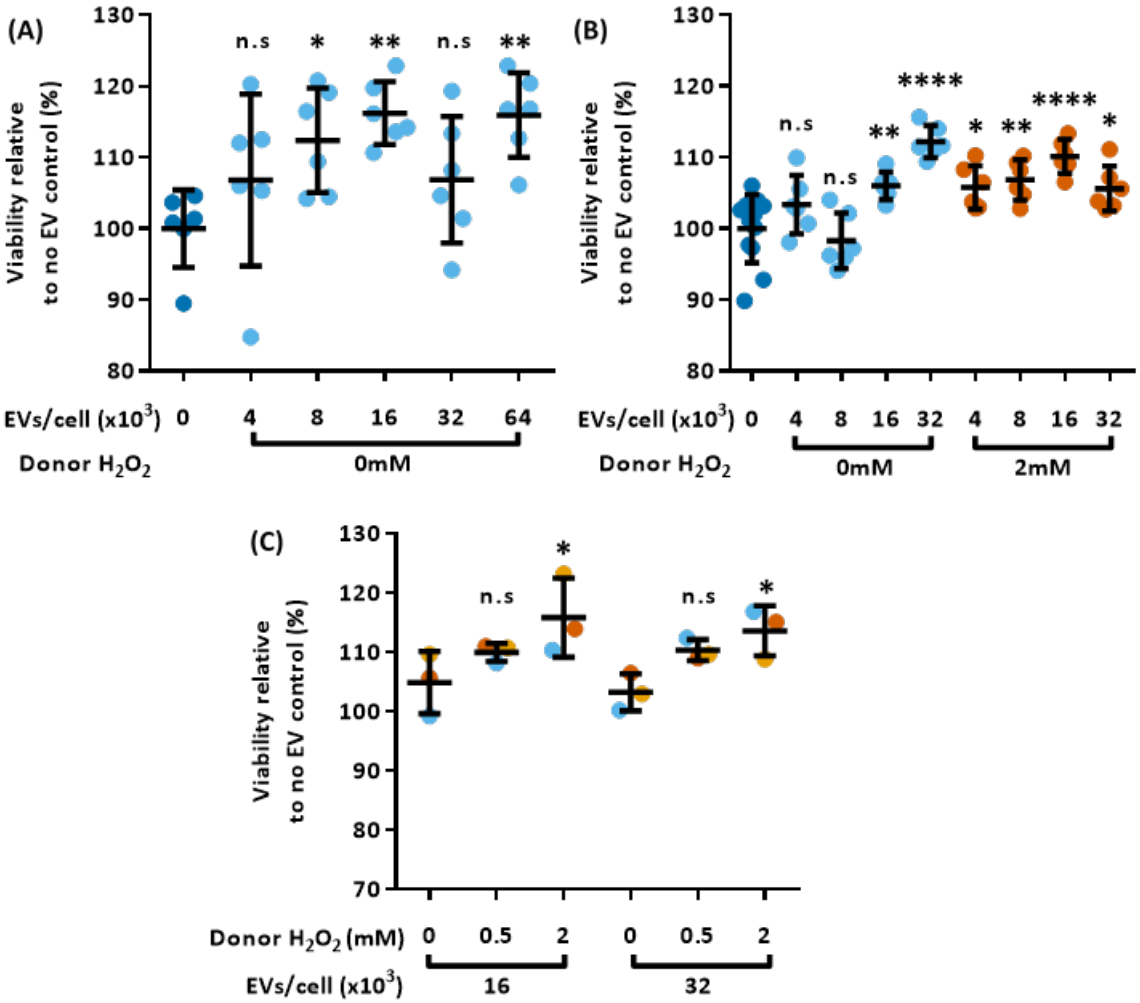


## Figure 4.1: Stress EVs increase signal in resazurin viability assay of recipient cells

*(A)-(C) Viability of S2R+ cells assessed using resazurin assay after 24 hours treatment with EVs derived from normal or $H_2O_2$ stressed donor cells. (A) Dose response for EVs from normal donor cells, showing mean and standard deviation of six technical replicates from one experiment. Statistical significance assessed by one-way ANOVA followed by Dunnett's multiple comparisons test. (B) Dose response for EVs from both normal and 2mM $H_2O_2$-stressed donor cells, showing mean and standard deviation of six technical replicates from one experiment. Statistical significance assessed by one-way ANOVA followed by Dunnett's multiple comparisons test. (C) Treatment with EVs from normal, 0.5mM and 2mM $H_2O_2$-stressed cells, showing the mean and standard deviation of three independent experiments, each independent experiment value the mean of six technical replicates. Statistical significance assessed by one-way ANOVA followed by Sidak's multiple comparisons test.*

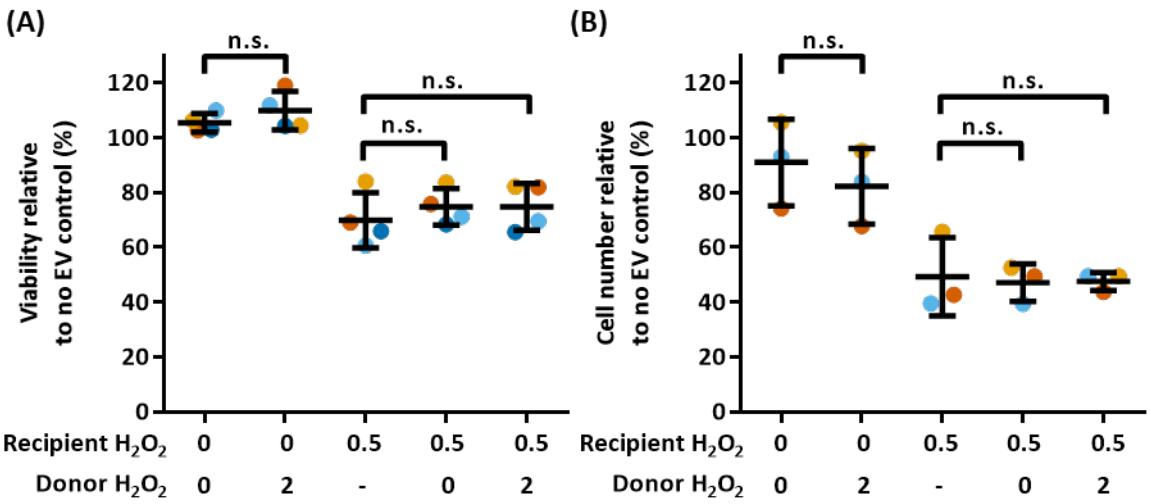


Figure 4.2: Three-hour EV treatment has no adaptive effect on recipient viability

*(A) Viability of S2R+ cells assessed using resazurin assay after 3-hour treatment with EVs derived from normal or 2mM $H_2O_2$-stressed cells, 1 hour direct 0.5mM $H_2O_2$ treatment, and 20-hour incubation in normal conditions. '–' represents no EV (PBS only) control. Graph shows the mean and standard from four independent experiments, each independent experiment value the mean of six technical replicates. (B) As for (A) but showing viable cell count as determined by trypan blue exclusion. Graph shows the mean and standard from three independent experiments, each independent experiment value the mean of three technical replicates. Each point normalised to the mean value of non-EV-treated control for that biological replicate. Statistical significance assessed by one-way ANOVA followed by Sidak's multiple comparisons test.*

### 4.3.3 EV treatment does not affect total mitotracker staining in recipient cells

Although utilised as a cytotoxicity or viability assay, the resazurin assay works by a colour change from blue resazurin to pink, fluorescent resorufin upon its reduction, and is thus a measure of overall reduction activity occurring within the cell population. As such, changes to assay signal could be representative of changes in cell number, either due to altered cell proliferation or cell death, or of changes to mitochondrial activity, which is believed to be the primary site of resazurin reduction. Active mitochondria maintain a highly polarised membrane, resulting in the accumulation and subsequent fluorescence of mitotracker orange dye. Therefore, staining intensity can be used as a readout of mitochondrial activity. Direct $H_2O_2$ treatment appeared to induce some decrease in the relative mitotracker staining intensity per cell, although this effect was not clearly dose-dependent as might be expected (Figure 4.3A). Upon EV treatment, given the increase in resazurin reduction, an increase in staining intensity was expected, but EVs derived from donor cells under either normal or stress conditions did not increase mitochondrial

activity at a three-hour treatment, showing no effect in one biological replicate, and a decrease in the other (Figure 4.3B). Whilst only representative of two independent biological replicates, this data indicates that EVs may not directly affect mitochondrial function, although it is also possible that quantification of total mitotracker fluorescence via immunocytochemistry may not be an appropriate assay method.

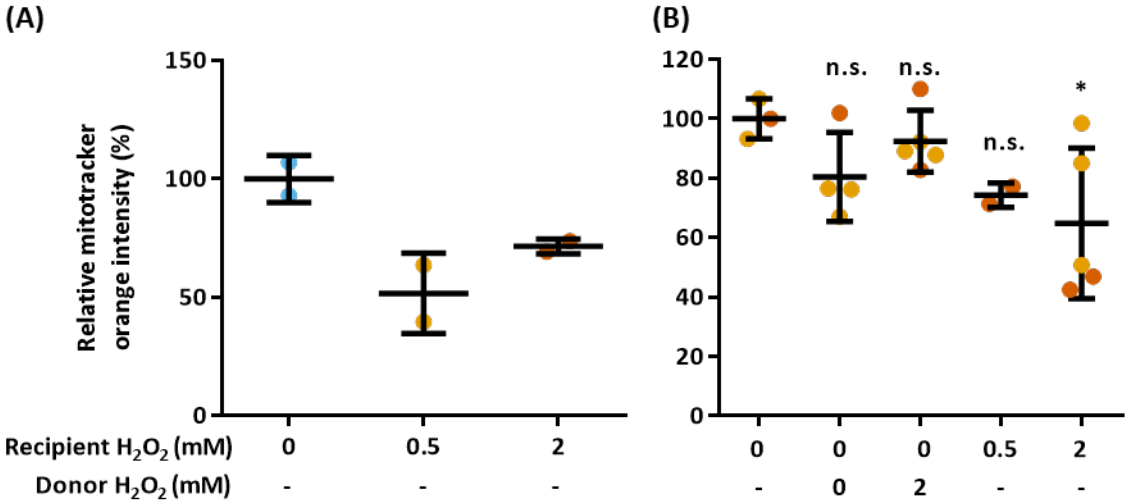


Figure 4.3: EVs have no effect on mitotracker orange staining in recipient cells

*(A) Quantification of mitotracker orange staining in direct $H_2O_2$ -stressed cells, showing mean and standard deviation for mean staining intensity of cells in two technical replicates of a single biological replicate. '–' represents no EV (PBS only) control. (B) Quantification of mitotracker staining in cells treated with EVs derived from normal or 2mM $H_2O_2$-stressed cells or direct $H_2O_2$ treatment. Graph shows mean and standard deviation for mean staining intensity of cells in 1-3 technical replicates of two independent experiments, technical replicates shown in yellow and orange. Statistical significance assessed with one-way ANOVA followed by Tukey's multiple comparisons test.*

### 4.3.4 Stress EVs may increase necroptotic cell death in recipient cells

Since EVs have been implicated in alterations to apoptotic responses, annexin V and propidium idiode (PI) flow cytometry was also used to further investigate effects of EVs on recipient cells. Although representative of only two independent biological replicates, these assays were carried out at three timepoints; 3-4 hours, 16 hours and 24 hours. At both 3-4 hours and 24 hours there was a decrease in the percentage of viable cells (annexin V and PI negative), and an increase in dead/dying (PI stained) cells that was only significant in high stress EV-treated cells relative to non-treated controls (Figure 4.4A, B). No difference in annexin V only staining was seen (Figure 4.4C), indicating that any effect was not through classical apoptotic pathways, but

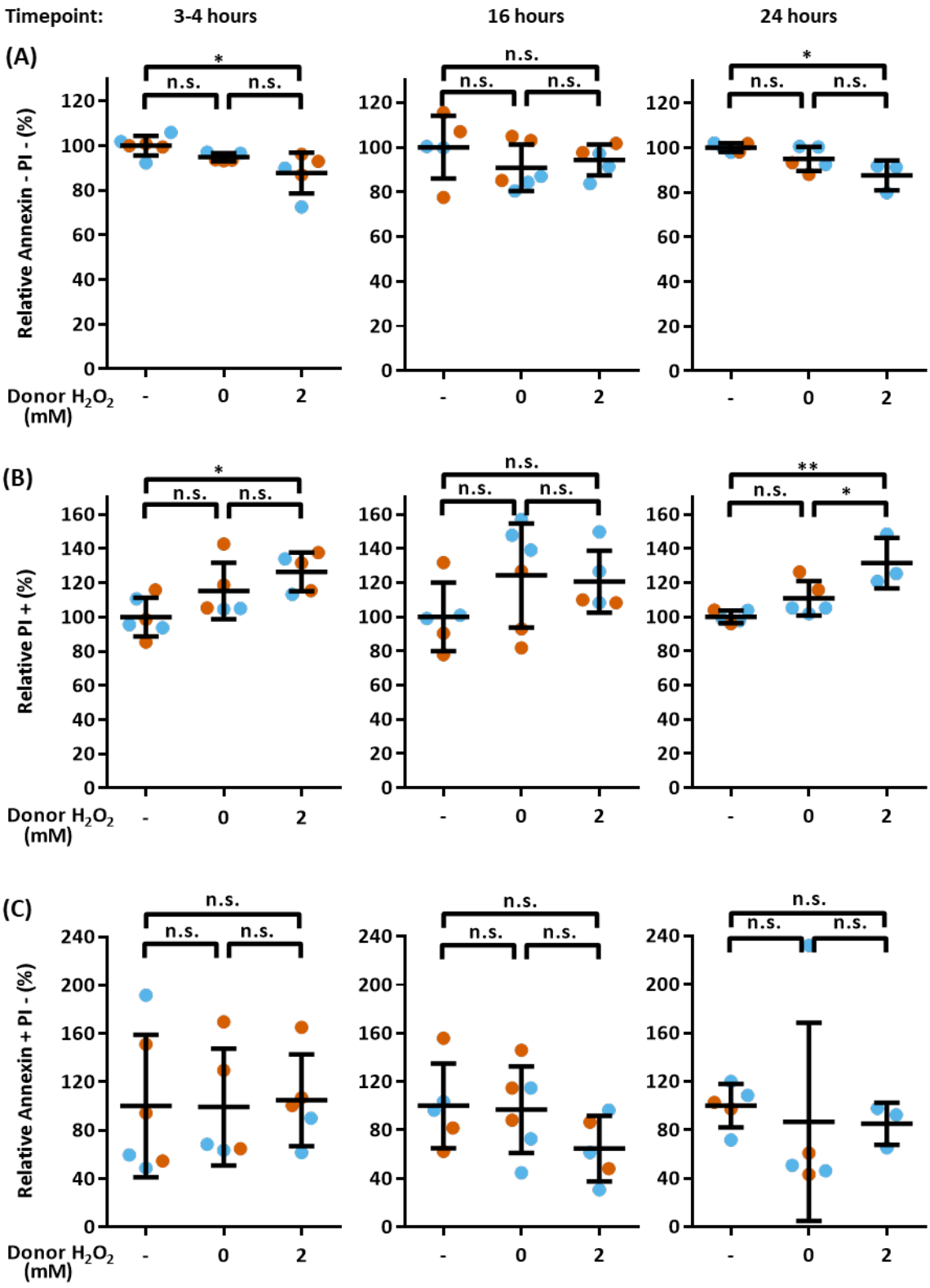


Figure 4.4: EV treatment increases propidium iodide staining in recipient cells

*(A)-(C) Flow cytometry of Annexin V and propidium iodide (PI) staining in live S2R+ cells after treatment with EVs derived from normal or 2mM $H_2O$-stressed donor cells. Results show percentages of total events across two independent experiments at three timepoints, 3-4 hours, 16 hours and 24 hours, with 2-3 technical replicates for each, shown in blue and orange. '–' represents no EV (PBS only) control. (A) Annexin negative, PI negative represent viable cells (B) combined PI positive stained events represent cell death, (C) Annexin positive PI negative represent early apoptosis. Statistical significance assessed with one-way ANOVA followed by Tukey's multiple comparisons test.*

rather through necroptosis. Although providing little explanation to previous results with resazurin assays, this data further supported the existence of some effect at the three-hour timepoint.

### 4.3.5 Stress EVs increase the variability of DNA damage response in recipient cells

Some studies have found that EV treatment may induce DNA damage (Al-Mayah *et al*., 2015; Xu *et al*., 2015; Bewicke-Copley *et al*., 2017) and yH2Ax phosphorylation as part of the DNA damage response (Dutta *et al*., 2014). Knowing that $H_2O_2$ treatment led to increased staining of the *Drosophila* counterpart, this assay was used to assess the effect of EVs at the three-hour timepoint. Results showed no significant effect of EVs derived under either normal or stress conditions (Figure 4.5A). However, what was evident was the increase in variability seen for biological replicates of stress EV treatments, with two replicates resulting in an increase in yH2Av and two resulting in decrease, whereas technical replicates tended to cluster very closely together (Figure 4.5B-E). It is possible that this difference in effect is related to the state of the recipient cell; since the baseline level was higher in both experiments where a decrease was seen; but it is also likely that this is impacted by the variability and purity of the EV preparations themselves.

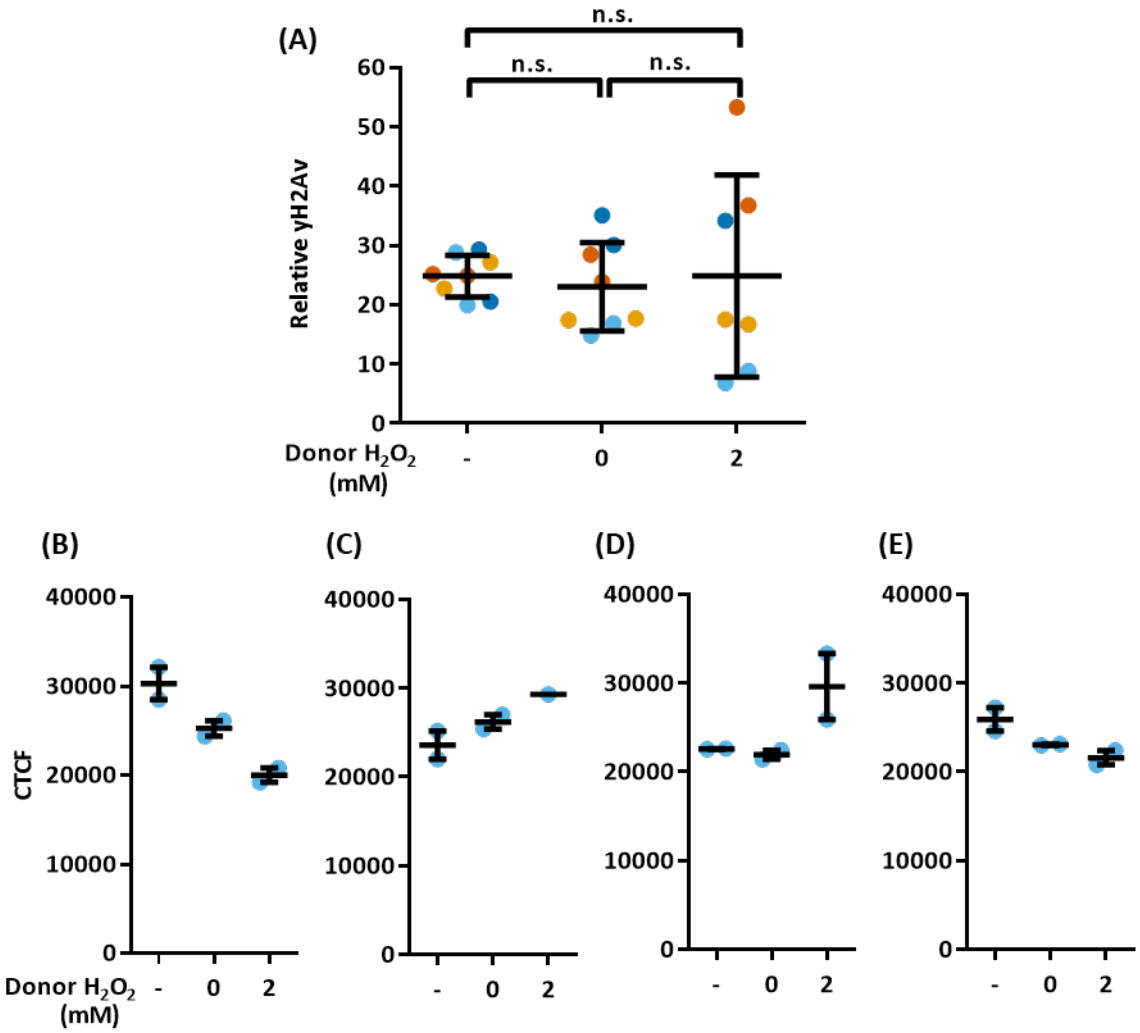


Figure 4.5: EV treatment increases variability of γH2Av staining in recipient cells

*(A)-(E) Quantification of γH2Av staining as indicator of DNA damage response in cells treated with EVs derived from normal or 2mM $H_2O_2$-stressed cells. (A) Graph shows mean and standard deviation of the percentage of cells showing staining intensity above 75% percentile of non-treated cells for two technical replicates of four independent experiments, technical replicates shown in yellow, orange, light blue and dark blue. '–' represents no EV (PBS only) control. Statistical significance assessed with one-way ANOVA followed by Tukey's multiple comparisons test. (B)-(E) Corrected total cell fluorescence for each independent experiment included in (A), each point represents median value for minimum 1300 cells.*

## 4.4 DISCUSSION

### 4.4.1 Use of resazurin reduction assay

The results in this chapter indicate that stress-cell-derived EVs do have some effect on recipient cells, likely increasing cell death via necroptosis. Initial results with the resazurin reduction assay indicated a significant effect of stress EVs on increasing cell viability, although subsequent follow-up assessments of cell number, death and mitochondrial activity indicate effects to be detrimental, calling into question the use of this assay. Numerous other studies have made use of similar multi-well colormetric or fluorescent assays such as tetrazolium MTT or MTS (Frühbeis *et al*., 2013; Eitan *et al*., 2015; Kore *et al*., 2018; Ma *et al*., 2018), and resazurin (Kumar Jella *et al*., 2014; Mutschelknaus *et al*., 2016) to show an effect of EVs on cell viability. EVs have been suggested to increase levels of ROS (Kumar Jella *et al*., 2014), so, since the resazurin assay is based on the reduction of blue resazurin to pink, fluorescent resorufin, these may interfere in the assay. However, the expected effect of any such interference would be a decrease in production of the fluorescent resorufin, not the increase that appears to have occurred.

The effects of stress-cell derived EVs seen in these cited studies vary, with EVs from cisplatin, heatshock and y-ray-treated cells found to reduce signal (Kumar Jella *et al*., 2014; Bewicke-Copley *et al*., 2017; Samuel *et al*., 2018), whilst Mutschelknaus *et al*. see an increase with y-rays, in line with the current data for $H_2O_2$. This indicates the possibility that different stressors may result in production of EVs which have very different effects on recipient cells. However, previous work has also suggested that an adaptive effect of EVs on direct $H_2O_2$ stress can be seen with a three hour EV incubation when using trypan blue exclusion of MC/9 mast cells, an effect that could not be observed with resazurin in S2R+ (Eldh *et al*., 2010). These differences further highlight the need to use more specific assays to elucidate which aspects of cell activity are affected.

### 4.4.2 Investigating mitochondrial activity in EV-treated cells

One avenue that was investigated was whether stress EVs had an impact on mitochondrial activity, but assays of total mitotracker staining showed no differences. Several studies have shown an effect of EVs on mitochondrial activity using alternative assays, for example the Seahorse XF Cell Mito Stress Test which is able to provide a measure of oxygen consumption under different conditions. In EV-treated mouse neuronal HT-22 cells, CTLL2 T-cells and human macrophages, EV-treated cells showed increased oxygen consumption (Phinney *et al*., 2015; Bland *et al*., 2018; Russell *et al*., 2019), whilst in C2C12 myotubes, EVs can rescue $H_2O_2$-induced decreases in capacity (Shuler *et al*., 2020). In the study by Russell *et al.*, despite increased oxygen consumption, no changes in membrane potential were observed, which is in line with the result seen here using mitotracker orange. Therefore, it is likely that the stress derived EVs may have effects on mitochondrial activity that were not measured in the mitotracker assay.

An additional area which could be explored is the effect of EVs on mitochondrial morphology, since stress is known to induce a shift from a tubular network of mitochondria to a more fragmented form (Fan *et al*., 2010). Some attempt was made to quantify punctate staining of the mitotracker orange-stained cells in a single replicate (data not shown), which indicated that EVs might have some effect on promoting a tubular morphology, in agreement with data in an ischemia reperfusion injury model in renal tubular epithelial cells (Gu *et al*., 2016).

### 4.4.3 Investigating cell death in EV-treated cells

In initial assays, annexin V and propidium iodide (PI) flow cytometry indicated an increased level of cell death, with higher relative PI-stained events at two timepoints, but no increase in annexin only stained events. In MCF-7, K562 and HeLa cells, EVs from heatshocked cells caused increased apoptosis, assayed by scoring the percentage of cells displaying fragmented nuclei (Bewicke-Copley *et al*., 2017). Several studies have implicated EVs as triggers for cell death, by transport of apoptosis-inducing ligands including TRAIL, Fas ligand and TNFα, particularly in an immune

context (Huber *et al*., 2005; Jeong *et al*., 2005; Tavakkoli *et al*., 2020). However, if cell death were occurring by apoptosis, the increase in PI staining at the early 3-4 hour timepoint would not be expected. In contrast, LDH release, an indicator of necrotic cell death, is detectable at two hours after $H_2O_2$ treatment, so the increase in PI staining at the early timepoint may indicate induction of necrosis by EVs (Helm *et al*., 2017). An increase in necroptosis, alongside apoptosis, was also indicated by work on 4T1 breast cancer cells treated with EL4 T-cell-line-derived EVs, in line with the data in S2R+ (Tavakkoli *et al*., 2020). Of particular interest, these increases in cell death were not seen with T41-cell-derived EVs, indicating that effects on recipients are likely dependent on the cell type, and the specificity of the EV cargo.

### 4.4.4 Investigating DNA damage response in EV-treated cells

Using induction of H2Av phosphorylation for assessment of DNA damage showed that there was no significant effect of either normal or stress EVs compared to no EV control. However, what was clearly evident was the increase in variability between biological, and not technical replicates. Phosphorylation of yH2Av induction is a rapid process, in one study of γ-irradiation occurring in just five minutes and returning to baseline in three hours (Madigan, 2002). However, for effects mediated by EVs, which may be reliant on EV uptake and cargo delivery, it could take significantly longer to induce an effect. EVs have been reported to be internalised within 10 minutes, although this increases over several hours, so, depending on the mechanisms of uptake, effects might be expected over a broad timeframe (Tian *et al*., 2014; Heusermann *et al*., 2016). Variation in the rate of uptake and delivery, possibly depending on the specific stress state of the cells, may be one explanation for the variability in yH2Av seen. Cells with yH2Av induction may also be those undergoing rapid cell death, so it may be that DNA damage was not detected successfully. Therefore, carrying out the same assay over a time course, including both shorter and longer timepoints, is likely to be informative.

### 4.4.5 Dosage and purity of EV preparations

In this work, the experimental design involved a set dosage of EVs in order to control for the effect of stress on increasing EV production. Given an approximate overnight doubling time of the S2R+ cell line, the 16,000 particles per seeded cell dose corresponds to around 2.5x equivalent of EVs. Given the unknown loss of EVs as a result of preparation, e.g. sticking to pipette tips and other plastics, this is within the range seen in the literature, in which a wide range of doses are used to see an effect, ranging through 1.7x dose (Eldh *et al*., 2010), 3x dose (Mutschelknaus *et al*., 2016), 10x (Samuel *et al*., 2018) to $1.5x10^7$ EVs per cell (de Jong *et al*., 2020). Although the numbers used by de Jong *et al.* are high, this is representative of repeated doses over a 10-day period, which may be more physiological than the single bolus approach taken here and in other studies. Therefore, additional work could involve continual dosing of recipient cells with low doses of EVs, which may be more likely to elicit measurable effects.

An additional factor to consider was that, due to the presence of FBS in the culture media, EV preparations also contained some quantity of small bovine-derived particles which, although likely not classical EVs, were quantifiable by NTA and may contain actin (Chapter 3). Whilst, on average, conditioned media contained 3x more particles than NCM, this was highly variable (Chapter 3). As a result, although particle number was normalised, each replicate may contain differing amounts of cell-derived EVs, and functional effects vary accordingly. Nevertheless, whilst the magnitude of the effect might thus differ between replicates, the trend between treatment groups would likely stay the same; a feature reflected in the data here. One approach that was considered to circumvent this problem was background correction against NTA counts in NCM controls. However, these bovine particles would likely also be internalised to some extent during cell incubation, and have previously been shown to affect cell proliferation, so may have introduced additional variability (Eitan *et al*., 2015). In addition, other cell-derived soluble factors might also be responsible for these effects, which would require more stringent purification procedures to rule out.

## 4.5 KEY FINDINGS

- The resazurin reduction assay is not a good technique for assessing functional effects of EVs on recipient cells.
- NTA-based EV normalisation is inappropriate when FBS is used in cell culture media.
- Stress EVs may act to increase DNA damage and necroptotic cell death in recipient cells.

# Chapter 5

## Profiling of EV and cell RNA

# 5 Profiling of EV and cell RNA

## 5.1 BACKGROUND

### 5.1.1 RNA in EVs

The discovery that EVs can contain RNAs contributed to an explosion in the study of EV-mediated intercellular communication (Baj-Krzyworzeka *et al*., 2006; Ratajczak *et al*., 2006; Valadi *et al*., 2007; Skog *et al*., 2008). These early studies demonstrated the presence of a range of mRNAs and microRNAs, whilst detection of tumour-specific RNAs indicated a potential novel source of disease biomarkers (Skog *et al*., 2008). In addition to this diagnostic use, these mRNAs were shown to be translatable, and thus likely functional, in cells treated with exogenous EVs (Valadi *et al*., 2007). Additional work implicated functional effects on cellular proliferation and viability as being mediated specifically by the RNA, indicating a wider importance in intercellular communication in other contexts (Ratajczak *et al*., 2006; Eldh *et al*., 2010).

Subsequent work has shown EVs to contain an even broader range of RNAs, including non-coding RNA types such as snoRNA, snRNA, lncRNA, vault RNA, Y-RNA, tRNA and rRNA, or fragments thereof, as outlined in section 1.2 (Nolte-'t Hoen *et al*., 2012; Jenjaroenpun *et al*., 2013; Kogure *et al*., 2013). Some evidence also suggests that these RNA types are functional in recipient cells (Rimer *et al*., 2018; Cooke *et al*., 2019). Alongside mammalian systems, RNAs have been demonstrated to be present in EVs of other organisms including bacteria (Sjöström *et al*., 2015), fungi (Da Silva *et al*., 2015), insects (Lefebvre *et al*., 2016) and plants (Baldrich *et al*., 2019), suggesting a conserved role, but the biological significance in these organisms remains poorly understood. Greater study is therefore needed to understand the range of cargo and how it is packaged, particularly across a wider range of organisms.

### 5.1.2 RNA loading into EVs

Alongside demonstrating the presence of RNA, the early seminal studies highlighted that correlation between RNA abundance in EVs and in their parental cells was poor, raising the possibility that some are specifically loaded (Valadi *et al*., 2007; Skog *et al*., 2008). MiRNAs have become the most studied RNA cargo of EVs, and consequently the focus of most work on RNA packaging. Several mechanisms, including non-templated RNA modifications, specific sequence motifs and structure, and association with a range of RNA-binding proteins have been elucidated (Villarroya-Beltri *et al*., 2013; Koppers-Lalic *et al*., 2014; Cha *et al*., 2015; Hagiwara *et al*., 2015; Shurtleff *et al*., 2016; Iavello *et al*., 2016; McKenzie *et al*., 2016; Mukherjee *et al*., 2016; Santangelo *et al*., 2016; Statello *et al*., 2018; Temoche-Diaz *et al*., 2019; Ghoshal *et al*., 2019; Barman *et al*., 2020; Wozniak *et al*., 2020; Leidal *et al*., 2020). Some study of incorporation of other RNA types has been carried out, on mRNA (Batagov *et al*., 2011; Bolukbasi *et al*., 2012; Kossinova *et al*., 2017; Leidal *et al*., 2020), tRNA (Tosar *et al*., 2015; Shurtleff *et al*., 2017; Gámbaro *et al*., 2019; Barman *et al*., 2020), Y-RNA (Shurtleff *et al*., 2017) and snoRNA (Barman *et al*., 2020; Leidal *et al*., 2020). These RNA biotypes are likely to have at least as much functional importance as miRNA, so further exploration into their EV association is greatly needed.

### 5.1.3 Effect of stress on RNA in EVs

A change in environmental conditions, such as the application of exogenous stressors like radiation or heatshock, may result in changes to RNA abundance due to transcription, processing or degradation of the RNA. Changes to RNA content of EVs has been reported in response to multiple different stressors including radiation (Arscott *et al*., 2013; Xu *et al*., 2015), oxidative stress (Eldh *et al*., 2010; Atienzar-Aroca *et al*., 2016) and hypoxia (de Jong *et al*., 2012; Kucharzewska *et al*., 2013). Several studies have also suggested, through ultraviolet or RNase treatment to inactivate the RNA, that these changes in cargo are specifically responsible for mediating functional effects on recipient cells (Eldh *et al*., 2010; Al-Mayah *et al*., 2012). However,

in many cases these changes in EV RNA content simply reflect changes in cellular abundance, so whether the induction of stress alters the underlying mechanisms of EV biogenesis and cargo loading is an open question.

## 5.2 AIMS AND OBJECTIVES

As discussed in section 1.1.4, the RNA cargo of EVs may be of relevance both in intercellular communication, such as by translation of delivered mRNA, activation of signalling receptors, or inhibitory binding by miRNAs, or as unwanted cellular material expelled from the producing cell. Characterising the content of EVs under different cellular conditions will therefore aid in the understanding of the specificity of EV cargo, and thus enable us to gain insights both into the basic mechanisms which govern EV biogenesis, and to the potential mechanisms of function of EVs in recipient cells. The aims of this chapter were therefore to:

1. Analyse how oxidative stress affects RNA content of EVs derived from *Drosophila* cells.
2. Compare EV to cellular RNA to explore mechanisms of EV RNA loading.
3. Identify candidate RNAs which may mediate stress response in recipient cells.

## 5.3 RESULTS

### 5.3.1 RNA in EV preparations is enriched over non-conditioned media

With an established method for purifying EVs from *Drosophila* cells under different stress conditions (chapter 3), total RNA was then extracted from EV preparations. Use of the Nanodrop for quantification indicated that S2 cells yielded 5.8x more EV-associated RNA than NCM, compared to only 1.8x more for S2R+ cells (Figure 5.1A). However, the nanodrop is known to perform poorly at low concentrations, where contaminants may have a significant impact on quantification. Quantification by Qubit, which relies on specific fluorescent dye incorporation, rather than absorbance, indicated much higher enrichment of up to 17-fold in the S2R+ cells. This enrichment of RNA was much higher than the 2.6-fold seen for particles (Figure 3.5B),

indicating that, despite some contamination of the EV preparations with bovine-derived particles, background was reduced when considering the RNA. Yield of RNA in the S2R+ cell line EVs was between 10-40 ng/µl, giving 250ng-1µg total RNA, thus suitable for downstream analysis with RNA sequencing. No difference in RNA content was seen between stress conditions in S2R+ EVs, either in total or after normalisation of RNA to particle number (Figure 5.1B), indicating that there was no effect of stress on the bulk amount of EV-associated RNA.

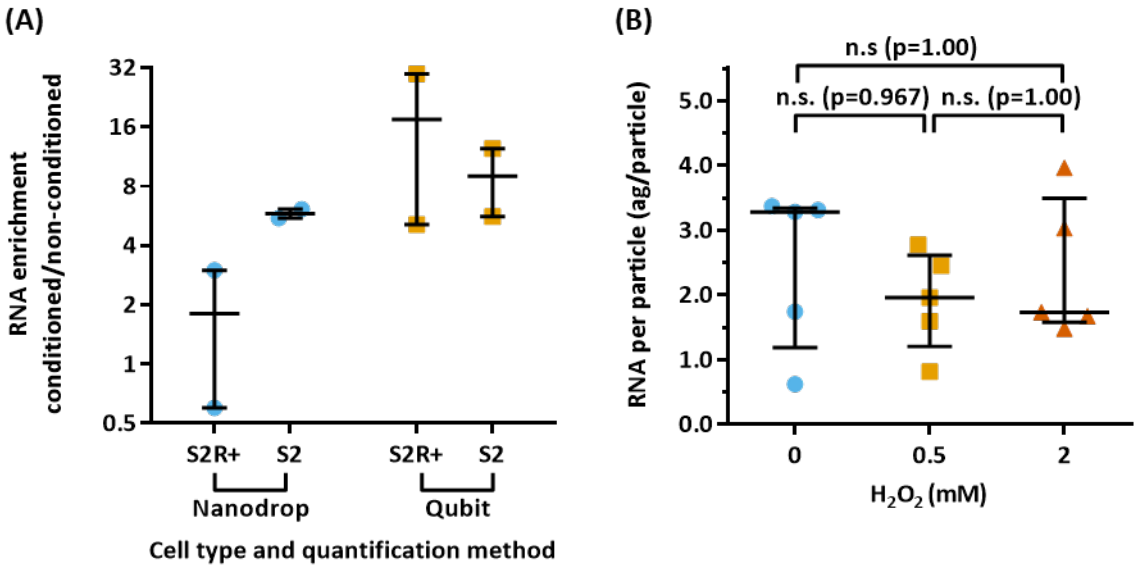


Figure 5.1: RNA is extracted from EV preparations with yield unaltered by stress

*(A) Total RNA extracted from SEC-purified EVs from media conditioned for 48 hours by S2 or S2R+ cells, expressed relative to matched media control. RNA was quantified by either Nanodrop or Qubit HS RNA kit. (B) RNA yield (attograms per particle) from S2R+ EVs after normalisation to particle count of sample using NTA. Graphs show median and (inter)quartile range, and statistical significance assessed with Kruskal-Wallis test followed by Dunn's multiple comparisons test.*

### 5.3.2 EV-associated RNA is predominantly small RNA

Further electrophoretic analysis of RNA extracted from S2R+ EVs and parental cells using agilent bioanalyser indicated that EV-associated RNA lacked the dominant ribosomal peaks seen in cellular RNA, and was instead highly enriched for RNAs between 25 and 200nt, regardless of stress treatment (Figure 5.2 and Supplementary Figure 5). The peaks shown in traces also indicated a broader range of small RNA sizes than seen in cellular RNA, which may represent either small RNA species, or fragments of longer RNAs. These results are consistent with the size range expected for exosomal, rather than MV or AB-associated RNA.

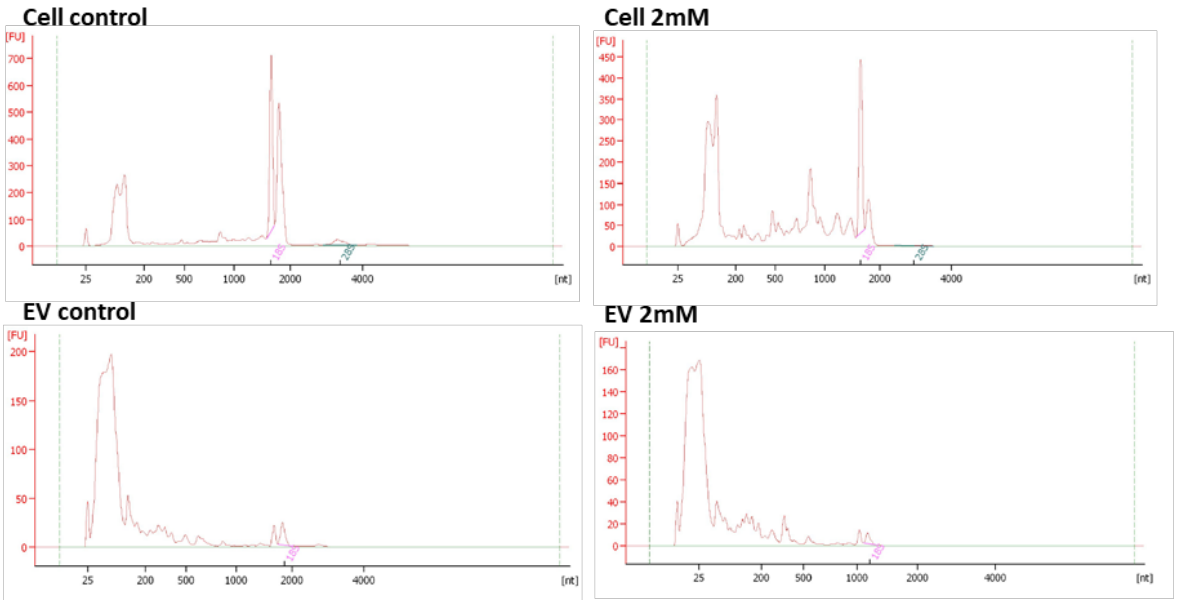


Figure 5.2: Small and/or fragmented RNA are predominant in EV samples

*Example traces from Agilent bioanalyser using RNA Nano Chip. Data provided by Liverpool Centre for Genomic Research (all traces shown in Supplementary Figure 5).*

### 5.3.3 Ribosomal RNA is the predominant species in EV-associated RNA

Next, paired end RNA sequencing was carried out on triplicate samples of RNA derived from control, 0.5mM and 2mM $H_2O_2$-stressed EVs and parental cells. No selection or depletion procedures were performed on EV samples, whilst parental cell RNA was ribo-depleted prior to library preparation. Quality control indicated that the sequencing was of good quality, although with warnings raised for sequence duplication and overrepresented sequences (Supplementary Figure 6). Initial mapping to the *Drosophila* genome showed low overall alignments, including for cellular RNA samples. BLAST searches of unmapped reads indicated that these reads constituted rRNA, transposon RNA and several viral species, including *Drosophila melanogaster totivirus SW-2009a* (DTV) and *Flock House Virus* (FHV). As a result, analysis was repeated with the aim of identifying all reads within the data, by iterative mapping to all *Drosophila* rRNA sequences, then transposon and repeat sequences, and then to the *Drosophila* genome. Following genome alignment, the remaining reads were mapped to a bovine genome and two

viral sequence files (one DTV, and the second all sequences for the *alphanodavirus* genus that includes FHV). Cumulatively, this mapping approach identified at least 98% of total reads in all EV samples, and at least 94% in all cell samples (Supplementary Figure 7). The EV-associated RNA was predominantly ribosomal under all conditions, at over 80% for all individual samples, with the next abundant group either *alphanodavirus* or RNA mapping to the *Drosophila* genome (Figure 5.3). These data were broadly similar to EVs of the same S2R+ cell line in Lefebvre *et al.* (2016), indicating suitability for further analysis and interrogation of differences induced by cellular stress (Supplementary Figure 8).

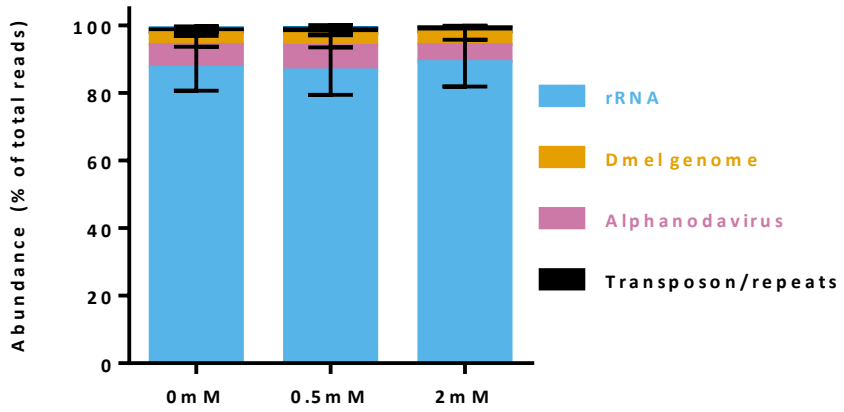


Figure 5.3: Alignment statistics for all EV samples

*Percentage of paired reads aligning to each type, relative to all sequenced reads.*

### 5.3.4 Ribosomal RNA maps almost exclusively to 28 and 18S subunits

Ribosomal RNA (rRNA) is expected to be the most abundant RNA biotype within cells, but, although direct comparison of EV and cell was not possible due to cell sample ribo-depletion, EV rRNA seemed overrepresented, constituting up to 94% of total reads (Figure 5.3). EV-associated rRNA has been little studied, although is known to be highly abundant (Jenjaroenpun *et al*., 2013; Wei *et al*., 2017), so read distribution analysis was carried out. This indicated that 96-99% of the rRNA mapped to 28S or 18S RNAs, with a small fraction to 5.8S (Figure 5.4A), identified in further analysis to map most closely to an rRNA pseudogene. The absence of 2S, 5S and 5.8S rRNAs is likely due to their small sizes at 30, 135 and 123nts, which have not been captured in

this dataset. Under $H_2O_2$ stress, there was a significant alteration in the relative content of 18S and 28S rRNA, with 18S rRNA increasing in abundance. Visualising the position of these reads using the Integrative Genome Viewer (IGV) showed multiple distinct peaks across the length of the 18S rRNA in particular (Figure 5.4B). However, to investigate whether these peaks have biological relevance requires comparison to non-ribo-depleted cellular rRNA.

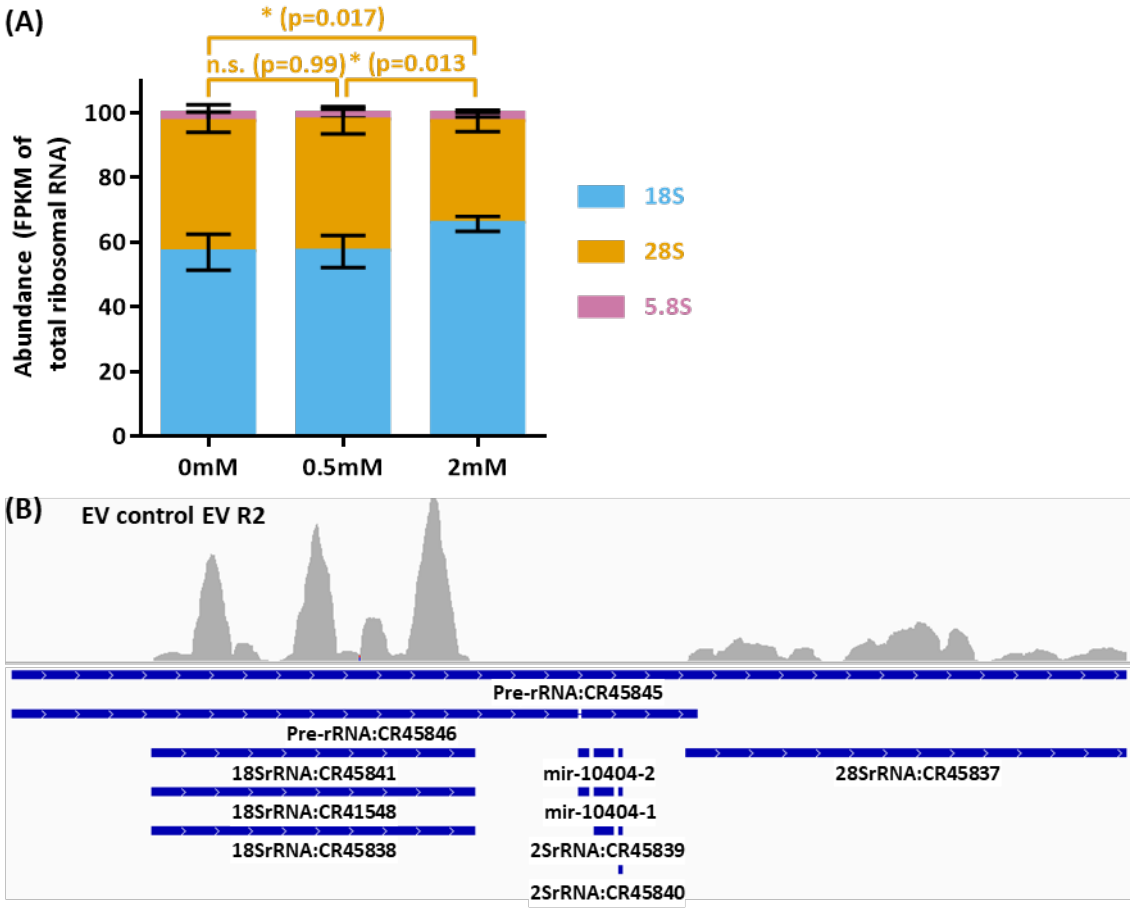


Figure 5.4: Ribosomal RNA reads align to both 18S and 28S rRNAs

*(A) Percentage of paired reads mapping to each ribosomal RNA. Statistical significance assessed with two-way ANOVA followed by Sidak's multiple comparisons test. (B) Screenshots of read distribution along CR45845 ribosomal locus on Integrative Genome Viewer.*

### 5.3.5 The Copia retrotransposon is abundant and enriched in EV-associated RNA

Previous work has indicated that repeat sequences and retrotransposons, such as *Copia* and *TART*, are enriched in EV RNA of *Drosophila* cells (Lefebvre *et al*., 2016; Ashley *et al*., 2018), so this was also investigated in the data under $H_2O_2$ stress conditions. To normalise for the ribo-

depletion carried out in cells, abundance was expressed as a percentage of non-ribosomal mapped *Drosophila* reads. Repeat sequences were found to be enriched in EVs relative to cells, but due to variability between biological replicates, this difference was only significant when pooling all stress conditions together (Figure 5.5A). EV abundance was at an average of 26±6.6%, lower than the 68±3.7% reported by Lefebvre *et al.* The *Copia* retrotransposon, which has been shown to be around 30-fold enriched in S2 cells, was then specifically investigated (Ashley *et al*., 2018), with analysis confirming *Copia* to be highly abundant at up to 86% of total repeat sequences. However, although significantly enriched in EVs under all conditions, the change was at a maximum of 2.6-fold and was not altered by stress (Figure 5.5B). These data further confirm *Copia* enrichment in EV-associated RNA and may indicate that it is specifically packaged.

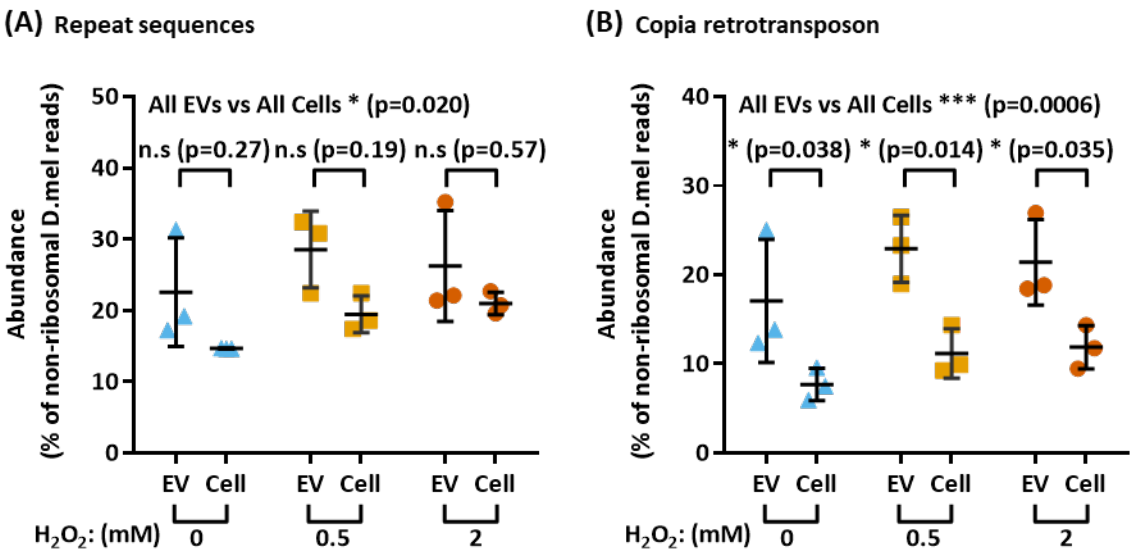


Figure 5.5: *Copia* retrotransposon is enriched in EV samples

*A) Combined percentage of paired reads aligning to Flybase transposon sequences and repeat masked sequences from UCSC Genome Browser for* Drosophila melanogaster*, after removal of ribosomal reads. (B) Percentage of paired reads mapping specifically to* Copia *retrotransposon. Graphs show mean and standard deviation of three biological replicates, and statistical significance assessed with two-way ANOVA followed by Sidak's multiple comparisons test.*

### 5.3.6 EV-associated RNA contains minimal bovine contamination

After mapping to rRNA, repeat sequences, and the *Drosophila* genome, unaligned reads were mapped against the bovine genome to check for contamination. This revealed that EVs

contained little bovine RNA, in fact less than in the parental cell RNA, although this difference was largely driven by two of nine cell samples (Figure 5.6). Whilst it is possible that some reads mapped to *Drosophila* may also map to the bovine reference, it can be concluded that there is minimal bovine-specific RNA present in the EV-RNA samples purified by SEC.

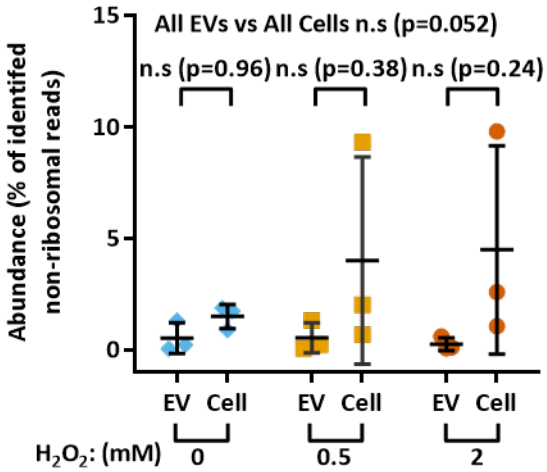


Figure 5.6: Bovine-specific RNA contamination is low in EV samples

*Percentage of paired reads aligning to bovine (bosTau8) genome after removal of ribosomal reads. Graph shows mean and standard deviation of three biological replicates, and statistical significance assessed with two-way ANOVA followed by Sidak's multiple comparisons test.*

.

### 5.3.7 Viral RNAs are differentially enriched in EV-associated RNA relative to cell

In addition to bovine RNA, a large proportion of non-*Drosophila* reads mapped to known viral sequences. Firstly, *Drosophila melanogaster totivirus* (DTV), a double-stranded RNA virus with a non-enveloped two-protein icosahedral virion of around 40nm. DTV reads made up ~1-2% of non-ribosomal reads in EV samples and were significantly depleted relative to cell samples, which contained up to 17% (Figure 5.7A). Secondly, several related members of the *alphanodavirus* genus, positive single-stranded RNA viruses with a non-enveloped three-protein icosahedral virion of around 30nm. These *alphanodavirus* reads were highly abundant in EVs, contributing up to 47% of non-ribosomal reads, and enriched relative to cells (Figure 5.7B). For both viruses, the variation between replicates was high, so no stress differences were evident.

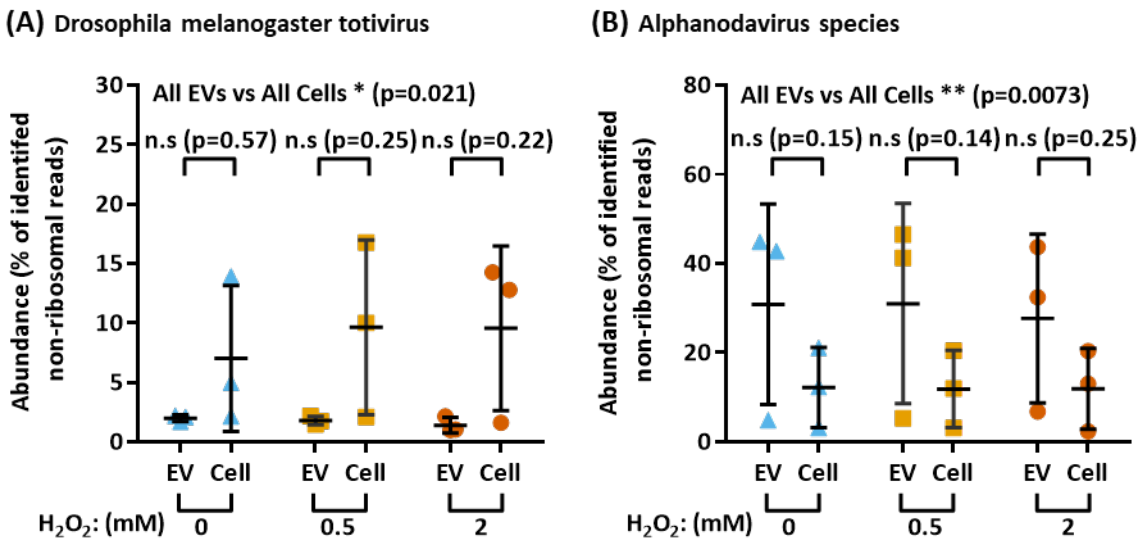


Figure 5.7: RNA of viral species is differentially enriched in EVs

*(A) Percentage of paired reads aligning to* Drosophila melanogaster totivirus *after removal of ribosomal reads. (B) Percentage of paired reads aligning to viral species in the* alphanodavirus *genus;* Flock house virus, Boolarra virus *and* black beetle virus. *Graphs show mean and standard deviation of three biological replicates and statistical significance assessed with two-way ANOVA followed by Sidak's multiple comparisons test.*

### 5.3.8 Altered gene expression confirms induction of stress in $H_2O_2$-treated cells

To investigate the effect of $H_2O_2$-induced stress on the genome mapping portion of RNA, the impact of the stress on the parental cells was first validated. Differential expression analysis found 177 RNAs with significantly altered expression under low stress conditions, rising to 854 under high stress, the majority (59% in high stress, 83% in low stress) comprising upregulation (Figure 5.8A). Gene ontology (GO) analysis of the upregulated genes returned a range of altered functions, including “response to stimulus” and “response to stress” (Figure 5.8B). These terms were more enriched under the high stress conditions, validating the dose-responsive induction of stress. Specific RNAs which were highly altered included *Gyc89Db*, encoding an oxygen-sensitive soluble guanylyl cyclase involved in response to hyperoxia and hypoxia, *Mmp1*, which has been used as a reporter of activation of the JNK stress response pathway, and a wide range of DNA damage response proteins (Figure 5.8C). Additionally, in the high stress conditions, RNAs such as *Sirup* and *SNF4Aγ*, which are involved in starvation response, were altered. These results together confirmed the induction of cellular stress in $H_2O_2$-treated cells.

(A)

| Condition | Number of altered genes | | |
|---|---|---|---|
| | Upregulated | Downregulated | Total |
| 0.5mM | 147 | 30 | 177 |
| 2mM | 504 | 350 | 854 |

(B)

| GO Term ID | Term source | Term name | Adjusted P-value | |
|---|---|---|---|---|
| | | | 0.5mM | 2mM |
| GO:0009888 | GO:BP | tissue development | 2.1E-06 | 1.5E-12 |
| GO:0008038 | GO:BP | neuron recognition | 2.1E-06 | 8.6E-08 |
| GO:0008037 | GO:BP | cell recognition | 2.3E-06 | 3.6E-08 |
| GO:0050896 | GO:BP | response to stimulus | 6.2E-06 | 1.2E-12 |
| GO:0006950 | GO:BP | response to stress | 1.1E-05 | 4.8E-09 |
| GO:0032989 | GO:BP | cellular component morphogenesis | 1.5E-05 | 1.7E-09 |
| GO:0007444 | GO:BP | imaginal disc development | 2.4E-05 | 1.5E-08 |
| GO:0016203 | GO:BP | muscle attachment | 2.8E-05 | 3.3E-05 |
| GO:0060429 | GO:BP | epithelium development | 3.4E-05 | 1.4E-10 |
| GO:0048513 | GO:BP | animal organ development | 4.0E-05 | 4.2E-10 |

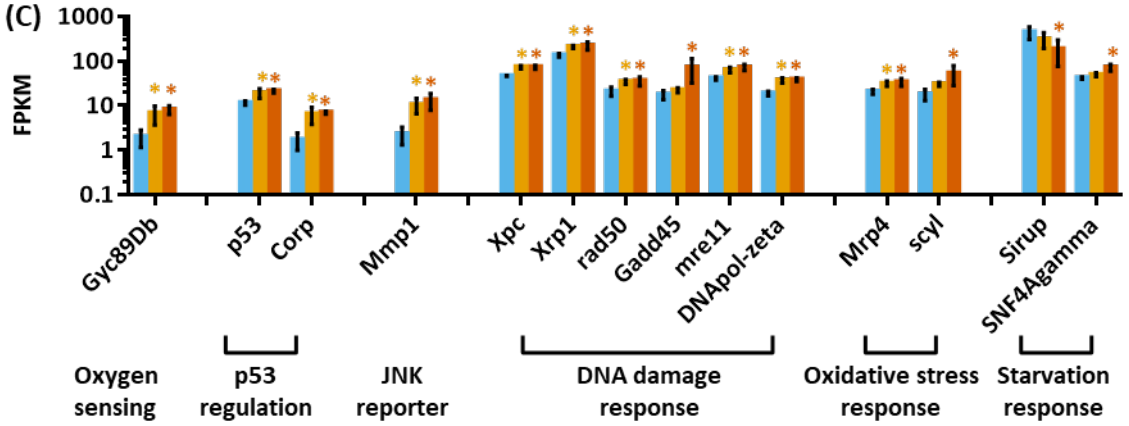


Figure 5.8: Differential expression confirms stress induction in $H_2O_2$-treated cells

*(A) All RNAs significantly altered in cells after treatment with 0.5 or 2mM $H_2O_2$. Differential expression determined by DESEQ2 with P-adj at 0.05. (B) Gene ontology analysis of 147 and 504 RNAs significantly upregulated in cells treated with 0.5 or 2mM $H_2O_2$ respectively, against a background of all annotated RNAs listed in Cufflinks file. Multiple testing correction by Benjamini-Hochberg false discovery rate with a cut-off at P-adj<0.001. (C) FPKM values for selected RNAs showing changes in expression.*

### 5.3.9 Expression of EV biogenesis components are altered under stress

In addition to confirmation of stress induction, since some evidence indicated an increase in EV release, cell data were also analysed for altered expression of genes involved in EV biogenesis (Figure 5.9). These results indicated that, of the *Drosophila* tetraspanins, *Tsp42Ed* (for which the closest mammalian ortholog is the EV marker CD63) was significantly altered under both levels

of stress. Of known genes involved in EV biogenesis, several ESCRT-III components (*Chmp1, Vps24, Vps60* and *CG5498*) were downregulated, reaching significance under the high stress conditions. In addition, Vps28, a component of the ESCRT-1 complex, was also significantly altered. Given that EV release appears to be increased under stress (Chapter 3), it is possible that these components are particularly important in regulating EV biogenesis under different physiological conditions.

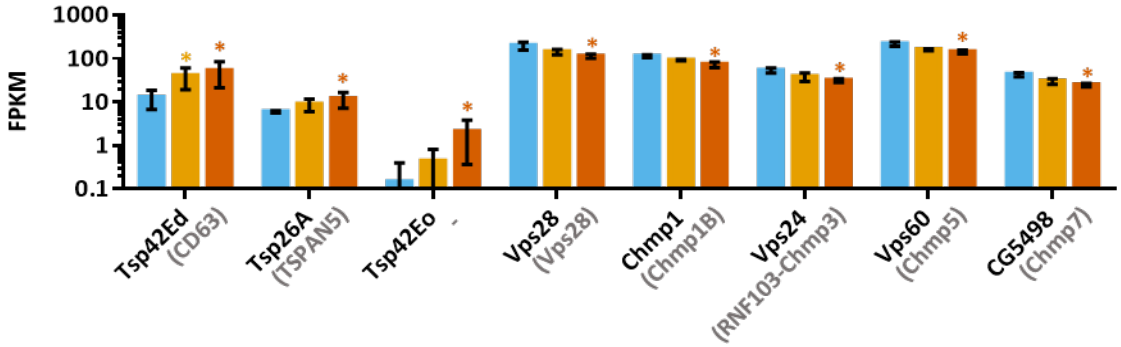


Figure 5.9: Expression of several ESCRT components altered in cells under stress

*FPKM abundance values in cells for all known tetraspanin and ESCRT component RNAs significantly altered in 2mM $H_2O_2$-treated cells relative to non-treated cells. Graph shows mean and standard deviation for three biological replicates, differential expression determined by DESEQ2 with P-adj at 0.05.*

### 5.3.10 RNA in EV preparations is partially enclosed within the vesicular membrane

With the majority of sequencing reads identified, and cellular stress induction confirmed, the remaining genome-mapping portion of the RNA content of EVs was investigated. To determine whether this RNA was located inside the EVs, an RNAse protection assay was carried out; treating samples with either RNase alone, or with Triton-X100 to disrupt the EV membrane and expose the internal RNA to subsequent RNAse. No difference in total RNA content was seen between samples treated with RNAse alone or Triton/RNase when quantifying by Qubit (Figure 5.10A). However, qPCR for mRNAs *Arc1* and *Rpl32* demonstrated near complete sensitivity with Triton/RNAse, but only partial sensitivity with RNAse alone, indicating that around 50% of the RNA was protected by the EV membrane (Figure 5.10B, C). Although variability was seen between different sample replicates, each showed very similar sensitivity for the two target RNAs, indicating that this result is likely to hold true for many other RNAs.

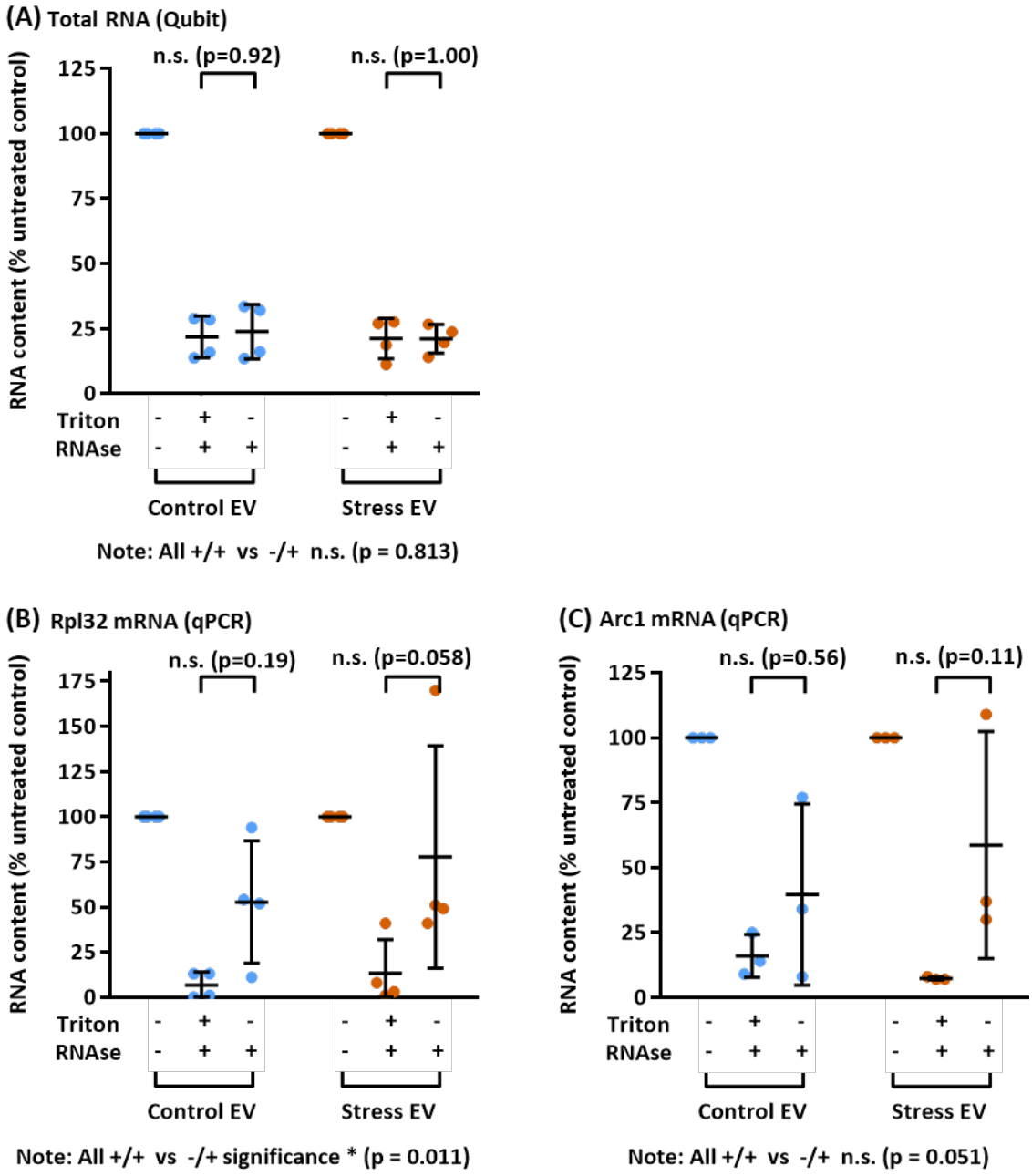


## Figure 5.10: mRNAs in EV samples show partial sensitivity to RNAse treatment

*(A) Relative quantity of total EV-associated RNA remaining after treatment with RNAse A alone, or when pre-treated with Triton X-100 detergent. EV samples derived from non-treated or 2mM $H_2O_2$-treated cells, were split into three aliquots before carrying out protection assay, total RNA extraction and quantification with Qubit HS RNA assay kit. (B) Relative quantity of* Rpl32 *mRNA remaining after treatments described in (A), quantified by qPCR. cDNA synthesis carried on 15-40ng of RNA from untreated control or equivalent volumes for RNAse A/Triton X-00 treatments. (C) As for (B) but for* Arc1 *mRNA. Graphs show mean and standard deviation for four or three biological replicates respectively. Statistical significance assessed with two-way ANOVA followed by Sidak's multiple comparisons test.*

### 5.3.11 Biotype abundance in EV associated RNA is not representative of the cell

Next, biotype abundance analysis was carried out on the top 1000 most abundant RNAs. This revealed mRNA to be the most abundant type in cells under control conditions, with a significant reduction under 2mM $H_2O_2$ stress (Figure 5.11A). However, this reduction under stress was not reflected in the EV samples, indicating that the EV-associated RNA was not completely representative of cellular RNA. Comparison of the enrichment of each EV-cell pair showed that although snoRNA and non-coding RNA were enriched under control, no significant differences were present under stress, likely in part due to increased variability (Figure 5.11B).

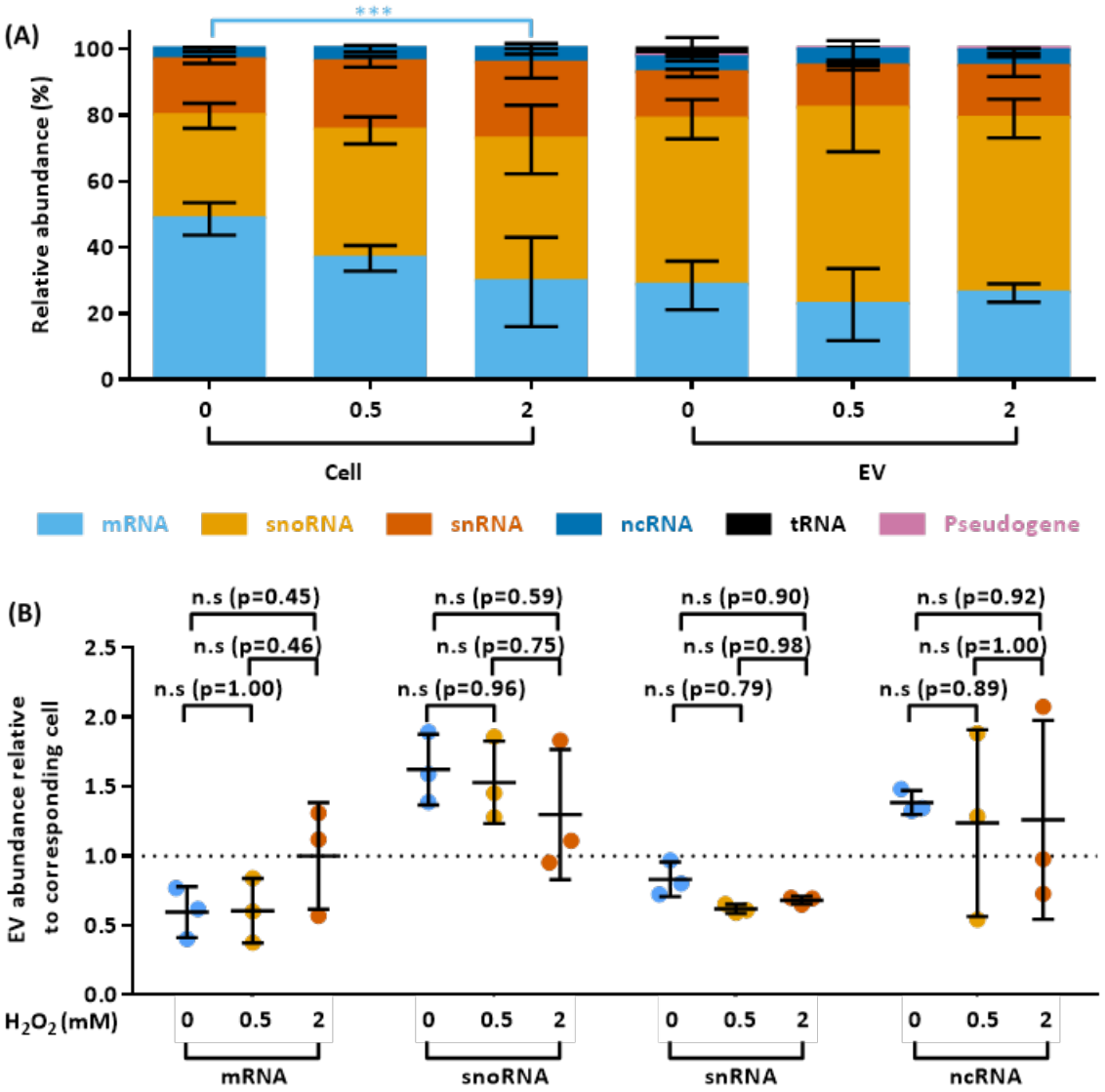


Figure 5.11: Relative abundance of EV RNA biotypes is not representative of cells

*(A) Relative biotypes of genome-mapped RNA for each of six sample types. (B) Enrichment of each biotype in EVs derived from non-treated, 0.5mM $H_2O_2$ and 2mM $H_2O_2$-stressed cells against parental cell sample. Graphs show mean and standard deviation of three biological replicates, and statistical significance assessed with two-way ANOVA followed by Tukey's multiple comparisons test.*

### 5.3.12 RNAs involved in ribosomal functions are enriched in EVs

Having identified the RNA biotypes present, any additional commonalities between the most abundant RNAs were investigated. Gene ontology (GO) analysis was carried out to look for functional similarities and revealed translation and ribosome related terms to be highly enriched in control EVs when compared to a genome-wide background (Figure 5.12A). However, since these terms also represent those associated with abundant cell RNAs, GO analysis was repeated using the top 1000 most abundant genes within the parental cells as background (Figure 5.12B). This again returned terms relating to translation and ribosomes, indicating that these enriched functions are likely not simply a result of concentration-dependent loading of cellular RNA. Under stress, enrichment of protein complexes became less significant, whilst several ribosomal terms became more significant. These results further indicated that ribosome production and function appear to be closely linked with EVs.

### 5.3.13 EV-cell correlation of mRNA, snoRNA and snRNA is stress-dependent

With the knowledge that there were differences in the abundance of different RNA biotypes, potential packaging of these RNAs was explored. Principal component analysis (PCA) was performed to look at sample similarity and confirmed that the sample type (cell or EV) was the strongest distinguishing component (Figure 5.13A). Control samples clustered well within their sample type, but greater differences were seen under stress, both between replicates and between sample types. For PCAs carried out on each biotype independently, sample type was again the strongest distinguishing component, although less distinct for snoRNA and snRNA than for mRNA and ncRNA, particularly under stress (Figure 5.13B-E). These data confirmed likely specificity in RNA incorporation into EVs in normal conditions but indicated that this specificity may be in part lost under stress.

**(A)**

| GO Term ID | Term source | Term name | Adjusted P-value | |
|---|---|---|---|---|
| | | | Control EV | Control Cell |
| GO:0005737 | GO:CC | cytoplasm | 1.4E-130 | 4.7E-127 |
| GO:0005622 | GO:CC | intracellular | 5.8E-112 | 4.1E-94 |
| GO:0002181 | GO:BP | cytoplasmic translation | 3.8E-89 | 1.4E-90 |
| GO:0005829 | GO:CC | cytosol | 1.2E-97 | 5.7E-81 |
| GO:0022626 | GO:CC | cytosolic ribosome | 7.4E-83 | 1.4E-80 |
| GO:0032991 | GO:CC | protein-containing complex | 2.5E-81 | 1.0E-70 |
| GO:0003735 | GO:MF | structural constituent of ribosome | 9.7E-64 | 1.0E-64 |
| GO:0006412 | GO:BP | translation | 1.8E-66 | 2.4E-64 |
| GO:0044391 | GO:CC | ribosomal subunit | 5.3E-64 | 2.1E-63 |
| GO:0005840 | GO:CC | ribosome | 6.4E-62 | 2.8E-61 |

**(B)**

| GO Term ID | Term source | Term name | Adjusted P-value | | | Dose-dependent change |
|---|---|---|---|---|---|---|
| | | | Control | 0.5mM | 2mM | |
| GO:0005829 | GO:CC | cytosol | 5.49E-10 | 1.04E-06 | 5.93E-09 | No |
| GO:0022626 | GO:CC | cytosolic ribosome | 4.98E-08 | 2.25E-06 | 1.44E-08 | No |
| GO:0005622 | GO:CC | intracellular | 3.44E-07 | 1.32E-04 | 2.82E-04 | Decrease |
| GO:0032991 | GO:CC | protein-containing complex | 1.29E-05 | 1.58E-05 | 9.78E-04 | Decrease |
| GO:0002181 | GO:BP | cytoplasmic translation | 2.15E-05 | 1.51E-06 | 1.22E-06 | Increase |
| GO:0043228 | GO:CC | non-membrane-bounded organelle | 7.43E-05 | 1.70E-05 | 9.78E-04 | No |
| GO:0043232 | GO:CC | intracellular non-membrane-bounded organelle | 7.43E-05 | 1.70E-05 | 9.78E-04 | No |
| GO:1990904 | GO:CC | ribonucleoprotein complex | 1.12E-04 | 1.88E-04 | #N/A | Decrease |
| GO:0022625 | GO:CC | cytosolic large ribosomal subunit | 2.06E-04 | #N/A | 3.58E-04 | No |
| GO:0005840 | GO:CC | ribosome | 3.77E-04 | 5.18E-04 | 4.33E-05 | No |
| GO:0044391 | GO:CC | ribosomal subunit | 6.43E-04 | 1.97E-04 | 2.16E-05 | Increase |
| GO:0043043 | GO:BP | peptide biosynthetic process | #N/A | 4.90E-04 | #N/A | No |
| GO:0043604 | GO:BP | amide biosynthetic process | #N/A | 4.90E-04 | #N/A | No |
| GO:0006412 | GO:BP | translation | #N/A | 8.39E-04 | #N/A | No |
| KEGG:03010 | KEGG | Ribosome | #N/A | 3.53E-04 | 2.63E-06 | Increase |
| GO:0015934 | GO:CC | large ribosomal subunit | #N/A | #N/A | 9.78E-04 | Increase |
| GO:0022627 | GO:CC | cytosolic small ribosomal subunit | #N/A | #N/A | 9.78E-04 | Increase |

## Figure 5.12: Gene ontology analysis for top 1000 most abundant RNAs in EVs

*(A) Gene ontology analysis for the top 1000 most abundant RNAs in EVs derived from non-treated cells, and in the cells themselves, against a background of all annotated RNAs listed in Cufflinks file. Multiple testing correction by Benjamini-Hochberg false discovery rate with a cut-off at P-adj<0.001. (B) Gene ontology analysis of top 1000 most abundant RNAs for EVs derived from non-treated, 0.5mM $H_2O_2$ and 2mM $H_2O_2$-treated cells, against a background of the top 1000 most abundant RNAs in corresponding cells.*

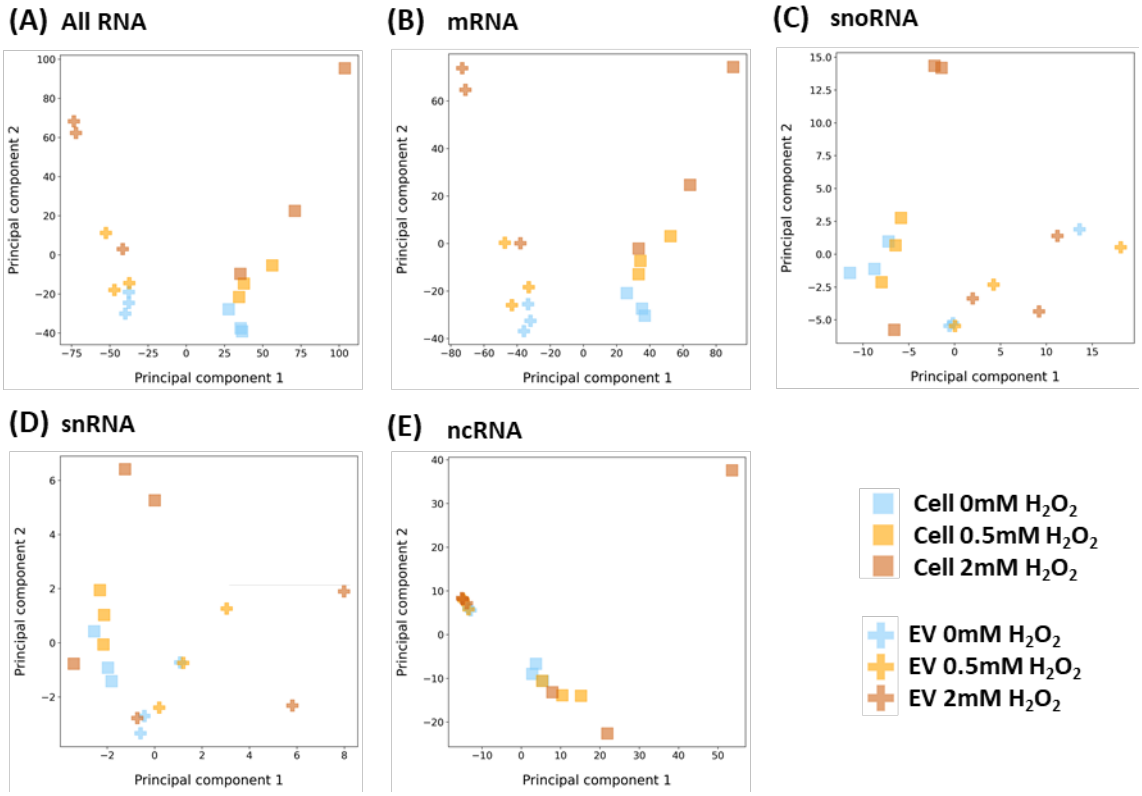


Figure 5.13: EV and cell samples cluster distinctly in principal component analysis

*Principal component analysis of all (A) genome-mapped RNA and (B)-(E) each individual biotype. Analysis was carried out by Claire Hill.*

Although PCA indicated greater differences between cell and EV samples under stress, this may be due to both technical variability between replicates, and biological differences. These aspects were quantified by correlation analysis and showed cell sample triplicates to correlate highly for all biotypes, whilst EV samples had lower correlation for mRNA, snRNA, and especially snoRNA (Figure 5.14A). In line with PCA, correlation was markedly reduced in all samples under stress, but was most evident in EV samples for mRNA and snoRNA. Pairwise correlations between each EV and parental cell sample showed the biggest difference was in snoRNA (Figure 5.14B). Under stress, correlation was reduced for both mRNA and snoRNA, whilst snRNA showed an increase.

Finally, what was evident from plots of EV-cell pairs was that there was high correlation between cells and EVs at high transcript abundance, but this was reduced at lowered abundance (Figure 5.14C). Taken together, these data provide evidence for selective packaging of RNA into EVs, that cellular abundance is a key factor, and that mRNA and snoRNA are most-stress dependent.

(A)

| $H_2O_2$ (mM) & type | Correlation between replicates | | | | |
|---|---|---|---|---|---|
| | All RNA | mRNA | ncRNA | snRNA | SnoRNA |
| 0 (EV) | 0.78 (0.77-0.80) | 0.77 (0.76-0.79) | 0.85 (0.79-0.91) | 0.75 (0.57-0.93) | 0.64 (0.53-0.73) |
| 0.5 (EV) | 0.77 (0.76-0.78) | 0.76 (0.75-0.77) | 0.87 (0.86-0.89) | 0.84 (0.76-0.90) | 0.74 (0.69-0.76) |
| 2 (EV) | 0.74 (0.73-0.75) | 0.73 (0.71-0.74) | 0.85 (0.85-0.85) | 0.78 (0.61-0.93) | 0.49 (0.35-0.67) |
| 0 (Cell) | 0.98 (0.98-0.99) | 0.98 (0.98-0.99) | 0.87 (0.86-0.87) | 0.96 (0.95-0.98) | 0.94 (0.94-0.95) |
| 0.5 (Cell) | 0.98 (0.98-0.99) | 0.98 (0.98-0.99) | 0.85 (0.83-0.87) | 0.92 (0.88-0.94) | 0.92 (0.90-0.93) |
| 2 (Cell) | 0.97 (0.97-0.98) | 0.97 (0.97-0.98) | 0.84 (0.84-0.84) | 0.94 (0.93-0.96) | 0.90 (0.86-0.93) |

(B)

| $H_2O_2$ (mM) | Correlation between EV-cell pairs | | | | |
|---|---|---|---|---|---|
| | All RNA | mRNA | ncRNA | snRNA | SnoRNA |
| 0 | 0.78 (0.77-0.79) | 0.78 (0.78-0.79) | 0.67 (0.59-0.71) | 0.57 (0.12-0.89) | 0.53 (0.40-0.67) |
| 0.5 | 0.77 (0.74-0.81) | 0.77 (0.73-0.81) | 0.66 (0.62-0.71) | 0.72 (0.50-0.89) | 0.51 (0.46-0.59) |
| 2 | 0.71 (0.65-0.79) | 0.71 (0.64-0.79) | 0.70 (0.66-0.73) | 0.85 (0.80-0.92) | 0.49 (0.29-0.62) |

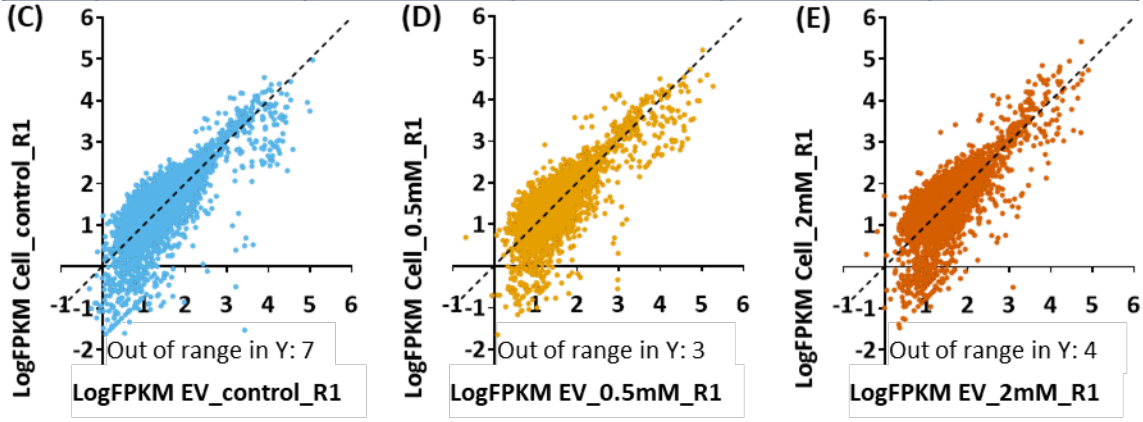


Figure 5.14: EV-Cell correlation decreases for mRNA and snoRNA under stress

*(A) Pairwise spearman correlation analysis of FPKM abundance values for triplicate samples of the six sample types, for all genome-mapped RNA and for each individual biotype. Coloured values show mean of three values, minimum and maximum shown in brackets. (B) Pairwise spearman correlation analysis of each EV sample with parental cell sample. (C)-(E) Graphs showing correlation of all genome-mapped RNAs for between EV and cell for replicate one, in (C) non-treated, (D) 0.5mM $H_2O_2$ and (E) 2mM $H_2O_2$ condition.*

### 5.3.14 Cytoskeletal and developmental GO terms are common in all conditions

Knowing that there were differences in EV and cell abundance at the biotype level, specific RNAs showing differential distribution were then assessed. Differential gene expression analysis of EV against cell indicated that more RNAs (837 in total) were differently distributed under control conditions than under either of the stress conditions (Figure 5.15A). In all three conditions the majority of significant changes observed were enrichment, although this may be due to depleted RNAs in EVs being less easy to detect, as a result of the lower sequencing depth. Comparison of these changes showed that 162 significantly enriched RNAs, or 18.3% of the total, were common

to all three conditions (Figure 5.15B). Interestingly, there were very few RNAs, only 4%, whose enrichment was shared under just the two stress conditions. A similar result was observed for EV-depleted RNAs, with 11.4% shared between all conditions, and only 5.2% shared under just the two stress conditions (Figure 5.15C).

**(A)**

| Condition | Number of altered RNAs | | |
|---|---|---|---|
| | Enriched | Depleted | Total |
| Control | 543 | 294 | 837 |
| 0.5mM | 466 | 225 | 691 |
| 2mM | 384 | 130 | 514 |

**(B)** Percentage of all EV-enriched RNAs

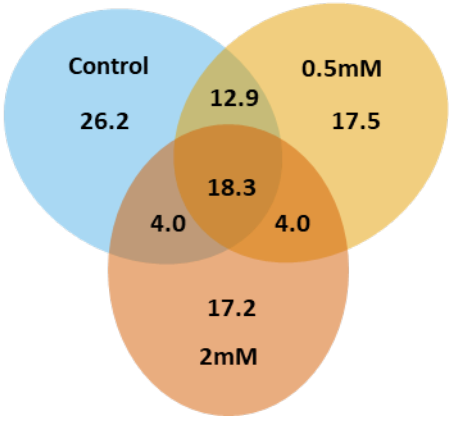


**(C)** Percentage of all EV-depleted RNAs

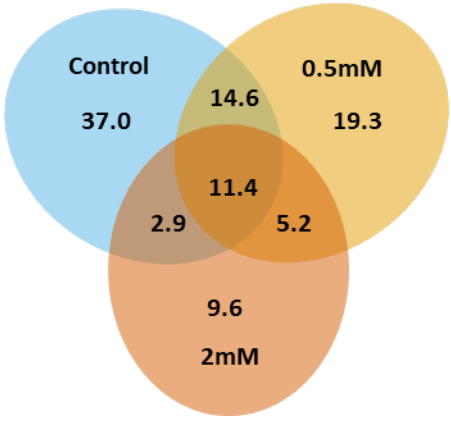


Figure 5.15:Overlaps between EV-cell RNA differences are small

*(A) All RNAs significantly altered in non-treated, 0.5mM and 2mM $H_2O_2$ EVs relative to cells. Differential expression determined by DESEQ2 with P-adj at 0.05. (B) Venn diagram showing overlap of significantly enriched RNAs, expressed as a percentage of total enriched RNAs under any condition. (C) As for (B), but for depleted RNAs.*

Although there was little overlap in the specific RNAs enriched or depleted under each stress condition, to look for functional similarities, GO term analysis was carried out. This identified multiple upregulated terms for the EV-enriched RNAs in control conditions, including several relating to the cytoskeleton, and an array of terms relating to development. Limiting the analysis to the subset of RNAs upregulated in common in all three conditions returned cytoskeletal and developmental terms as the most significant in EV-enriched RNA (Figure 5.16D), and mitochondria-related term in EV-depleted RNA (Figure 5.16E). These mitochondrial terms arise from mt:ND1-ND4, mt:Cyt-b, mt:Col, and mt:ColI, all of which are mitochondrially encoded and translated by the mitoribosome, so would be expected to be contained within the mitochondria.

**(A) Common to EV-enriched RNAs**

| GO Term ID | Term source | Term name | Adjusted P-value |
|---|---|---|---|
| GO:0048731 | GO:BP | system development | 2.72E-16 |
| GO:0048468 | GO:BP | cell development | 9.10E-16 |
| GO:0009653 | GO:BP | anatomical structure morphogenesis | 9.69E-16 |
| GO:0008092 | GO:MF | cytoskeletal protein binding | 3.51E-15 |
| GO:0007275 | GO:BP | multicellular organism development | 3.66E-15 |
| GO:0048513 | GO:BP | animal organ development | 6.39E-15 |
| GO:0030154 | GO:BP | cell differentiation | 7.40E-15 |
| GO:0048869 | GO:BP | cellular developmental process | 8.76E-15 |
| GO:0048856 | GO:BP | anatomical structure development | 1.34E-14 |
| GO:0007010 | GO:BP | cytoskeleton organization | 1.22E-13 |

**(B) Common to EV-depleted RNAs**

| GO Term ID | Term source | Term name | Adjusted P-value |
|---|---|---|---|
| GO:0031224 | GO:CC | intrinsic component of membrane | 3.82E-07 |
| GO:0031967 | GO:CC | organelle envelope | 3.82E-07 |
| GO:0016021 | GO:CC | integral component of membrane | 3.82E-07 |
| GO:0031975 | GO:CC | envelope | 3.82E-07 |
| GO:0005746 | GO:CC | mitochondrial respirasome | 1.59E-06 |
| GO:0031090 | GO:CC | organelle membrane | 1.59E-06 |
| GO:0098803 | GO:CC | respiratory chain complex | 1.59E-06 |
| GO:0070469 | GO:CC | respirasome | 1.88E-06 |
| GO:0031966 | GO:CC | mitochondrial membrane | 2.67E-06 |
| GO:0098800 | GO:CC | inner mitochondrial membrane protein complex | 2.67E-06 |

Figure 5.16: EV enriched RNAs in common relate to cytoskeleton and development

*(A) Gene ontology analysis of 162 RNAs enriched in EVs under all conditions, against a background of all annotated RNAs listed in Cufflinks file. Multiple testing correction by Benjamini-Hochberg false discovery rate with cut-off at P-adj<0.001. (B) As for (A) but for 51 RNAs depleted in EVs under all conditions.*

GO term analysis of the full set of RNAs enriched in EVs under each condition was then carried out and compared. When filtering these terms to only those which showed dose-dependent changes under stress, cytoskeleton terms were found to be highly reduced in significance (Figure 5.17A). Terms relating to wing disc development increased in significance under stress, although other terms relating to development were decreased. For EV-depleted RNAs, fewer associated terms were upregulated, relating primarily to the membrane/endoplasmic reticulum, and these were less significant under stress (Figure 5.17B). The similarity of the terms associated with stress-induced changes to those which are common under all three conditions indicates that these processes are likely key to EV function, and indeed if delivered to recipient cells, could alter cellular behaviour.

**(A) Gene ontology changes in enriched RNAs**

| GO Term ID | Term source | Term name | Adjusted P-value | | | Dose-dependent change |
|---|---|---|---|---|---|---|
| | | | 0mM | 0.5mM | 2mM | |
| GO:0030036 | GO:BP | actin cytoskeleton organization | 1.0E-17 | 1.2E-14 | 5.3E-06 | Decrease |
| GO:0030029 | GO:BP | actin filament-based process | 6.6E-19 | 1.1E-16 | 3.4E-07 | Decrease |
| GO:0051641 | GO:BP | cellular localization | 1.9E-14 | 1.2E-12 | 8.0E-04 | Decrease |
| GO:0005856 | GO:CC | cytoskeleton | 3.3E-14 | 3.8E-09 | 7.5E-04 | Decrease |
| GO:0051179 | GO:BP | localization | 6.9E-18 | 1.9E-12 | 7.8E-08 | Decrease |
| GO:0033036 | GO:BP | macromolecule localization | 1.0E-12 | 8.6E-12 | 6.8E-04 | Decrease |
| GO:1902531 | GO:BP | regulation of intracellular signal transduction | 4.4E-15 | 1.9E-14 | 2.4E-06 | Decrease |
| GO:0050794 | GO:BP | regulation of cellular process | 8.3E-16 | 2.0E-14 | 1.8E-07 | Decrease |
| GO:0007017 | GO:BP | microtubule-based process | 1.5E-12 | 1.7E-11 | 2.5E-04 | Decrease |
| GO:0044085 | GO:BP | cellular component biogenesis | 4.7E-13 | 3.3E-09 | 7.0E-05 | Decrease |
| GO:0022607 | GO:BP | cellular component assembly | 2.3E-13 | 2.1E-10 | 2.0E-05 | Decrease |
| GO:0050789 | GO:BP | regulation of biological process | 2.2E-14 | 7.5E-13 | 4.2E-07 | Decrease |
| GO:0065007 | GO:BP | biological regulation | 2.4E-15 | 8.8E-14 | 2.5E-08 | Decrease |
| GO:0048477 | GO:BP | oogenesis | 8.9E-20 | 9.0E-18 | 6.9E-13 | Decrease |
| GO:0051128 | GO:BP | regulation of cellular component organization | 3.4E-15 | 9.7E-15 | 1.3E-08 | Decrease |
| GO:0007292 | GO:BP | female gamete generation | 6.1E-19 | 2.9E-16 | 2.0E-12 | Decrease |
| GO:0023052 | GO:BP | signalling | 6.1E-14 | 2.3E-11 | 5.9E-08 | Decrease |
| GO:0007154 | GO:BP | cell communication | 2.8E-14 | 9.0E-12 | 2.0E-08 | Decrease |
| GO:0048469 | GO:BP | cell maturation | 9.2E-12 | 1.3E-10 | 5.6E-06 | Decrease |
| GO:0044093 | GO:BP | positive regulation of molecular function | 6.6E-10 | 1.7E-06 | 4.0E-04 | Decrease |
| GO:0022412 | GO:BP | cellular process involved in reproduction in multicellular organism | 4.7E-17 | 2.2E-15 | 1.7E-11 | Decrease |
| GO:0007165 | GO:BP | signal transduction | 8.4E-13 | 1.8E-11 | 2.4E-07 | Decrease |
| GO:0007281 | GO:BP | germ cell development | 7.0E-18 | 5.2E-16 | 2.0E-12 | Decrease |
| GO:0005912 | GO:CC | adherens junction | 4.2E-09 | 5.7E-09 | 7.5E-04 | Decrease |
| GO:0001738 | GO:BP | morphogenesis of a polarized epithelium | 2.9E-04 | 4.3E-05 | 2.1E-09 | Increase |
| GO:0021700 | GO:BP | developmental maturation | 3.4E-11 | 2.4E-10 | 4.7E-06 | Decrease |
| GO:0016477 | GO:BP | cell migration | 1.6E-11 | 2.8E-11 | 1.4E-06 | Decrease |
| GO:0019953 | GO:BP | sexual reproduction | 6.1E-13 | 3.1E-11 | 5.2E-08 | Decrease |
| GO:0044703 | GO:BP | multi-organism reproductive process | 6.3E-13 | 3.2E-11 | 5.3E-08 | Decrease |
| GO:0007276 | GO:BP | gamete generation | 3.3E-15 | 8.8E-14 | 2.5E-10 | Decrease |
| GO:0030951 | GO:BP | establishment or maintenance of microtubule cytoskeleton polarity | 1.4E-08 | 2.8E-06 | 7.7E-04 | Decrease |
| GO:0048609 | GO:BP | multicellular organismal reproductive process | 1.7E-12 | 3.4E-11 | 5.6E-08 | Decrease |
| GO:0050793 | GO:BP | regulation of developmental process | 4.0E-16 | 1.7E-15 | 1.3E-11 | Decrease |
| GO:0032501 | GO:BP | multicellular organismal process | 1.5E-15 | 8.8E-14 | 4.3E-11 | Decrease |
| GO:0040011 | GO:BP | locomotion | 1.3E-10 | 2.1E-09 | 3.7E-06 | Decrease |
| GO:2000026 | GO:BP | regulation of multicellular organismal development | 1.6E-15 | 4.8E-14 | 3.7E-11 | Decrease |
| GO:0030952 | GO:BP | establishment or maintenance of cytoskeleton polarity | 2.6E-08 | 3.1E-07 | 5.0E-04 | Decrease |
| GO:0007476 | GO:BP | imaginal disc-derived wing morphogenesis | 1.4E-05 | 4.6E-07 | 7.3E-10 | Increase |
| GO:0048737 | GO:BP | imaginal disc-derived appendage development | 3.4E-06 | 3.6E-10 | 3.3E-10 | Increase |
| GO:0048736 | GO:BP | appendage development | 4.3E-06 | 4.8E-10 | 4.3E-10 | Increase |
| GO:0035295 | GO:BP | tube development | 2.0E-16 | 4.2E-16 | 2.0E-12 | Decrease |
| GO:0003002 | GO:BP | regionalization | 2.3E-13 | 1.3E-10 | 2.1E-09 | Decrease |
| GO:0035114 | GO:BP | imaginal disc-derived appendage morphogenesis | 6.3E-06 | 7.6E-10 | 7.6E-10 | Increase |
| GO:0035107 | GO:BP | appendage morphogenesis | 7.7E-06 | 9.5E-10 | 9.2E-10 | Increase |
| GO:0051239 | GO:BP | regulation of multicellular organismal process | 8.4E-15 | 1.2E-12 | 6.1E-11 | Decrease |
| GO:0051704 | GO:BP | multi-organism process | 4.9E-13 | 5.7E-10 | 1.9E-09 | Decrease |
| GO:0048583 | GO:BP | regulation of response to stimulus | 1.0E-12 | 1.2E-11 | 3.7E-09 | Decrease |

| | | | | | | |
|---|---|---|---|---|---|---|
| GO:0048646 | GO:BP | anatomical structure formation involved in morphogenesis | 9.7E-10 | 1.4E-07 | 3.3E-06 | Decrease |
| GO:0003006 | GO:BP | developmental process involved in reproduction | 9.0E-15 | 1.3E-13 | 2.9E-11 | Decrease |
| GO:0007472 | GO:BP | wing disc morphogenesis | 2.9E-06 | 7.1E-08 | 1.6E-09 | Increase |
| GO:0009966 | GO:BP | regulation of signal transduction | 5.3E-14 | 1.1E-11 | 8.3E-11 | Decrease |
| GO:0007389 | GO:BP | pattern specification process | 1.6E-13 | 1.5E-11 | 1.9E-10 | Decrease |
| GO:0051716 | GO:BP | cellular response to stimulus | 1.2E-10 | 3.6E-10 | 1.2E-07 | Decrease |
| GO:0050896 | GO:BP | response to stimulus | 5.8E-11 | 3.9E-10 | 5.2E-08 | Decrease |
| GO:0048584 | GO:BP | positive regulation of response to stimulus | 1.5E-08 | 5.1E-08 | 1.2E-05 | Decrease |
| GO:0035282 | GO:BP | segmentation | 7.3E-09 | 1.0E-08 | 5.6E-06 | Decrease |
| GO:0022414 | GO:BP | reproductive process | 1.8E-11 | 1.3E-10 | 6.9E-09 | Decrease |
| GO:0032504 | GO:BP | multicellular organism reproduction | 4.0E-09 | 8.7E-09 | 1.4E-06 | Decrease |
| GO:0007298 | GO:BP | border follicle cell migration | 1.5E-07 | 3.1E-07 | 5.1E-05 | Decrease |
| GO:0002065 | GO:BP | columnar/cuboidal epithelial cell differentiation | 7.8E-13 | 1.1E-12 | 2.3E-10 | Decrease |
| GO:0009967 | GO:BP | positive regulation of signal transduction | 2.1E-08 | 6.7E-08 | 5.1E-06 | Decrease |
| GO:0007297 | GO:BP | ovarian follicle cell migration | 1.7E-07 | 2.8E-07 | 3.8E-05 | Decrease |
| GO:0048732 | GO:BP | gland development | 9.6E-04 | 4.0E-04 | 7.6E-06 | Increase |
| GO:0007391 | GO:BP | dorsal closure | 3.1E-09 | 5.9E-09 | 3.7E-07 | Decrease |
| GO:0007310 | GO:BP | oocyte dorsal/ventral axis specification | 8.3E-07 | 1.8E-05 | 7.3E-05 | Decrease |
| GO:0023014 | GO:BP | signal transduction by protein phosphorylation | 6.7E-06 | 4.1E-05 | 5.6E-04 | Decrease |
| GO:0016331 | GO:BP | morphogenesis of embryonic epithelium | 7.6E-09 | 1.2E-08 | 5.0E-07 | Decrease |
| GO:0005829 | GO:CC | cytosol | 7.5E-09 | 4.0E-07 | 4.2E-07 | Decrease |
| GO:0048518 | GO:BP | positive regulation of biological process | 2.2E-12 | 7.2E-11 | 1.2E-10 | Decrease |
| GO:0043408 | GO:BP | regulation of MAPK cascade | 1.3E-05 | 2.6E-05 | 5.0E-04 | Decrease |
| GO:0010720 | GO:BP | positive regulation of cell development | 8.9E-07 | 2.2E-07 | 4.2E-08 | Increase |
| GO:1905879 | GO:BP | regulation of oogenesis | 7.2E-05 | 1.3E-05 | 5.0E-06 | Increase |
| GO:0009950 | GO:BP | dorsal/ventral axis specification | 2.9E-06 | 1.8E-05 | 4.0E-05 | Decrease |
| GO:0000003 | GO:BP | reproduction | 1.5E-08 | 1.8E-08 | 1.5E-07 | Decrease |
| GO:0010970 | GO:BP | transport along microtubule | 1.3E-04 | 5.1E-04 | 9.5E-04 | Decrease |
| GO:0000165 | GO:BP | MAPK cascade | 6.9E-05 | 1.1E-04 | 4.5E-04 | Decrease |
| GO:0045597 | GO:BP | positive regulation of cell differentiation | 6.8E-07 | 6.7E-07 | 1.2E-07 | Increase |
| GO:0051240 | GO:BP | positive regulation of multicellular organismal process | 1.2E-07 | 1.1E-07 | 4.7E-08 | Increase |
| GO:0051094 | GO:BP | positive regulation of developmental process | 8.4E-08 | 8.5E-08 | 1.3E-07 | Decrease |

**(B) Gene ontology changes in depleted RNAs**

| GO Term ID | Term source | Term name | Adjusted P-value | | | Dose-dependent change |
|---|---|---|---|---|---|---|
| | | | Control | 0.5mM | 2mM | |
| GO:0016020 | GO:CC | membrane | 9.0E-20 | 8.8E-08 | 2.8E-05 | Decrease |
| GO:0005783 | GO:CC | endoplasmic reticulum | 2.3E-16 | 7.4E-06 | 3.0E-04 | Decrease |
| GO:0016021 | GO:CC | integral component of membrane | 1.2E-16 | 5.0E-08 | 1.4E-04 | Decrease |
| GO:0031224 | GO:CC | intrinsic component of membrane | 1.9E-16 | 5.0E-08 | 1.7E-04 | Decrease |
| GO:0031090 | GO:CC | organelle membrane | 9.2E-14 | 5.0E-08 | 2.8E-06 | Decrease |
| GO:0110165 | GO:CC | cellular anatomical entity | 4.3E-12 | 1.7E-06 | 8.1E-06 | Decrease |
| KEGG:04141 | KEGG | Protein processing in endoplasmic reticulum | 2.8E-07 | 3.2E-04 | 3.2E-04 | Decrease |
| GO:0051179 | GO:BP | localization | 5.5E-04 | 1.4E-05 | 9.9E-06 | Increase |

Figure 5.17: Gene ontology terms associated with RNAs of differential abundance in EV vs cell that are dose-dependently altered by stress

*A) Filtered table of gene ontology analysis carried out on 543, 466 and 384 RNAs respectively enriched in non-treated, 0.5mM and 2mM $H_2O_2$ EVs relative to cells, against a background of all annotated RNAs listed in Cufflinks file. Multiple testing correction by Benjamini-Hochberg false discovery rate with a cut-off at P-adj<0.001. Differential expression determined via DESEQ2, with P-adj at 0.05. Results filtered to display only terms showing $H_2O_2$-dose-dependent changes in term significance. (B) As for (A) but for 294, 225 and 130 RNAs respectively depleted in non-treated, 0.5mM and 2mM $H_2O_2$ EVs relative to cells.*

### 5.3.15 Differential abundance affecting snoRNA and snRNA is lost under stress

Next, differential distribution between cell and EV RNA was analysed at the biotype level. Under control conditions, snoRNAs were proportionally the most enriched type, but with a strikingly far lower percentage under stress, a trend also seen for snRNAs to a lesser extent (Figure 5.18A). A lower proportion of RNAs of any type were depleted in EVs, with snRNAs showing the most prominent difference under stress (Figure 5.18B). These data indicate that the mechanisms controlling selectivity of snoRNAs and snRNA may be compromised under conditions of stress.

**(A)**

| Biotype | EV enriched RNAs (%) | | |
|---|---|---|---|
| | 0mM $H_2O_2$ | 0.5mM $H_2O_2$ | 2mM $H_2O_2$ |
| mRNA | 4.6 | 3.8 | 3.1 |
| ncRNA | 2.8 | 2.5 | 2.4 |
| snoRNA | 32 | 25 | 5.8 |
| snRNA | 14 | 13 | 4.2 |
| Pseudogene | 13 | 14 | 13 |

**(B)**

| Biotype | EV depleted RNAs (%) | | |
|---|---|---|---|
| | 0mM $H_2O_2$ | 0.5mM $H_2O_2$ | 2mM $H_2O_2$ |
| mRNA | 2.9 | 2.1 | 1.2 |
| ncRNA | 0.0 | 0.2 | 0.1 |
| snoRNA | 0.8 | 1.4 | 0.0 |
| snRNA | 4.8 | 4.2 | 0.0 |
| Pseudogene | 0.0 | 0.0 | 0.0 |

Figure 5.18 Differential distribution of snoRNA and snRNA most affected by stress

*(A) Percentage of RNAs of each biotype, with FPKM greater than zero in cells, that are detected as significantly enriched in EVs over cells. Differential expression determined via DESEQ2, with P-adj at 0.05. (B) As for (A), but for EV-depleted RNAs.*

### 5.3.16 Dose-responsive changes are seen in stress EVs compared to control EVs

Although enrichment of EVs relative to parental cells is informative in understanding the mechanisms determining differential abundance, a direct comparison of RNA abundance between EV samples is more relevant to understanding of the functional effects on recipient cells. Differential expression analysis was therefore carried out to compare EVs from both 0.5mM and 2mM $H_2O_2$ stress to control. Under 2mM stress, 67 RNAs were significantly upregulated, with GO term analysis highlighting multiple terms relating to development, along

with ‘response to stress’ and ‘programmed cell death’ (Figure 5.19A). The enrichment of these latter terms indicates that, if mRNAs can be delivered and translated in recipient cells, it is plausible that they act to alter cellular stress response, cell growth and death. These changes in EVs were also compared to those seen in cells, revealing that, whilst 32 of the 67 RNAs were also significantly upregulated in cells under stress, for 35 the change was EV-specific (Figure 5.19B and Supplementary Figure 9). Under 0.5mM $H_2O_2$ stress, only *Arc1* mRNA was statistically significantly upregulated, but with a trend towards increases in other RNAs (Figure 5.19C). Consideration of RNAs downregulated in stress EVs revealed only 7 RNAs that were significant under high stress, with associated GO terms relating exclusively to cytoskeletal functions (Figure 5.21A). In contrast to upregulated RNAs, there was no overlap with cell changes (Figure 5.21B), whilst non-significant dose-dependent changes were again seen (Figure 5.21C). These observations of stress-dose-responsive effects gives confidence that these differences may have biological relevance, with the specific RNAs identified providing candidates for investigation of the effects of RNA cargo on recipient cells.

To validate the differential distribution identified in RNA sequencing data, qPCR was carried out on two mRNAs. Firstly *Uba1*, significantly enriched 3.3-fold in EVs from 2mM $H_2O_2$-stressed cells compared to normal EVs, and *Akap200*, 2.7-fold depleted under stress, using *Rpl32* as a housekeeping gene, as this RNA was identified as stably expressed in sequencing data. Differences in *Uba1* and *Akap200* expression were at the boundary of statistical significance when assessing by qPCR, but in the expected direction for both mRNAs, with statistical significance lacking due to the high variability between biological replicates (Figure 5.20). Nevertheless, these data support the validity of the conclusions drawn from the RNA sequencing data more widely.

(A)

| GO Term ID | Term source | Term name | Adjusted P-value |
|---|---|---|---|
| GO:0050896 | GO:BP | response to stimulus | 2.2E-04 |
| GO:0007275 | GO:BP | multicellular organism development | 4.1E-04 |
| GO:0048856 | GO:BP | anatomical structure development | 4.1E-04 |
| GO:0060429 | GO:BP | epithelium development | 4.1E-04 |
| GO:0048513 | GO:BP | animal organ development | 4.8E-04 |
| GO:0006950 | GO:BP | response to stress | 5.4E-04 |
| GO:0009888 | GO:BP | tissue development | 7.2E-04 |
| GO:0032502 | GO:BP | developmental process | 7.2E-04 |
| GO:0032501 | GO:BP | multicellular organismal process | 8.6E-04 |
| GO:0012501 | GO:BP | programmed cell death | 9.0E-04 |
| GO:0045177 | GO:CC | apical part of cell | 4.0E-05 |

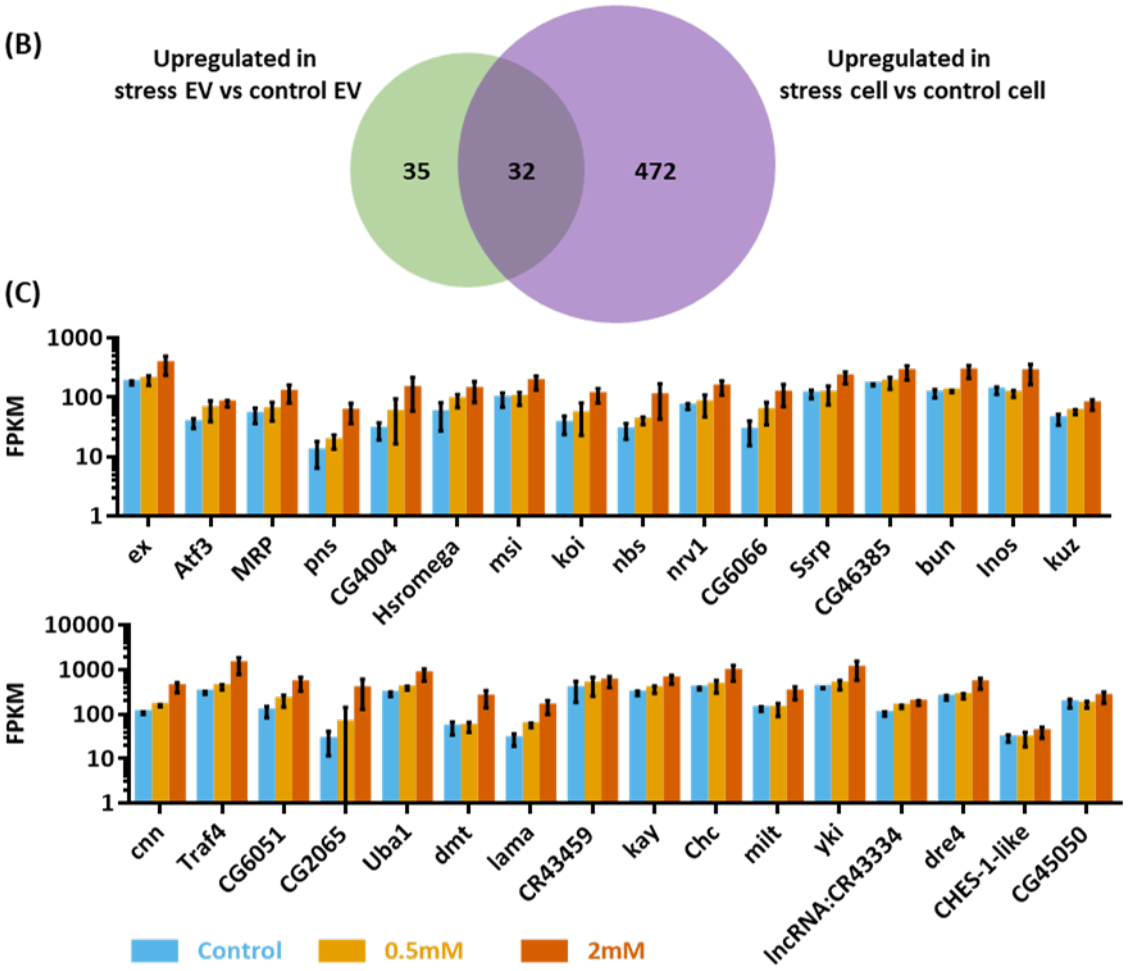


## Figure 5.19 RNA upregulation in stress EVs is strongly stress-dose-dependent

*A) Gene ontology analysis of 67 RNAs significantly upregulated in EVs derived from 2mM $H_2O_2$-treated cells relative to EVs derived from non-treated, against a background of all annotated RNAs listed in Cufflinks file. Multiple testing correction by Benjamini-Hochberg false discovery rate with a cut-off at P-adj<0.001. Differential expression determined via DESEQ2, with P-adj at 0.05. (B) Venn diagram showing overlap of RNA significantly upregulated in 2mM $H_2O_2$ EVs vs non-treated EVs, and RNAs significantly upregulated in 2mM $H_2O_2$ cells vs non-treated cells. (C) FPKM abundance values in EVs for 32 RNAs detected as significantly upregulated in EVs but not cells under 2mM $H_2O_2$ stress.*

(A)

| GO Term ID | Term source | Term name | Adjusted P-value |
|---|---|---|---|
| GO:0044837 | GO:BP | actomyosin contractile ring organization | 1.3E-04 |
| GO:0032506 | GO:BP | cytokinetic process | 2.4E-04 |
| GO:0030866 | GO:BP | cortical actin cytoskeleton organization | 4.4E-04 |
| GO:0030865 | GO:BP | cortical cytoskeleton organization | 5.4E-04 |
| GO:0000281 | GO:BP | mitotic cytokinesis | 6.1E-04 |
| GO:0030036 | GO:BP | actin cytoskeleton organization | 7.4E-04 |
| GO:0030029 | GO:BP | actin filament-based process | 8.0E-04 |
| GO:0031032 | GO:BP | actomyosin structure organization | 8.7E-04 |
| GO:0005826 | GO:CC | actomyosin contractile ring | 3.2E-04 |

(B)




(C)

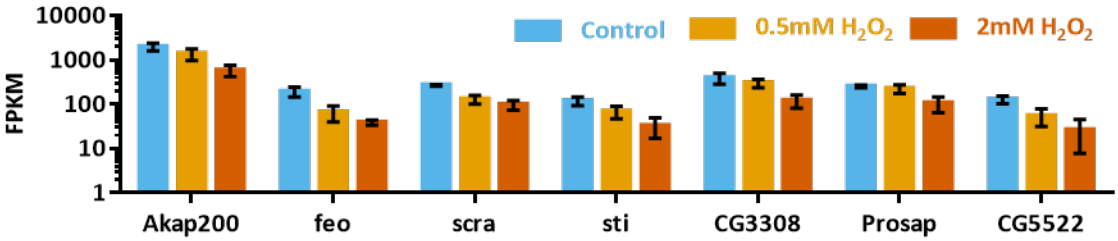


Figure 5.21 Downregulated RNAs in stress EVs are cytoskeleton function related

*(A) Gene ontology analysis of 7 RNAs significantly downregulated in EVs derived from 2mM $H_2O_2$-treated cells relative to EVs derived from non-treated cells, against a background of all annotated RNAs listed in Cufflinks file. Multiple testing correction by Benjamini-Hochberg false discovery rate with a cut-off at P-adj<0.001. Differential expression determined via DESEQ2, with P-adj at 0.05. (B) Venn diagram showing overlap of RNA significantly downregulated in 2mM $H_2O_2$ EVs vs non-treated EVs, and RNAs significantly downregulated in 2mM $H_2O_2$ cells vs non-treated cells. (C) FPKM abundance values in EVs for all RNAs detected as significantly downregulated in EVs under 2mM $H_2O_2$* stress.

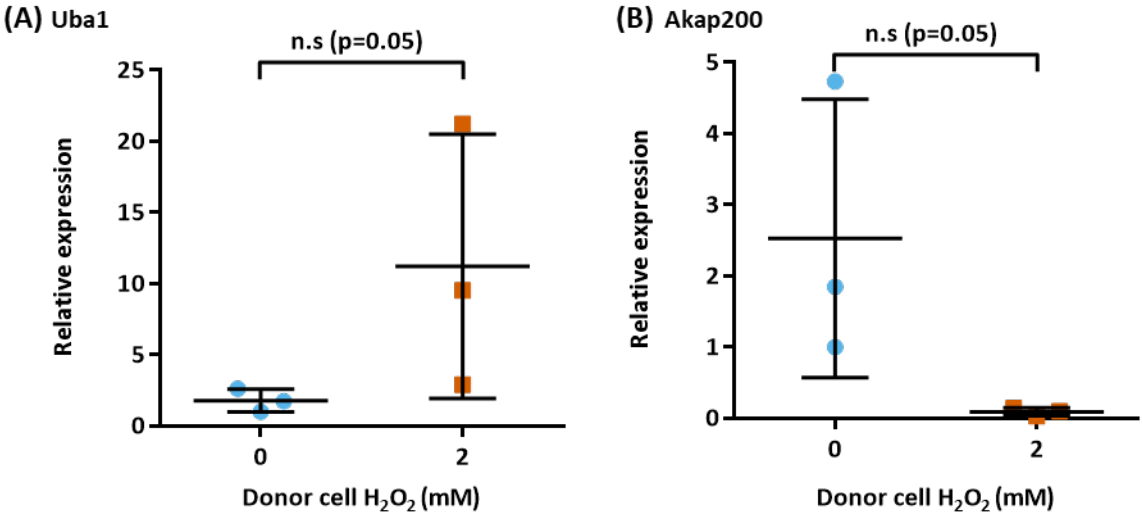


Figure 5.20 qPCR confirms up and downregulation in RNA sequencing data

*qPCR data for A)* Uba1 *and B)* Akap200 *identified as up and downregulated respectively in differential expression of RNAs sequencing data, normalised to* Rpl32 *housekeeping gene. Mean and standard deviation for three biological replicates, statistical significance assessed by one-tailed Mann Whitney test.*

### 5.3.17 Few specific gene changes in stress EVs are evolutionarily conserved

Finally, study of *Drosophila* systems may give insight into cellular responses in mammalian systems through the identification of conserved changes. Evolutionary conservation of RNAs altered in stress EV RNAs relative to control EVs was therefore carried out using an existing published microarray dataset of mouse mast cells also treated with an $IC_{50}$ concentration of $H_2O_2$ (Eldh *et al*., 2010). Differential expression analysis using GEO2R indicated that no changes in this dataset reached a significant adjusted p-value at the 0.05 threshold, so unadjusted p-values were used, as in the original paper, along with a fold change of at least 2. For 1980 RNAs that showed upregulation in any of its probes in the microarray, 1285 had at least one ortholog with a DRSC Integrative Ortholog Prediction Tool (DIOPT) score of 4 or more. 15 of these *Drosophila* orthologs also showed significant changes in the same direction as a mouse RNA probe. GO term analysis of the 16 mouse RNAs, against a background of the 1285 with an identified ortholog, showed enrichment of terms relating to mitochondrial localisation (Figure 5.22). In contrast, of 687 *Drosophila* orthologs for 1401 downregulated mouse RNAs, 16 showed significant changes, but the majority in the opposite direction. These data point towards the existence of minimal stress-induced changes to EV RNA content that are conserved at this evolutionary distance.

| GO Term ID | Term source | Term name | Adjusted P-value |
|---|---|---|---|
| GO:0034643 | GO:BP | establishment of mitochondrion localization, microtubule-mediated | 1.5E-03 |
| GO:0047497 | GO:BP | mitochondrion transport along microtubule | 1.5E-03 |
| GO:0051646 | GO:BP | mitochondrion localization | 1.5E-03 |
| GO:0051654 | GO:BP | establishment of mitochondrion localization | 1.5E-03 |

Figure 5.22 Conserved $H_2O_2$-induced changes in EV RNAs relate to mitochondria

*Gene ontology analysis of 16 mouse RNAs showing corresponding changes in* Drosophila*, against background containing 1285 RNAs with at least one identified ortholog with DIOPT score >4. Multiple testing correction by Benjamini-Hochberg false discovery rate with a cut-off at P-adj<0.001.*

## 5.4 DISCUSSION

### 5.4.1 Ribosomal RNA in EV preparations

Although studies on EV-associated RNA have thus far largely considered miRNAs and mRNAs to be the most important, a much wider range of RNA species have been identified as present in EVs and have been subject to little investigation (Pérez-Boza *et al*., 2018). In this work, bioanalyser analysis indicated the predominance of small or fragmented RNAs in EV preparations, alongside the presence of some full-length rRNA. The presence of a strong small RNA peak is indicative of high density (i.e. small) EVs, whilst full-length rRNA of ABs and/or MVs, so together likely indicating a mixed population (Crescitelli *et al*., 2013; Willms *et al*., 2016; Lässer *et al*., 2017; Wei *et al*., 2017). However, although these full-length rRNA peaks were small in bioanalyser profiles, the dominant species in RNA sequencing data was rRNA, therefore implying fragmented rRNA, seen previously in both total RNA and small RNA libraries (Jenjaroenpun *et al*., 2013; Wei *et al*., 2017). Notably, in this latter study, despite differences in intact rRNA abundance between large and small EVs in bioanalyser profiles, in sequencing the rRNA reads, at 89.6-92.5% of the total, were similarly dominant in both EV types. An increasing body of work indicates that rRNA fragmentation is highly regulated and may have an important functions in controlling cell proliferation, apoptosis, stress and DNA-damage response (Lee *et al*., 2009b; Wang *et al*., 2016; Chen *et al*., 2017; Zhu *et al*., 2018; Cherlin *et al*., 2020) . In addition, it has also been suggested that EVs could play a role as a selective clearance mechanism for rRNAs (Lefebvre *et al*., 2016). Whilst more in-depth study is therefore needed to elucidate whether the rRNA fragments are found within the EVs or are non-vesicular, and if they are of functional importance, data nonetheless confirms their presence in EV-associated RNA of *Drosophila* cells.

### 5.4.2 Topology of EV-associated RNA

A key question for studies of EV components, such as RNA, is whether they have luminal or surface topology. Here, RNAse protection data indicated that there is no difference between total quantified RNA in RNase only or detergent plus RNAse treated samples. Since sequencing was carried out on non-RNAse-treated samples, and rRNA made up vast majority (up to 94%) of reads, this may indicate that the rRNA is located outside of the EVs. Indeed, work by Chiou *et al*. (2018) found that, whilst EV fractions in sucrose gradients demonstrated partial protection against RNAse for a range of RNA species (including 18S rRNA), non-vesicular fractions showed no protection for 18S rRNA, in agreement with the *Drosophila* EV data. Furthermore, non-vesicular extracellular RNA has been shown to contain primarily rRNA, indicating the presence of extracellular ribosomes (Tosar *et al*., 2020). Therefore, it is possible that the rRNA fragments in the EV samples may be due to extracellular, but non-vesicular, rRNA.

In contrast to total RNA quantification, qPCR of RNAse protection samples demonstrated around 50% sensitivity of high abundance mRNAs *Arc1* and *Rpl32.* Whilst a number of studies have suggested complete protection of EV-associated RNA species such as miRNA, snoRNA and CRISPR/Cas9 guide RNA (Rimer *et al*., 2018; Temoche-Diaz *et al*., 2019; de Jong *et al*., 2020), others have indicated varying levels of partial protection (Enderle *et al*., 2015; Shurtleff *et al*., 2017; Chiou *et al*., 2018; Ter-Ovanesyan, 2019). What was evident in the *Drosophila* data was that, whilst the level of RNase sensitivity between biological replicates was highly variable, the level of sensitivity for both mRNAs in matched samples was very similar. This indicates that sample preparation is likely key, with differing EV purification procedures an important contributing factor in these studies. However, notably, the two studies from the same group, Shurtleff *et al*., and Temoche-Diaz *et al.,* showed very different results for miRNA and mRNA, suggesting that there may be biological differences in the location of these RNAs, with more mRNA found outside the EV, in agreement with data in the current work. Alternatively, since the combination of RNAse with detergent treatment does not completely degrade total RNA, some

species may be shielded from RNase activity by non-vesicular protein complexes. Therefore, use of protease treatment in combination with RNAse and detergent is necessary to enable determination of the mechanism of RNase protection. Nonetheless, data here support the existence of mRNA both within and outside of the EV membrane, whilst indicating that other RNA such as rRNA, may be primarily non-vesicular.

### 5.4.3 Bovine RNA contamination

In this work, since the aim was to investigate the effect of stress on EV-RNA content, EV-depleted FBS was added to cell culture media rather than using serum-free, to minimise generation of stress in control samples. Previous work has indicated that both FBS and alternative chemical supplements may contain bovine RNA, with EV RNA from four publicly available datasets containing 3-17% bovine-specific RNA reads, much higher than in cellular RNA (Wei *et al*., 2016; Auber *et al*., 2019). However, in the *Drosophila* EV samples, the abundance of bovine-specific RNA was at a maximum of 1.3% of reads, in fact lower than in the corresponding cell samples. It may be that this is due to the difference in sequencing type, with longer RNAs studied in this work more efficiently depleted from FBS than the small RNAs assessed in the cited studies. However, despite the similarity of the current work with Lefebvre *et al.*, the EV samples here contained less bovine-specific RNA (Supplementary Figure 10, indicating that the SEC method used here is more efficient at removal of contaminating non-vesicular RNA than the UC method used by Lefebvre *et al.*). These results highlight that the SEC method may be more appropriate for ensuring clean EV preparations for RNA sequencing.

### 5.4.4 Transposon content of EVs

Within the *Drosophila* data, repeat sequences, in particular the *Copia* retrotransposon, were found to be abundant and enriched within EV-associated RNA, in agreement with the findings of Ashley *et al.* (2018) and Lefebvre *et al.* (2016). The proportion of total repeat RNA though, at 26±6.6% in the data generated here, was much lower than the 68±3.7% reported by Lefebvre *et*

*al*. However, reanalysis of data from Lefebvre *et al.* gave a more similar percentage of 18±4.0%, due to identification of a higher number of rRNA reads than in the original study (Supplementary Figure 8 and Supplementary Figure 11). In the current work the magnitude of *Copia* enrichment was also around 10-fold lower than found by Ashley *et al*. This difference can, at least in part, be attributed to the fact that the latter study used poly(A)-selected libraries rather than sequencing total RNA. Since the non-coding RNA biotypes which make up a greater proportion of EV RNA are absent in such libraries, the relative enrichment of the poly(A) tailed retrotransposon is likely inflated. This highlights the importance of clear methodologies in comparison of samples which are known to have very different RNA type content, such as cells and EVs.

Other work has also found a variety of mobile genetic elements to be enriched in EVs (Balaj *et al*., 2011; Lefebvre *et al*., 2016; Evdokimova *et al*., 2019; Hardy *et al*., 2019). Transcription of transposons is known to increase under stress conditions, and indeed an increase in cellular abundance of repeat sequences under stress was observed, but no increase was detected in EVs. In contrast, in another study, induction of oxidative stress through sodium arsenate treatment resulted in EV-enrichment of Long Terminal Repeats (LTRs), Human endogenous retroviruses (HERVs) and Long interspersed nuclear elements (LINEs) in A4573, TC32 and TC71 cells, above the EV enrichment seen in normal conditions (Evdokimova *et al*., 2019). EV targeting may provide a means to rid the cell of transposon RNA, which could be especially important under stress conditions, whilst it has also suggested that EVs provide a means for adaptive horizontal transfer of retroviral-like elements (Lefebvre *et al*., 2016). This has been further evidenced through demonstration of the enrichment of a LINE-1 retrotransposon-egfp construct which is capable of retrotransposition in recipient cells, albeit at a very low frequency of ~0.0001% (Kawamura *et al*., 2019). The enrichment of transposon RNA in EVs therefore support the idea that its packaging may have important implications for both producing and receiving cells, particularly under cellular stress conditions.

### 5.4.5 Similarities between viral RNA and EV RNA packaging

In both data generated here, and in reanalysis of data from Lefebvre *et al.,* reads mapping to viral RNA sequences were evident, with *alphanodavirus* reads enriched in the EV preparations and DTV reads depleted (Supplementary Figure 12). What is unclear is whether these reads represent the presence of co-purified viral particles, viral particles contained within EVs, or viral RNA alone associated with the EVs. EVs have been found to contain viral particles or genomes from a number of different non-enveloped positive single-stranded RNA viruses, the same type as *alphanodavirus*, with this form of *en bloc* transmission suggested to aid their infectivity, so viral RNA may be an important biological cargo of EVs (Altan-Bonnet *et al*., 2019).

Small RNA sequencing studies have identified viral reads to be commonplace in *Drosophila* cell lines (and flies), with up to 30% of reads documented (Wu *et al*., 2010; Webster *et al*., 2016). DTV and FHV-like viruses were the biggest contributors in S2 and S2R+ cell lines, leading to conclusions of persistent, non-lytic infection. In the current work, no evidence of infection was noted in cell cultures, and indeed cell counts demonstrated no correlation between the abundance of viral reads and viable cell number (Supplementary Figure 13). In addition, mitotracker staining imaging data from chapter 4 demonstrates that the cells do not show the perinuclear mitochondrial localisation found to be characteristic of lytic, but not persistent infection (Venter *et al*., 2009; Jovel and Schneemann, 2011). Interestingly, these studies also suggest persistent infection to be characterised by production of defective viral RNAs rather than genomic viral RNAs, with short viral reads from both generated by RNA interference (RNAi). Since Ago2, part of the RNAi machinery, has been linked to RNA loading into EVs (McKenzie *et al*., 2016), the activation of RNAi by such defective RNAs may influence the overall RNA content of EVs.

To complicate still further the distinctions between viruses and EVs, viral particles in themselves have been demonstrated to contain a range of host cell RNAs (Onafuwa-Nuga *et al*., 2005, 2006;

Routh *et al*., 2012). Both HIV-1 and virus-like particles (VLPs) packaged non-coding *7SL* RNA (Onafuwa-Nuga *et al*., 2006), which was both abundant and significantly enriched within preparations from control but not 2mM $H_2O_2$-stress here, and enriched within EVs in other studies (Nolte-'t Hoen *et al*., 2012; Tosar *et al*., 2015; Shurtleff *et al*., 2017). Furthermore, in addition to *7SL*, Moloney Murine Leukaemia virus was found to contain a range of snRNAs, again found in the current work and in other EV data (Nolte-'t Hoen *et al*., 2012; Lässer *et al*., 2017; Chiou *et al*., 2018; Driedonks *et al*., 2018). Finally, expression of the capsid precursor *α* RNA of FHV or *Nudaurelia capensis* omega virus in the insect cell line *Spodoptera frugiperda* results in spontaneous formation of non-infectious VLPs (Routh *et al*., 2012). In the absence of viral genome amplification, these VLPs package host cell RNAs, predominantly rRNA, transposable elements, and small amounts of microsatellite RNA, ncRNA and mRNA, highly reminiscent of the RNA from *Drosophila* EV preparations. Since viruses and EVs share very similar biophysical characteristics, purification of pure EVs or pure viral particles is difficult and many existing studies likely contain significant population overlap (Zhou *et al*., 2020). However, since RNA viruses and EVs share common biogenesis pathways, an alternative explanation is that that they also share common mechanisms of RNA packaging (Hoen *et al*., 2016; Margolis and Sadovsky, 2019). Further work, especially in the case of the defective viral RNAs likely present here, is needed to understand the similarities and differences of viruses and EVs, and the significance of the packaged RNA.

### 5.4.6 Correlation of RNA types in EV and cell samples

In the *Drosophila* samples, cellular and EV mRNA profiles were found to be highly distinct from one another through PCA analysis, although with significant variability, particularly under stress. However, spearman correlation coefficients between triplicate samples ranged from 0.77-0.80 for EV samples compared to 0.98-0.99 for cell samples, similar variability to that reported in colorectal cancer cell lines, 0.76-0.95 in EV samples and 0.91-0.94 in cell samples (Hinger *et al*.,

2018). This difference may reflect non-specific loading processes, or greater technical variability within EV samples, due to greater processing requirements for EVs. This sample variability has been shown to predominantly affect long RNA over small RNA for an unknown reason; one possibility is that a greater propensity for long RNA to be present in non-vesicular extracellular RNA increases the effect of technical variability (Hinger *et al*., 2018). In the current work, whilst there was a strong concentration-dependent aspect determining packaging of RNA into EVs, with high abundance cell RNAs tending to be highly abundant in EVs, there is evidence of a degree of specific loading, with 514-837 RNAs significantly differentially distributed. This is in agreement with work on miRNAs, which has proposed the existence of both non-selective and selective mechanisms for RNA incorporation (Tosar *et al*., 2015). What was surprising to see was that there was little overlap in RNAs that were differentially enriched or depleted in EVs under each stress condition, with a core set of only 18.3% of the total enriched RNAs and 11.4% of the depleted RNAs. Some comparison of RNA enrichment has been carried out between diffferent cell lines; with three isogenic colorectal cell (CRC) lines showing 51% overlap in long RNA and 17% in miRNA, whilst in three other CRC lines overlap was 27% for mRNA and 5% for small RNA (Cha *et al*., 2015; Chen *et al*., 2016; Hinger *et al*., 2018). Thus, there seems to be little commonality in the specific RNAs packaged into EVs in both similar cell types and different conditions. It is therefore unsurprising that minimal conservation of specific RNA changes under $H_2O_2$ stress were seen between EVs from *Drosophila* and mouse cell lines. Nevertheless, the RNAs commonly enriched in all conditions in the current work appeared to show functional similarity, relating to the cytoskeleton and development in GO term analysis. Together these data indicate that there is little similarity in the specific RNAs that are loaded into EVs under different conditions, but indicate that there may be other fundamental features of the RNAs, including biophysical aspects or cellular localisation, which may determine their incorporation.

### 5.4.7 Enrichment of snoRNA

In the data the snoRNA biotype was found to be enriched in EVs compared to cells. Previous work has suggested snoRNA to be depleted in EVs, but in small RNA sequencing of RNAs <90nt in length (Nolte-'t Hoen *et al*., 2012; Baglio *et al*., 2015; Tosar *et al*., 2015; Wei *et al*., 2017; Chiou *et al*., 2018). At 46-316nt length in *Drosophila*, snoRNAs sit at the boundary between small (<200nt) and long (>200nt) RNAs. Using very similar total RNA sequencing methods to those used here, Lefebvre *et al.* identified a strong enrichment of snoRNA in *Drosophila* D17 EVs relative to cells, with an overall biotype distribution in EVs not dissimilar to that here (45.6% snoRNA, 17.9% snRNA, 13.2% mRNA, compared to 50.2±5.9% snoRNA, 14.0±1.2% snRNA, 28.5±7.4% mRNA), although in the corresponding S2R+ EVs, mRNA was more dominant at 74.5%. In sequencing of human HepG2 and A431 cells and EVs in the same work, snoRNAs were at much lower abundance, and depleted in EVs, suggested there may be species-specific factor in determining this cargo. Of interest, vault RNAs and Y-RNAs, which are major species of the high abundance miscellaneous RNA grouping in human cell EVs, are not present (or at least not currently known) in *Drosophila* (Perreault *et al*., 2007; Duarte Junior *et al*., 2019). Given the enrichment of snoRNA in EVs seen in current work, this supports existing evidence that, in *Drosophila*, snoRNA may be an especially important RNA cargo of EVs.

SnoRNAs have undergone little study beyond their role in methylation and pseudouridylation of rRNA. However, recent work suggests that they have additional functions in regulating response to stress, in particular oxidative stress (Stepanov *et al*., 2015; Lee *et al*., 2016). It was therefore interesting to see that the correlation and differential expression of snoRNAs was strikingly altered under stress. Recently, snoRNAs were identified to be the most affected biotype of the LDELS mechanism, whilst incorporation was also affected by the endoplasmic reticulum protein VAPA (Barman *et al*., 2020; Leidal *et al*., 2020). SnoRNAs are primarily found in the nucleus, but four *Rpl13*-intron-derived snoRNAs have been shown to accumulate in the cytoplasm under

doxorubicin-induced oxidative stress (Holley *et al*., 2015), so this change in localisation may be a strong determinant underpinning the availability for EV packaging under changing cellular conditions.

## 5.5 KEY FINDINGS

- EV preparations contain primarily rRNA fragments, the majority mapping to the 18S small ribosomal subunit, with a relative increase under oxidative stress.
- *Copia* retrotransposon RNA is abundant and enriched in EV-associated RNA.
- EV preparations purified by SEC contain minimal contaminating bovine-specific RNA.
- *Alphanodavirus* RNAs are enriched in EV preparations whilst DTV RNAs are depleted.
- Some mRNA is protected from RNase degradation by the vesicular membrane.
- Abundance of EV-associated RNA biotypes do not reflect abundance in the cell.
- EV-cell correlation of mRNA, snoRNA and snRNA is dependent on cell stress.
- Abundant EV-associated RNA is involved in ribosomal functions, whilst EV-enriched RNA is involved in cytoskeletal and developmental functions.

# Chapter 6

## Exploring mRNA loading in EVs

# 6 Exploring mRNA loading in EVs

## 6.1 BACKGROUND

### 6.1.1 Functionality of mRNA in EVs

Since the discovery that EVs can contain mRNAs that appear to be delivered to recipient cells and translated (Valadi *et al*., 2007), there have been conflicting reports as to both their presence in EVs, and delivery to recipient cells. Some studies have demonstrated, through the use of reporter systems (e.g. Cre-loxP gfp, β-lactamase), that mRNA is present and seems to be functionally delivered to recipient cells, although some questions remain about the possible trace presence of protein mediating this effect (Ridder *et al*., 2014, 2015; Zomer *et al*., 2015; Hinger *et al*., 2018; Albanese *et al*., 2020). However another study found, using a luciferase reporter, that whilst full-length mRNA is present in EVs, no functional reporter activation in recipient cells could be detected (Kanada *et al*., 2015). Notably, the transfer of luciferase detected by Albanese *et al*. was only seen when EV-producing cells were co-transfected with vesicular stomatitis virus G plasmids, which incorporate into the EV membrane and promote fusion with recipient cells. These results highlight that delivery of translatable mRNA is highly dependent on EV uptake and endosomal escape, so a move towards study in an *in vivo* context is likely to lead to a better understanding of its physiological relevance (Hung and Leonard, 2016; Heath *et al*., 2019; de Jong *et al*., 2020).

Although some intact, translatable mRNAs seem to be present in EVs, these have been estimated to be present at approximately 1 molecule per 10 EVs, whilst smaller intronic or exonic fragments are estimated to be more abundant, at 1 fragment per EV (Wei *et al*., 2017). No specific function has yet been described for these fragments, but several studies have found that UTR regions, particularly 3' UTRs, are overrepresented, indicating the possibility that they may be specifically loaded, or preferentially stable products of the degradation of full-length mRNAs (Nolte-'t Hoen *et al*., 2012; Batagov and Kurochkin, 2013; Wei *et al*., 2017; Pérez-Boza

*et al*., 2018). Therefore, more work is needed to understand how these fragments are generated and loaded into EVs, and what biological relevance they may have.

### 6.1.2 The role of sequence motifs in EV-mRNA loading

As outlined in section 1.3.2, several studies have identified sequence motifs that may be important in packaging of mRNA into EVs, particularly in combination with RBPs (Batagov *et al*., 2011; Bolukbasi *et al*., 2012; Szostak *et al*., 2014; Kossinova *et al*., 2017). However, the 25nt "zipcode" motif (ACCCTGCCGCCTGGACTCCGCCTGT) discovered in primary glioblastoma and melanoma cell lines, and validated in HEK293T cells through an effect on eGFP loading (Bolukbasi *et al*., 2012), was not enriched in EVs of the hepatic cell line MLP29, and did not have an effect on loading of *HChrR6* mRNA in HEK-293 cells (Szostak *et al*., 2014; Forterre *et al*., 2020). Szostak *et al.* instead identified C[TA]G[GC][AGT]G[CT]C[AT]GG[GA] as an EV enriched motif, suggesting that sequence motifs are likely important, but may be highly context dependent. Therefore, more work is needed to establish whether motifs act to enhance EV loading in other non-mammalian organisms, in order to understand whether these loading mechanisms are evolutionarily conserved.

### 6.1.3 Differential loading of mRNA under stress conditions

Although numerous studies have shown that the mRNA content is altered under different types of cellular stress (section 1.1.5), very little is known about how these changes occur. Three possibilities exist. Firstly, that any change in EV abundance simply reflects the change in abundance in parental cells. However, as demonstrated in chapter 5, 52% of RNAs statistically significantly upregulated in EVs under 2mM $H_2O_2$-stress were *not* also upregulated in the parental cells, indicating potential changes in loading mechanisms (Figure 5.19). A second possibility is that under stress, there is differential regulation of mechanisms which exist under normal conditions. For example, in study of miRNA loading, oxidative-stress induced phosphorylation of caveolin-1 resulted in O-GlcNAc glycosylation of hnRNPA2B1, altering miRNA

binding (Lee *et al*., 2019). Finally, it is also possible that here are additional mechanisms that only come into play under stress conditions. Given the importance of EVs and their cargo in a wide range of pathologies, understanding *how* RNA loading is modulated under different cellular conditions is vitally important, but a largely open question.

## 6.2 AIMS AND OBJECTIVES

Although EV RNA incorporation is being increasingly studied, much of the work has focused on small RNA rather than on mRNA. In addition, little is known about whether the mechanisms discovered are conserved under different conditions, and in different species. Therefore, understanding of the basic mechanisms underlying this packaging process will help to determine both its physiological relevance, to the producing cell and in intercellular communication, and how it can be best leveraged for therapeutic use. The aims of this chapter were therefore to:

1. Use bioinformatic analysis to assess mRNA length as a determinant of loading into EVs.
2. Identify any sequence motifs enriched within EV-associated mRNAs, in both control and oxidative stress conditions.
3. Test the effect of enriched sequence motifs on promoting EV loading of mRNA *in vitro*.
4. Explore other features that are enriched in EV mRNAs relative to cellular mRNAs.

## 6.3 RESULTS

### 6.3.1 EVs are enriched for reads mapping to longer RNAs

Having carried out characterisation of the full range of total RNA present in all samples, to further explore the mechanisms underlying RNA differential abundance in cell and EV samples, any common characteristics to enriched or depleted mRNAs were then investigated. mRNAs range widely in length from 152-56489nt, so length may put some restriction on packageability. Although a splice variant-level analysis could not be carried out due to low read depth in the EV samples (junction saturation analysis in Supplementary Figure 14), length was analysed by

considering the median length of all known splice variants. The size distribution of the top 1000 most abundant mRNAs revealed that, although most mRNAs detected were in the 500-1000nt size range, mRNAs at over 6000nt could be detected (Figure 6.1A). Visualisation of mapping locations using Integrative Genome Viewer (IGV) confirmed that reads spanned the full length of the transcripts, including longer mRNAs such as *Khc* (5012nt) and *Tud* (9592nt) (Figure 6.1C, D). Although detected mRNAs were predominantly 500-1000nt in EVs, the distribution of lengths was highly similar in cell samples, indicating no strong preference for shorter transcripts as has been suggested elsewhere. Analysis of the abundance of these mRNAs, by considering relative FPKM values, further demonstrated that transcripts of 500-1000nt were the most prominent in both cell and EV sample types (Figure 6.1B). Unexpectedly, long transcripts of >6000nt in length appeared to be enriched in EV samples (Figure 6.1A, B). To further investigate this finding, the lengths of all mRNAs found (by DESEQ2) to be statistically significantly enriched or depleted in EVs, were compared. This revealed that EV-enriched mRNAs were highly significantly longer than depleted mRNAs in normal conditions, but under stress the significance was reduced (Figure 6.2A). This result further strengthened the case for the presence of loading of longer mRNAs into EVs but indicated that under conditions of stress, length may be a less important determinant than in normal conditions.

During length analysis it was also noted that the number of known splice variants per gene was higher in EV-enriched mRNAs compared to depleted mRNAs (Figure 6.2B). Since many proteins involved in splicing have been detected in EVs (Pavlyukov *et al*., 2018), these differences might be a direct length effect, or an indirect effect of longer RNAs being subjected to more splicing. To distinguish these factors the number of exons per gene, after normalising for gene length, was compared. Using this measure, no significant differences between enriched and depleted mRNAs were seen, indicating that the enrichment of longer mRNAs in EVs under normal conditions were likely direct, and not a result of increased splicing complexity (Figure 6.2C).

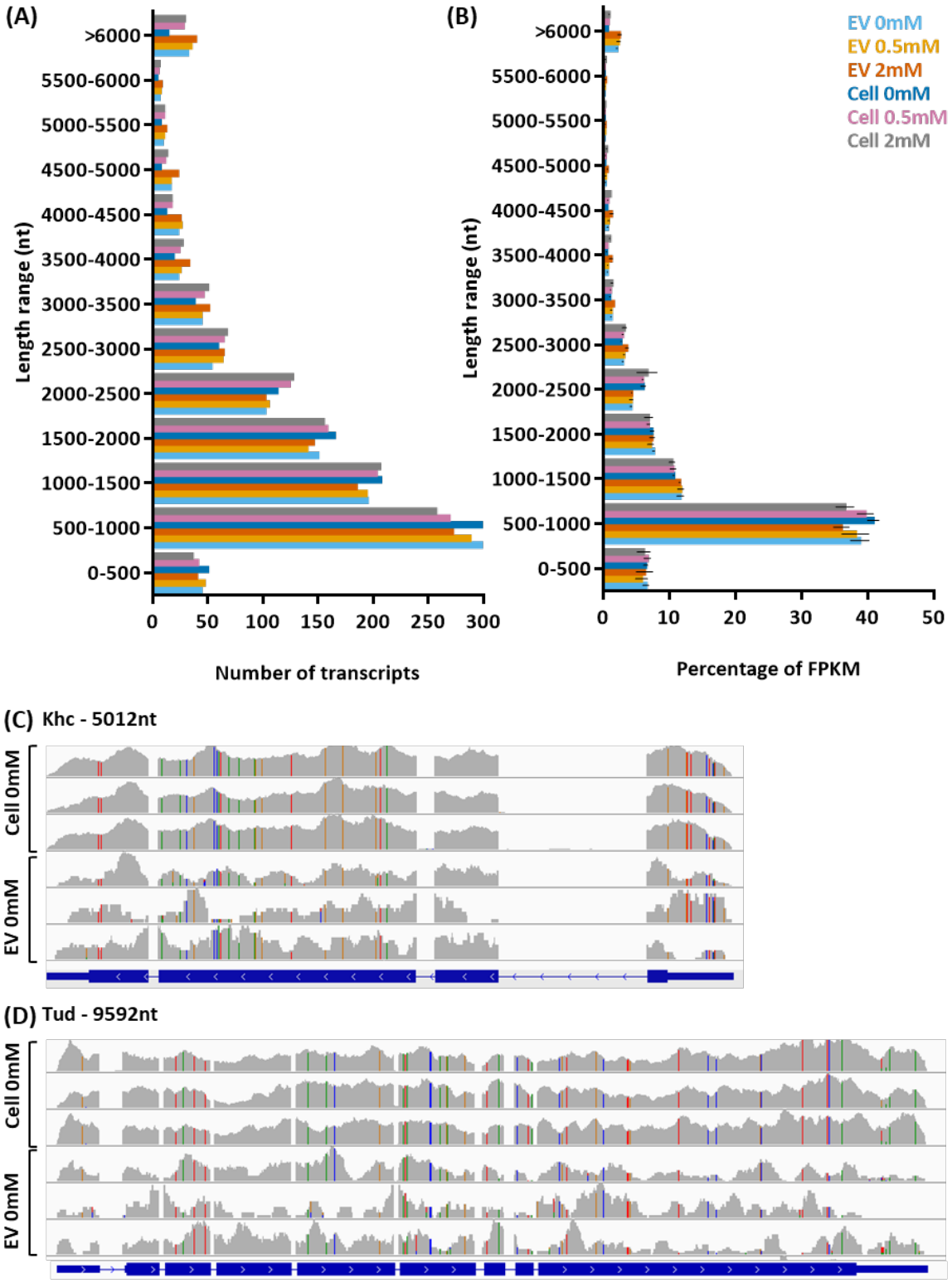


Figure 6.1: EVs contain reads derived from both long and short mRNAs

*(A) Length distribution of the top 1000 most abundant mRNAs (excluding* Arc1*) detected in EV and cell samples. (B) As for (A) but with normalised FPKM abundance values generated by Cufflinks. (C) and (D) Screenshots of read distribution along* Khc *and* Tud *loci on Integrative Genome Viewer.*

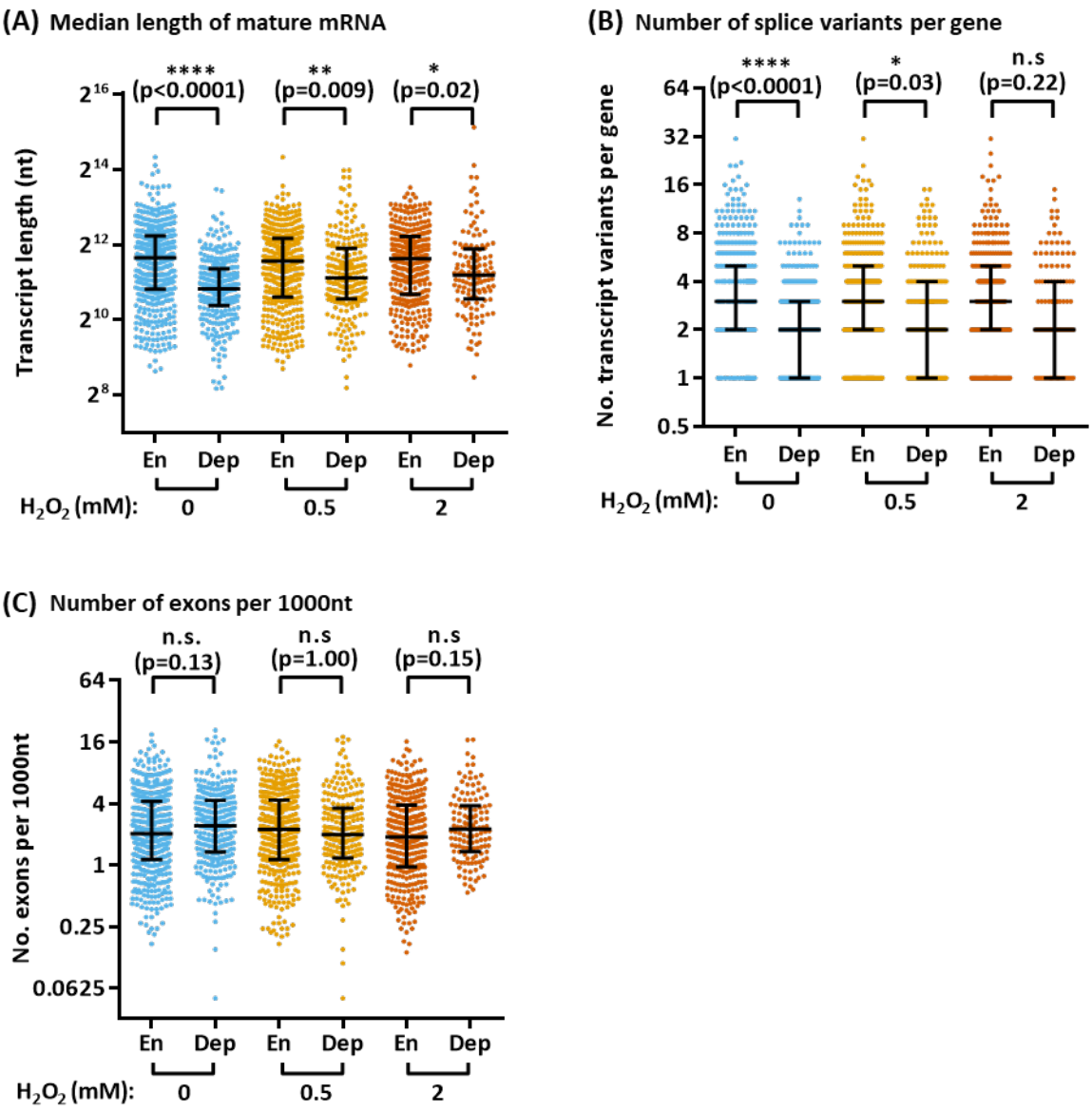


Figure 6.2: Significantly enriched EV mRNAs are longer than EV-depleted mRNAs

*(A) Median total length of spliced mRNA variants for all mRNAs detected as statistically significantly enriched or depleted in EVs, determined via DESEQ2, with P-adj at 0.05. (B) Number of known splice variants per gene and (C) total number of exons per gene, after normalisation to total gene length. Graphs show median and interquartile range, and statistical significance assessed with by Kruskal Wallis test followed by Dunn's multi-comparison test.*

### 6.3.2 Intronic reads become more abundant in EVs with increasing stress

Although some mRNAs showed the coverage expected for a full-length, spliced RNA, this does not confirm them to be intact. To further investigate whether mRNAs were present as fragments, the read distribution of the total mapped reads was evaluated. In control cells, 75% of reads mapped to coding exons (CDS), with no significant changes under stress (Figure 6.3A).

In the EVs, however, there was a strong significant reduction in the CDS region, with a significant increase in intronic mapping and a slight increase in 3'UTRs. Comparing the enrichment in each matched EV-cell pair also showed that under stress, there was a significant relative enrichment of introns, 3'UTRs and 5'UTRs relative to the CDS (Figure 6.3B), whilst visualisation using IGV confirmed that individual genes demonstrating these patterns could be found (Figure 6.4). Since these region enrichments were not found for all genes, this indicated that specific features within them may have importance for determining EV-RNA packaging.

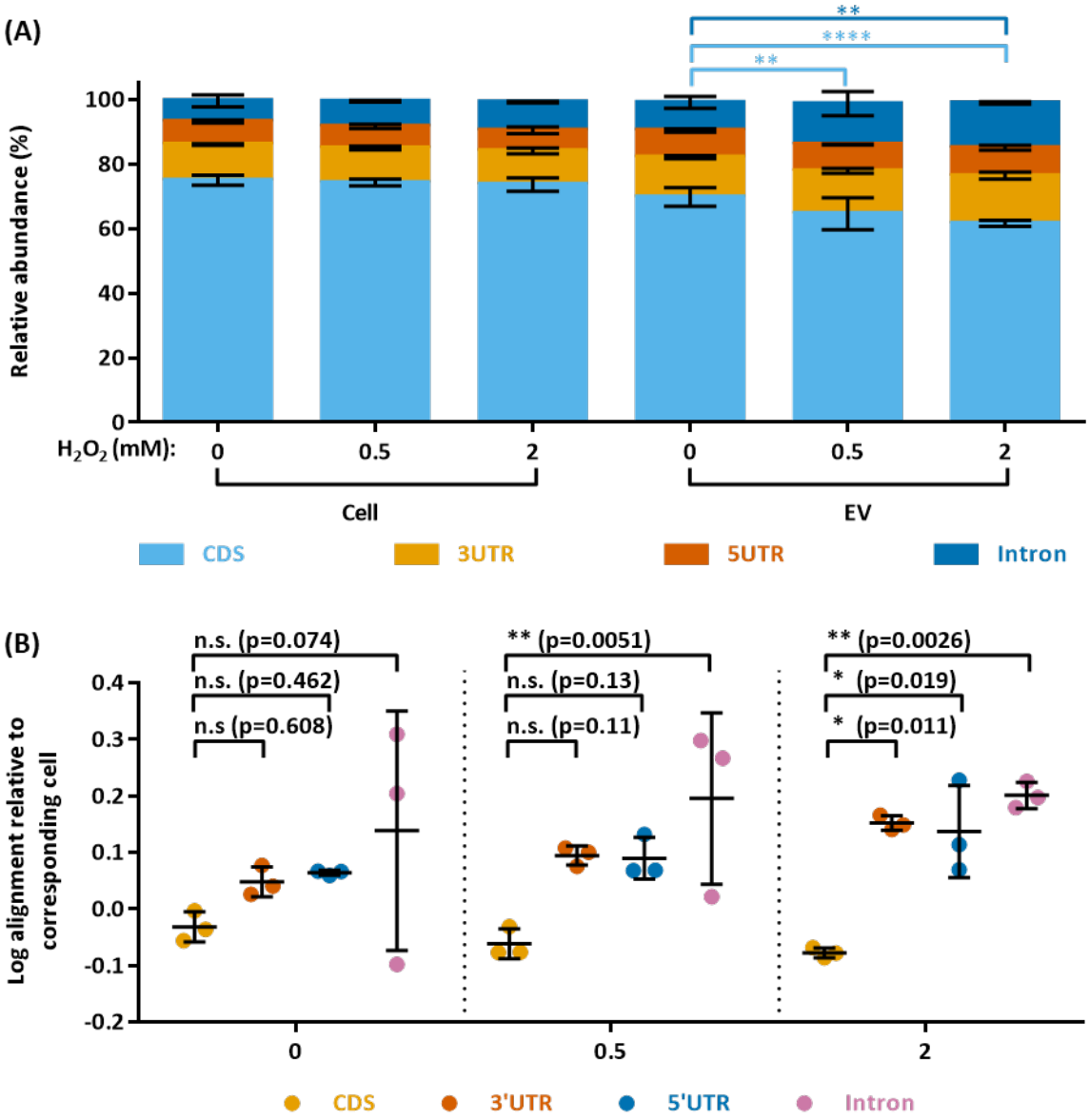


Figure 6.3: Intronic, 3'UTR and 5'UTR reads are enriched in EVs under stress

*(A) Relative abundance of sequencing reads in each mRNA region. (B) Enrichment of each region in EVs derived from non-treated, 0.5mM $H_2O_2$ and 2mM $H_2O_2$-stressed cells against parental cell samples. Graphs show mean and standard deviation of three biological replicates, and statistical significance assessed with two-way ANOVA followed by Tukey's multiple comparisons test.*

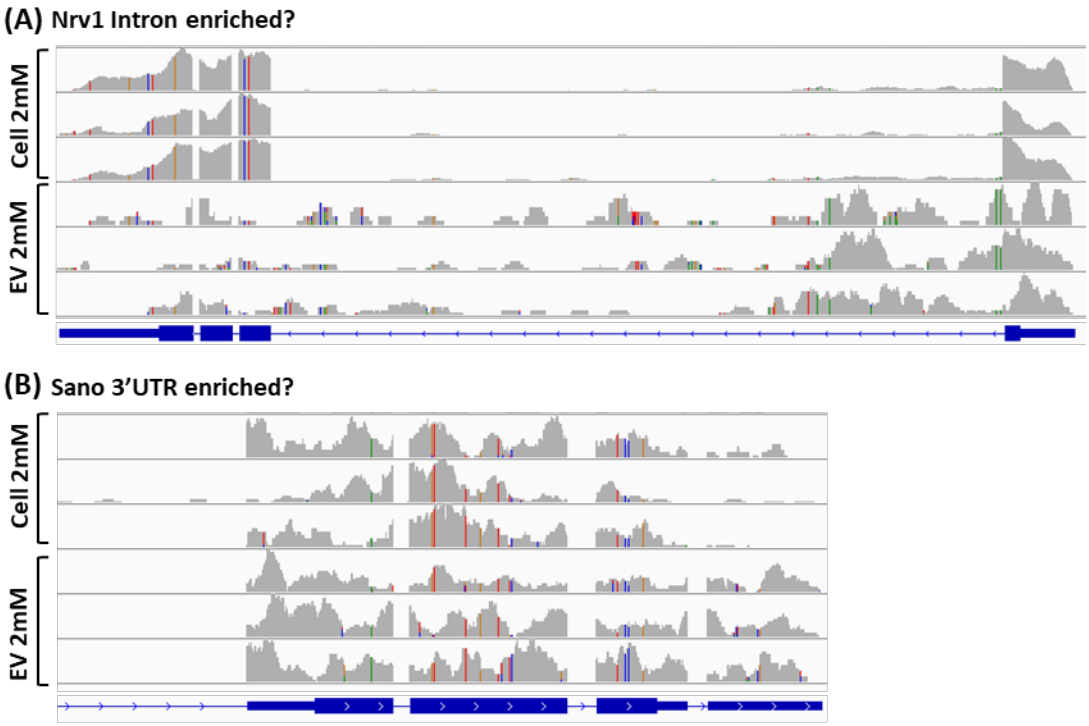


Figure 6.4: Example genes showing region specific enrichment

*(A) and (B) Screenshots of read distribution along* Nrv1 *and* Sano *loci on Integrative Genome Viewer, showing intron and 3'UTR enrichment respectively, in EV and cell RNA under 2mM $H_2O_2$ stress.*

### 6.3.3 Base mismatch is higher EV samples under stress conditions

Given the tendency for low alignment rates in EV samples reported by others (Cha *et al*., 2015; Tosar *et al*., 2015; Yang *et al*., 2017; Hinger *et al*., 2018), the quality of sequencing read alignment was next analysed, examining the base mismatch rate of each sample relative to the reference sequence. This showed a striking increase in mismatch rate in transcribed regions of EVs under high stress, an increase that was not seen in the cell samples (Figure 6.5A). Region-specific evaluation revealed a significant enrichment of mismatches in 3'UTRs, which was maintained under all three stress levels (Figure 6.5B). Visual inspection with IGV confirmed that some mismatches occurred in the same location in all cell and EV samples, some in single samples only, and some at a higher rate in several EV samples only (data not shown). However, the differences in read depth between these samples prevented any meaningful quantification of these group types. One possibility for increased total rate of mismatch is a higher rate of non-templated base modifications/additions that alter reads during reverse transcription (Hinger *et*

*al*., 2018). However, a second possibility is that these mismatches are sequence errors within the mRNA, indicative of aberrant mRNAs that are targeted to EVs.

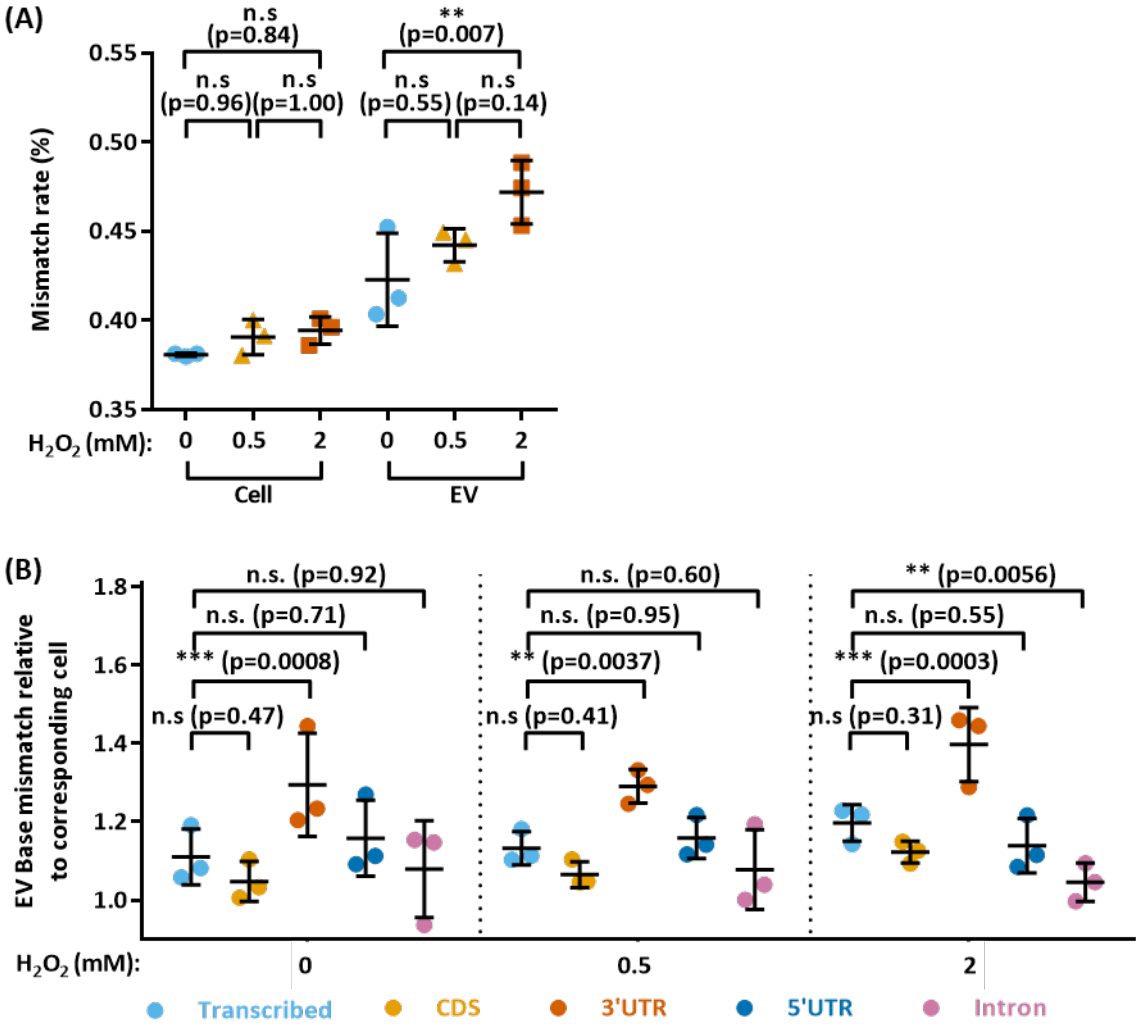


Figure 6.5: Read alignment mismatch rate is increased in EVs under stress

*(A) Mismatch rate for sequencing read alignments in all transcribed regions. (B) Relative mismatch rate of EVs derived from non-treated, 0.5mM $H_2O_2$ and 2mM $H_2O_2$-stressed cells against parental cell samples. Graphs show mean and standard deviation for three biological replicates, and statistical significance assessed with (A) one-way ANOVA followed by Sidak's multiple comparisons test or (B) two-way ANOVA followed by Tukey's multiple comparisons test.*

### 6.3.4 3' end gene coverage is lower in EV samples under stress conditions

If aberrant mRNAs are indeed targeted to EVs, they may be those which are intended for degradation, implying that EVs contain the products of mRNA degradation. To investigate this possibility, the RSeQC tools were used to quantitively assess coverage across gene length. The gene body coverage profile indicated that, for both cell and EV samples, coverage was lower at 5' and 3' ends, the latter more so (Figure 6.6A), which are known effects of RNA fragmentation

and random hexamer priming during library preparation (Wang *et al.*, 2009). Quantification of this coverage bias was carried out using the tool RNASeqMetrics, which calculates the mean coverage of the 100 most 3' or 5' bases divided by the mean coverage of the whole transcript, with relative 5'/3' bias giving an indication of degradation. These results showed that there was no significant effect of stress on degradation of mRNA in cell samples, but it was significant in EV samples (Figure 6.6B). Since this tool calculates bias for the 1000 most abundant transcripts, it is unlikely to be an effect of read depth. In addition, since $H_2O_2$-containing culture media was removed before conditioning for EV purification, and EVs samples treated identically, it seems unlikely that the effect is due to exogenous degradation, but more likely representative of biological differences, such as specific loading of degradation products. In this case the reduced coverage at the 3' end of RNA indicates that EVs may be enriched for products of 3'-' decay.

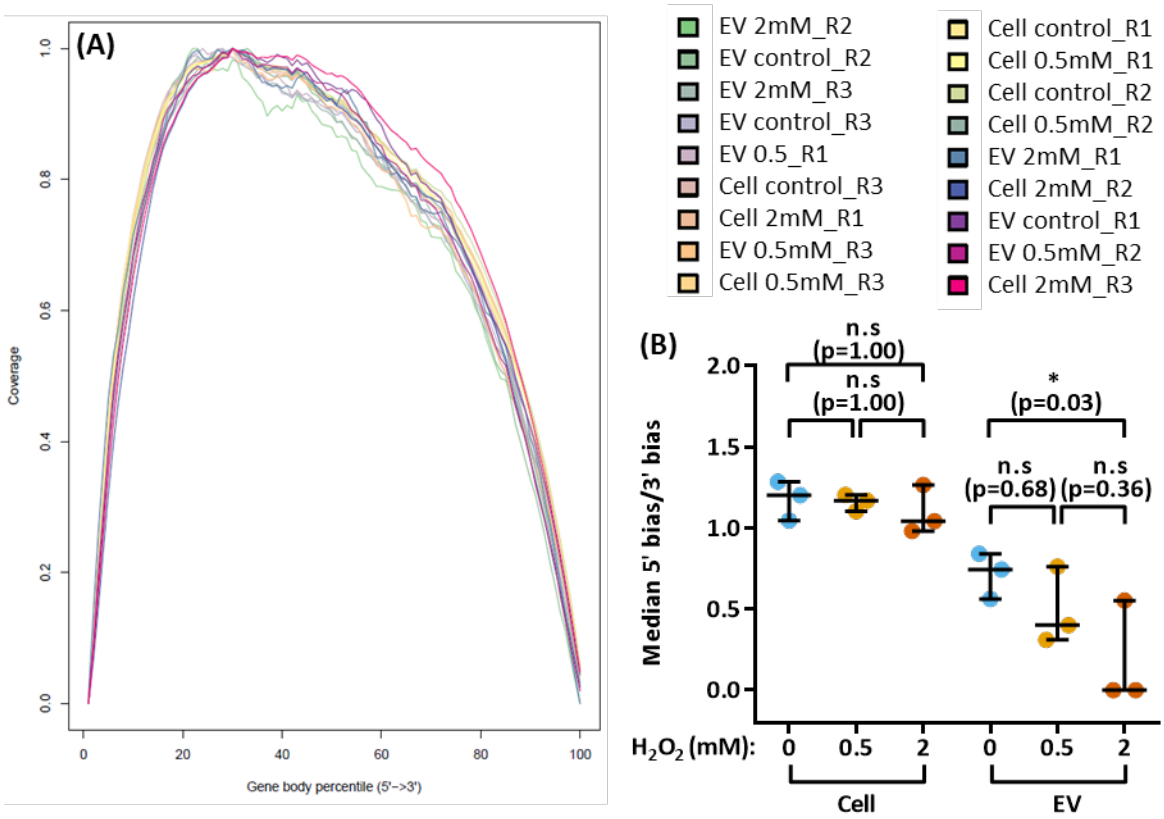


## Figure 6.6: EV RNAs exhibit greater 3' end degradation under stress

*(A) Gene body coverage determined by RSeQC of all eighteen sequenced samples (*Arc1 *and* mdg-4 *trans-spliced gene excluded). (B) 5'/3' bias of all samples, representing the ratio of mean coverage of the 100 most 5' bases divided by the mean coverage of the whole transcript, to the mean coverage of the 100 most 3' bases divided by the mean coverage of the whole transcript, for the 1000 most abundant transcripts. Graph shows mean and standard deviation of three biological replicates, and statistical significance assessed by one-way ANOVA followed by Sidak's multi-comparison test.*

### 6.3.5 Control EV enriched motifs are abundant in all stress conditions

Sequence motifs have been proposed to be important in packaging of a range of RNA biotypes into EVs, so any potential such motifs in the *Drosophila* mRNA were next investigated. To do so a pipeline for classification of mRNAs was set up, separating them into mRNAs expressed in the cell only, and those expressed in the EV only or highly enriched (at least four-fold) in EV relative to cell (Figure 6.7). Initially this was carried out with a low stringency threshold, with a minimum read count of 5 in at least one cell replicate, or 1 in at least one EV replicate.

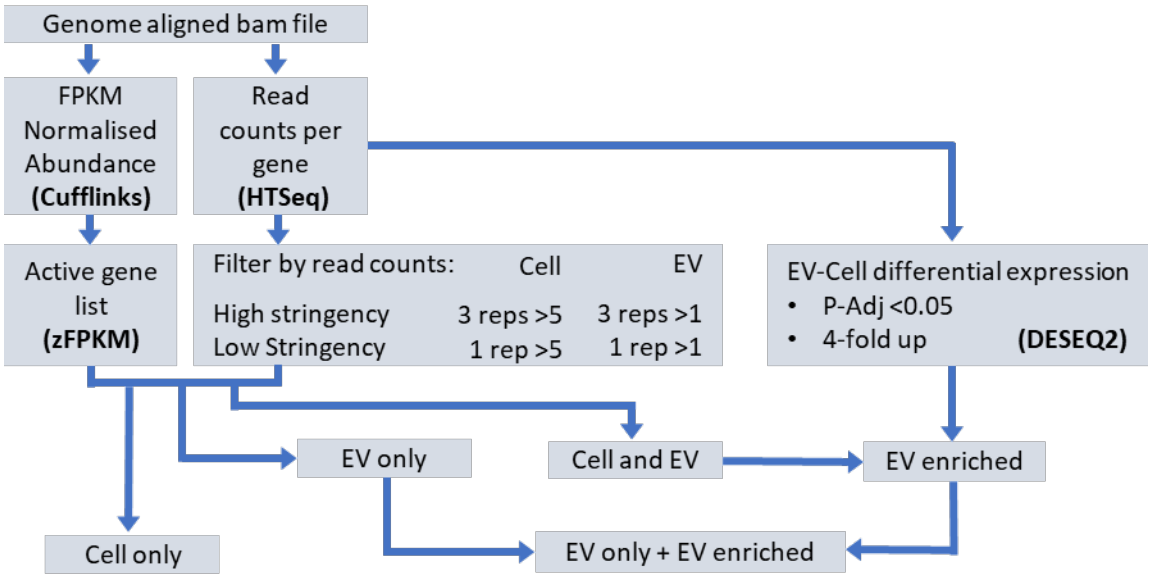


Figure 6.7: Outline of pipeline for grouping mRNAs for motif analysis

This grouping process gave 314 "EV only/EV enriched" and 776 "cell only" mRNAs in control conditions, for which the 3'UTR sequences of all transcript variants were input, as target and background groups respectively, into the MEME Suite programme "Multiple EM for Motif Elicitation" (MEME), which discovers ungapped motifs. Using a second programme "Find Individual Motif Occurrences" (FIMO), the 30 motifs output from MEME were searched within the 3'UTR sequences from all mRNAs. mRNAs with motif hits with a q-value of less than 0.05 in any of its splice variants were then considered as motif-containing mRNAs. Of 30 motifs, six showed an enriched abundance in EV samples relative to cells in control conditions (Figure 6.8A, B). These same six motifs were also detected as enriched in EVs under both stress conditions,

although with a slightly lowered abundance in EVs and slightly higher in cells. To determine whether the hits in these different groups were simply in the same mRNA sequences, the overlaps between "EV only/EV enriched" mRNAs under each condition were checked. This showed that only 5.1% of the mRNAs within this group overlapped between all three conditions (Figure 6.8C). However, motif hits were detected in mRNAs found exclusively in any one of the control, low or high stress conditions, whilst the highest rates for motifs 1,3,4 and 7 were in the mRNAs whose EV-enrichment was common to all three conditions (Figure 6.8D). The six motifs were also found to be enriched in EVs relative to cells in each stress condition when analysing all enriched and depleted mRNAs without the 4-fold cut-off or filtering process, indicating that the motif discovery pipeline was robust (Supplementary Figure 15A). Comparison of motifs to those from the literature revealed similarity of motif-2 to those of Batagov *et al.* (2011) and Szostak *et al.* (2014), although this was not statistically significant (Supplementary Figure 15B). Nevertheless, these motifs do appear to be enriched in EV mRNAs under each stress condition, suggesting they may have a basal role in mRNA packaging in *Drosophila*.

### 6.3.6 3'UTR motifs do not specifically increase EV localisation of mRNA *in vitro*

With bioinformatic analysis indicating that the motifs identified were enriched within the EV mRNAs relative to cells, next the sufficiency of these motifs for enhancement of mRNA packaging was assessed. To do so, a Cre-LoxP reporter system, developed by Claire Hill for use in *Drosophila in vitro* and *in vivo*, was used. Modelled on a system used for study of EV transfer in mice (Ridder *et al*., 2014; Zomer *et al*., 2015), this makes use of two complementary plasmids, the first encoding Cre recombinase (Cre), and the second encoding myristoylated gfp, with a LoxP-flanked stop cassette between the promoter and coding region. To first test whether the presence of motifs increased packaging of RNA into EVs, three additional versions of the Cre plasmid were produced; firstly, one containing the 25-nt motif identified by Bolukbasi *et al.* in mammalian cells (Cre-25nt). Secondly, one containing the 3'UTR of FBtr0344944, one variant of

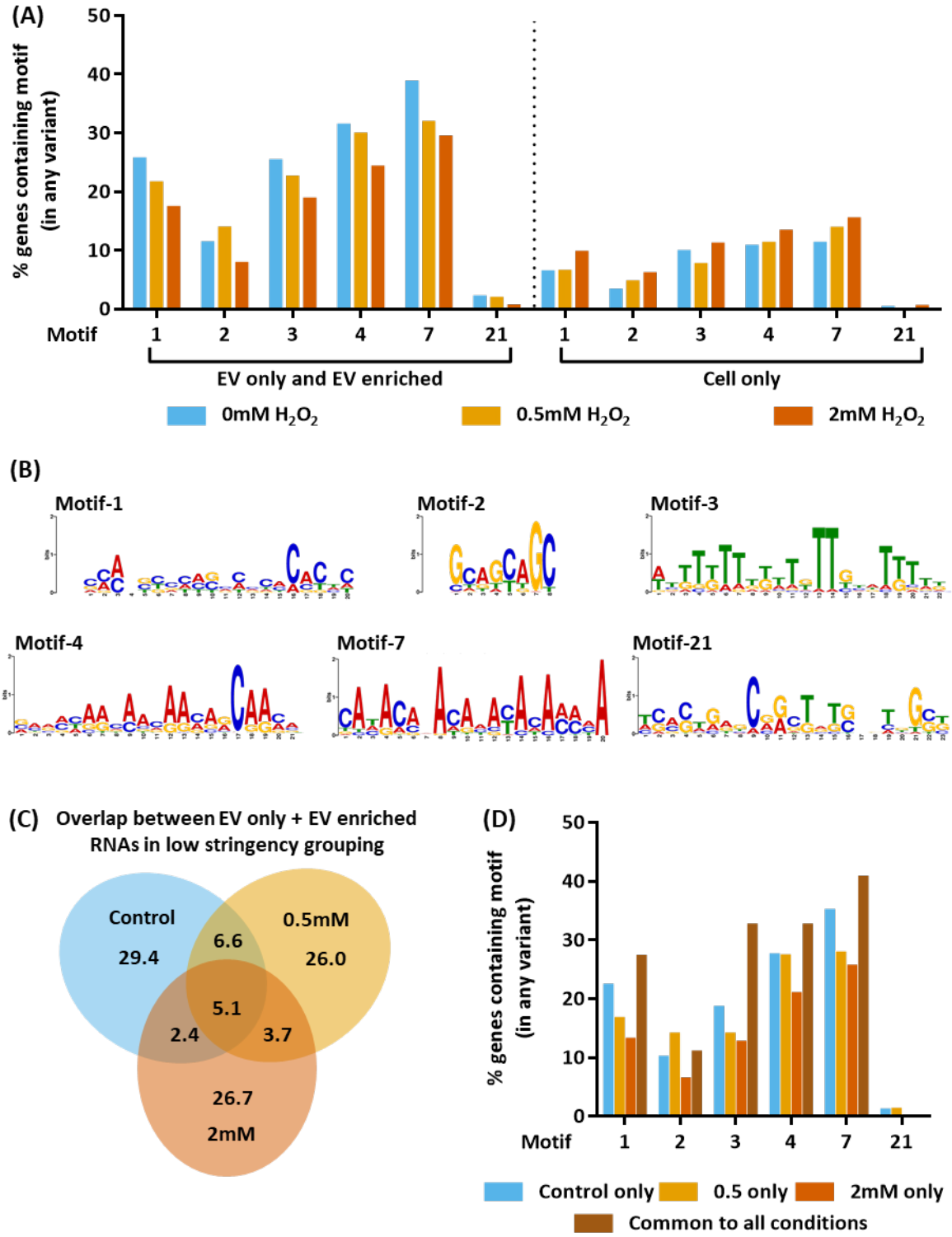


Figure 6.8: EV-enriched motifs from control conditions also abundant under stress

*(A) Abundancies of 30 motifs in low stringency control set found by searching of 3'UTR sequences using MEME, in each mRNA set. (B) Graphical representation of each motif showing significant hits. (C) Percentage overlap of the "EV only and EV enriched group" in each stress condition; total 314 mRNAs in control conditions, 300 in 0.5mM $H_2O_2$ and 274 in 2mM $H_2O_2$. (D) Abundance of each motif in the fully overlapping or condition-specific mRNAs from (C).*

*Drosophila paralytic (para)* mRNA, an 185-nt sequence containing occurrences of low stringency motifs 1,2,3,4 and 7 (Cre-Para WT). Finally, one containing the *para* 3'UTR with three of these motifs shuffled (Cre-ParaShuffled) (Supplementary Figure 16). RNA was then extracted from EVs purified from S2R+ cells transfected with these constructs. RNase protection assays (treatment with either RNase alone, or Triton-X100 to disrupt the EV membrane and expose the internal RNA to subsequent RNAse) showed that all Cre types tested showed near complete sensitivity with RNAse and Triton, but only partial sensitivity with RNAse alone, indicating that some RNA was protected from degradation by the EV membrane, in line with results seen for *Arc1* and *Rpl32* in chapter 5 (Figure 6.9A). To assess the effect on EV loading, the relative EV-cell expression ratio was then compared for each Cre type using qPCR. This indicated that, whilst Cre-25nt showed no differences in expression, there was a trend towards an increased EV/cell ratio for both Cre-ParaWT and Cre-ParaShuffled (Figure 6.9B). Therefore, it is likely that the remaining unshuffled motifs may be more important, or that the 3'UTR addition acts to increase EV packaging independently of the specific motifs present.

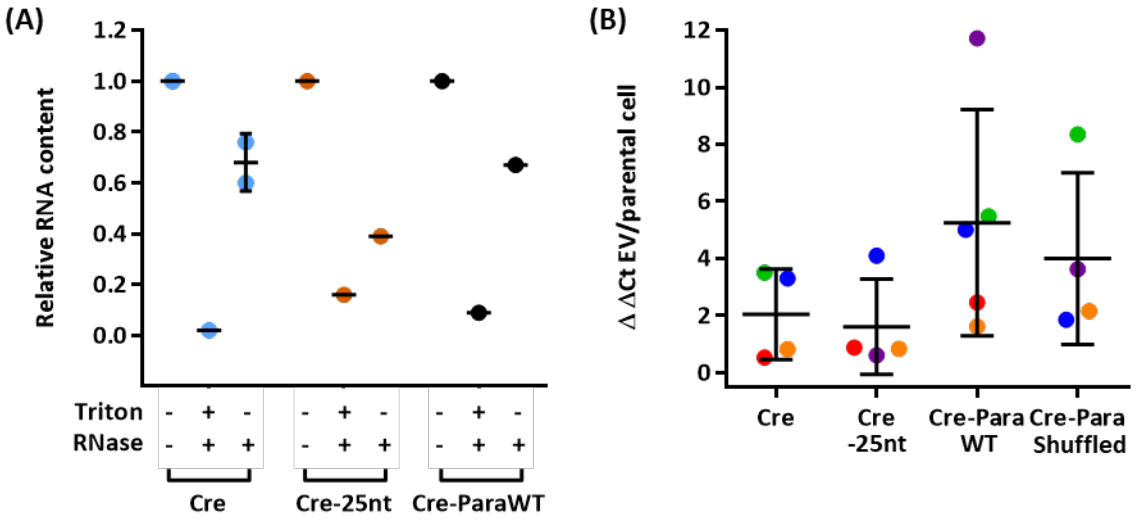


## Figure 6.9: WT and shuffled Para 3'UTR show tendency to increased EV Cre

*(A) Relative quantity of Cre mRNA remaining after treatment with RNAse A alone, or when pre-treated with Triton X-100 detergent. EV samples derived from cells transfected with normal Cre, Cre-25nt, Cre-ParaWT or Cre-ParaShuffled. cDNA synthesis carried on 15-40ng of RNA from untreated control or equivalent volumes for RNAse A/Triton X-100 treatments. (B) Relative expression of Cre in each EV sample, normalised to the expression level in its parental cell sample by ΔΔCt method. Graphs show mean and standard deviation of two to five biological replicates.*

### 6.3.7 No high abundance stress-specific EV-enriched motifs can be identified

Having detected some motifs under control conditions that demonstrated EV enrichment, the next aim was to assess whether any stress-specific EV loading motifs could be identified. This next motif search was carried out with a higher readcount threshold, with a minimum read count of 5 in all three cell replicates, or 1 in all three EV replicates, referred to from this point as high stringency conditions. Motif searching was carried out in three ways: firstly comparing the "EV only/EV enriched" group for 2mM $H_2O_2$ EV mRNAs relative to 2mM $H_2O_2$ "cell only". Secondly, 2mM $H_2O_2$ "EV only/EV enriched" relative to control "EV only/EV enriched". Thirdly, mRNAs found exclusively (non-overlapping with control or 0.5mM $H_2O_2$) in 2mM $H_2O_2$ "EV only/EV enriched" group relative to 2mM $H_2O_2$ cells. In each case, this search returned motifs that predominantly fit one of two types: firstly high (> ~20%) abundance in mRNAs in the in 2mM $H_2O_2$ "EV only/EV enriched" group but present and enriched in "EV only/EV enriched" under all stress conditions, in fact often more abundant under control conditions (Figure 6.10). Secondly, more abundant in 2mM $H_2O_2$ "EV only/EV enriched" EVs compared to control "EV only/EV enriched" but very low (<5%) overall abundance. Almost all motifs in the first high abundance motif group showed significant similarity to one or more of the low stringency motifs identified in the control conditions. Together, these results indicated that stress-specific EV loading motifs likely do not play a role in mRNA packaging, but strengthens the case that the higher abundance motifs detected are important in all conditions, and represent an underlying mechanism which could be altered by additional levels of regulation in different cellular contexts.

### 6.3.8 RNA binding proteins Smooth and PAPI may have a role in mRNA loading

Since RNA-binding proteins (RBPs) have been recognised as important in mRNA incorporation into EVs in several studies (section 1.3.3), the next aim was to investigate whether the motifs discovered in *Drosophila* cells might be functioning via RBP-binding. To do so, motifs showing above ~10% abundance in EVs from each of the four motif sets were compared to an existing

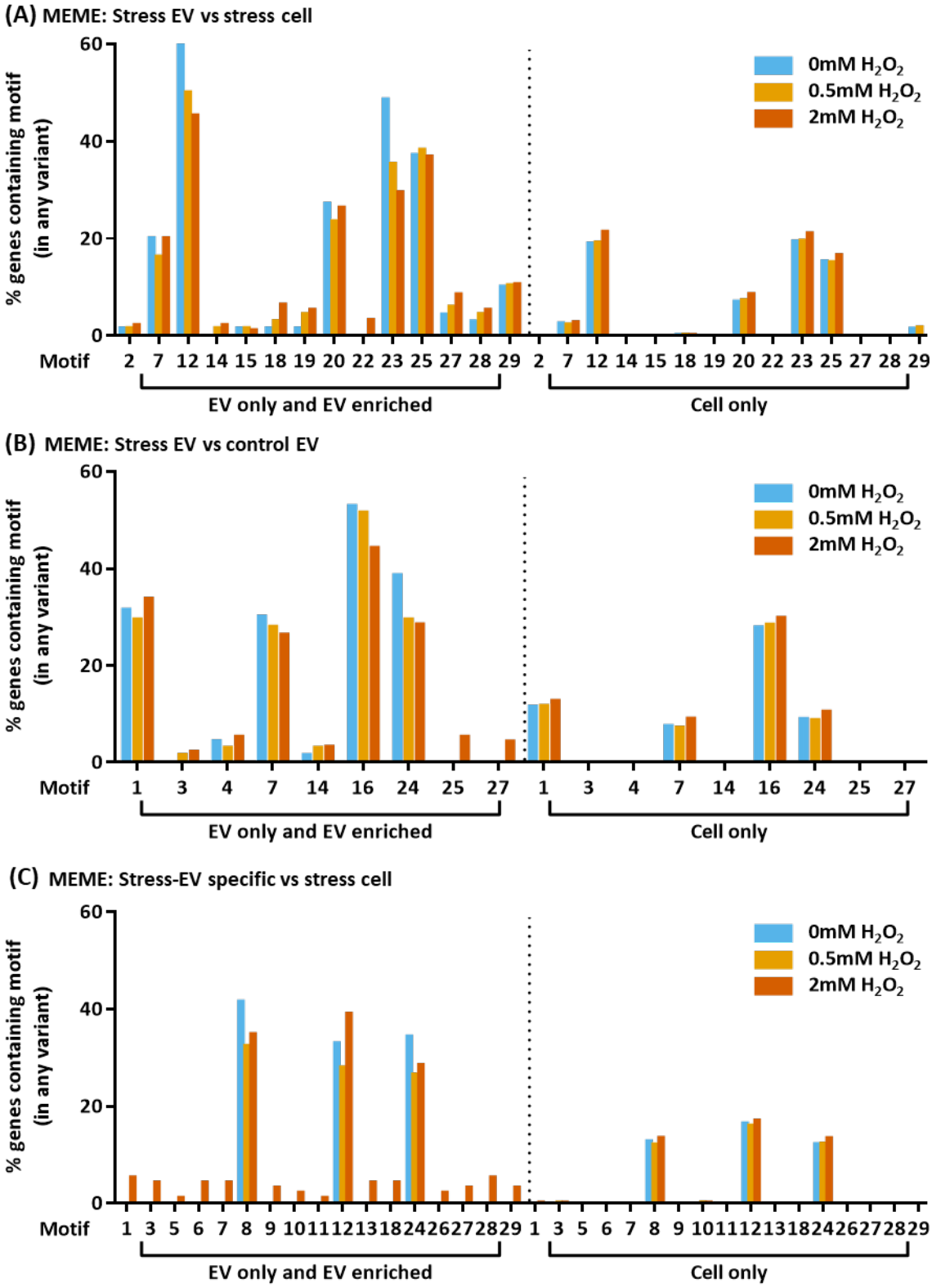


Figure 6.10: No high abundance stress-specific EV motifs can be identified

*(A) Abundancies of the 30 motifs in high stringency set of 2mM $H_2O_2$ "EV only plus EV enriched" group compared to 2mM $H_2O_2$ cells. (B) Abundancies of the 30 motifs in high stringency set of 2mM $H_2O_2$ "EV only plus EV enriched" group compared to control "EV only plus EV group". (C) Abundancies of the 30 motifs in high stringency set of mRNAs present exclusively in 2mM $H_2O_2$ "EV only plus EV enriched" group compared to 2mM $H_2O_2$ cells.*

database of 68 Drosophila RBP motifs, across 51 unique RBPs (Ray et al., 2013). Using a q-value cut-off of 0.05, this revealed six RBPs to show similarity to one or more potential EV motifs using TOMTOM (Figure 6.11). Strikingly, both Smooth and CNOT4 showed significant similarity to at least one motif in each of the sets, with PAPI and ARET also displaying high significance matches.

**(A)**

| Motif set | Motif number | RNA binding protein | | | | | |
|---|---|---|---|---|---|---|---|
| | | SM | CNOT4 | ROX8 | CPO | PAPI | ARET |
| Low stringency Control EV vs Control Cell | Motif-1 | 0.0407 | | | | | |
| | Motif-2 | | | | | | |
| | Motif-3 | | | | | | |
| | Motif-4 | | | | | | |
| | Motif-7 | 0.0184 | 0.0184 | | | | |
| High stringency 2mM EV vs 2mM Cell | Motif-7 | | | 0.0146 | | | |
| | Motif-12 | | | | | | |
| | Motif-20 | 0.0115 | 0.0115 | | 0.0115 | | |
| | Motif-23 | | | | | | |
| | Motif-25 | | | | | | |
| High stringency 2mM EV vs control EV | Motif-1 | | | | | 0.0002 | 0.0007 |
| | Motif-7 | 0.0028 | 0.0050 | | | | |
| | Motif-16 | | | | | | |
| | Motif-24 | | | | | | |
| | Motif-25 | | | | | | |
| High stringency Only in 2mM EV vs 2mM cell | Motif-8 | 0.0006 | 0.0033 | | | | |
| | Motif-12 | | | | | | |
| | Motif-24 | | | | | | |

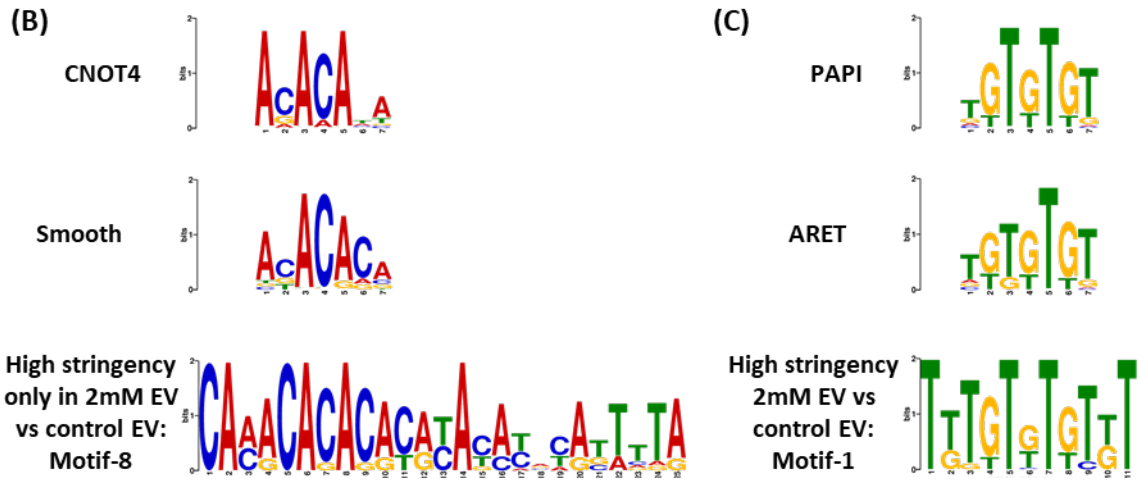


Figure 6.11: EV-enriched motifs shown similarity to known RBP motifs

*(A) Comparison of each motif set with known RBP motifs from Ray* et al. *(2013) using TOMTOM. Only q-values below 0.05 shown. (B) and (C) Graphical representation of highest significance motif comparisons.*

Since some of the motifs generated by MEME had a high level of degeneracy, RBP motifs in the 3'UTR sequences were searched for directly with FIMO. This returned significant matches for Smooth, PAPI and ARET that were enriched in "EV only/EV enriched" groups relative to "cell only" under all conditions, strengthening the case for the involvement of these proteins in RNA loading (Figure 6.12A). Finally, the expression level of the mRNAs encoding these proteins was assessed in cells, to see whether protein was likely to be expressed in sufficient quantities to mediate an effect in EVs. This showed that, whilst *Aret* showed very low expression at <1 FPKM, *Smooth* and *Papi* showed higher expression at 7-30 FPKMs (Figure 6.12B). Together, these data implicate PAPI and Smooth as the most likely RBP candidates with an effect on mRNA-packaging in *Drosophila* EVs.

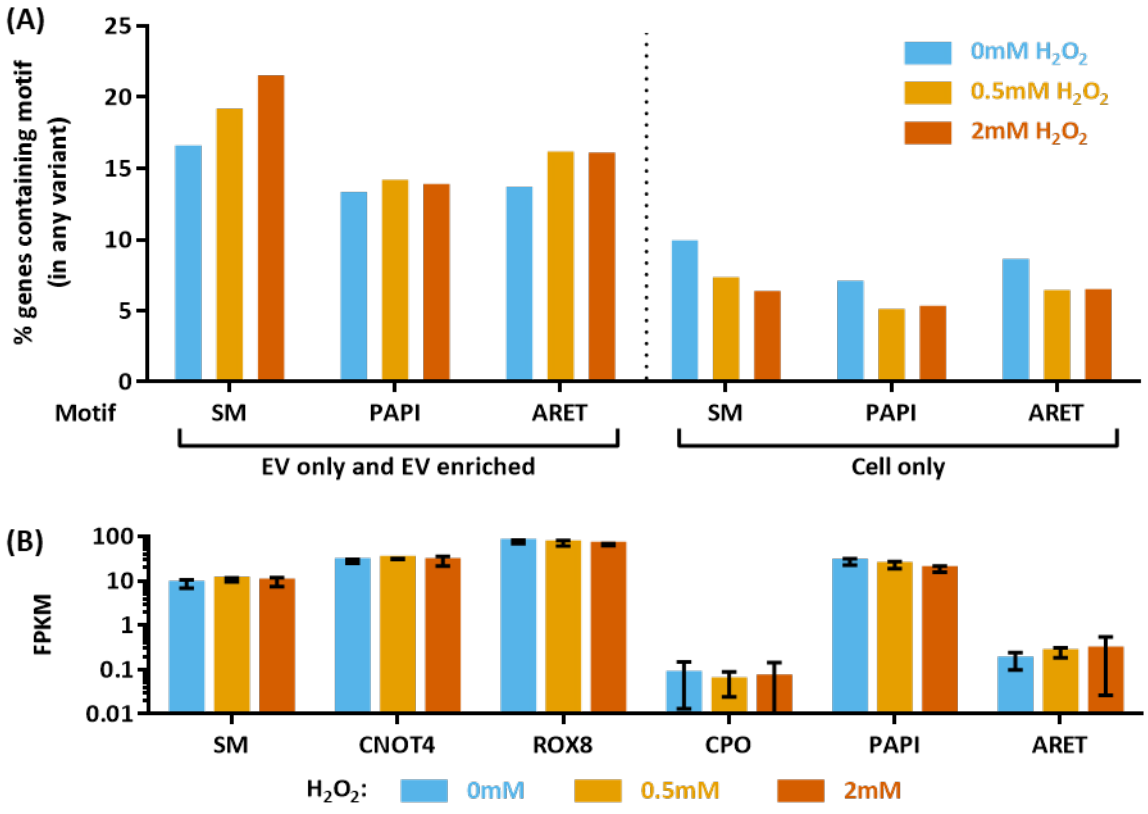


Figure 6.12: Smooth and PAPI are RBP candidates for involvement in mRNA loading

*(A) Abundancies of the hits of 68 RBP motifs in the Ray* et al*. (2013) database in each set of mRNAs in low stringency conditions. (B). FPKM abundance values from Cufflinks for each of the RBPs identified in (A). Graph shows mean and standard deviation of three biological replicates.*

### 6.3.9 CAG trinucleotide repeats are enriched within the CDS of EV-mRNAs

Initial motif searching was carried out in 3'UTRs due to a) its enrichment under stress, b) its known involvement in regulating mRNA localisation, stability and degradation, and c) the ease of testing *in vitro*. However, since testing indicated minimal specific effects of the motifs discovered, the bioinformatic search using MEME was broadened to include all the entire sequence. Using high stringency thresholding, cDNA sequences for all transcript variants of control "EV only/EV enriched" and "cell only" groups were input, as target and background groups respectively, into MEME. FIMO was then used to search for the 30 motifs in each of CDS, 3'UTR and 5'UTR regions. This process revealed that motifs were preferentially found within the CDS region, and also enriched within EVs relative to cells under all three stress conditions (Figure 6.13A-C). However, visual inspection found many of these motifs to be highly similar variations on a CAG trinucleotide repeat, with comparison using the MEME Suite tool TOMTOM further indicating their significant similarity (Supplementary Figure 17). These CAG-repeat motifs were also found within the 3'UTR and 5'UTR regions under all three stress conditions (Figure 6.13B, C). These data therefore suggest that mRNAs containing CAG-repeats in any region, but most frequently in the CDS, may be particularly prone to preferential packaging into EVs. In addition, considering the combinatorial effect of motifs, or other features, within all regions of the mRNA is necessary to understand its propensity to be packaged into EVs.

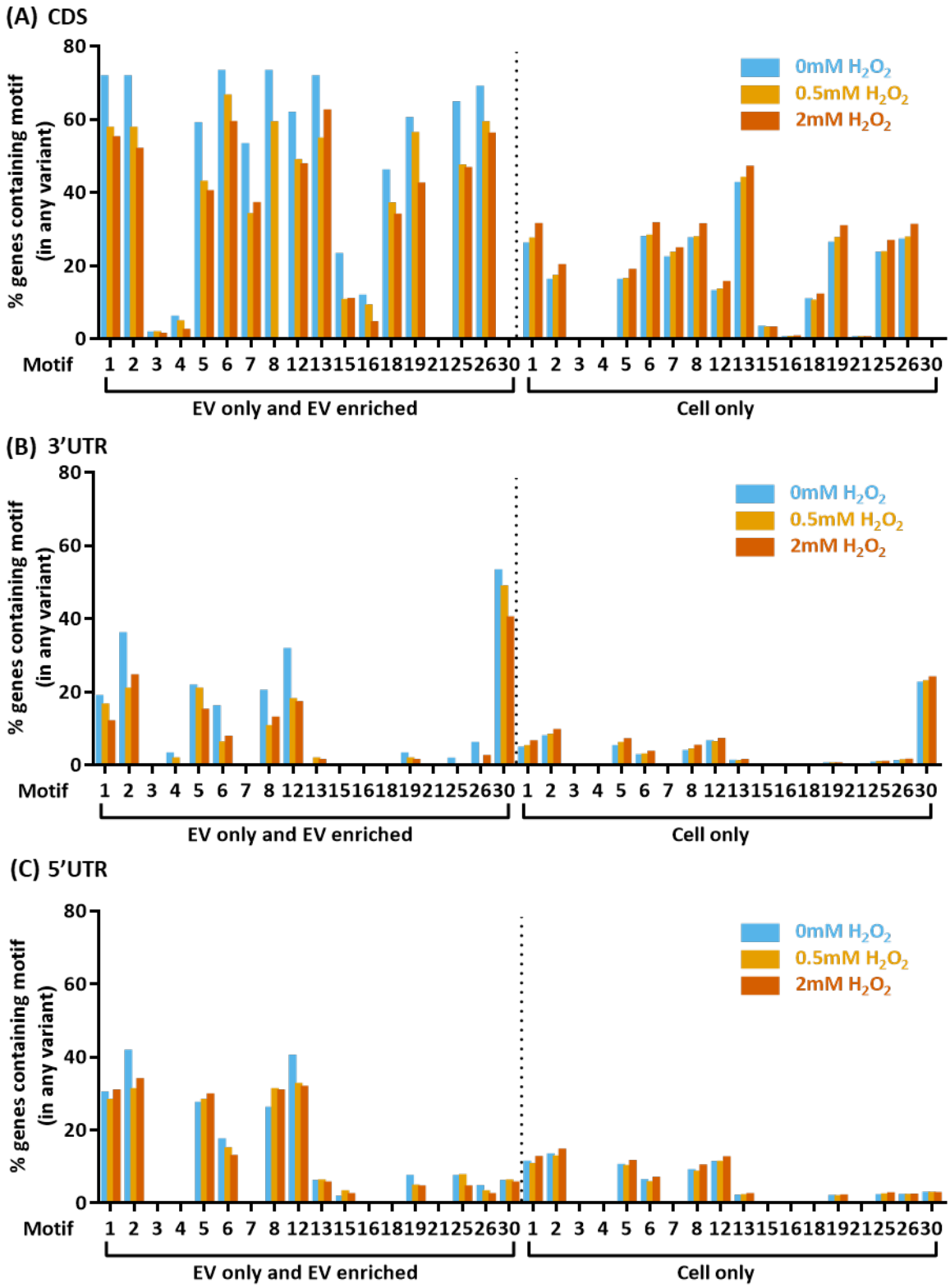


Figure 6.13: EV-enriched motifs are present in all mRNA regions

*(A)-(C) Abundancies of the 30 motifs in high stringency control set found by searching of cDNA sequences using MEME, in each of region of the mRNA; (A) CDS, (B) 3'UTR and (C) 5' UTR, in each set of mRNAs.*

## 6.4 DISCUSSION

### 6.4.1 No preference for shorter mRNAs in EV samples

The data presented in this chapter demonstrate that sequence reads of RNA from EV samples map to mRNAs from up to and over 6000nt, with coverage over the full-length of many of these mRNAs. Although some studies have suggested a size limitation of ~1000nt mRNA loading, this is as a result of being unable to detect longer mRNAs using qPCR, so may be due to the greater technical challenges faced in amplifying longer RNAs, particularly from low input RNA such as EVs (Wei *et al*., 2017; Hinger *et al*., 2018). Other qPCR-based studies have detected longer mRNAs of up to 5000bp in length (Enderle *et al*., 2015; Matsuno *et al*., 2019). Whilst a preference for shorter, particularly 500-1000nt transcripts in EVs was found in RNA sequencing data in one study (Shurtleff *et al*., 2017), in another the overall transcript length distribution showed no preference for shorter transcripts, highly similar to the findings here in *Drosophila* EVs (Wei *et al*., 2017). In this latter study, the long mRNAs were detectable in sequencing data despite the lack of detection by qPCR. Some of the differences between studies may be due to the different methods of EV purification employed, and thus represent variation in EV populations and non-vesicular material. Nonetheless, the data here further argue towards the presence mRNA derived from the full range of mRNA lengths, either in an intact or fragmented state.

Through a comparison of the length of statistically significantly EV-enriched and depleted mRNAs, the data here also indicated the possibility that EV enriched mRNAs were longer, an effect which was less evident under stress. This observation could be an artefact of RNA sequencing, which is biased towards the detection of longer RNAs, especially since the effective read depth in EV samples was much lower than in cell samples. However, since read depth for EVs under each of the stress conditions was similar, and this length difference between enriched and depleted mRNAs was reduced under stress, this may indicate that the difference detected has biological significance. For example, a possible connection between RNA granules and RNA-

protein complex secretion in EVs has been postulated, with many RBPs that are thought to be involved in EV-RNA packaging (HnrnpA2B1, HnrnpA1, HnrnpU, IGP2BP1, Syncrip, Ybx-1, Fmr1, Ago1, Ago2) also known to localise to stress granules and P-bodies (Markmiller *et al*., 2018; Wolozin and Ivanov, 2019; Leidal and Debnath, 2020). Stress granule-associated mRNAs have been shown to have longer CDS and 3'UTR regions, with length differences also seen in different granule types and under arsenite-induced oxidative stress (Khong *et al*., 2017; Matheny *et al*., 2019). Therefore, it is possible that the differences in length represent RNA granule-linked loading, which is altered under conditions of stress. However, the low read depth in EVs limits conclusions that may be made from this dataset. Since stress granule-enriched mRNAs also have a tendency for lower abundance, greater sequencing depth is likely even more critical to uncovering such potential links (Khong *et al*., 2017). Therefore, along with other lines of evidence, a tendency towards longer mRNAs in EVs hints towards the possible involvement of RNA granules in the loading process but requires more in-depth investigation to confirm.

### 6.4.2 Increased intronic and UTR reads in EVs under stress conditions

An additional feature uncovered in the data was an altered read distribution, with reduced CDS content, and relative enrichment of intronic and UTR regions, particularly under oxidative stress. Several studies have reported increased mapping to intronic regions in some EV populations, in both small RNA sequencing (Nolte-'t Hoen *et al*., 2012; Li *et al*., 2013; Wei *et al*., 2017) and total RNA sequencing (Kossinova *et al*., 2017; Hardy *et al*., 2019). High intronic mapping in EV samples was reduced by DNAse treatment in one study, which might suggest more DNA within the stress EV samples (Shurtleff *et al*., 2017). Although the *Drosophila* RNA samples were DNAse treated before sequencing, since both apoptotic and necroptotic cell death increase extracellular release of DNA, it is a plausible possibility that the increase in intronic reads is due to contaminating DNA. However, alternative explanations include an increase in non-spliced pre-mRNA, as would be the case for nuclear fractions (Sultan *et al*., 2014), or intron retention events,

and would suggest that RNA packaging to be in some way linked to RNA processing, possibilities which require further investigation.

In addition to the increase in relative intron content, under high stress conditions, both 3'UTR and 5'UTR regions were also enriched in EVs relative to cells. Several studies have found this to be the case in normal conditions, in both regions in some studies (Nolte-'t Hoen *et al*., 2012; Wei *et al*., 2017) and the 3'UTR only in others (Batagov and Kurochkin, 2013). Studies by Batagov and Kurochkin and Wei *et al.* both make use of data from primary glioblastoma cell lines, so it may be that the enrichment of UTRs is primarily a result of stress but seen as a result of the specific cell origin or increased sensitivity of these primary cells.

It has been reported in several studies that 3'UTRs may be differentially expressed from the CDS region, particularly within the brain (Mercer *et al*., 2011; Kocabas *et al*., 2015). Furthermore, an additional study found isolated 3'UTR expression to be tightly correlated with oxidative stress in neuronal populations, reflecting the difference observed in the *Drosophila* cell EVs (Sudmant *et al*., 2018). Kocabas *et al.* find that the 3'UTR/CDS expression ratio varies greatly, but with the high ratio group enriched for GO terms relating to development, reminiscent of the GO term analysis of EV enriched RNAs in Chapter 5, and thus raising the possibility that their expression has functional importance. Classification of mRNAs into groups based on their UTR enrichment, an approach taken by one group (Pérez-Boza *et al*., 2018), would be a useful future strategy, but in the current work this was precluded by low read depth. Despite this limitation, these data strongly support the enrichment of UTR regions within RNA of EV samples but, in contrast to previous work, only under conditions of stress.

### 6.4.3 Presence of degraded mRNAs in EVs

In contrast with read distribution analysis which showed an enrichment of UTR regions under stress, analysis of gene-body coverage (which assesses coverage at the 100 most 3' and 5' nts of the mRNA), showed lower coverage at the most 3' end, indicative of degradation. Since

exogenous degradation is expected to be the same between all EV samples, it is suspected that this difference may represent alterations in RNA packaging but, since RNAse inhibitors were not employed, it is possible that stress EVs samples contained greater endogenous RNAses which accelerated degradation post-purification. Therefore, in the future the use of a spike-in RNA as a control to monitor degradation would be a useful approach to rule out this possibility.

RNA degradation in the 3'-5' direction is an early event in apoptosis, occurring via DIS3L2-mediated degradation of uridylated intermediates (Thomas *et al*., 2015; Liu *et al*., 2018). Increased levels of dying cells were seen in $H_2O_2$-treated cells in chapter 3 (Figure 3.8), and bioanalyser analysis indicated the presence of some full-length rRNA in chapter 5, suggestive of a mixed EV population that includes ABs (Figure 5.2). Therefore, the stress EVs may contain an increased proportion of RNAs degraded as part of the apoptotic process. On the other hand, these degraded mRNAs may be specifically loaded into EVs. Indeed, in small RNA sequencing, EVs have been found to be enriched for mRNA fragments under normal conditions (Van Balkom *et al*., 2015). Furthermore, Y-RNAs, which have been suggested to play a role in regulating refolding or decay of variant and misfolded RNAs (U2 snRNA and pre-5S rRNA) through the Ro60 ribonucleoprotein complex are similarly known to be highly enriched in EVs (Chen et al., 2003; Fuchs et al., 2006; Nolte-'t Hoen et al., 2012; Tosar et al., 2015; Van Balkom et al., 2015; Cambier et al., 2017; Wei et al., 2017). Given the increased abundance of partially degraded mRNAs in *Drosophila* EVs under stress, together these data indicate that EVs could play a role in release of degradation products of many different RNA biotypes, which may be an important function in both EV-producing and EV-receiving cells.

### 6.4.4 Increased mismatch rate in stress EVs

An intriguing finding in the data was that EV samples showed an increase in the percentage of base mismatches between sequencing reads and reference genome compared to cells, a rate that was strikingly increased under stress. Whilst not directly reported previously, a higher rate

of mismatch has been proposed as an explanation for the lower mapping rate seen for EVs in both total RNA sequencing and small RNA sequencing (Cha *et al*., 2015; Tosar *et al*., 2015; Yang *et al*., 2017; Hinger *et al*., 2018). This has been suggested to be due to non-templated RNA base modifications or additions that alter reads during reverse transcription (Hinger *et al*., 2018). Poly-uridylated miRNAs have been shown to be significantly enriched in EVs, whilst the existence of an unidentified modification has been proposed as a mechanism for specific incorporation of tRNAs, so these modifications could act as a broader mechanism to control RNA packaging (Koppers-Lalic *et al*., 2014; Shurtleff *et al*., 2017). RNA modification is thought to be especially important in stress conditions, with N6-methyladenosine modification increased in hypoxic conditions, and shown to be a mechanism by which mRNAs are directed to heat or sodium arsenate-induced stress granules (Fry *et al*., 2017; Anders *et al*., 2018). Since the data here show that the rate of base mismatch in EVs rose significantly under oxidative stress, it is possible that RNA modifications may be an underlying determinant of the differences in RNA content. However, existing techniques for the identification of modified bases, such as meRIP and miCLIP, are likely especially challenging to apply to low-yield RNA from EVs. An alternative explanation is that these mismatches represent sequence errors, and that these aberrant RNAs are intended for degradation. Since this rate of mismatch increased significantly in EVs under stress, where errors are more likely to be occurring, and given the evidence of 3' end degradation in the EVs under stress, this seems a strong possibility that merits further investigation.

### 6.4.5 3'UTR motifs alone are not a strong determinant of mRNA loading

In this work, multiple 8-25nt sequence motifs were identified as enriched in EV-mRNAs in the 3'UTR region. Despite the low level of overlap between mRNAs present in control and stress EVs, searches for enriched motifs in each condition identified similar motifs that were present under all conditions, possibly implying their basal importance in the packaging process. However, these novel motifs showed limited similarity to those implicated as determinants of mRNA loading in

mammalian studies, with only low stringency motif-2 showing some, non-significant, similarity (Batagov *et al*., 2011; Bolukbasi *et al*., 2012; Szostak *et al*., 2014). Given the wide evolutionary differences between mammals and *Drosophila*, this could be interpreted as evidence for species differences, but it must also be noted that at present no identified mRNA motifs in mammalian cell lines have been independently validated. Despite confirmation of the effect of the 25nt zipcode motif on *eGFP* mRNA loading in HEK-293T cells in the initial study, this was not reproduced in *HChrR6* mRNA loading in HEK-293 cells (Bolukbasi *et al*., 2012; Forterre *et al*., 2020). In such a similar cellular context, this may suggest that mRNA packaging is also highly dependent on other factors such as expression level, mRNA length, or additional *cis* factors within other region of the mRNA. Indeed, broadening the motif search to include the full mRNA yielded multiple derivatives of a CAG repeat, enriched in EVs in all regions, but most abundant in the CDS. Trinucleotide repeat motifs such as CAG are important factors in the pathogenesis of many neurodegenerative diseases, and may be located in any region e.g. CDS in Huntingtin's disease and 3'UTRs in type 1 myotonic dystrophy (Zhang and Ashizawa, 2017). Recent work has shown that the an expanded CAG repeat within *huntingtin* mRNA showed an increase in EV incorporation compared to normal *huntingtin* in mouse striatal neurons, although this was not statistically significant (Zhang *et al*., 2016). Alongside the importance to disease pathology, the high prevalence of these CAG repeats within the CDS points towards the importance of considering the full sequence length of any mRNA to understand its propensity for EV loading.

In the current work, *in vitro,* Cre constructs containing either the wild-type *para* 3'UTR*,* with intact motifs, or the shuffled motifs, showed a non-significant trend towards increased EV prevalence, whilst the 25nt zipcode did not. Although the shuffling process did not disrupt all motifs, and other sequences or structures that promote loading may be present, one explanation for the effect of both constructs is a non-specific consequence of the increase in 3'UTR length to 185nt. This might be due to altered stability of the RNA, with data on tRNA loading demonstrating stability as a key factor determining packaging into EVs in the producing

cell (Gámbaro et al., 2019). Increased stability might also promote an increased lifetime within any recipient cells. One explanation for the lack of significant effect on differential distribution *in vitro* is that the actin promoter drives high expression within the cells, which appears to be a strong determinant of secretion in itself (Chapter 5; Gezer *et al*., 2014; Sork *et al*., 2020). Therefore, with the use of a lower expression promoter, the effect of the 3'UTR addition would likely become more evident. Nonetheless, given that longer mRNAs also appeared to be enriched in EVs over cells, this data again points to the importance of mRNA length as a determinant of packaging into EVs.

Since analysis of individual splice variants could not be meaningfully carried out, one aspect that was not investigated was the number of motifs, either the same or different, present in a single mRNA. In other cases, such as the AU-rich elements involved in regulating mRNA decay, multiple copies of the same or similar motif are found within a single 3'UTR (Barreau *et al*., 2005). Thus, investigation of repeating motifs, and their location, is an additional area for further study.

### 6.4.6 The RBP Smooth may link EV mRNA loading to mRNA degradation

Since RBPs are increasingly being implicated in EV loading of small RNAs, the *Drosophila* motifs were compared to known RBP motifs, with at least one high abundance motif in each motif set showing significant similarity to the binding site for Smooth. The CA-repeats of this motif have also been suggested to be involved in binding to EV loading motifs in the human homolog of Smooth, hnRNP L, providing hints towards a potentially conserved mechanism of mRNA packaging (NGUYEN and FERGUSON, 2018). HnRNP L has been reported to bind to CA-repeats in the CDS of *MTNR1A* mRNA to cause a stabilising effect, and the 3'UTR of *Bcl-2* and *iNOS* mRNAs to cause a destabilising effect (Söderberg *et al*., 2007; Lee *et al*., 2009a; Huang *et al*., 2021). Of particular interest, binding of HnRNP L has also been found to override nonsense-mediated decay targeting features such as long 3'UTRs, including of aberrant *Bcl-2* transcripts in

B-cell lymphoma (Kishor *et al*., 2019). Therefore, the role of RBP binding in determination of RNA packaging into EVs may be highly interconnected with RNA degradation.

## 6.5 KEY FINDINGS

- There is no preference for shorter mRNAs within EV-associated RNA.
- Intron, 3'UTR and 5'UTR reads are enriched in EV-associated RNA under $H_2O_2$ stress.
- Base mismatch is higher in EV-enriched RNAs under $H_2O_2$ stress, especially in 3'UTRs.
- EV-enriched motifs found in control conditions are present in 3'UTRs in all stress conditions, but no high abundance stress-specific motifs can be discovered.
- RNA binding proteins Smooth and PAPI are candidates for further investigation as mediators of mRNA-loading in *Drosophila* EVs.
- CAG motifs are enriched within the CDS region of EV-associated mRNAs.

# Chapter 7

## Discussion and Future Directions

# 7 Discussion and future directions

## 7.1 SUMMARY OF KEY FINDINGS

In this thesis the first aim was to establish a *Drosophila* cell culture model to investigate EV-biology, to complement work being done by Claire Hill to establish a model in *Drosophila* larvae. Here, SEC has been demonstrated to work effectively for purification of S2R+ EVs from cells under normal and $H_2O_2$ stress conditions, confirmed by particle/protein separation and TEM imaging to perform very similarly to use in mammalian cell lines. In place of the canonical tetraspanin markers CD81, CD63 and CD9 in mammalian systems, it adds weight to existing data showing Latebloomer to be a protein marker of small EVs in *Drosophila*. Using this *in vitro* system, the effect of $H_2O_2$ oxidative stress on EV production was investigated, and showed that, whilst the stress does not alter the size of EVs produced, it may increase their number. EV preparations from these $H_2O_2$-stressed cells were found to induce cell death in recipient cells, although understanding the nature of this process requires more in-depth study. Through this work, several methodological aspects of importance have also been demonstrated. Whilst EV-depletion of FBS by UC does appear to remove EVs, small non-EV like particles remain, in addition to actin, highlighting the importance of NCM media controls in all EV work. Furthermore, whilst cell 'viability' assays such as resazurin reduction and MTT are widely used to assess functional effects of EVs on recipient cells, work here has emphasised the need for alternative assays to confirm the specific nature of these effects.

The second main aim of this thesis was to investigate the RNA cargo of EVs and assess how this is altered under $H_2O_2$-stress. It was shown that EV preparations contain primarily rRNA fragments, the majority mapping to the 18S small ribosomal subunit, and with a relative increase under $H_2O_2$-stress. Through a complete characterisation of the long RNA content in EV preparations and in the parental cells, it was found that the abundance of EV-associated RNA biotypes does not reflect their abundance in the cells; mRNA is underrepresented whilst snoRNA

is overrepresented. It was further shown that the overall correlation between specific transcript abundances is reduced under stress, in mRNA and snoRNA in particular. Through GO term analysis the most abundant EV-associated RNAs were seen to be involved in ribosomal functions, whilst those for which enrichment in EVs over cells is altered under stress relate primarily to cytoskeletal and developmental functions. In line with existing data, the *Copia* retrotransposon was found to be highly abundant, and significantly enriched, within EV preparations. Whilst the expression of viral RNA within the samples was not expected, the differential enrichment of the two predominant groups; *alphanodavirus* species and DTV, as enriched and depleted respectively, highlights the overlap between EV and virus production and RNA packaging.

With regards to the mechanisms which may determine mRNA packaging in EVs, this work found no preference for shorter mRNA transcripts. Enrichment of intronic, 3'UTR and 5'UTR reads in EV-associated RNA under $H_2O_2$-stress, and evidence of 3' end degradation, support existing evidence that EV-associated RNA contains a mixed population of intact and fragmented mRNA. Investigation of potential loading motifs in mRNA 3'UTRs revealed a number of sequences that were enriched in EV mRNAs compared to cells under both normal and $H_2O_2$-stress conditions, with RBPs Smooth and PAPI identified as potential candidates for mediating this loading. Stress-specific motifs, however, could not be discovered. Other features of mRNA have also been identified as potential mechanisms of interest for promoting EV-loading. Testing of motifs *in vitro* unexpectedly revealed a possible role for RNA stability in determining localisation to EVs, whilst a striking increase in base mismatch in the RNA of EV preparations under stress was also found, possibly indicative of either targeting of aberrant RNA to EVs, or of RNA modification. Together these results present strong evidence that the RNA content of EVs is altered under $H_2O_2$-stress and provides several avenues for further investigation of the mechanisms by which this may occur.

## 7.2 EFFECTS OF $H_2O_2$ ON EV PROPERTIES IN CELL CULTURE

Multiple studies have shown an increase in EV production under stress conditions by a range of techniques, in most cases using NTA technology (Hedlund *et al*., 2011; King *et al*., 2012; Kumar Jella *et al*., 2014; Mutschelknaus *et al*., 2016). The data here supports an effect of $H_2O_2$ on stimulating EV production, although it must be noted that NTA cannot distinguish between true EVs, aggregates or other particles, such as those found in the EV-depleted FBS (Brennan *et al*., 2020). More specific quantification techniques are reliant on protein-based capture and have at present mostly been limited to CD81, CD63 and CD9 tetraspanins not present in *Drosophila*, but future developments will likely improve accuracy of quantification. Using NTA technology, no difference between the size of normal and stress-cell derived EVs could be observed, although again, this may be reflective of the limitations of NTA (Kestens *et al*., 2017). Nevertheless, these results suggest that $H_2O_2$ -treatment, and cell stress more widely, may increase production of EVs, which may increase both the ability of producing cell to expel unwanted material, and the degree to which they can contribute to interactions with recipient cells.

Since stress appeared to increase EV number, analysis of protein markers by Western blotting was performed to test whether EV composition differed between conditions, with loading normalised by total protein content. The tetraspanin latebloomer was validated as a genuine marker of small EVs, in agreement with work from three other groups (Koles *et al*., 2012; Parchure *et al*., 2015; González-Méndez *et al*., 2020). However, no overt differences were seen between control and stress conditions, although in the absence of an appropriate loading control, no quantification of this was carried out. Notably, of other classical EV markers, TSG101 was absent, and Alix variable. Given that these components of the ESCRT machinery are also involved in viral replication and budding (Vietri *et al*., 2020), since variable expression of viral RNAs was identified in sequencing, persistent viral infection may have influenced protein expression. In support of this, infection of lung-carcinoma-derived A549 cells with respiratory

syncytial virus was found to increase Alix expression in CD63 positive EVs (Chahar *et al*., 2018). In one study, TSG101 was found to be present in EVs of transfected *Drosophila* S2 cells but not control cells, indicating high variability that is dependent on either technical aspects of the EV preparation, or altered biogenesis in parental cells (Gradilla *et al*., 2014). Given that analysis of unmapped reads in published datasets of *Drosophila* EVs also showed the presence of viral reads (data not shown), unacknowledged viral infection may have a significant impact on "EV marker" expression more widely in the literature. This finding underscores the importance of efforts to identify *all* reads in RNA sequencing, not just those mapping to the genome of primary interest, and further highlighting the interplay between virus and EV biogenesis.

Knowledge of the heterogeneity of EVs released under different conditions is of critical importance to understanding of their function, so comparison of a wider range of protein markers for the S2R+ EVs would be of use in future work. Of particular interest, a previous study has shown that expression of Rab11a is increased under glutamine deprivation, suggested to be indicative of EV release from recycling endosomes, rather than late endosomes, and thus reflective of altered biogenesis routes under stress (Fan *et al*., 2020). Additionally, many studies have demonstrated that viruses can utilise Rab11 recycling endosomes for assembly and budding, including the influenza virus that was found to make use of the RBP Ybx-1 for trafficking to Rab11 compartments (Kawaguchi *et al*., 2012; Vale-Costa and Amorim, 2016). RNA cargo of Rab11 EVs has not been studied, but since *alphanodavirus* RNAs were enriched in the *Drosophila* cell EV preparations, these recycling endosome derived EVs represent an interesting area of study, particularly under cellular stress.

## 7.3 UNDERSTANDING EV PACKAGING OF RNA

Several features of the RNA content of the EVs in the data generated; the enrichment of intronic regions, snoRNAs and potentially of longer mRNAs, are reminiscent of the expected RNA content of the nucleus (Sultan *et al*., 2014; Bouvrette *et al*., 2018). One study characterising the

comparative cargo of high and low density EVs found that the high density EVs (likely more representative of an exosome population) were enriched for snRNA and snoRNA, but also for nuclear proteins, leading the authors to propose that high density EV production is associated in some way with the nucleus (Lässer *et al*., 2017). In addition, some snoRNAs have also been found to localise to the cytoplasm rather than the nucleus under doxorubicin-induced oxidative stress (Holley *et al*., 2015), highlighting that changes in subcellular RNA localisation may be critical to understanding how EV-RNA loading processes may differ under altered cellular conditions. Given also that the endocytic recycling compartment, from which Rab11a recycling endosomes derive, is localised close to the nucleus (Grant and Donaldson, 2009), and the increase in Rab11a EVs under some stresses (Fan *et al*., 2020), this increase in nuclear-like RNA cargo is likely indicative of altered EV biogenesis. Therefore, whilst increasing the technical experimental complexity, an informative approach would be to compare RNA content of sub-cellular fractions, such as the nuclear and insoluble fractions (Bouvrette *et al*., 2018), with EV RNA, rather than with total cell RNA.

Multiple studies have demonstrated that there is a strong regulatory link between autophagy and EV biogenesis. Several studies have observed reduced production of EVs and cargo upon treatment with rapamycin, used widely to induce autophagy, whilst bafilomycin treatment, to inhibit lysosomal acidification, increases EV production (Alvarez-Erviti *et al*., 2011; Abdulrahman *et al*., 2018; Fan *et al*., 2020; Leidal *et al*., 2020). In addition, several components of the autophagy machinery, including ATG3, ATG5, ATG7, ATG12, ATG16L1, have been demonstrated to have some involvement in controlling EV biogenesis, although seemingly independent of their role in autophagic degradation (Murrow *et al*., 2015; Guo *et al*., 2017; Abdulrahman *et al*., 2018; Leidal *et al*., 2020). Of particular interest, the study by Leidal *et al.* (2020) demonstrated that knockout of *Atg7* or *Atg12* significantly altered the small RNA content of EVs, most strongly of snoRNAs, through the proposed LC3-dependent extracellular vesicle loading and secretion (LDELS) system. This same biotype was found in the current work to be overrepresented in EVs,

and have its differential distribution strongly affected by stress, indicating that further interaction between EV biogenesis and autophagy pathways may be occurring. In addition, *Drosophila* EV preparations were shown here to be enriched for RNA of the *Copia* retrotransposon; whilst mammalian LINE-1 and Alu retrotransposons have previously been demonstrated to colocalise with LC3 for degradation by autophagy (Guo *et al*., 2014). The authors suggest that this may occur via stress granules or P-bodies, as an efficient means to degrade bulk RNA, a route confirmed for stress granule degradation in yeast and mammalian cells in a second study (Buchan *et al*., 2013). Given that the EV-enriched mRNAs in *Drosophila* appeared slightly longer than depleted mRNAs, a feature associated with stress granules, the possibility that EVs may contain RNA intended for autophagic degradation should therefore be considered.

Alongside granule-mediated RNA degradation, studies have also demonstrated that RNA may be taken up to lysosomal compartments directly via LAMP2C and SIDT2 transporters (Fujiwara *et al*., 2013; Aizawa *et al*., 2016). In the latter study, the cytosolic region of LAMP2C was shown to interact with multiple RBPs in either HeLa cell lysates or mouse brains, including hnRNPA1, hnRNPU, Lupus La, FMR1 and SYNCRIP, all of which are implicated in RNA loading into EVs, thus strengthening a case for interaction between these processes. Knockout of *Xrn1* exonuclease, blocking mRNA decay, results in a shift towards autophagy-mediated RNA degradation (Buchan *et al*., 2013), so it is possible that an analogous compensatory switch towards EV release occurs upon the inhibition of autophagy. Since some features of the mRNA within the *Drosophila* EVs; their possible fragmentation, an increase in base mismatch and 5'/3' end bias under oxidative stress, are suggestive of aberrant or degraded RNA, it seems likely that there is a link between RNA degradation and EV RNA cargo that warrants further investigation.

The current work, through enrichment of binding motifs within the EV RNAs, identified Smooth and PAPI as specific RBPs which may be involved in EV loading of mRNAs. Since both *Copia*

retrotransposon and *alphanodavirus* RNAs were enriched within the EV preparations, it is interesting to note that the human homolog of Smooth, hnRNPL, binds to LINE-1 retrotransposons and several viruses; hepatitis C and foot and mouth virus, both positive single-stranded RNA viruses like alphanodaviruses (Peddigari *et al*., 2013; Li *et al*., 2014; Sun *et al*., 2020), Since other hnRNP proteins implicated in EV-RNA loading, such as SYNCRIP, also bind to hepatitis viruses (Choi *et al*., 2004; Liu *et al*., 2009), these proteins may have a wider role in determining the RNA content of EVs beyond mRNA.

Further work to validate RBP involvement could involve firstly the knockdown of each RBP *in vitro* and *in vivo*, to assess the effect on *Cre* localisation and reporter signalling. Secondly, validation of the direct binding e.g. through pulldown of proteins binding to EV RNA. Alongside these potential new targets, the development of the parallel *in vitro* and *in vivo* systems in this thesis and that of Claire Hill provides an opportunity to test the evolutionary conservation of proteins implicated in RNA loading in mammalian systems. One such primary protein of interest is Ybx-1, thought to be involved in loading of a range of RNA biotypes, including mRNA, tRNA and miRNA (Shurtleff *et al*., 2016, 2017; Kossinova *et al*., 2017). Since sodium arsenite-induced oxidative stress has also shown an increase in Ybx-1 in conditioned cell media, likely secreted via EVs (Guarino *et al*., 2018), it may provide a means by which RNA content of EVs is altered under stress conditions. Study of Ybx-1 in human cells, zebrafish and the *Drosophila* homolog, YPS, has also recently shown binding to 5-methylcytosine modifications in all RNA biotypes, including mRNA (Chen *et al*., 2019; Yang *et al*., 2019; Zou *et al*., 2020). Given the increases seen in mismatch rate in the EVs under increasing oxidative stress that may represent increased RNA modification, this provides a plausible mechanism for altered EV RNA loading under stress.

Of the sequence motifs identified in mRNA under low stringency conditions, motif-3, a T-rich sequence (encoded as U in RNA), stands out, as uridylation is associated with targeting for RNA decay (Thomas *et al*., 2015; Liu *et al*., 2018). Alongside the presence of such tracts in 3'UTRs of

mRNA, transposons and viruses undergo widespread uridylation (Huo *et al*., 2016; Warkocki *et al*., 2018). Therefore, the *Copia* transposon and viral RNAs enriched in EVs in this work may have co-opted this mechanism to allow their intercellular spread.

Data from testing of motifs also unexpectedly showed that, rather than a specific motif effect, the introduction of either the wild-type or shuffled 185nt 3'UTR of *paralytic* appeared to increase the EV/cell ratio of *Cre* mRNA, indicating a possible effect of 3'UTR length on mRNA stability. Some other evidence suggests that packaging of RNAs into EVs may be related to their stability within the cellular environment, with EV-associated mRNAs found to have shorter half-lives than cell retained RNAs in both B-cells and fibroblasts (Batagov *et al*., 2011). A study comparing apoptotic small EV RNA with apoptotic body RNA also determined that a) ABs were more similar to cells, and b) that small EV RNA had higher predicted minimum free energy (MFE) (Hardy *et al*., 2019). A higher MFE corresponds to a less stable, unfolded dynamic state, so it is likely that these RNAs may have a lower half-life *in vitro and in vivo.* Although Hardy *et al.* do not compare their apoptotic small EVs to normal EVs, along with the evidence that 3'UTR length increases *Cre* RNA packaging in the *Drosophila* EVs, it hints that stability may be a factor of broader importance in EV loading.

## 7.4 FUNCTIONALITY OF EV-RNA

A critical question in the EV field is how RNA cargo can be delivered in sufficient quantities to elicit measurable functional effects in recipient cells. Although evidence presented in this thesis does indicate that *Cre* mRNA is loaded into EVs, it is possible that this is a feature of its high expression level, as in physiological conditions it is estimated that the most abundant intact mRNA is present at around 1 copy per 1000 EVs (Wei *et al*., 2017). Results from the analysis of the RNA sequencing data here; the majority rRNA reads, the enrichment of UTR reads in EVs under $H_2O_2$-stress, and evidence of 3' end degradation, support existing data suggesting that EV-associated RNA contains a mixed population of intact and fragmented mRNA. This is in line with

estimates that mRNA fragments are present at ten times the abundance of intact RNAs (Wei *et al*., 2017), so it seems probable that these fragments may play at least as important a function as intact RNA. Existing work has provided evidence for the role of different EV RNA biotypes in the activation of toll-like receptors (TLRs) (Fabbri *et al*., 2012; Moroishi *et al*., 2016; Nabet *et al*., 2017), so degraded and fragmented RNAs within EVs may also act in this way. The *7SL* RNA studied by Nabet *et al.* in stromal cells was notably also enriched in the *Drosophila* S2R+ EVs. The data presented here also indicates that EVs derived from stressed cells likely have an effect on inducing cell death, via necroptosis, which has also been suggested in 4T1 breast cancer cells treated with EL4-T cell line derived EVs (Tavakkoli *et al*., 2020). Activation of TLRs is a known pathway by which cell death can be induced, so it seems reasonable that RNA fragments in EVs could be, at least in part, driving this effect. Poly(U)-rich RNAs are known pathogen associated molecular patterns (PAMPs) that stimulate signalling via TLR7, TLR8, and RIG1 receptors, so the enrichment of U-rich sequences in EVs, such as low stringency motif-3, may have functional importance in recipient cells as well as in EV-loading. Alongside transposons and repeat sequences, the enrichment of U-rich trinucleotides and pentanucleotides were confirmed in small apoptotic EVs of HUVEC cells of one study, although their effects on recipient cells were not investigated (Hardy *et al*., 2019). The characterisation in this thesis therefore confirms that the EV RNA has the capability of stimulating signalling receptors in recipient cells, which may result in subsequent cell death.

The RNase protection assays in this work suggest that, for mRNA, a portion of free RNA is contained within the vesicular membrane, whilst some non-vesicular RNA is co-isolated. Alongside ribosomes, Tosar *et al.* (2020) demonstrate the presence of full-length, non-degraded mRNAs within non-vesicular fractions, using both qPCR and long RNA sequencing (Oxford Nanopore). Use of such long-read RNA sequencing technology is key to understanding whether intact mRNAs are the exception, or the rule, and whether they are primarily associated with EVs or non-vesicular fractions. This study additionally demonstrated that the non-vesicular RNA

fractions were able to stimulate activation of dendritic cells, but induce cell death at high concentrations, so the effects seen in the S2R+ cells may also be due to non-vesicular RNAs (Tosar *et al*., 2020). Together the data shows that, whilst at least some RNA is present inside the EVs, the phenotypic effects seen on recipient cells cannot yet be attributed specifically to vesicular-contained RNA.

Fully understanding the role of EVs and their RNA cargo requires the study of uptake and delivery processes that were not directly investigated in this work. Several studies have indicated that irradiation stress increases EV uptake in recipient cells, through the use of PKH67 or PKH26 lipid binding dyes to label EVs (Arscott *et al*., 2013; Mutschelknaus *et al*., 2016). However, these dyes are non-specific and may form micelles that are internalised by recipient cells, and may thus give false conclusions on EV-specific effects. An alternative is to use EV marker proteins, such as CD81 and CD63, tagged with fluorescent proteins, a technique of which use is rapidly expanding in mammalian systems. In *Drosophila* Latebloomer is a good candidate, although evidence suggests that GFP-tagged human CD63 also localises to MVBs and secreted EVs of *Drosophila*, so could be used in its place (Corrigan *et al*., 2014). Use of lipophilic dyes in combination with this specific protein labelling, might also help to determine any effects mediated by any remaining bovine EVs in culture media, of which internalisation might also be altered by stress.

## 7.5 FINAL CONCLUSIONS AND FUTURE DIRECTIONS

To date, the study of EV-RNA loading mechanisms has focused primarily on sequence motifs, and associated RNA binding proteins. Carrying out complementary mass spectrometry of EV samples to identify changes in protein abundance under stress conditions could therefore help to determine RBPs that are responsible for altered loading mechanisms. With the knowledge that RNA content of *Drosophila* EVs is similar to that of mammalian EVs, testing of homologs of proteins identified in mammalian systems, such as Yps (Ybx-1) and Hrb98DE (hnRNPA2B1) would also aid in understanding of the evolutionary conservation of RNA packaging processes. In

addition, particularly when assessing the effects of different cellular conditions such as stress, post-translational modifications of these proteins should be studied, as these appear to be a key player in controlling RNA packaging.

However, since RBPs may act to alter EV loading indirectly, effects on subcellular RNA distribution need also be considered. Given evidence that RNA loading of EVs is linked to organellar structures such as the nucleus, endoplasmic reticulum and lysosomal system (Lässer et al., 2017; Barman et al., 2020; Leidal et al., 2020), and that cellular RNA distribution is highly assymetric (Khong et al., 2017; Bouvrette et al., 2018; Matheny et al., 2019), future work to directly compare the RNA content of EVs to sub-cellular fractions will aid in pinpointing where, and thus how, packaging is occuring. However, since EV biogenesis is highly heterogenous, this must necessarily be linked to an improvement in our ability to distinguish and purify different EV subpopulations, such as through immuno-affinity capture technqiues. The ability to define and separate these sub-populations will also aid in characterising how biogenesis is altered under stress, and thus the implications for both EV producer and EV recipient cells.

Of particular interest to understanding the loading and function of EV RNA would be determining the cause of the increased mismatch rate in EVs under stress; whether this is due to RNA modifications or sequence errors, and if this is coupled to RNA degradation pathways. Specific approaches to identify modified bases such as meRIP and miCLIP may be of use, although at present may be technically too challenging to apply to EVs. Comparison of the characteristics of the RNA content of EVs, such as the mismatch rate, with knockdown or overexpression of components of the RNA degradation machinery such as the 3'–5' exoribonuclease *DIS3L2*, an approach recently employed to great effect for components of the autophagy machinery, would also be of interest to probe this link.

The evidence in this thesis, alongside others, provides some refutation for the suggestion that long RNAs, or at least fragments of them, are not present in EVs. Indeed, it hints that longer

parental RNAs could in fact be enriched in EVs, which may have important implications for understanding of EV RNA loading mechanisms, such as a link with stress granules. Initial evidence that increased 3'UTR length, independently of the presence of EV "loading motifs", may promote packaging into EVs is a promising avenue for future work, so testing the effect of a range of 3'UTR lengths on the incorporation of *Cre* should be carried out in future.

One of the major limitations of this work was that sequencing depth was too low to carry out splice variant specific analysis. Whilst some improvement in read depth would likely be gained from RiboZero treatment to remove rRNA, this treatment was notably poor in stress cells, likely as a result of the facts that a) no commercially available kits are available specifically for *Drosophila,* and b) RiboZero performs poorly on fragmented rRNA. Use of recently developed methods for the design of larger sets of short probes for rRNA depletion such as "RiboPop" would likely improve efficiency and enable higher read depth of other coding and non-coding RNAs present at low abundance in EVs (Thompson *et al.,* 2020). An additional technology that could be employed to great effect in EVs is long read sequencing technology such as Oxford Nanopore. This would permit a transcriptome-wide assessment of the fragmentation state of the RNA content of EVs, which would provide an unequivocal answer as to whether the mRNAs within can code for protein production.

However, if EV RNA *is* primarily degraded RNA, this function is not mutually exclusive with a signalling role in intercellular communication. Indeed, it seems likely that EV-RNAs may function as damage-associated molecular patterns (DAMPs) to stimulate inflammatory responses and cell death in recipient cells. These data would indicate that the role of EVs in disposal and intercellular communication may of greater importance under conditions of cellular stress, which would be of significant pathological importance. Future work therefore will require the study of response pathways in recipient cells to assess if they are stimulated specifically by the EV-RNAs, and which individual RNAs might be most potent at doing so.

# Supplementary Materials

# 8 Supplementary Materials

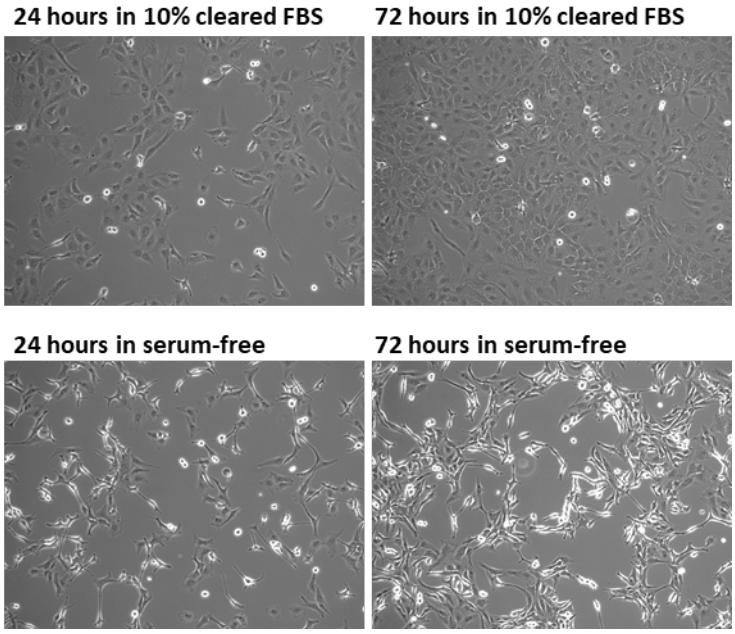


Supplementary Figure 1: SKOV3 cells tolerate serum-free conditions for 72 hours

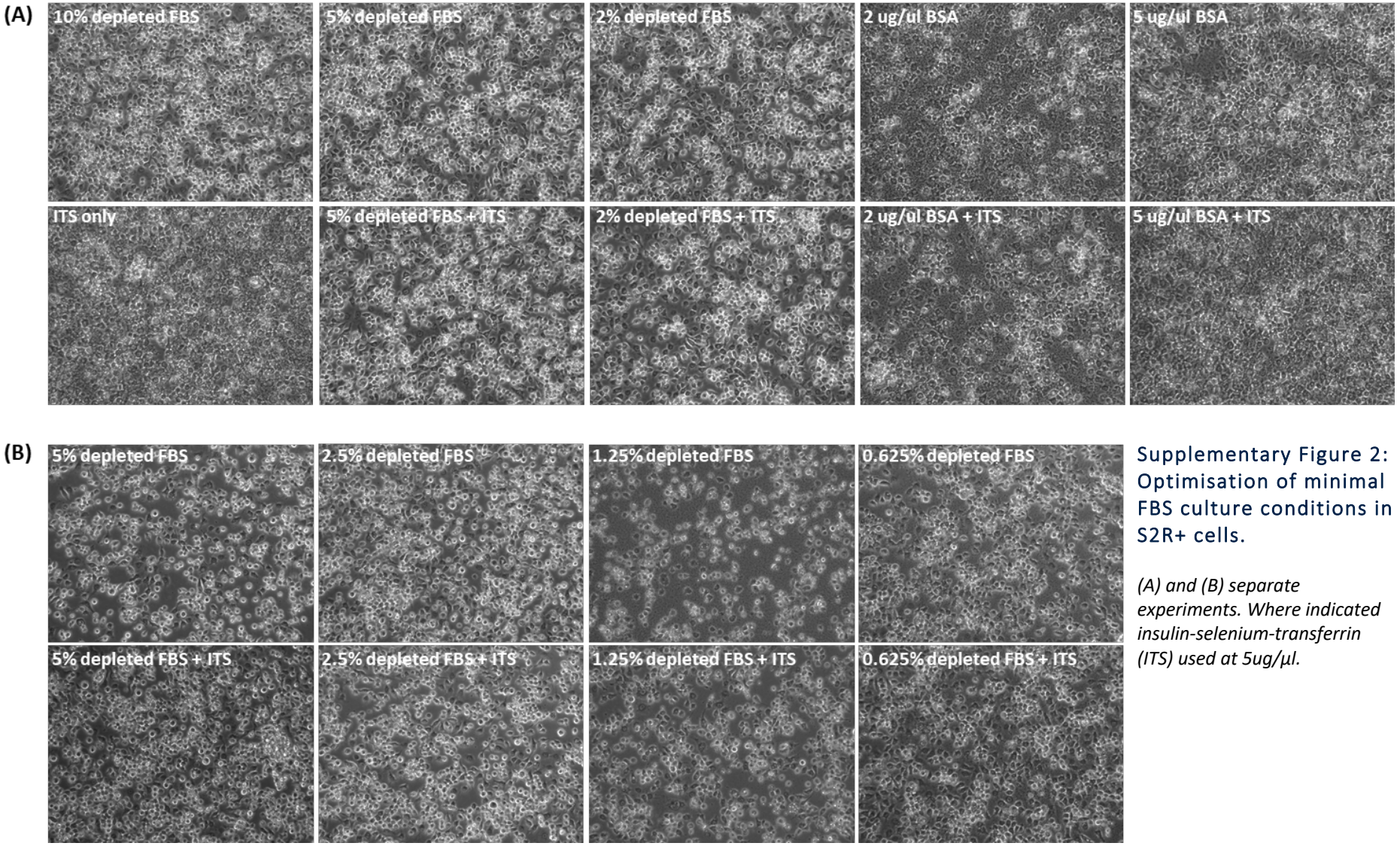


Supplementary Figure 2: Optimisation of minimal FBS culture conditions in S2R+ cells.

*(A) and (B) separate experiments. Where indicated insulin-selenium-transferrin (ITS) used at 5ug/µl.*

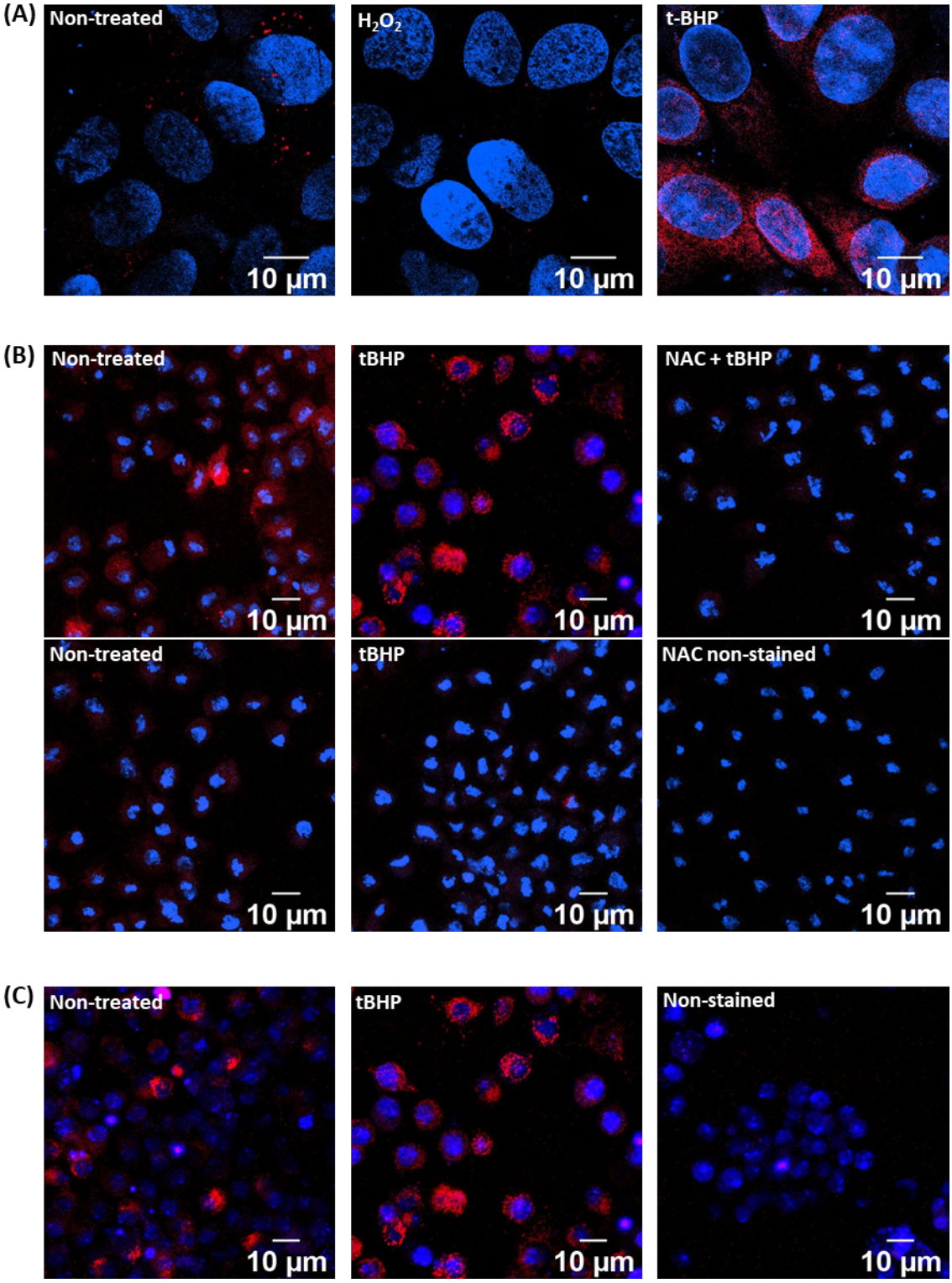


## Supplementary Figure 3: Testing of CellROX staining in MCF7 and S2R+ cells

*(A) Representative images of MCF-7 cells stained with Hoechst and CellROX after treatment with 222µM $H_2O_2$ or 47µM tBHP. (B) Representative images of CellROX staining in fixed S2R+ cells, showing high variability within conditions. Where indicated, cells pre-treated with 1mg/ml of the antioxidant N-acetylcysteine (NAC) as control for 2 hours, followed by treatment with 20um tBHP. (C) Representative images of staining in live S2R+ cells.*

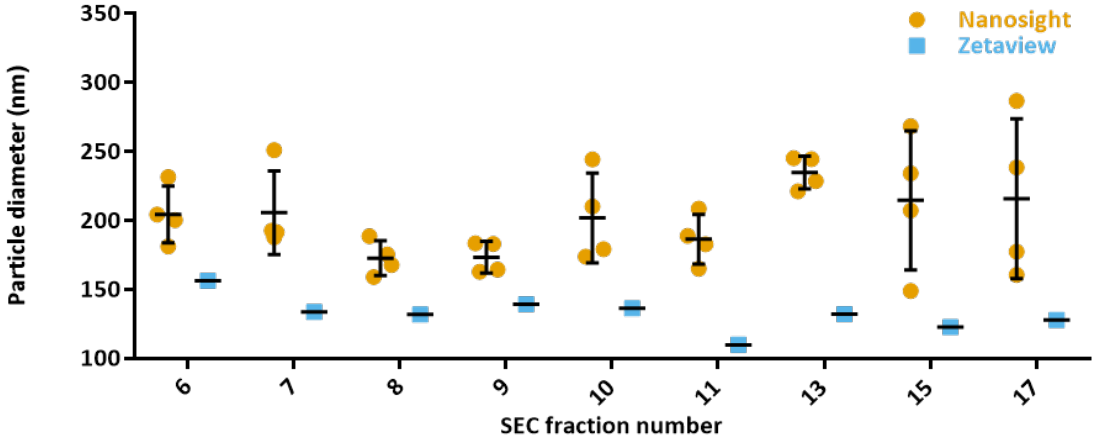


Supplementary Figure 4: Comparison of median particle size by Nanosight and Zetaview

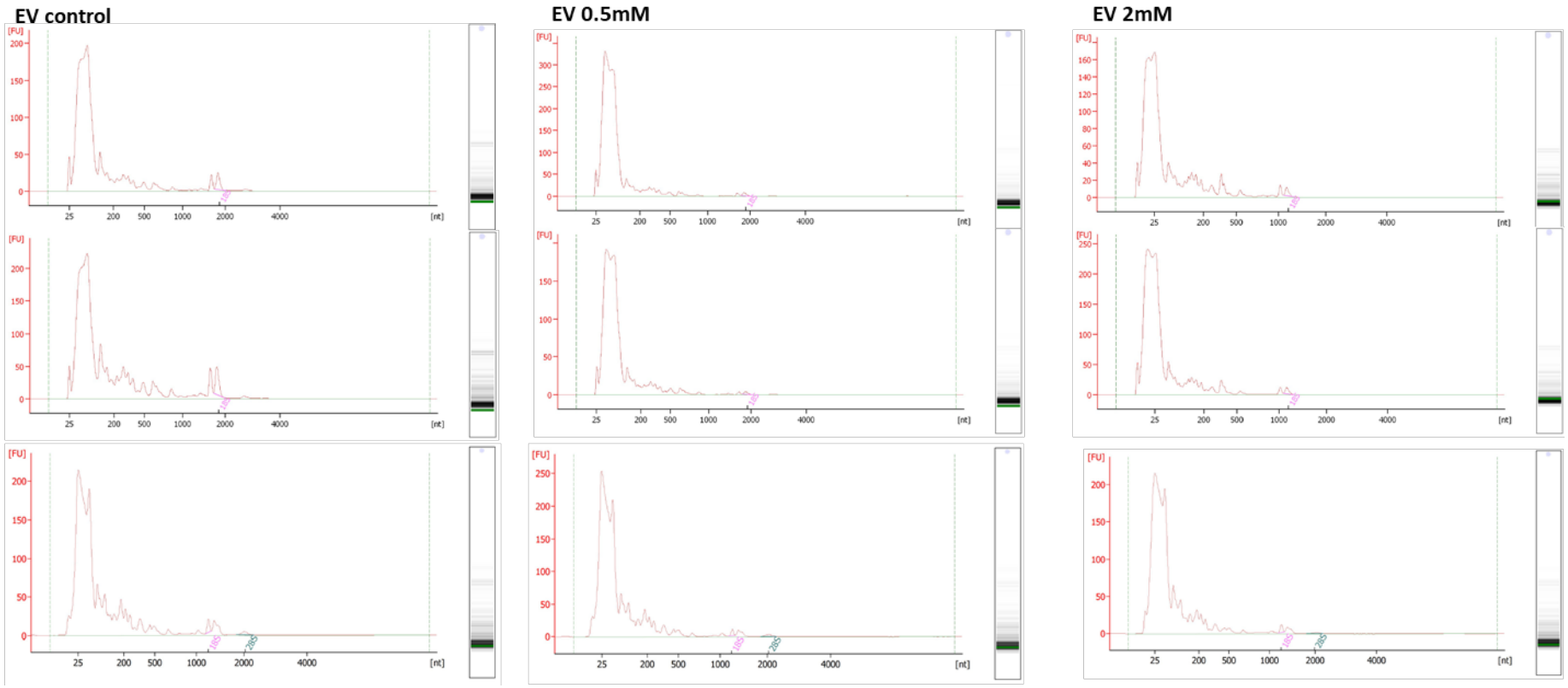
EV control
EV 0.5mM
EV 2mM
[FU]
[nt]
25
200
500
1000
2000
4000
18S
28S

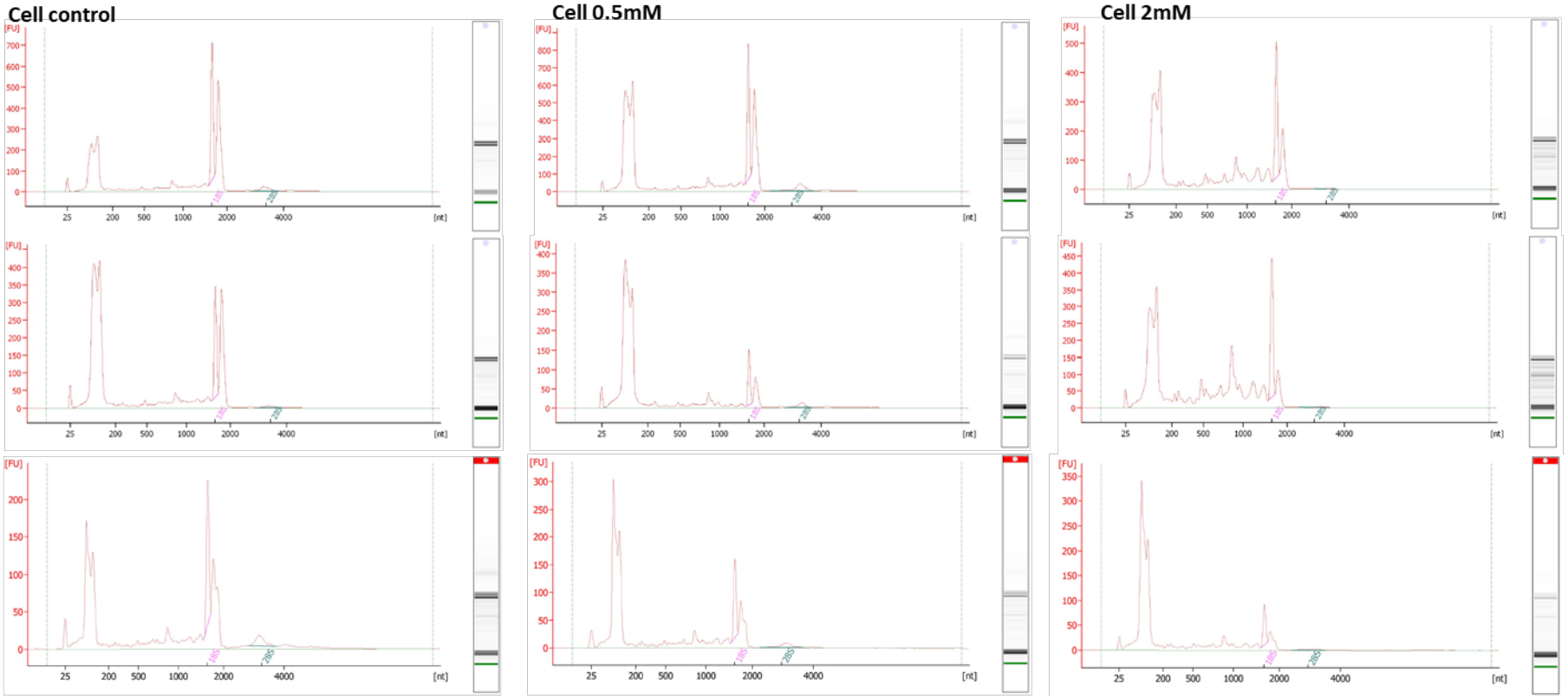


Supplementary Figure 5: Agilent bioanalyser traces for all sequenced RNA samples




## Supplementary Figure 6: FastQC quality control data for all sequenced samples

*Graphical display of quality scores for all 18 sequenced samples. FastQC classifies quality as either high (green), medium (yellow) or low (red). Sequence duplication, overrepresented sequences and GC content flagged as low quality, likely due to the presence of ribosomal RNA.*

**(A)**

| Reference sequence | Reads mapped to reference | | | | | | | | | | | | | | | | | | | |
|---|---|---|---|---|---|---|---|---|---|---|---|---|---|---|---|---|---|---|---|---|
| | EV control R1 | EV Control R2 | EV Control R3 | Cell Control R1 | Cell Control R2 | Cell Control R3 | EV 2mM R1 | EV 2mM R2 | EV 2mM R3 | Cell 2mM R1 | Cell 2mM R2 | Cell 2mM R3 | EV 0.5mM R1 | EV 0.5mM R2 | EV 0.5mM R3 | Cell 0.5mM R1 | Cell 0.5mM R2 | Cell 0.5mM R3 | EV Lefebvre R1 | EV Lefebvre R2 |
| Total | 25135922 | 16769682 | 20105170 | 24126694 | 22368262 | 21672928 | 20718340 | 18443406 | 18017858 | 21280766 | 18584410 | 23599080 | 20032144 | 25142152 | 22120348 | 17839120 | 22444988 | 23536440 | 33450610 | 41133748 |
| rRNA (Bowtie2 end-to-end) | 21089788 | 15691226 | 16292528 | 1662020 | 2783380 | 912566 | 18593328 | 17197048 | 14402284 | 3241810 | 5488346 | 3664012 | 16853518 | 23375806 | 17554230 | 1743232 | 4590348 | 1280978 | 30563192 | 39419108 |
| Transposon (Bowtie2 end-to-end) | 325578 | 122012 | 176484 | 2394170 | 2368772 | 1486762 | 205494 | 173308 | 356436 | 2182392 | 2145520 | 2242228 | 314666 | 253748 | 330920 | 2422368 | 2535550 | 1966966 | 92038 | 96262 |
| Repeat mask (Bowtie2 end-to-end) | 8996 | 11470 | 10184 | 89650 | 150004 | 204004 | 13208 | 12802 | 8592 | 96498 | 107084 | 83680 | 11614 | 15162 | 11032 | 88898 | 118298 | 114100 | 3760 | 2878 |
| Drosophila genome (HISAT2) | 694214 | 620974 | 755114 | 13596078 | 13717090 | 9217038 | 742980 | 659814 | 631470 | 7207420 | 8675242 | 8256302 | 653270 | 893344 | 732722 | 8093208 | 10890880 | 9227952 | 500378 | 355208 |
| Bovine genome (Bowtie2 end-to-end) | 10738 | 11374 | 2204 | 400280 | 352940 | 200248 | 2282 | 5684 | 2838 | 1780412 | 322280 | 222298 | 9512 | 17838 | 2870 | 327536 | 1590104 | 163472 | 88888 | 53456 |
| Totivirus (Bowtie2 end-to-end) | 107140 | 14026 | 100720 | 1102076 | 384746 | 3052484 | 24086 | 9124 | 95228 | 2493718 | 188794 | 2616550 | 86354 | 22458 | 86034 | 1569008 | 343246 | 3936234 | 74004 | 20380 |
| Alphanodavirus (Bowtie2 end-to-end) | 1721256 | 29366 | 1742470 | 1842736 | 413048 | 3133014 | 599738 | 26048 | 1461544 | 1391332 | 168596 | 2811508 | 1313090 | 46452 | 2067542 | 1219820 | 350998 | 3199686 | 286046 | 17448 |
| Alphanodavirus (Bowtie2 local) | 454240 | 13294 | 552500 | 1017490 | 172482 | 1705506 | 175486 | 40528 | 558312 | 974250 | 125836 | 1518548 | 384736 | 25338 | 776974 | 730260 | 187388 | 1792580 | 16354 | 1564 |
| rRNA (Bowtie2 local) | 285804 | 141718 | 171380 | 19080 | 31080 | 13954 | 209438 | 229342 | 218028 | 61434 | 57958 | 39058 | 149076 | 284580 | 204736 | 20640 | 68140 | 15756 | 167766 | 75452 |
| Drosophila genome (Bowtie2 local) | 40838 | 21736 | 31484 | 935556 | 912220 | 667724 | 26878 | 24850 | 39390 | 554976 | 569928 | 633708 | 29004 | 36816 | 36594 | 595990 | 705312 | 653354 | 34918 | 22214 |
| Totivirus (Bowtie2 local) | 4742 | 652 | 6362 | 56478 | 19088 | 137442 | 858 | 436 | 4064 | 95248 | 9948 | 103130 | 2726 | 1082 | 4762 | 65802 | 16170 | 156964 | 4356 | 1130 |
| Drosophila C virus (Bowtie2 local) | | | | | | | | | | | | | | | | | | | 186600 | 249636 |
| Enterobacteria phage (Bowtie2 local) | | | | | | | | | | | | | | | | | | | 128018 | 124290 |

**(B)**

| Reference sequence | Percentage of total reads mapped to reference | | | | | | | | | | | | | | | | | | | |
|---|---|---|---|---|---|---|---|---|---|---|---|---|---|---|---|---|---|---|---|---|
| | EV control R1 | EV Control R2 | EV Control R3 | Cell Control R1 | Cell Control R2 | Cell Control R3 | EV 2mM R1 | EV 2mM R2 | EV 2mM R3 | Cell 2mM R1 | Cell 2mM R2 | Cell 2mM R3 | EV 0.5mM R1 | EV 0.5mM R2 | EV 0.5mM R3 | Cell 0.5mM R1 | Cell 0.5mM R2 | Cell 0.5mM R3 | EV Lefebvre R1 | EV Lefebvre R2 |
| rRNA (Bowtie2 end-to-end) | 83.9 | 93.6 | 81.0 | 6.9 | 12.4 | 4.2 | 89.7 | 93.2 | 79.9 | 15.2 | 29.5 | 15.5 | 84.1 | 93.0 | 79.4 | 9.8 | 20.5 | 5.4 | 91.4 | 95.8 |
| Transposon (Bowtie2 end-to-end) | 1.3 | 0.7 | 0.9 | 9.9 | 10.6 | 6.9 | 1.0 | 0.9 | 2.0 | 10.3 | 11.5 | 9.5 | 1.6 | 1.0 | 1.5 | 13.6 | 11.3 | 8.4 | 0.3 | 0.2 |
| Repeat mask (Bowtie2 end-to-end) | 0.0 | 0.1 | 0.1 | 0.4 | 0.7 | 0.9 | 0.1 | 0.1 | 0.0 | 0.5 | 0.6 | 0.4 | 0.1 | 0.1 | 0.0 | 0.5 | 0.5 | 0.5 | 0.0 | 0.0 |
| Drosophila genome (HISAT2) | 2.8 | 3.7 | 3.8 | 56.4 | 61.3 | 42.5 | 3.6 | 3.6 | 3.5 | 33.9 | 46.7 | 35.0 | 3.3 | 3.6 | 3.3 | 45.4 | 48.5 | 39.2 | 1.5 | 0.9 |
| Bovine genome (Bowtie2 end-to-end) | 0.0 | 0.1 | 0.0 | 1.7 | 1.6 | 0.9 | 0.0 | 0.0 | 0.0 | 8.4 | 1.7 | 0.9 | 0.0 | 0.1 | 0.0 | 1.8 | 7.1 | 0.7 | 0.3 | 0.1 |
| Totivirus (Bowtie2 end-to-end) | 0.4 | 0.1 | 0.5 | 4.6 | 1.7 | 14.1 | 0.1 | 0.0 | 0.5 | 11.7 | 1.0 | 11.1 | 0.4 | 0.1 | 0.4 | 8.8 | 1.5 | 16.7 | 0.2 | 0.0 |
| Alphanodavirus (Bowtie2 end-to-end) | 6.8 | 0.2 | 8.7 | 7.6 | 1.8 | 14.5 | 2.9 | 0.1 | 8.1 | 6.5 | 0.9 | 11.9 | 6.6 | 0.2 | 9.3 | 6.8 | 1.6 | 13.6 | 0.9 | 0.0 |
| Alphanodavirus (Bowtie2 local) | 1.8 | 0.1 | 2.7 | 4.2 | 0.8 | 7.9 | 0.8 | 0.2 | 3.1 | 4.6 | 0.7 | 6.4 | 1.9 | 0.1 | 3.5 | 4.1 | 0.8 | 7.6 | 0.0 | 0.0 |
| rRNA (Bowtie2 local) | 1.1 | 0.8 | 0.9 | 0.1 | 0.1 | 0.1 | 1.0 | 1.2 | 1.2 | 0.3 | 0.3 | 0.2 | 0.7 | 1.1 | 0.9 | 0.1 | 0.3 | 0.1 | 0.5 | 0.2 |
| Drosophila genome (Bowtie2 local) | 0.2 | 0.1 | 0.2 | 3.9 | 4.1 | 3.1 | 0.1 | 0.1 | 0.2 | 2.6 | 3.1 | 2.7 | 0.1 | 0.1 | 0.2 | 3.3 | 3.1 | 2.8 | 0.1 | 0.1 |
| Totivirus (Bowtie2 local) | 0.0 | 0.0 | 0.0 | 0.2 | 0.1 | 0.6 | 0.0 | 0.0 | 0.0 | 0.4 | 0.1 | 0.4 | 0.0 | 0.0 | 0.0 | 0.4 | 0.1 | 0.7 | 0.0 | 0.0 |
| Drosophila C virus (Bowtie2 local) | | | | | | | | | | | | | | | | | | | 0.6 | 0.6 |
| Enterobacteria phage (Bowtie2 local) | | | | | | | | | | | | | | | | | | | 0.4 | 0.3 |
| Total | 98.4 | 99.5 | 98.7 | 95.8 | 95.2 | 95.7 | 99.4 | 99.7 | 98.7 | 94.4 | 96.1 | 94.0 | 98.9 | 99.3 | 98.6 | 94.6 | 95.3 | 95.6 | 96.1 | 98.3 |

## Supplementary Figure 7: Alignment statistics for all sequenced samples

*(A) Paired reads aligned to each reference sequence, with alignment tool and setting shown in brackets. (B) Percentage of total sequenced reads aligned to each reference.*

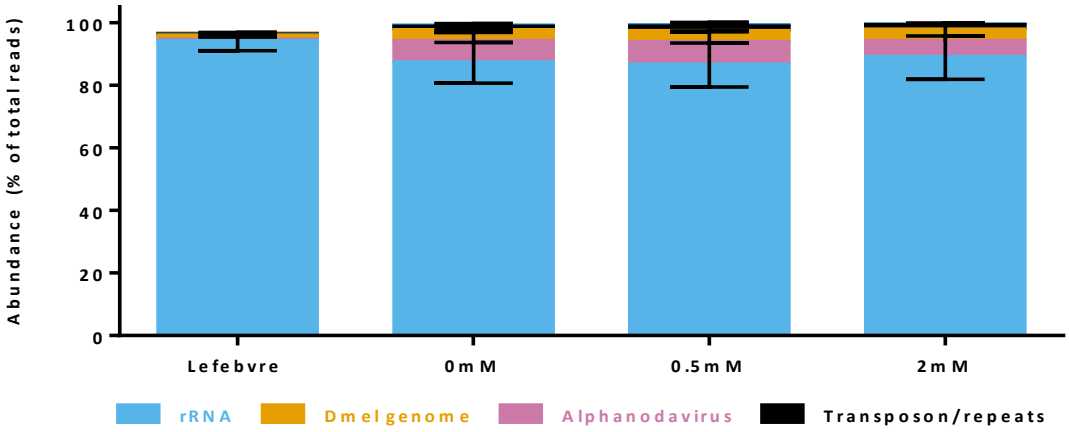


## Supplementary Figure 8: Alignment statistics for all EV samples

*Percentage of paired reads aligning to each RNA type relative to all sequenced reads, for each of the 18 sequenced samples and S2R+ EV samples from Lefebvre et al. (2016).*

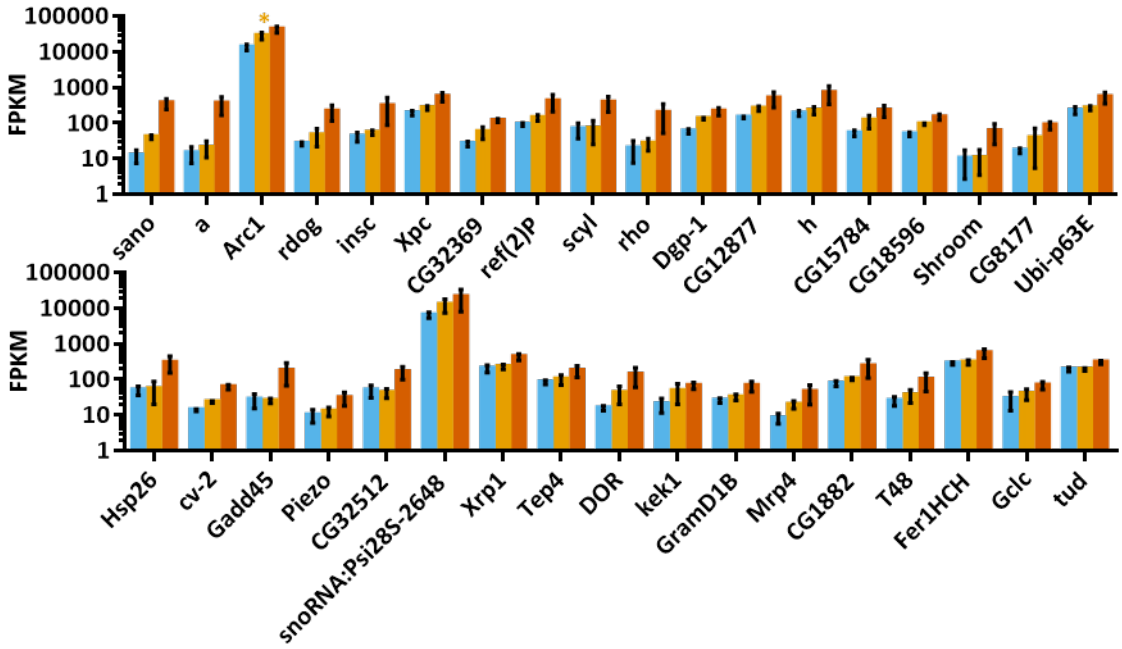


## Supplementary Figure 9: RNAs upregulated in both cells and EVs under stress

*FPKM abundance values in EVs for 35 RNAs detected as significantly upregulated in EVs as well as cells under 2mM $H_2O_2$ stress, by DESEQ2 with p-adj at 0.05.*

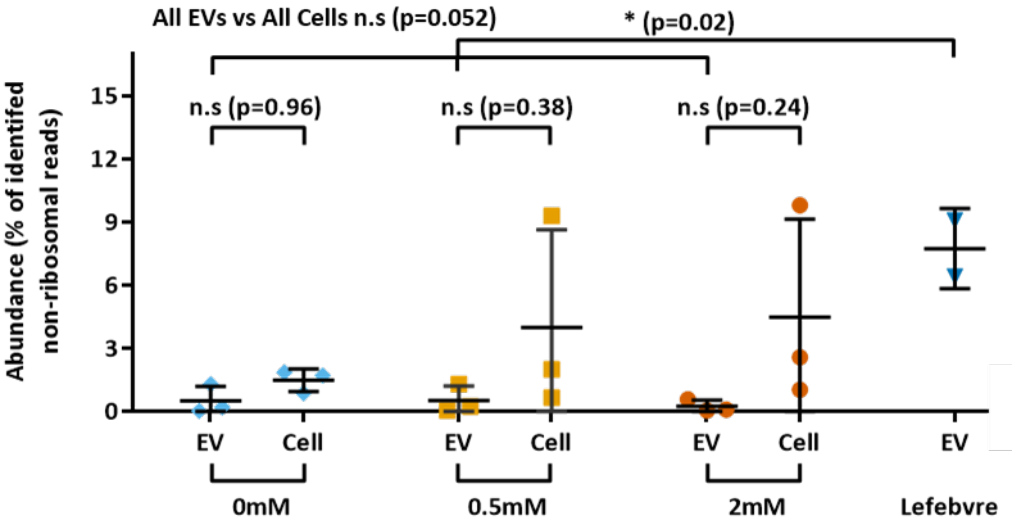


## Supplementary Figure 10: Bovine-specific RNA contamination in all samples

*Percentage of paired reads aligning to bovine (bosTau8) genome after removal of ribosomal reads, for each of the 18 sequenced samples and S2R+ EV samples from Lefebvre et al. (2016). Mean and standard deviation shown, and statistical significance assessed with two-way ANOVA followed by Sidak's multiple comparisons test.*

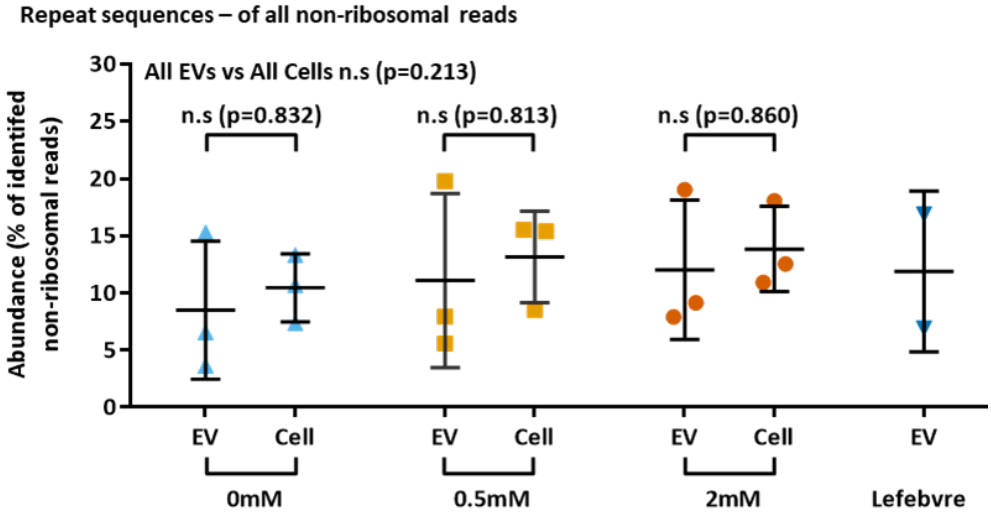


## Supplementary Figure 11: Repeat sequences/transposons in all samples

*Combined percentage of paired reads aligning to Flybase transposon sequences and repeat masked sequences from UCSC Genome Browser for* Drosophila melanogaster*, after removal of ribosomal reads, for each of the 18 sequenced samples and S2R+ EV samples from Lefebvre et al (2016). Mean and standard deviation shown, and statistical significance assessed with two-way ANOVA followed by Sidak's multiple comparisons test.*

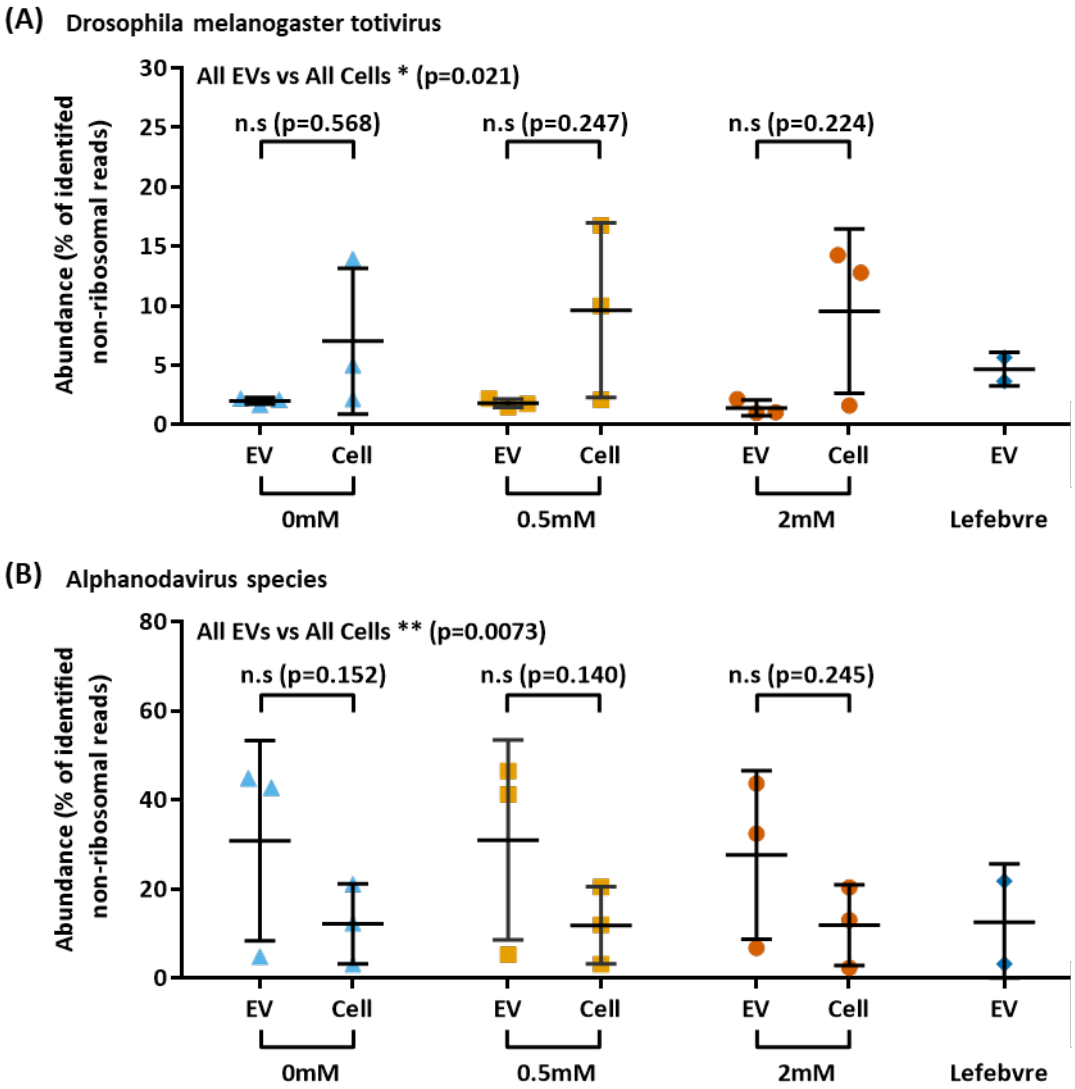


## Supplementary Figure 12: Viral RNA content of all samples

*(A) Percentage of paired reads aligning to* Drosophila melanogaster totivirus *after removal of ribosomal reads. (B) Percentage of paired reads aligning to viral species in the alphanodavirus genus; Flock house virus, Boolarra virus and black beetle virus, for each of the 18 sequenced samples and S2R+ EV samples from Lefebvre et al (2016). Mean and standard deviation shown, and statistical significance assessed with two-way ANOVA followed by Sidak's multiple comparisons test.*

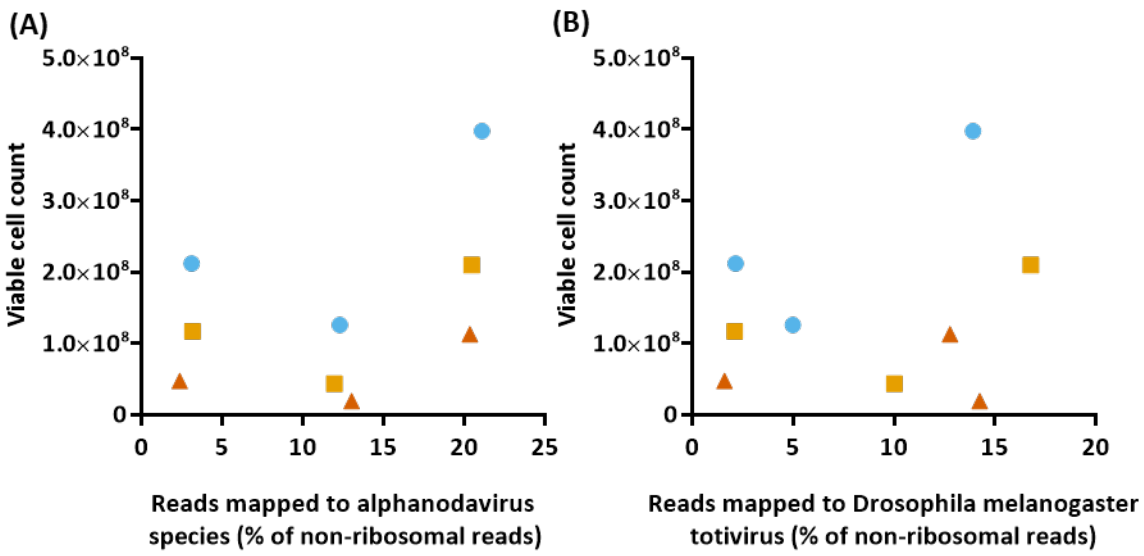


## Supplementary Figure 13: Effect of viral infection on viable cell count

*(A) Correlation between viral read percentage for* alphanodavirus *in cell samples and viable cell count, as measured by trypan blue exclusion. (B) As for (A) but for* Drosophila melanogaster totivirus*.*

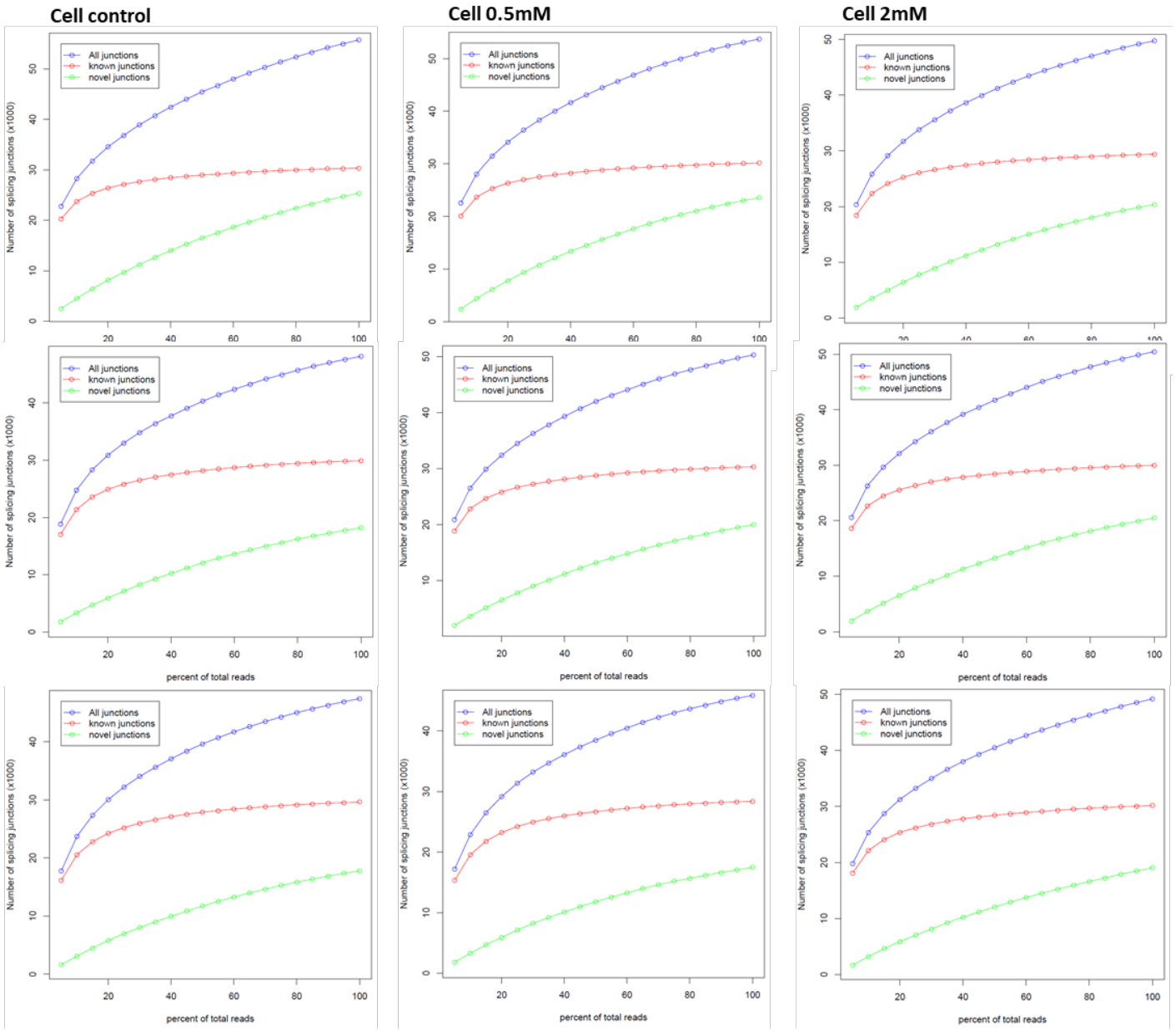
Cell control
Cell 0.5mM
Cell 2mM
All junctions
known junctions
novel junctions
Number of splicing junctions (x1000)
percent of total reads

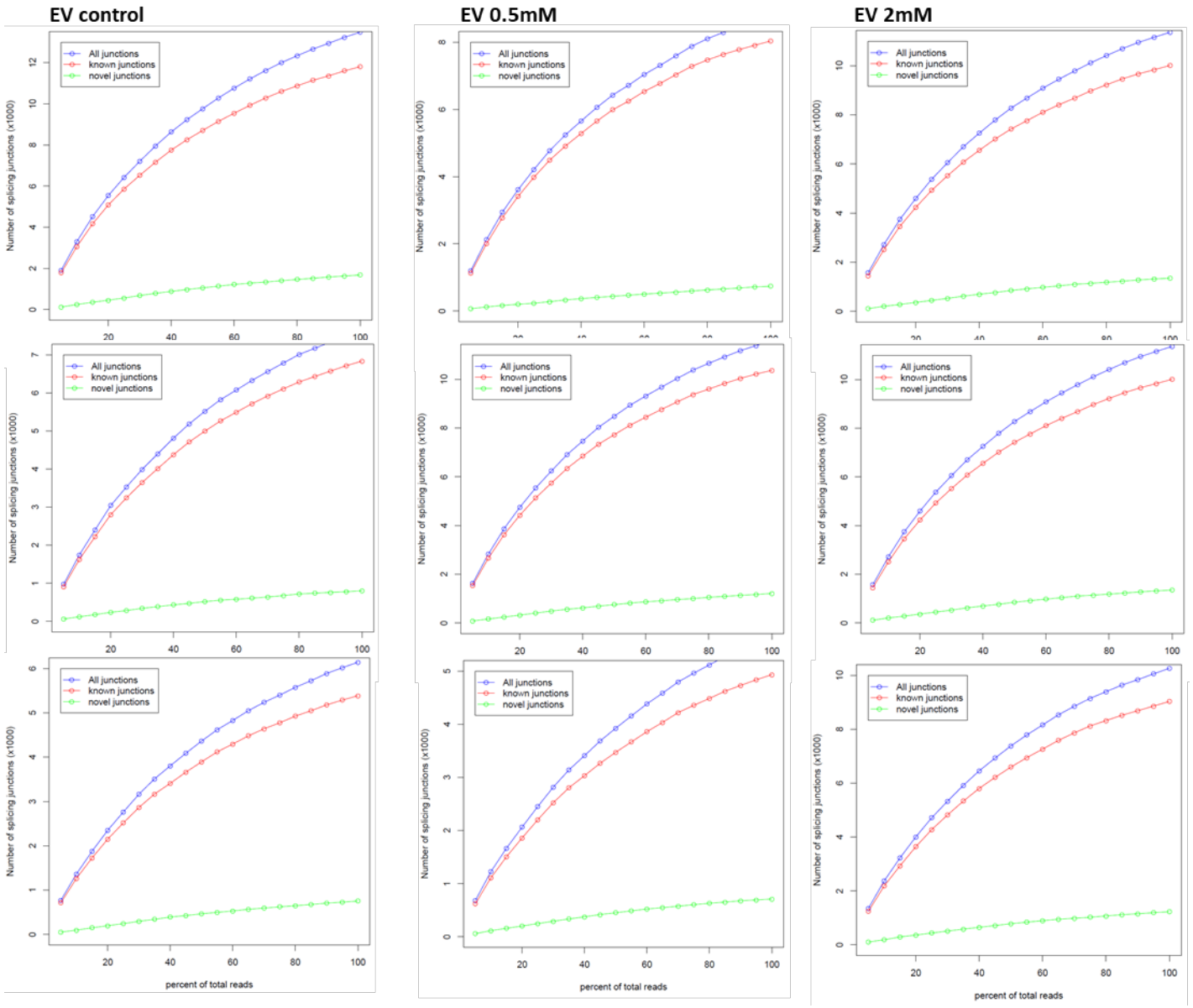


## Supplementary Figure 14: Junction saturation analysis

*Indicates read depth is not sufficient to saturate splice junctions to enable transcript variant level analysis.*

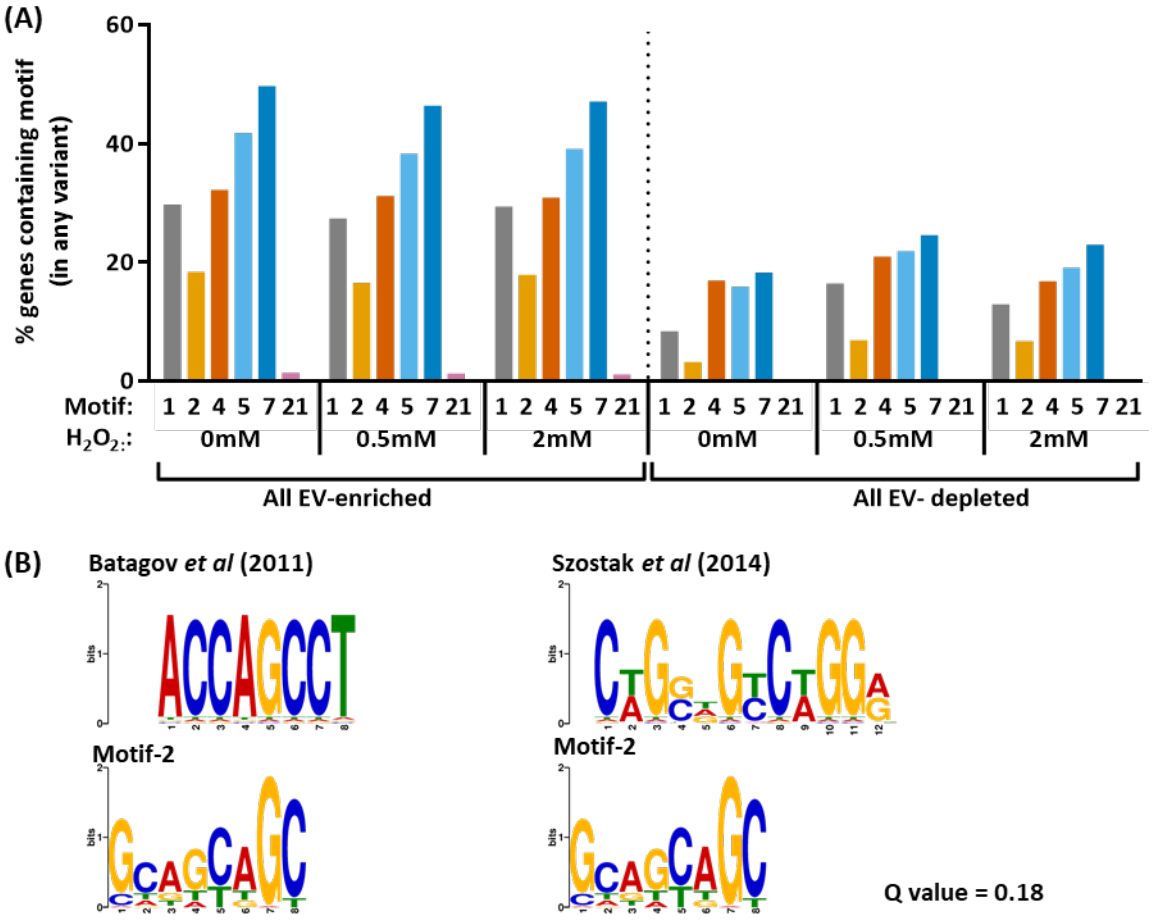


Supplementary Figure 15: Validation of low stringency control motif set

*(A) Abundancies of 30 motifs in low stringency control set found by searching of 3'UTR sequences using MEME, in all mRNA found as significantly enriched or depleted in EVs by DESEQ2, at any fold change with p-adj at 0.05. (B) Graphical representation of highest significance hits with TOMTOM comparison of motifs to those in literature, but both with q-value of 0.18.*

**(A) ParaWT 3'UTR**

TGAGCCAGGCCTCGCCCCCCCCTCCAAGATGCACGCGAGTATTAGCATGAGTACGTGTTGGATGTTGCATGTTG
CATCAGCGATGCAGCAGCGACAGTGAGCTAACAACAACAGCAACAAGGCGAACAACAAGCATAATTTTCTGCT
ATATAATGAAAGAACACCATACAAACAAATACAACAACAAT

**(B) ParaShuffled 3'UTR**

TGAGCCAGGCCTCGCCCCCCCCTCCAAGATGCACGCGAGTATTAGCATGAGT**TAATTGTGTTGGGCTTGTACG**
GCATCAGCGATGCAGCAGCGACAGT**AATCCCAAGAAAAAACGGCAC**AGGCGAACAACAAGCATAATTTTCTG
CTATATAATGAAAGAA**ACAAAAACACAACCAATACAACT**CAAT

Motif-1 Motif-2 Motif-3 Motif-4 Motif-7

Supplementary Figure 16: 3'UTR sequences for motif constructs

*Motif hits in 3'UTR sequences with q-value <0.05 in FIMO for A) ParaWT, and B) Para with shuffled motifs. Motif-1 and motif-2 remain present.*

| Motif number | Adjusted p-value |
|---|---|
| Motif-1 | 4.52E-05 |
| Motif-2 | 1.80E-05 |
| Motif-3 | 0.896851 |
| Motif-4 | 0.342552 |
| Motif-5 | 5.94E-08 |
| Motif-6 | 0.000152 |
| Motif-7 | 0.244074 |
| Motif-8 | 8.39E-07 |
| Motif-9 | 0.050226 |
| Motif-11 | 0.908107 |
| Motif-12 | 0.00105 |
| Motif-13 | 0.036032 |
| Motif-14 | 0.887915 |
| Motif-15 | 9.08E-05 |
| Motif-16 | 0.701492 |
| Motif-17 | 0.016337 |
| Motif-18 | 0.003489 |
| Motif-19 | 0.144857 |
| Motif-21 | 0.111645 |
| Motif-22 | 0.227235 |
| Motif-24 | 0.912345 |
| Motif-25 | 0.001704 |
| Motif-26 | 0.051109 |
| Motif-27 | 0.864977 |
| Motif-28 | 0.028585 |
| Motif-29 | 0.881367 |

## Supplementary Figure 17: Comparison of cDNA motifs to $(CAG)_6$

*Table showing TOMTOM comparison of 30 motifs in high stringency control set found by searching of cDNA sequences using MEME, to $(CAG)_6$ repeat motif. Significant matches highlighted in green.*

# References

# 9 References


Abdulrahman, B. A., Abdelaziz, D. H., and Schatzl, H. M. (2018). Autophagy regulates exosomal release of prions in neuronal cells. *J. Biol. Chem.* 293, 8956–8968. doi:10.1074/jbc.RA117.000713.

Afgan, E., Baker, D., van den Beek, M., Blankenberg, D., Bouvier, D., Čech, M., et al. (2016). The Galaxy platform for accessible, reproducible and collaborative biomedical analyses: 2016 update. *Nucleic Acids Res.* 44, W3–W10. doi:10.1093/nar/gkw343.

Aizawa, S., Fujiwara, Y., Contu, V. R., Hase, K., Takahashi, M., Kikuchi, H., et al. (2016). Lysosomal putative RNA transporter SIDT2 mediates direct uptake of RNA by lysosomes. *Autophagy* 12, 565–578. doi:10.1080/15548627.2016.1145325.

Al-Mayah, A., Bright, S., Chapman, K., Irons, S., Luo, P., Carter, D., et al. (2015). The non-targeted effects of radiation are perpetuated by exosomes. *Mutat. Res. - Fundam. Mol. Mech. Mutagen.* 772, 38–45. doi:10.1016/j.mrfmmm.2014.12.007.

Al-Mayah, A. H. J., Irons, S. L., Pink, R. C., Carter, D. R. F., and Kadhim, M. A. (2012). Possible Role of Exosomes Containing RNA in Mediating Nontargeted Effect of Ionizing Radiation. *Radiat. Res.* 177, 539–545. doi:10.1667/RR2868.1.

Albanese, M., Chen, Y.-F. A., Hüls, C., Gärtner, K., Tagawa, T., Mejias-Perez, E., et al. (2020). Micro RNAs are minor constituents of extracellular vesicles and are hardly delivered to target cells. *bioRxiv*, 2020.05.20.106393. doi:10.1101/2020.05.20.106393.

Alexandre, J., Hu, Y., Lu, W., Pelicano, H., and Huang, P. (2007). Novel action of paclitaxel against cancer cells: Bystander effect mediated by reactive oxygen species. *Cancer Res.* 67, 3512–3517. doi:10.1158/0008-5472.CAN-06-3914.

Altan-Bonnet, N., Perales, C., and Domingo, E. (2019). Extracellular vesicles: Vehicles of en bloc viral transmission. *Virus Res.* 265, 143–149. doi:10.1016/j.virusres.2019.03.023.

Alvarez-Erviti, L., Seow, Y., Schapira, A. H., Gardiner, C., Sargent, I. L., Wood, M. J. A., et al. (2011). Lysosomal dysfunction increases exosome-mediated alpha-synuclein release and transmission. *Neurobiol. Dis.* 42, 360–367. doi:10.1016/j.nbd.2011.01.029.

Anders, M., Chelysheva, I., Goebel, I., Trenkner, T., Zhou, J., Mao, Y., et al. (2018). Dynamic m6a methylation facilitates mRNA triaging to stress granules. *Life Sci. Alliance* 1. doi:10.26508/lsa.201800113.

Anders, S., Pyl, P. T., and Huber, W. (2015). HTSeq--a Python framework to work with high-throughput sequencing data. *Bioinformatics* 31, 166–169. doi:10.1093/bioinformatics/btu638.

Andreu, Z., and Yáñez-Mó, M. (2014). Tetraspanins in extracellular vesicle formation and function. *Front. Immunol.* 5, 442. doi:10.3389/fimmu.2014.00442.

Andrews, S. Babraham Bioinformatics - FastQC A Quality Control tool for High Throughput Sequence Data. Available at: https://www.bioinformatics.babraham.ac.uk/projects/fastqc/ [Accessed March 9, 2021].

Arora, S. (2012). Identifying and targeting cellular mechanisms to enhance cisplatin

chemotherapeutic response in cancer. Available at: http://utdr.utoledo.edu/cgi/viewcontent.cgi?article=1277&context=theses-dissertations [Accessed March 10, 2017].

Arroyo, J. D., Chevillet, J. R., Kroh, E. M., Ruf, I. K., Pritchard, C. C., Gibson, D. F., et al. (2011). Argonaute2 complexes carry a population of circulating microRNAs independent of vesicles in human plasma. *Proc. Natl. Acad. Sci. U. S. A.* 108, 5003–5008. doi:10.1073/pnas.1019055108.

Arscott, W. T., Tandle, A. T., Zhao, S., Shabason, J. E., Gordon, I. K., Schlaff, C. D., et al. (2013). Ionizing Radiation and Glioblastoma Exosomes: Implications in Tumor Biology and Cell Migration. *Transl. Oncol.* 6, 638-IN6. doi:10.1593/tlo.13640.

Ashley, J., Cordy, B., Lucia, D., Fradkin, L. G., Budnik, V., and Thomson, T. (2018). Retrovirus-like Gag Protein Arc1 Binds RNA and Traffics across Synaptic Boutons. *Cell* 172, 262-274.e11. doi:10.1016/j.cell.2017.12.022.

Atay, S., Gercel-Taylor, C., and Taylor, D. D. (2011). Human Trophoblast-Derived Exosomal Fibronectin Induces Pro-Inflammatory Il-1β Production by Macrophages. *Am. J. Reprod. Immunol.* 66, 259–269. doi:10.1111/j.1600-0897.2011.00995.x.

Atienzar-Aroca, S., Flores-Bellver, M., Serrano-Heras, G., Martinez-Gil, N., Barcia, J. M., Aparicio, S., et al. (2016). Oxidative stress in retinal pigment epithelium cells increases exosome secretion and promotes angiogenesis in endothelial cells. *J. Cell. Mol. Med.* 20, 1457–1466. doi:10.1111/jcmm.12834.

Auber, M., Fröhlich, D., Drechsel, O., Karaulanov, E., and Krämer-Albers, E. M. (2019). Serum-free media supplements carry miRNAs that co-purify with extracellular vesicles. *J. Extracell. Vesicles* 8, 1656042. doi:10.1080/20013078.2019.1656042.

Aubertin, K., Silva, A. K. A., Luciani, N., Espinosa, A., Djemat, A., Charue, D., et al. (2016). Massive release of extracellular vesicles from cancer cells after photodynamic treatment or chemotherapy. *Sci. Rep.* 6. doi:10.1038/srep35376.

Azzam, E. I., de Toledo, S. M., and Little, J. B. (2001). Direct evidence for the participation of gap junction-mediated intercellular communication in the transmission of damage signals from alpha -particle irradiated to nonirradiated cells. *Proc. Natl. Acad. Sci. U. S. A.* 98, 473–478. doi:10.1073/pnas.011417098.

Baglio, S. R., Rooijers, K., Koppers-Lalic, D., Verweij, F. J., Pérez Lanzón, M., Zini, N., et al. (2015). Human bone marrow- and adipose-mesenchymal stem cells secrete exosomes enriched in distinctive miRNA and tRNA species. *Stem Cell Res. Ther.* 6, 127. doi:10.1186/s13287-015-0116-z.

Bailey, T. L., Boden, M., Buske, F. A., Frith, M., Grant, C. E., Clementi, L., et al. (2009). MEME Suite: Tools for motif discovery and searching. *Nucleic Acids Res.* 37, W202–W208. doi:10.1093/nar/gkp335.

Bailey, T. L., and Elkan, C. (1994). Fitting a mixture model by expectation maximization to discover motifs in biopolymers. *Proc. Int. Conf. Intell. Syst. Mol. Biol.* 2, 28–36.

Baj-Krzyworzeka, M., Szatanek, R., Węglarczyk, K., Baran, J., Urbanowicz, B., Brański, P., et al. (2006). Tumour-derived microvesicles carry several surface determinants and mRNA of tumour cells and transfer some of these determinants to monocytes. *Cancer Immunol.*

*Immunother.* 55, 808–818. doi:10.1007/s00262-005-0075-9.

Balaj, L., Lessard, R., Dai, L., Cho, Y. J., Pomeroy, S. L., Breakefield, X. O., et al. (2011). Tumour microvesicles contain retrotransposon elements and amplified oncogene sequences. *Nat. Commun.* 2, 1–9. doi:10.1038/ncomms1180.

Baldrich, P., Rutter, B. D., Karimi, H. Z., Podicheti, R., Meyers, B. C., and Innes, R. W. b. (2019). Plant extracellular vesicles contain diverse small RNA species and are enriched in 10- to 17-nucleotide "Tiny" RNAs. *Plant Cell* 31, 315–324. doi:10.1105/tpc.18.00872.

Barman, B., Ping, J., Krystofiak, E., and Allen, R. (2020). Biogenesis of RNA-containing extracellular vesicles at endoplasmic reticulum membrane contact sites. *bioRxiv*, 2020.12.04.412379. doi:10.1101/2020.12.04.412379.

Barreau, C., Paillard, L., and Osborne, H. B. (2005). AU-rich elements and associated factors: Are there unifying principles? *Nucleic Acids Res.* 33, 7138–7150. doi:10.1093/nar/gki1012.

Barrett, T., Wilhite, S. E., Ledoux, P., Evangelista, C., Kim, I. F., Tomashevsky, M., et al. (2013). NCBI GEO: Archive for functional genomics data sets - Update. *Nucleic Acids Res.* 41, D991–D995. doi:10.1093/nar/gks1193.

Bartel, D. P. (2004). MicroRNAs: Genomics, Biogenesis, Mechanism, and Function. *Cell* 116, 281–297. doi:10.1016/S0092-8674(04)00045-5.

Batagov, A. O., and Kurochkin, I. V. (2013). Exosomes secreted by human cells transport largely mRNA fragments that are enriched in the 3'-untranslated regions. *Biol. Direct* 8, 1–8. doi:10.1186/1745-6150-8-12.

Batagov, A. O., Kuznetsov, V. A., and Kurochkin, I. V. (2011). Identification of nucleotide patterns enriched in secreted RNAs as putative cis-acting elements targeting them to exosome nano-vesicles. *BMC Genomics* 12, S18. doi:10.1186/1471-2164-12-S3-S18.

Baxter, A. A., Phan, T. K., Hanssen, E., Liem, M., Hulett, M. D., Mathivanan, S., et al. (2019). Analysis of extracellular vesicles generated from monocytes under conditions of lytic cell death. *Sci. Rep.* 9, 1–13. doi:10.1038/s41598-019-44021-9.

Bayer-Santos, E., Aguilar-Bonavides, C., Rodrigues, S. P., Cordero, E. M., Marques, A. F., Varela-Ramirez, A., et al. (2013). Proteomic analysis of trypanosoma cruzi secretome: Characterization of two populations of extracellular vesicles and soluble proteins. *J. Proteome Res.* 12, 883–897. doi:10.1021/pr300947g.

Beckett, K., Monier, S., Palmer, L., Alexandre, C., Green, H., Bonneil, E., et al. (2013). Drosophila S2 Cells Secrete Wingless on Exosome-Like Vesicles but the Wingless Gradient Forms Independently of Exosomes. *Traffic* 14, 82–96. doi:10.1111/tra.12016.

Beer, K. B., and Wehman, A. M. (2017). Mechanisms and functions of extracellular vesicle release in vivo—What we can learn from flies and worms. *Cell Adhes. Migr.* 11, 135–150. doi:10.1080/19336918.2016.1236899.

Beira, J. V., and Paro, R. (2016). The legacy of Drosophila imaginal discs. *Chromosoma* 125, 573–592. doi:10.1007/s00412-016-0595-4.

Bellingham, S. A., Coleman, B. M., and Hill, A. F. (2012). Small RNA deep sequencing reveals a distinct miRNA signature released in exosomes from prion-infected neuronal cells. *Nucleic*

*Acids Res.* 40, 10937–10949. doi:10.1093/nar/gks832.

Benedikter, B. J., Bouwman, F. G., Vajen, T., Heinzmann, A. C. A., Grauls, G., Mariman, E. C., et al. (2017). Ultrafiltration combined with size exclusion chromatography efficiently isolates extracellular vesicles from cell culture media for compositional and functional studies. *Sci. Rep.* 7, 1–13. doi:10.1038/s41598-017-15717-7.

Bewicke-Copley, F., Mulcahy, L. A., Jacobs, L. A., Samuel, P., Akbar, N., Pink, R. C., et al. (2017). Extracellular vesicles released following heat stress induce bystander effect in unstressed populations. *J. Extracell. Vesicles* 6, 1340746. doi:10.1080/20013078.2017.1340746.

Bianco, F., Perrotta, C., Novellino, L., Francolini, M., Riganti, L., Menna, E., et al. (2009). Acid sphingomyelinase activity triggers microparticle release from glial cells. *EMBO J.* 28, 1043–1054. doi:10.1038/emboj.2009.45.

Bier, E. (2005). Drosophila, the golden bug, emerges as a tool for human genetics. *Nat. Rev. Genet.* 6, 9–23. doi:10.1038/nrg1503.

Bland, C. L., Byrne-Hoffman, C. N., Fernandez, A., Rellick, S. L., Deng, W., and Klinke, D. J. (2018). Exosomes derived from B16F0 melanoma cells alter the transcriptome of cytotoxic T cells that impacts mitochondrial respiration. *FEBS J.* 285, 1033–1050. doi:10.1111/febs.14396.

Böing, A. N., van der Pol, E., Grootemaat, A. E., Coumans, F. A. W., Sturk, A., and Nieuwland, R. (2014). Single-step isolation of extracellular vesicles by size-exclusion chromatography. *J. Extracell. Vesicles* 3. doi:10.3402/jev.v3.23430.

Bolukbasi, M. F., Mizrak, A., Ozdener, G. B., Madlener, S., Ströbel, T., Erkan, E. P., et al. (2012). MiR-1289 and “zipcode”-like sequence enrich mRNAs in microvesicles. *Mol. Ther. - Nucleic Acids* 1, e10. doi:10.1038/mtna.2011.2.

Bonsergent, E., Grisard, E., Buchrieser, J., Schwartz, O., Théry, C., and Lavieu, G. (2021). Quantitative characterization of extracellular vesicle uptake and content delivery within mammalian cells. *Nat. Commun.* 12, 1864. doi:10.1038/s41467-021-22126-y.

Bouvrette, L. P. B., Cody, N. A. L., Bergalet, J., Lefebvre, F. A., Diot, C., Wang, X., et al. (2018). CeFra-seq reveals broad asymmetric mRNA and noncoding RNA distribution profiles in Drosophila and human cells. *Rna* 24, 98–113. doi:10.1261/rna.063172.117.

Brand, A. H., and Perrimon, N. (1993). Targeted gene expression as a means of altering cell fates and generating dominant phenotypes. *Development* 118, 401–415.

Bratkovič, T., Bozič, J., and Rogelj, B. (2020). Functional diversity of small nucleolar RNAs. *Nucleic Acids Res.* 48, 1627–1651. doi:10.1093/nar/gkz1140.

Brennan, K., Martin, K., FitzGerald, S. P., O’Sullivan, J., Wu, Y., Blanco, A., et al. (2020). A comparison of methods for the isolation and separation of extracellular vesicles from protein and lipid particles in human serum. *Sci. Rep.* 10, 1–13. doi:10.1038/s41598-020-57497-7.

Brister, J. R., Ako-Adjei, D., Bao, Y., and Blinkova, O. (2015). NCBI viral Genomes resource. *Nucleic Acids Res.* 43, D571–D577. doi:10.1093/nar/gku1207.

Brown, B. D., Gentner, B., Cantore, A., Colleoni, S., Amendola, M., Zingale, A., et al. (2007). Endogenous microRNA can be broadly exploited to regulate transgene expression

according to tissue, lineage and differentiation state. *Nat. Biotechnol.* 25, 1457–1467. doi:10.1038/nbt1372.

Buchan, J. R., Kolaitis, R. M., Taylor, J. P., and Parker, R. (2013). Eukaryotic stress granules are cleared by autophagy and Cdc48/VCP function. *Cell* 153, 1461. doi:10.1016/j.cell.2013.05.037.

Bushnell, B. BBtools. Available at: https://sourceforge.net/projects/bbmap/ [Accessed March 9, 2021].

Buzas, E. I., György, B., Nagy, G., Falus, A., and Gay, S. (2014). Emerging role of extracellular vesicles in inflammatory diseases. *Nat. Rev. Rheumatol.* 10, 356–364. doi:10.1038/nrrheum.2014.19.

Cambier, L., de Couto, G., Ibrahim, A., Echavez, A. K., Valle, J., Liu, W., et al. (2017). Y RNA fragment in extracellular vesicles confers cardioprotection via modulation of IL-10 expression and secretion. *EMBO Mol. Med.* 9, 337–352. doi:10.15252/emmm.201606924.

Camussi, G., Deregibus, M. C., Bruno, S., Cantaluppi, V., and Biancone, L. (2010). Exosomes/microvesicles as a mechanism of cell-to-cell communication. *Kidney Int.* 78, 838–848. doi:10.1038/ki.2010.278.

Carnino, J. M., Ni, K., and Jin, Y. (2020). Post-translational Modification Regulates Formation and Cargo-Loading of Extracellular Vesicles. *Front. Immunol.* 11, 948. doi:10.3389/fimmu.2020.00948.

Carollo, E., Paris, B., Samuel, P., Pantazi, P., Bartelli, T. F., Dias-Neto, E., et al. (2019). Detecting ovarian cancer using extracellular vesicles: Progress and possibilities. *Biochem. Soc. Trans.* 47, 295–304. doi:10.1042/BST20180286.

Caruso, S., and Poon, I. K. H. (2018). Apoptotic cell-derived extracellular vesicles: More than just debris. *Front. Immunol.* 9. doi:10.3389/fimmu.2018.01486.

Cha, D. J., Franklin, J. L., Dou, Y., Liu, Q., Higginbotham, J. N., Demory Beckler, M., et al. (2015). KRAS-dependent sorting of miRNA to exosomes. *Elife* 4. doi:10.7554/eLife.07197.

Chen, L., Wang, Y., Pan, Y., Zhang, L., Shen, C., Qin, G., et al. (2013). Cardiac progenitor-derived exosomes protect ischemic myocardium from acute ischemia/reperfusion injury. *Biochem. Biophys. Res. Commun.* 431, 566–571. doi:10.1016/j.bbrc.2013.01.015.

Chen, M., Xu, R., Ji, H., Greening, D. W., Rai, A., Izumikawa, K., et al. (2016). Transcriptome and long noncoding RNA sequencing of three extracellular vesicle subtypes released from the human colon cancer LIM1863 cell line. *Sci. Rep.* 6, 38397. doi:10.1038/srep38397.

Chen, X., Li, A., Sun, B. F., Yang, Y., Han, Y. N., Yuan, X., et al. (2019). 5-methylcytosine promotes pathogenesis of bladder cancer through stabilizing mRNAs. *Nat. Cell Biol.* 21, 978–990. doi:10.1038/s41556-019-0361-y.

Chen, X., Smith, J. D., Shi, H., Yang, D. D., Flavell, R. A., and Wolin, S. L. (2003). The Ro Autoantigen Binds Misfolded U2 Small Nuclear RNAs and Assists Mammalian Cell Survival after UV Irradiation. *Curr. Biol.* 13, 2206–2211. doi:10.1016/j.cub.2003.11.028.

Chen, Z., Sun, Y., Yang, X., Wu, Z., Guo, K., Niu, X., et al. (2017). Two featured series of rRNA-derived RNA fragments (rRFs) constitute a novel class of small RNAs. *PLoS One* 12,

e0176458. doi:10.1371/journal.pone.0176458.

Cherlin, T., Magee, R., Jing, Y., Pliatsika, V., Loher, P., and Rigoutsos, I. (2020). Ribosomal RNA fragmentation into short RNAs (rRFs) is modulated in a sex- and population of origin-specific manner. *BMC Biol.* 18, 38. doi:10.1186/s12915-020-0763-0.

Chinnadurai, M., Chidambaram, S., Ganesan, V., Baraneedharan, U., Sundaram, L., Paul, S. F. D., et al. (2011). Bleomycin, neocarzinostatin and ionising radiation-induced bystander effects in normal diploid human lung fibroblasts, bone marrow mesenchymal stem cells, lung adenocarcinoma cells and peripheral blood lymphocytes. *Int. J. Radiat. Biol.* 87, 673–682. doi:10.3109/09553002.2010.549536.

Chiou, N. T., Kageyama, R., and Ansel, K. M. (2018). Selective Export into Extracellular Vesicles and Function of tRNA Fragments during T Cell Activation. *Cell Rep.* 25, 3356-3370.e4. doi:10.1016/j.celrep.2018.11.073.

Choi, K. S., Mizutani, A., and Lai, M. M. C. (2004). SYNCRIP, a Member of the Heterogeneous Nuclear Ribonucleoprotein Family, Is Involved in Mouse Hepatitis Virus RNA Synthesis. *J. Virol.* 78, 13153–13162. doi:10.1128/jvi.78.23.13153-13162.2004.

Coleman, M. L., Sahai, E. A., Yeo, M., Bosch, M., Dewar, A., and Olson, M. F. (2001). Membrane blebbing during apoptosis results from caspase-mediated activation of ROCK I. *Nat. Cell Biol.* 3, 339–345. doi:10.1038/35070009.

Cooke, W. R., Cribbs, A., Zhang, W., Kandzija, N., Motta-Mejia, C., Dombi, E., et al. (2019). Maternal circulating syncytiotrophoblast-derived extracellular vesicles contain biologically active 5'-tRNA halves. *Biochem. Biophys. Res. Commun.* 518, 107–113. doi:10.1016/j.bbrc.2019.08.015.

Corrigan, L., Redhai, S., Leiblich, A., Fan, S. J., Perera, S. M. W., Patel, R., et al. (2014). BMP-regulated exosomes from Drosophila male reproductive glands reprogram female behavior. *J. Cell Biol.* 206, 671–688. doi:10.1083/jcb.201401072.

Crescitelli, R., Lässer, C., Szabó, T. G., Kittel, A., Eldh, M., Dianzani, I., et al. (2013). Distinct RNA profiles in subpopulations of extracellular vesicles: Apoptotic bodies, microvesicles and exosomes. *J. Extracell. Vesicles* 2, 20677. doi:10.3402/jev.v2i0.20677.

Da Silva, R. P., Puccia, R., Rodrigues, M. L., Oliveira, D. L., Joffe, L. S., César, G. V., et al. (2015). Extracellular vesicle-mediated export of fungal RNA. *Sci. Rep.* 5, 1–12. doi:10.1038/srep07763.

Das, A., Valkov, N., Salvador, A. M., Kur, I., Ziegler, O., Yeri, A., et al. (2019). Red blood cell-derived extracellular vesicles mediate intercellular communication in ischemic heart failure. *bioRxiv*, 624841. doi:10.1101/624841.

de Jong, O. G., Murphy, D. E., Mäger, I., Willms, E., Garcia-Guerra, A., Gitz-Francois, J. J., et al. (2020). A CRISPR-Cas9-based reporter system for single-cell detection of extracellular vesicle-mediated functional transfer of RNA. *Nat. Commun.* 11, 1113. doi:10.1038/s41467-020-14977-8.

de Jong, O. G., Verhaar, M. C., Chen, Y., Vader, P., Gremmels, H., Posthuma, G., et al. (2012). Cellular stress conditions are reflected in the protein and RNA content of endothelial cell-derived exosomes. *J. Extracell. Vesicles* 1, 18396. doi:10.3402/jev.v1i0.18396.

Del Conde, I., Shrimpton, C. N., Thiagarajan, P., and López, J. A. (2005). Tissue-factor-bearing microvesicles arise from lipid rafts and fuse with activated platelets to initiate coagulation. *Blood* 106, 1604–1611. doi:10.1182/blood-2004-03-1095.

Desdín-Micó, G., and Mittelbrunn, M. (2017). Role of exosomes in the protection of cellular homeostasis. *Cell Adh. Migr.* 11, 127–134. doi:10.1080/19336918.2016.1251000.

DeVeaux, L. C., Durtschi, L. S., Case, J. G., and Wells, D. P. (2006). Bystander effects in unicellular organisms. *Mutat. Res. - Fundam. Mol. Mech. Mutagen.* 597, 78–86. doi:10.1016/j.mrfmmm.2005.06.033.

Di Vizio, D., Kim, J., Hager, M. H., Morello, M., Yang, W., Lafargue, C. J., et al. (2009). Oncosome formation in prostate cancer: Association with a region of frequent chromosomal deletion in metastatic disease. *Cancer Res.* 69, 5601–5609. doi:10.1158/0008-5472.CAN-08-3860.

Di Vizio, D., Morello, M., Dudley, A. C., Schow, P. W., Adam, R. M., Morley, S., et al. (2012). Large oncosomes in human prostate cancer tissues and in the circulation of mice with metastatic disease. *Am. J. Pathol.* 181, 1573–1584. doi:10.1016/j.ajpath.2012.07.030.

Diebold, S. S., Kaisho, T., Hemmi, H., Akira, S., and Reis E Sousa, C. (2004). Innate Antiviral Responses by Means of TLR7-Mediated Recognition of Single-Stranded RNA. *Science (80-. ).* 303, 1529–1531. doi:10.1126/science.1093616.

Dobin, A., Davis, C. A., Schlesinger, F., Drenkow, J., Zaleski, C., Jha, S., et al. (2013). STAR: ultrafast universal RNA-seq aligner. *Bioinformatics* 29, 15–21. doi:10.1093/bioinformatics/bts635.

Driedonks, T. A. P., van der Grein, S. G., Ariyurek, Y., Buermans, H. P. J., Jekel, H., Chow, F. W. N., et al. (2018). Immune stimuli shape the small non-coding transcriptome of extracellular vesicles released by dendritic cells. *Cell. Mol. Life Sci.* 75, 3857–3875. doi:10.1007/s00018-018-2842-8.

Duarte Junior, F. F., Bueno, P. S. A., Pedersen, S. L., Rando, F. dos S., Pattaro Júnior, J. R., Caligari, D., et al. (2019). Identification and characterization of stem-bulge RNAs in Drosophila melanogaster. *RNA Biol.* 16, 330–339. doi:10.1080/15476286.2019.1572439.

Dutta, S., Warshall, C., Bandyopadhyay, C., Dutta, D., and Chandran, B. (2014). Interactions between Exosomes from Breast Cancer Cells and Primary Mammary Epithelial Cells Leads to Generation of Reactive Oxygen Species Which Induce DNA Damage Response, Stabilization of p53 and Autophagy in Epithelial Cells. *PLoS One* 9, e97580. doi:10.1371/journal.pone.0097580.

Eitan, E., Zhang, S., Witwer, K. W., and Mattson, M. P. (2015). Extracellular vesicle-depleted fetal bovine and human sera have reduced capacity to support cell growth. *J. Extracell. Vesicles* 4, 1–10. doi:10.3402/jev.v4.26373.

Ekström, K., Valadi, H., Sjöstrand, M., Malmhäll, C., Bossios, A., Eldh, M., et al. (2012). Characterization of mRNA and microRNA in human mast cell-derived exosomes and their transfer to other mast cells and blood CD34 progenitor cells. *J. Extracell. Vesicles* 1. doi:10.3402/jev.v1i0.18389.

Eldh, M., Ekström, K., Valadi, H., Sjöstrand, M., Olsson, B., Jernås, M., et al. (2010). Exosomes Communicate Protective Messages during Oxidative Stress; Possible Role of Exosomal Shuttle RNA. *PLoS One* 5, 1–8. doi:10.1371/journal.pone.0015353.

Emmanouilidou, E., Melachroinou, K., Roumeliotis, T., Garbis, S. D., Ntzouni, M., Margaritis, L. H., et al. (2010). Cell-produced α-synuclein is secreted in a calcium-dependent manner by exosomes and impacts neuronal survival. *J. Neurosci.* 30, 6838–6851. doi:10.1523/JNEUROSCI.5699-09.2010.

Enderle, D., Spiel, A., Coticchia, C. M., Berghoff, E., Mueller, R., Schlumpberger, M., et al. (2015). Characterization of RNA from Exosomes and Other Extracellular Vesicles Isolated by a Novel Spin Column-Based Method. *PLoS One* 10, e0136133. doi:10.1371/journal.pone.0136133.

Evdokimova, V., Ruzanov, P., Gassmann, H., Zaidi, S. H., Peltekova, V., Heisler, L. E., et al. (2019). Exosomes transmit retroelement RNAs to drive inflammation and immunosuppression in Ewing Sarcoma. *bioRxiv*. doi:10.1101/806851.

Fabbri, M., Paone, A., Calore, F., Galli, R., Gaudio, E., Santhanam, R., et al. (2012). MicroRNAs bind to Toll-like receptors to induce prometastatic inflammatory response. *Proc. Natl. Acad. Sci. U. S. A.* 109, E2110–E2116. doi:10.1073/pnas.1209414109.

Fan, S., Kroeger, B., Marie, P. P., Bridges, E. M., Mason, J. D., McCormick, K., et al. (2020). Glutamine deprivation alters the origin and function of cancer cell exosomes. *EMBO J.* 39. doi:10.15252/embj.2019103009.

Fan, X., Hussien, R., and Brooks, G. A. (2010). H2O2-induced mitochondrial fragmentation in C2C12 myocytes. *Free Radic. Biol. Med.* 49, 1646–1654. doi:10.1016/j.freeradbiomed.2010.08.024.

Fatica, A., and Bozzoni, I. (2014). Long non-coding RNAs: New players in cell differentiation and development. *Nat. Rev. Genet.* 15, 7–21. doi:10.1038/nrg3606.

Forterre, A. V., Wang, J. H., Delcayre, A., Kim, K., Green, C., Pegram, M. D., et al. (2020). Extracellular vesicle–mediated in vitro transcribed mRNA delivery for treatment of HER2þ breast cancer xenografts in mice by prodrug CB1954 without general toxicity. *Mol. Cancer Ther.* 19, 858–867. doi:10.1158/1535-7163.MCT-19-0928.

Frühbeis, C., Fröhlich, D., Kuo, W. P., Amphornrat, J., Thilemann, S., Saab, A. S., et al. (2013). Neurotransmitter-Triggered Transfer of Exosomes Mediates Oligodendrocyte-Neuron Communication. *PLoS Biol.* 11, e1001604. doi:10.1371/journal.pbio.1001604.

Fry, N. J., Law, B. A., Ilkayeva, O. R., Holley, C. L., and Mansfield, K. D. (2017). N6-methyladenosine is required for the hypoxic stabilization of specific mRNAs. *RNA* 23, 1444–1455. doi:10.1261/rna.061044.117.

Fuchs, G., Stein, A. J., Fu, C., Reinisch, K. M., and Wolin, S. L. (2006). Structural and biochemical basis for misfolded RNA recognition by the Ro autoantigen. *Nat. Struct. Mol. Biol.* 13, 1002–1009. doi:10.1038/nsmb1156.

Fujiwara, Y., Furuta, A., Kikuchi, H., Aizawa, S., Hatanaka, Y., Konya, C., et al. (2013). Discovery of a novel type of autophagy targeting RNA. *Autophagy* 9, 403–409. doi:10.4161/auto.23002.

Gámbaro, F., Li Calzi, M., Fagúndez, P., Costa, B., Greif, G., Mallick, E., et al. (2019). Stable tRNA halves can be sorted into extracellular vesicles and delivered to recipient cells in a concentration-dependent manner. *RNA Biol.*, 1–15. doi:10.1080/15476286.2019.1708548.

Gardiner, C., Vizio, D. Di, Sahoo, S., Théry, C., Witwer, K. W., Wauben, M., et al. (2016). Techniques used for the isolation and characterization of extracellular vesicles: Results of a worldwide survey. *J. Extracell. Vesicles* 5, 32945. doi:10.3402/jev.v5.32945.

Gezer, U., Özgür, E., Cetinkaya, M., Isin, M., and Dalay, N. (2014). Long non-coding RNAs with low expression levels in cells are enriched in secreted exosomes. *Cell Biol. Int.* 38, 1076–1079. doi:10.1002/cbin.10301.

Ghoshal, A., Rodrigues, L. C., Gowda, C. P., Elcheva, I. A., Liu, Z., Abraham, T., et al. (2019). Extracellular vesicle-dependent effect of RNA-binding protein IGF2BP1 on melanoma metastasis. *Oncogene* 38, 4182–4196. doi:10.1038/s41388-019-0797-3.

Gibbings, D. J., Ciaudo, C., Erhardt, M., and Voinnet, O. (2009). Multivesicular bodies associate with components of miRNA effector complexes and modulate miRNA activity. *Nat. Cell Biol.* 11, 1143–1149. doi:10.1038/ncb1929.

González-Méndez, L., Gradilla, A., Sánchez-Hernández, D., González, E., Aguirre-Tamaral, A., Jiménez-Jiménez, C., et al. (2020). Polarized sorting of Patched enables cytoneme-mediated Hedgehog reception in the Drosophila wing disc. *EMBO J.* doi:10.15252/embj.2019103629.

Goodenbour, J. M., and Pan, T. (2006). Diversity of tRNA genes in eukaryotes. *Nucleic Acids Res.* 34, 6137–6146. doi:10.1093/nar/gkl725.

Görgens, A., Bremer, M., Ferrer-Tur, R., Murke, F., Tertel, T., Horn, P. A., et al. (2019). Optimisation of imaging flow cytometry for the analysis of single extracellular vesicles by using fluorescence-tagged vesicles as biological reference material. *J. Extracell. Vesicles* 8. doi:10.1080/20013078.2019.1587567.

Gradilla, A. C., González, E., Seijo, I., Andrés, G., Bischoff, M., González-Mendez, L., et al. (2014). Exosomes as Hedgehog carriers in cytoneme-mediated transport and secretion. *Nat. Commun.* 5, 5649. doi:10.1038/ncomms6649.

Grant, B. D., and Donaldson, J. G. (2009). Pathways and mechanisms of endocytic recycling. *Nat. Rev. Mol. Cell Biol.* 10, 597–608. doi:10.1038/nrm2755.

Grant, C. E., Bailey, T. L., and Noble, W. S. (2011). FIMO: scanning for occurrences of a given motif. *Bioinformatics* 27, 1017–1018. doi:10.1093/bioinformatics/btr064.

Grimm, D., Streetz, K. L., Jopling, C. L., Storm, T. A., Pandey, K., Davis, C. R., et al. (2006). Fatality in mice due to oversaturation of cellular microRNA/short hairpin RNA pathways. *Nature* 441, 537–541. doi:10.1038/nature04791.

Gross, J. C., Chaudhary, V., Bartscherer, K., and Boutros, M. (2012). Active Wnt proteins are secreted on exosomes. *Nat. Cell Biol.* 14, 1036–1045. doi:10.1038/ncb2574.

Gu, D., Zou, X., Ju, G., Zhang, G., Bao, E., and Zhu, Y. (2016). Mesenchymal Stromal Cells Derived Extracellular Vesicles Ameliorate Acute Renal Ischemia Reperfusion Injury by Inhibition of Mitochondrial Fission through miR-30. *Stem Cells Int.* 2016, 1–12. doi:10.1155/2016/2093940.

Guarino, A. M., Troiano, A., Pizzo, E., Bosso, A., Vivo, M., Pinto, G., et al. (2018). Oxidative Stress Causes Enhanced Secretion of YB-1 Protein that Restrains Proliferation of Receiving Cells. *Genes (Basel).* 9, 513. doi:10.3390/genes9100513.

Guo, B. B., Bellingham, S. A., and Hill, A. F. (2015). The neutral sphingomyelinase pathway regulates packaging of the prion protein into exosomes. *J. Biol. Chem.* 290, 3455–3467. doi:10.1074/jbc.M114.605253.

Guo, H., Chitiprolu, M., Gagnon, D., Meng, L., Perez-Iratxeta, C., Lagace, D., et al. (2014). Autophagy supports genomic stability by degrading retrotransposon RNA. *Nat. Commun.* 5, 1–11. doi:10.1038/ncomms6276.

Guo, H., Chitiprolu, M., Roncevic, L., Javalet, C., Hemming, F. J., Trung, M. T., et al. (2017). Atg5 Disassociates the V1V0-ATPase to Promote Exosome Production and Tumor Metastasis Independent of Canonical Macroautophagy. *Dev. Cell* 43, 716-730.e7. doi:10.1016/j.devcel.2017.11.018.

Gupta, S., Stamatoyannopoulos, J. A., Bailey, T. L., and Noble, W. S. (2007). Quantifying similarity between motifs. *Genome Biol.* 8, R24. doi:10.1186/gb-2007-8-2-r24.

Hagiwara, K., Katsuda, T., Gailhouste, L., Kosaka, N., and Ochiya, T. (2015). Commitment of Annexin A2 in recruitment of microRNAs into extracellular vesicles. *FEBS Lett.* 589, 4071–4078. doi:10.1016/j.febslet.2015.11.036.

Haimovich, G., Ecker, C. M., Dunagin, M. C., Eggan, E., Raj, A., Gerst, J. E., et al. (2017). Intercellular mRNA trafficking via membrane nanotube-like extensions in mammalian cells. *Proc. Natl. Acad. Sci. U. S. A.* 114, E9873–E9882. doi:10.1073/pnas.1706365114.

Harding, C., Heuser, J., and Stahl, P. (1984). Endocytosis and intracellular processing of transferrin and colloidal gold-transferrin in rat reticulocytes: Demonstration of a pathway for receptor shedding. *Eur. J. Cell Biol.* 35, 256–263. Available at: https://europepmc.org/article/med/6151502 [Accessed April 14, 2021].

Hardy, M. P., Audemard, É., Migneault, F., Feghaly, A., Brochu, S., Gendron, P., et al. (2019). Apoptotic endothelial cells release small extracellular vesicles loaded with immunostimulatory viral-like RNAs. *Sci. Rep.* 9, 1–14. doi:10.1038/s41598-019-43591-y.

Hart, T., Komori, H. K., LaMere, S., Podshivalova, K., and Salomon, D. R. (2013). Finding the active genes in deep RNA-seq gene expression studies. *BMC Genomics* 14, 778. doi:10.1186/1471-2164-14-778.

Havaki, S., Kotsinas, A., Chronopoulos, E., Kletsas, D., Georgakilas, A., and Gorgoulis, V. G. (2015). The role of oxidative DNA damage in radiation induced bystander effect. *Cancer Lett.* 356, 43–51. doi:10.1016/j.canlet.2014.01.023.

Heath, N., Osteikoetxea, X., De Oliveria, T. M., Lázaro-Ibáñez, E., Shatnyeva, O., Schindler, C., et al. (2019). Endosomal escape enhancing compounds facilitate functional delivery of extracellular vesicle cargo. *Nanomedicine* 14, 2799–2814. doi:10.2217/nnm-2019-0061.

Hedlund, M., Nagaeva, O., Kargl, D., Baranov, V., and Mincheva-Nilsson, L. (2011). Thermal- and oxidative stress causes enhanced release of NKG2D ligand-bearing immunosuppressive exosomes in leukemia/lymphoma T and B cells. *PLoS One* 6, e16899. doi:10.1371/journal.pone.0016899.

Hei, T. K., Zhou, H., Ivanov, V. N., Hong, M., Lieberman, H. B., Brenner, D. J., et al. (2008). Mechanism of radiation-induced bystander effects: a unifying model. *J. Pharm. Pharmacol.* 60, 943–950. doi:10.1211/jpp.60.8.0001.

Helm, K., Beyreis, M., Mayr, C., Ritter, M., Jakab, M., Kiesslich, T., et al. (2017). In Vitro Cell Death Discrimination and Screening Method by Simple and Cost-Effective Viability Analysis. *Cell. Physiol. Biochem.* 41, 1011–1019. doi:10.1159/000460910.

Heusermann, W., Hean, J., Trojer, D., Steib, E., von Bueren, S., Graff-Meyer, A., et al. (2016). Exosomes surf on filopodia to enter cells at endocytic hot spots, traffic within endosomes, and are targeted to the ER. *J. Cell Biol.* 213, 173–184. doi:10.1083/jcb.201506084.

Hewson, C., Capraro, D., Burdach, J., Whitaker, N., and Morris, K. V. (2016). Extracellular vesicle associated long non-coding RNAs functionally enhance cell viability. *Non-coding RNA Res.* 1, 3–11. doi:10.1016/j.ncrna.2016.06.001.

Hinger, S. A., Cha, D. J., Franklin, J. L., Higginbotham, J. N., Dou, Y., Ping, J., et al. (2018). Diverse Long RNAs Are Differentially Sorted into Extracellular Vesicles Secreted by Colorectal Cancer Cells. *Cell Rep.* 25, 715-725.e4. doi:10.1016/j.celrep.2018.09.054.

Hoen, E. N., Cremer, T., Gallo, R. C., and Margolis, L. B. (2016). Extracellular vesicles and viruses: Are they close relatives? *Proc. Natl. Acad. Sci. U. S. A.* 113, 9155–9161. doi:10.1073/pnas.1605146113.

Holley, C. L., Li, M. W., Scruggs, B. S., Matkovich, S. J., Ory, D. S., and Schaffer, J. E. (2015). Cytosolic accumulation of small nucleolar RNAs (snoRNAs) is dynamically regulated by NADPH oxidase. *J. Biol. Chem.* 290, 11741–11748. doi:10.1074/jbc.M115.637413.

Holm, M. M., Kaiser, J., and Schwab, M. E. (2018). Extracellular Vesicles: Multimodal Envoys in Neural Maintenance and Repair. *Trends Neurosci.* 41, 360–372. doi:10.1016/j.tins.2018.03.006.

Hoshino, A., Costa-Silva, B., Shen, T. L., Rodrigues, G., Hashimoto, A., Tesic Mark, M., et al. (2015). Tumour exosome integrins determine organotropic metastasis. *Nature* 527, 329–335. doi:10.1038/nature15756.

Hoshino, A., Kim, H. S., Bojmar, L., Gyan, K. E., Cioffi, M., Hernandez, J., et al. (2020). Extracellular Vesicle and Particle Biomarkers Define Multiple Human Cancers. *Cell* 182, 1044-1061.e18. doi:10.1016/j.cell.2020.07.009.

Hu, Y., Flockhart, I., Vinayagam, A., Bergwitz, C., Berger, B., Perrimon, N., et al. (2011). An integrative approach to ortholog prediction for disease-focused and other functional studies. *BMC Bioinformatics* 12. doi:10.1186/1471-2105-12-357.

Hu, Y., Sopko, R., Foos, M., Kelley, C., Flockhart, I., Ammeux, N., et al. (2013). FlyPrimerBank: An Online Database for Drosophila melanogaster Gene Expression Analysis and Knockdown Evaluation of RNAi Reagents. doi:10.1534/g3.113.007021.

Huang, Y., Lu, K., Chao, H., Chen, A., Chao, T., Guo, C., et al. (2021). The MTNR1A mRNA is stabilized by the cytoplasmic hnRNPL in renal tubular cells. *J. Cell. Physiol.* 236, 2023–2035. doi:10.1002/jcp.29988.

Huber, V., Fais, S., Iero, M., Lugini, L., Canese, P., Squarcina, P., et al. (2005). Human colorectal cancer cells induce T-cell death through release of proapoptotic microvesicles: Role in immune escape. *Gastroenterology* 128, 1796–1804. doi:10.1053/j.gastro.2005.03.045.

Hung, M. E., and Leonard, J. N. (2016). A platform for actively loading cargo RNA to elucidate limiting steps in EV-mediated delivery. *J. Extracell. Vesicles* 5. doi:10.3402/jev.v5.31027.

Huo, Y., Shen, J., Wu, H., Zhang, C., Guo, L., Yang, J., et al. (2016). Widespread 3'-end uridylation in eukaryotic RNA viruses. *Sci. Rep.* 6, 1–9. doi:10.1038/srep25454.

Hyenne, V., Ghoroghi, S., Collot, M., Bons, J., Follain, G., Harlepp, S., et al. (2019). Studying the Fate of Tumor Extracellular Vesicles at High Spatiotemporal Resolution Using the Zebrafish Embryo. *Dev. Cell* 48, 554-572.e7. doi:10.1016/j.devcel.2019.01.014.

Iavello, A., Frech, V. S. L., Gai, C., Deregibus, M. C., Quesenberry, P. J., and Camussi, G. (2016). Role of Alix in miRNA packaging during extracellular vesicle biogenesis. *Int. J. Mol. Med.* 37, 958–966. doi:10.3892/ijmm.2016.2488.

Ischiropoulos, H., and Beckman, J. S. (2003). Oxidative stress and nitration in neurodegeneration: Cause, effect, or association? *J. Clin. Invest.* 111, 163–169. doi:10.1172/JCI200317638.

Janas, T., Janas, M. M., Sapoń, K., and Janas, T. (2015). Mechanisms of RNA loading into exosomes. *FEBS Lett.* 589, 1391–1398. doi:10.1016/j.febslet.2015.04.036.

Janas, T., Janas, P., Sapoń, K., and Janas, T. (2020). Binding of RNA Aptamers to Membrane Lipid Rafts: Implications for Exosomal miRNAs Transfer from Cancer to Immune Cells. *Int. J. Mol. Sci.* 21, 8503. doi:10.3390/ijms21228503.

Janas, T., Janas, T., and Yarus, M. (2006). Specific RNA binding to ordered phospholipid bilayers. *Nucleic Acids Res.* 34, 2128–2136. doi:10.1093/nar/gkl220.

Janas, T., Janas, T., and Yarus, M. (2012). Human tRNASec associates with HeLa membranes, cell lipid liposomes, and synthetic lipid bilayers. *RNA* 18, 2260–2268. doi:10.1261/rna.035352.112.

Jenjaroenpun, P., Kremenska, Y., Nair, V. M., Kremenskoy, M., Joseph, B., and Kurochkin, I. V. (2013). Characterization of RNA in exosomes secreted by human breast cancer cell lines using next-generation sequencing. *PeerJ* 1, e201. doi:10.7717/peerj.201.

Jeong, W. K., Wieckowski, E., Taylor, D. D., Reichert, T. E., Watkins, S., and Whiteside, T. L. (2005). Fas ligand-positive membranous vesicles isolated from sera of patients with oral cancer induce apoptosis of activated T lymphocytes. *Clin. Cancer Res.* 11, 1010–1020.

Jeppesen, D. K., Hvam, M. L., Primdahl-Bengtson, B., Boysen, A. T., Whitehead, B., Dyrskjøt, L., et al. (2014). Comparative analysis of discrete exosome fractions obtained by differential centrifugation. *J. Extracell. Vesicles* 3, 25011. doi:10.3402/jev.v3.25011.

Jeyaram, A., and Jay, S. M. (2018). Preservation and Storage Stability of Extracellular Vesicles for Therapeutic Applications. *AAPS J.* 20. doi:10.1208/s12248-017-0160-y.

Joshi, B. S., de Beer, M. A., Giepmans, B. N. G., and Zuhorn, I. S. (2020). Endocytosis of Extracellular Vesicles and Release of Their Cargo from Endosomes. *ACS Nano* 14, 4444–4455. doi:10.1021/acsnano.9b10033.

Jovel, J., and Schneemann, A. (2011). Molecular characterization of Drosophila cells persistently infected with Flock House virus. *Virology* 419, 43–53. doi:10.1016/j.virol.2011.08.002.

Kanada, M., Bachmann, M. H., Hardy, J. W., Frimannson, D. O., Bronsart, L., Wang, A., et al. (2015). Differential fates of biomolecules delivered to target cells via extracellular vesicles. *Proc. Natl. Acad. Sci. U. S. A.* 112, E1433–E1442. doi:10.1073/pnas.1418401112.

Karikó, K., Ni, H., Capodici, J., Lamphier, M., and Weissman, D. (2004). mRNA Is an Endogenous Ligand for Toll-like Receptor 3. *J. Biol. Chem.* 279, 12542–12550. doi:10.1074/jbc.M310175200.

Karolchik, D., Hinricks, A. S., Furey, T. S., Roskin, K. M., Sugnet, C. W., Haussler, D., et al. (2004). The UCSC table browser data retrieval tool. *Nucleic Acids Res.* 32. doi:10.1093/nar/gkh103.

Kawaguchi, A., Matsumoto, K., and Nagata, K. (2012). YB-1 Functions as a Porter To Lead Influenza Virus Ribonucleoprotein Complexes to Microtubules. *J. Virol.* 86, 11086–11095. doi:10.1128/jvi.00453-12.

Kawamura, Y., Sanchez Calle, A., Yamamoto, Y., Sato, T.-A., and Ochiya, T. (2019). Extracellular vesicles mediate the horizontal transfer of an active LINE-1 retrotransposon. *J. Extracell. Vesicles* 8. doi:10.1080/20013078.2019.1643214.

Kestens, V., Bozatzidis, V., De Temmerman, P. J., Ramaye, Y., and Roebben, G. (2017). Validation of a particle tracking analysis method for the size determination of nano- and microparticles. *J. Nanoparticle Res.* 19, 1–16. doi:10.1007/s11051-017-3966-8.

Khong, A., Matheny, T., Jain, S., Mitchell, S. F., Wheeler, J. R., and Parker, R. (2017). The Stress Granule Transcriptome Reveals Principles of mRNA Accumulation in Stress Granules. *Mol. Cell* 68, 808-820.e5. doi:10.1016/j.molcel.2017.10.015.

Kim, D., Langmead, B., and Salzberg, S. L. (2015). HISAT: A fast spliced aligner with low memory requirements. *Nat. Methods* 12, 357–360. doi:10.1038/nmeth.3317.

King, H. W., Michael, M. Z., and Gleadle, J. M. (2012). Hypoxic enhancement of exosome release by breast cancer cells. *BMC Cancer* 12, 421. doi:10.1186/1471-2407-12-421.

Kocabas, A., Duarte, T., Kumar, S., and Hynes, M. A. (2015). Widespread Differential Expression of Coding Region and 3' UTR Sequences in Neurons and Other Tissues. *Neuron* 88, 1149–1156. doi:10.1016/j.neuron.2015.10.048.

Kogure, T., Yan, I. K., Lin, W. L., and Patel, T. (2013). Extracellular Vesicle-Mediated Transfer of a Novel Long Noncoding RNA TUC339: A Mechanism of Intercellular Signaling in Human Hepatocellular Cancer. *Genes and Cancer* 4, 261–272. doi:10.1177/1947601913499020.

Koles, K., Nunnari, J., Korkut, C., Barria, R., Brewer, C., Li, Y., et al. (2012). Mechanism of evenness interrupted (Evi)-exosome release at synaptic boutons. *J. Biol. Chem.* 287, 16820–16834. doi:10.1074/jbc.M112.342667.

Koppen, T., Weckmann, A., Müller, S., Staubach, S., Bloch, W., Dohmen, R. J., et al. (2011). Proteomics analyses of microvesicles released by Drosophila Kc167 and S2 cells. *Proteomics* 11, 4397–4410. doi:10.1002/pmic.201000774.

Koppers-Lalic, D., Hackenberg, M., Bijnsdorp, I. V., van Eijndhoven, M. A. J., Sadek, P., Sie, D., et al. (2014). Nontemplated Nucleotide Additions Distinguish the Small RNA Composition in Cells from Exosomes. *Cell Rep.* 8, 1649–1658. doi:10.1016/j.celrep.2014.08.027.

Kore, R. A., Edmondson, J. L., Jenkins, S. V, Jamshidi-Parsian, A., Dings, R. P. M., Reyna, N. S., et al. (2018). Hypoxia-derived exosomes induce putative altered pathways in biosynthesis and ion regulatory channels in glioblastoma cells. *Biochem. Biophys. reports* 14, 104–113. doi:10.1016/j.bbrep.2018.03.008.

Korkut, C., Ataman, B., Ramachandran, P., Ashley, J., Barria, R., Gherbesi, N., et al. (2009). Trans-synaptic transmission of vesicular Wnt signals through Evi/Wntless. *Cell* 139, 393–404. doi:10.1016/j.cell.2009.07.051.

Korkut, C., Li, Y., Koles, K., Brewer, C., Ashley, J., Yoshihara, M., et al. (2013). Regulation of postsynaptic retrograde signaling by presynaptic exosome release. *Neuron* 77, 1039–46. doi:10.1016/j.neuron.2013.01.013.

Kossinova, O. A., Gopanenko, A. V., Tamkovich, S. N., Krasheninina, O. A., Tupikin, A. E., Kiseleva, E., et al. (2017). Cytosolic YB-1 and NSUN2 are the only proteins recognizing specific motifs present in mRNAs enriched in exosomes. *Biochim. Biophys. Acta - Proteins Proteomics* 1865, 664–673. doi:10.1016/j.bbapap.2017.03.010.

Kucharzewska, P., and Belting, M. (2013). Emerging roles of extracellular vesicles in the adaptive response of tumour cells to microenvironmental stress. *J. Extracell. Vesicles* 2. doi:10.3402/jev.v2i0.20304.

Kucharzewska, P., Christianson, H. C., Welch, J. E., Svensson, K. J., Fredlund, E., Ringnér, M., et al. (2013). Exosomes reflect the hypoxic status of glioma cells and mediate hypoxia-dependent activation of vascular cells during tumor development. *Proc. Natl. Acad. Sci. U. S. A.* 110, 7312–7317. doi:10.1073/pnas.1220998110.

Kulp, A., and Kuehn, M. J. (2010). Biological Functions and biogenesis of secreted bacterial outer membrane vesicles. *Annu. Rev. Microbiol.* 64, 163–184. doi:10.1146/annurev.micro.091208.073413.

Kumar Jella, K., Rani, S., O'Driscoll, L., McClean, B., Byrne, H. J., and Lyng, F. M. (2014). Exosomes Are Involved in Mediating Radiation Induced Bystander Signaling in Human Keratinocyte Cells. *Radiat. Res.* 181, 138–145. doi:10.1037//0022-3514.81.6.1001.

Lai, C. P., Kim, E. Y., Badr, C. E., Weissleder, R., Mempel, T. R., Tannous, B. A., et al. (2015). Visualization and tracking of tumour extracellular vesicle delivery and RNA translation using multiplexed reporters. *Nat. Commun.* 6, 1–12. doi:10.1038/ncomms8029.

Langmead, B., and Salzberg, S. L. (2012). Fast gapped-read alignment with Bowtie 2. *Nat. Methods* 9, 357–359. doi:10.1038/nmeth.1923.

Larkin, A., Marygold, S. J., Antonazzo, G., Attrill, H., dos Santos, G., Garapati, P. V., et al. (2021). FlyBase: Updates to the Drosophila melanogaster knowledge base. *Nucleic Acids Res.* 49, D899–D907. doi:10.1093/nar/gkaa1026.

Lässer, C., Seyed Alikhani, V., Ekström, K., Eldh, M., Torregrosa Paredes, P., Bossios, A., et al. (2011). Human saliva, plasma and breast milk exosomes contain RNA: Uptake by macrophages. *J. Transl. Med.* 9, 9. doi:10.1186/1479-5876-9-9.

Lässer, C., Shelke, G. V., Yeri, A., Kim, D. K., Crescitelli, R., Raimondo, S., et al. (2017). Two distinct extracellular RNA signatures released by a single cell type identified by microarray and next-generation sequencing. *RNA Biol.* 14, 58–72. doi:10.1080/15476286.2016.1249092.

Lee, D. H., Lim, M. H., Youn, D. Y., Jung, S. E., Ahn, Y. S., Tsujimoto, Y., et al. (2009a). hnRNP L binds to CA repeats in the 3'UTR of bcl-2 mRNA. *Biochem. Biophys. Res. Commun.* 382, 583–587. doi:10.1016/j.bbrc.2009.03.069.

Lee, H. C., Chang, S. S., Choudhary, S., Aalto, A. P., Maiti, M., Bamford, D. H., et al. (2009b). QiRNA

is a new type of small interfering RNA induced by DNA damage. *Nature* 459, 274–277. doi:10.1038/nature08041.

Lee, H., Li, C., Zhang, Y., Zhang, D., Otterbein, L. E., and Jin, Y. (2019). Caveolin-1 selectively regulates microRNA sorting into microvesicles after noxious stimuli. *J. Exp. Med.* 216, 2202–2220. doi:10.1084/jem.20182313.

Lee, J., Harris, A. N., Holley, C. L., Mahadevan, J., Pyles, K. D., Lavagnino, Z., et al. (2016). Rpl13a small nucleolar RNAs regulate systemic glucose metabolism. *J. Clin. Invest.* 126, 4616–4625. doi:10.1172/JCI88069.

Lefebvre, F. A., Benoit Bouvrette, L. P., Perras, L., Blanchet-Cohen, A., Garnier, D., Rak, J., et al. (2016). Comparative transcriptomic analysis of human and Drosophila extracellular vesicles. *Sci. Rep.* 6, 27680. doi:10.1038/srep27680.

Leidal, A. M., and Debnath, J. (2020). Unraveling the mechanisms that specify molecules for secretion in extracellular vesicles. *Methods* 177, 15–26. doi:10.1016/j.ymeth.2020.01.008.

Leidal, A. M., Huang, H. H., Marsh, T., Solvik, T., Zhang, D., Ye, J., et al. (2020). The LC3-conjugation machinery specifies the loading of RNA-binding proteins into extracellular vesicles. *Nat. Cell Biol.* 22, 187–199. doi:10.1038/s41556-019-0450-y.

Li, C. C. Y., Eaton, S. A., Young, P. E., Lee, M., Shuttleworth, R., Humphreys, D. T., et al. (2013). Glioma microvesicles carry selectively packaged coding and noncoding RNAs which alter gene expression in recipient cells. *RNA Biol.* 10, 1333–1344. doi:10.4161/rna.25281.

Li, J., Lee, Y., Johansson, H. J., Mäger, I., Vader, P., Nordin, J. Z., et al. (2015). Serum-free culture alters the quantity and protein composition of neuroblastoma-derived extracellular vesicles. *J. Extracell. Vesicles* 4, 1–12. doi:10.3402/jev.v4.26883.

Li, Y., Masaki, T., Shimakami, T., and Lemon, S. M. (2014). hnRNP L and NF90 Interact with Hepatitis C Virus 5'-Terminal Untranslated RNA and Promote Efficient Replication. *J. Virol.* 88, 7199–7209. doi:10.1128/jvi.00225-14.

Li, Z., Yang, J., and Huang, H. (2006). Oxidative stress induces H2AX phosphorylation in human spermatozoa. *FEBS Lett.* 580, 6161–6168. doi:10.1016/j.febslet.2006.10.016.

Liao, Y., Smyth, G. K., and Shi, W. (2014). featureCounts: an efficient general purpose program for assigning sequence reads to genomic features. *Bioinformatics* 30, 923–930. doi:10.1093/bioinformatics/btt656.

Liégeois, S., Benedetto, A., Garnier, J. M., Schwab, Y., and Labouesse, M. (2006). The V0-ATPase mediates apical secretion of exosomes containing Hedgehog-related proteins in Caenorhabditis elegans. *J. Cell Biol.* 173, 949–961. doi:10.1083/jcb.200511072.

Linares, R., Tan, S., Gounou, C., Arraud, N., and Brisson, A. R. (2015). High-speed centrifugation induces aggregation of extracellular vesicles. *J. Extracell. Vesicles* 4, 29509. doi:10.3402/jev.v4.29509.

Ling, D., and Salvaterra, P. M. (2011). Robust RT-qPCR data normalization: Validation and selection of internal reference genes during post-experimental data analysis. *PLoS One* 6, e17762. doi:10.1371/journal.pone.0017762.

Little, J. B. (1971). Repair of Potentially-lethal Radiation Damage in Mammalian Cells:

Enhancement by Conditioned Medium from Stationary Cultures. *Int. J. Radiat. Biol. Relat. Stud. Physics, Chem. Med.* 20, 87–92. doi:10.1080/09553007114550921.

Liu, H. M., Aizaki, H., Choi, K. S., Machida, K., Ou, J. J. H., and Lai, M. M. C. (2009). SYNCRIP (synaptotagmin-binding, cytoplasmic RNA-interacting protein) is a host factor involved in hepatitis C virus RNA replication. *Virology* 386, 249–256. doi:10.1016/j.virol.2009.01.018.

Liu, X., Fu, R., Pan, Y., Meza-Sosa, K. F., Zhang, Z., and Lieberman, J. (2018). PNPT1 Release from Mitochondria during Apoptosis Triggers Decay of Poly(A) RNAs. *Cell* 174, 187-201.e12. doi:10.1016/j.cell.2018.04.017.

Lobb, R. J., Becker, M., Wen, S. W., Wong, C. S. F., Wiegmans, A. P., Leimgruber, A., et al. (2015). Optimized exosome isolation protocol for cell culture supernatant and human plasma. *J. Extracell. Vesicles* 4, 27031. doi:10.3402/jev.v4.27031.

Loboda, A., Damulewicz, M., Pyza, E., Jozkowicz, A., and Dulak, J. (2016). Role of Nrf2/HO-1 system in development, oxidative stress response and diseases: an evolutionarily conserved mechanism. *Cell. Mol. Life Sci.* 73, 3221–3247. doi:10.1007/s00018-016-2223-0.

Lorincz, Á. M., Timár, C. I., Marosvári, K. A., Veres, D. S., Otrokocsi, L., Kittel, Á., et al. (2014). Effect of storage on physical and functional properties of extracellular vesicles derived from neutrophilic granulocytes. *J. Extracell. Vesicles* 3. doi:10.3402/jev.v3.25465.

Love, M. I., Huber, W., and Anders, S. (2014). Moderated estimation of fold change and dispersion for RNA-seq data with DESeq2. *Genome Biol.* 15, 550. doi:10.1186/s13059-014-0550-8.

Lu, P., Li, H., Li, N., Singh, R. N., Bishop, C. E., Chen, X., et al. (2017). MEX3C interacts with adaptor-related protein complex 2 and involves in miR-451a exosomal sorting. *PLoS One* 12, e0185992. doi:10.1371/journal.pone.0185992.

Ma, X., Wang, J., Li, J., Ma, C., Chen, S., Lei, W., et al. (2018). Loading MiR-210 in Endothelial Progenitor Cells Derived Exosomes Boosts Their Beneficial Effects on Hypoxia/Reoxygeneation-Injured Human Endothelial Cells via Protecting Mitochondrial Function. *Cell. Physiol. Biochem.* 46, 664–675. doi:10.1159/000488635.

Madamanchi, N. R., Vendrov, A., and Runge, M. S. (2005). Oxidative stress and vascular disease. *Arterioscler. Thromb. Vasc. Biol.* 25, 29–38. doi:10.1161/01.ATV.0000150649.39934.13.

Madigan, J. P. (2002). DNA double-strand break-induced phosphorylation of Drosophila histone variant H2Av helps prevent radiation-induced apoptosis. *Nucleic Acids Res.* 30, 3698–3705. doi:10.1093/nar/gkf496.

Margolis, L., and Sadovsky, Y. (2019). The biology of extracellular vesicles: The known unknowns. *PLOS Biol.* 17, e3000363. doi:10.1371/journal.pbio.3000363.

Markmiller, S., Soltanieh, S., Server, K. L., Mak, R., Jin, W., Fang, M. Y., et al. (2018). Context-Dependent and Disease-Specific Diversity in Protein Interactions within Stress Granules. *Cell* 172, 590-604.e13. doi:10.1016/j.cell.2017.12.032.

Matera, A. G., Terns, R. M., and Terns, M. P. (2007). Non-coding RNAs: Lessons from the small nuclear and small nucleolar RNAs. *Nat. Rev. Mol. Cell Biol.* 8, 209–220. doi:10.1038/nrm2124.

Matheny, T., Rao, B. S., and Parker, R. (2019). Transcriptome-Wide Comparison of Stress Granules and P-Bodies Reveals that Translation Plays a Major Role in RNA Partitioning. *Mol. Cell. Biol.* 39. doi:10.1128/MCB.00313-19.

Mathieu, M., Martin-Jaular, L., Lavieu, G., and Théry, C. (2019). Specificities of secretion and uptake of exosomes and other extracellular vesicles for cell-to-cell communication. *Nat. Cell Biol.* 21, 9–17. doi:10.1038/s41556-018-0250-9.

Matsuno, Y., Kanke, T., Maruyama, N., Fujii, W., Naito, K., and Sugiura, K. (2019). Characterization of mRNA profiles of the exosome-like vesicles in porcine follicular fluid. *PLoS One* 14, e0217760–e0217760. doi:10.1371/journal.pone.0217760.

Matusek, T., Wendler, F., Polès, S., Pizette, S., D'Angelo, G., Fürthauer, M., et al. (2014). The ESCRT machinery regulates the secretion and long-range activity of Hedgehog. *Nature* 516, 99–103. doi:10.1038/nature13847.

McKenzie, A. J., Hoshino, D., Hong, N. H., Cha, D. J., Franklin, J. L., Coffey, R. J., et al. (2016). KRAS-MEK Signaling Controls Ago2 Sorting into Exosomes. *Cell Rep.* 15, 978–987. doi:10.1016/j.celrep.2016.03.085.

Mercer, T. R., Wilhelm, D., Dinger, M. E., Soldà, G., Korbie, D. J., Glazov, E. A., et al. (2011). Expression of distinct RNAs from 3' untranslated regions. *Nucleic Acids Res.* 39, 2393–2403. doi:10.1093/nar/gkq1158.

Minciacchi, V. R., Freeman, M. R., and Di Vizio, D. (2015). Extracellular vesicles in cancer: exosomes, microvesicles and the emerging role of large oncosomes. *Semin. Cell Dev. Biol.* 40, 41–51. doi:10.1016/j.semcdb.2015.02.010.

Mittelbrunn, M., Gutiérrez-Vázquez, C., Villarroya-Beltri, C., González, S., Sánchez-Cabo, F., González, M. Á., et al. (2011). Unidirectional transfer of microRNA-loaded exosomes from T cells to antigen-presenting cells. *Nat. Commun.* 2. doi:10.1038/ncomms1285.

Mol, E. A., Goumans, M. J., Doevendans, P. A., Sluijter, J. P. G., and Vader, P. (2017). Higher functionality of extracellular vesicles isolated using size-exclusion chromatography compared to ultracentrifugation. *Nanomedicine Nanotechnology, Biol. Med.* 13, 2061–2065. doi:10.1016/j.nano.2017.03.011.

Montecalvo, A., Larregina, A. T., Shufesky, W. J., Stolz, D. B., Sullivan, M. L. G., Karlsson, J. M., et al. (2012). Mechanism of transfer of functional microRNAs between mouse dendritic cells via exosomes. *Blood* 119, 756–766. doi:10.1182/blood-2011-02-338004.

Morishita, M., Takahashi, Y., Nishikawa, M., Sano, K., Kato, K., Yamashita, T., et al. (2015). Quantitative analysis of tissue distribution of the B16BL6-derived exosomes using a streptavidin-lactadherin fusion protein and Iodine-125-Labeled biotin derivative after intravenous injection in mice. *J. Pharm. Sci.* 104, 705–713. doi:10.1002/jps.24251.

Moroishi, T., Hayashi, T., Pan, W. W., Fujita, Y., Holt, M. V., Qin, J., et al. (2016). The Hippo Pathway Kinases LATS1/2 Suppress Cancer Immunity. *Cell* 167, 1525-1539.e17. doi:10.1016/j.cell.2016.11.005.

Mothersill, C., and Seymour, C. (1997). Medium from irradiated human epithelial cells but not human fibroblasts reduces the clonogenic survival of unirradiated cells. *Int. J. Radiat. Biol.* 71, 421–427. doi:10.1080/095530097144030.

Mukherjee, K., Ghoshal, B., Ghosh, S., Chakrabarty, Y., Shwetha, S., Das, S., et al. (2016). Reversible HuR-micro RNA binding controls extracellular export of miR-122 and augments stress response. *EMBO Rep.* 17, 1184–1203. doi:10.15252/embr.201541930.

Mulcahy, L. A., Pink, R. C., and Carter, D. R. F. (2014). Routes and mechanisms of extracellular vesicle uptake. *J. Extracell. Vesicles* 3, 24641. doi:10.3402/jev.v3.24641.

Muralidharan-Chari, V., Clancy, J., Plou, C., Romao, M., Chavrier, P., Raposo, G., et al. (2009). ARF6-Regulated Shedding of Tumor Cell-Derived Plasma Membrane Microvesicles. *Curr. Biol.* 19, 1875–1885. doi:10.1016/j.cub.2009.09.059.

Murrow, L., Malhotra, R., and Debnath, J. (2015). ATG12-ATG3 interacts with Alix to promote basal autophagic flux and late endosome function. *Nat. Cell Biol.* 17, 300–310. doi:10.1038/ncb3112.

Mutschelknaus, L., Peters, C., Winkler, K., Yentrapalli, R., Heider, T., Atkinson, M. J., et al. (2016). Exosomes derived from squamous head and neck cancer promote cell survival after ionizing radiation. *PLoS One* 11, e0152213. doi:10.1371/journal.pone.0152213.

Nabet, B. Y., Qiu, Y., Shabason, J. E., Wu, T. J., Yoon, T., Kim, B. C., et al. (2017). Exosome RNA Unshielding Couples Stromal Activation to Pattern Recognition Receptor Signaling in Cancer. *Cell* 170, 352-366.e13. doi:10.1016/j.cell.2017.06.031.

Nabhan, J. F., Hu, R., Oh, R. S., Cohen, S. N., and Lu, Q. (2012). Formation and release of arrestin domain-containing protein 1-mediated microvesicles (ARMMs) at plasma membrane by recruitment of TSG101 protein. *Proc. Natl. Acad. Sci. U. S. A.* 109, 4146–4151. doi:10.1073/pnas.1200448109.

Nagasawa, S., and Little, J. B. (1992). Induction of Sister Chromatid Exchanges by Extremely Low Doses of α-particles. *Cancer Res.* 52, 6394–6396. Available at: http://www.ncbi.nlm.nih.gov/pubmed/1423287 [Accessed March 10, 2017].

NGUYEN, J., and FERGUSON, S. (2018). Compositions and methods for loading extracellular vesicles with chemical and biological agents/molecules cross reference to related applications.

Nolte-'t Hoen, E. N. M., Buermans, H. P. J., Waasdorp, M., Stoorvogel, W., Wauben, M. H. M., 't Hoen, P. A. C., et al. (2012). Deep sequencing of RNA from immune cell-derived vesicles uncovers the selective incorporation of small non-coding RNA biotypes with potential regulatory functions. *Nucleic Acids Res.* 40, 9272–9285. doi:10.1093/nar/gks658.

Nordin, J. Z., Lee, Y., Vader, P., Mäger, I., Johansson, H. J., Heusermann, W., et al. (2015). Ultrafiltration with size-exclusion liquid chromatography for high yield isolation of extracellular vesicles preserving intact biophysical and functional properties. *Nanomedicine Nanotechnology, Biol. Med.* 11, 879–883. doi:10.1016/j.nano.2015.01.003.

O'Brien, K., Breyne, K., Ughetto, S., Laurent, L. C., and Breakefield, X. O. (2020). RNA delivery by extracellular vesicles in mammalian cells and its applications. *Nat. Rev. Mol. Cell Biol.*, 1–22. doi:10.1038/s41580-020-0251-y.

Oliveira, D. L., Nakayasu, E. S., Joffe, L. S., Guimarães, A. J., Sobreira, T. J. P., Nosanchuk, J. D., et al. (2010). Characterization of Yeast Extracellular Vesicles: Evidence for the Participation of Different Pathways of Cellular Traffic in Vesicle Biogenesis. *PLoS One* 5, e11113. doi:10.1371/journal.pone.0011113.

Onafuwa-Nuga, A. A., King, S. R., and Telesnitsky, A. (2005). Nonrandom Packaging of Host RNAs in Moloney Murine Leukemia Virus. *J. Virol.* 79, 13528–13537. doi:10.1128/jvi.79.21.13528-13537.2005.

Onafuwa-Nuga, A. A., Telesnitsky, A., and King, S. R. (2006). 7SL RNA, but not the 54-kd signal recognition particle protein, is an abundant component of both infectious HIV-1 and minimal virus-like particles. *RNA* 12, 542–546. doi:10.1261/rna.2306306.

Pan, B. T., and Johnstone, R. M. (1983). Fate of the transferrin receptor during maturation of sheep reticulocytes in vitro: Selective externalization of the receptor. *Cell* 33, 967–978. doi:10.1016/0092-8674(83)90040-5.

Parchure, A., Vyas, N., Ferguson, C., Parton, R. G., and Mayor, S. (2015). Oligomerization and endocytosis of Hedgehog is necessary for its efficient exovesicular secretion. *Mol. Biol. Cell* 26, 4700–4717. doi:10.1091/mbc.E15-09-0671.

Park, J. S., Lee, S. H., Na, H. J., Pyo, J. H., Kim, Y. S., and Yoo, M. A. (2012). Age- and oxidative stress-induced DNA damage in Drosophila intestinal stem cells as marked by Gamma-H2AX. *Exp. Gerontol.* 47, 401–405. doi:10.1016/j.exger.2012.02.007.

Park, S. J., Jeon, H., Yoo, S. M., and Lee, M. S. (2018). The effect of storage temperature on the biological activity of extracellular vesicles for the complement system. *Vitr. Cell. Dev. Biol. - Anim.* 54, 423–429. doi:10.1007/s11626-018-0261-7.

Parolini, I., Federici, C., Raggi, C., Lugini, L., Palleschi, S., De Milito, A., et al. (2009). Microenvironmental pH is a key factor for exosome traffic in tumor cells. *J. Biol. Chem.* 284, 34211–34222. doi:10.1074/jbc.M109.041152.

Pavlyukov, M. S., Yu, H., Bastola, S., Minata, M., Shender, V. O., Lee, Y., et al. (2018). Apoptotic Cell-Derived Extracellular Vesicles Promote Malignancy of Glioblastoma Via Intercellular Transfer of Splicing Factors. *Cancer Cell* 34, 119-135.e10. doi:10.1016/j.ccell.2018.05.012.

Peddigari, S., Li, P. W. L., Rabe, J. L., and Martin, S. L. (2013). HnRNPL and nucleolin bind LINE-1 RNA and function as host factors to modulate retrotransposition. *Nucleic Acids Res.* 41, 575–585. doi:10.1093/nar/gks1075.

Pérez-Boza, J., Lion, M., and Struman, I. (2018). Exploring the RNA landscape of endothelial exosomes. *RNA* 24, 423–435. doi:10.1261/rna.064352.117.

Perez-Hernandez, D., Gutiérrez-Vázquez, C., Jorge, I., López-Martín, S., Ursa, A., Sánchez-Madrid, F., et al. (2013). The intracellular interactome of tetraspanin-enriched microdomains reveals their function as sorting machineries toward exosomes. *J. Biol. Chem.* 288, 11649–11661. doi:10.1074/jbc.M112.445304.

Perreault, J., Perreault, J. P., and Boire, G. (2007). Ro-associated Y RNAs in metazoans: Evolution and diversification. *Mol. Biol. Evol.* 24, 1678–1689. doi:10.1093/molbev/msm084.

Phinney, D. G., Di Giuseppe, M., Njah, J., Sala, E., Shiva, S., St Croix, C. M., et al. (2015). Mesenchymal stem cells use extracellular vesicles to outsource mitophagy and shuttle microRNAs. *Nat. Commun.* 6, 8472. doi:10.1038/ncomms9472.

Picard Tools - By Broad Institute Available at: http://broadinstitute.github.io/picard/ [Accessed March 9, 2021].

Pickering, A. M., Vojtovich, L., Tower, J., and Davies, K. J. A. (2013). Oxidative stress adaptation with acute, chronic, and repeated stress. *Free Radic. Biol. Med.* 55, 109–118. doi:10.1016/j.freeradbiomed.2012.11.001.

Pizzino, G., Irrera, N., Cucinotta, M., Pallio, G., Mannino, F., Arcoraci, V., et al. (2017). Oxidative Stress: Harms and Benefits for Human Health. *Oxid. Med. Cell. Longev.* 2017. doi:10.1155/2017/8416763.

Poon, I. K. H., Lucas, C. D., Rossi, A. G., and Ravichandran, K. S. (2014). Apoptotic cell clearance: Basic biology and therapeutic potential. *Nat. Rev. Immunol.* 14, 166–180. doi:10.1038/nri3607.

Purschke, M., Laubach, H.-J., Anderson, R. R., and Manstein, D. (2010). Thermal injury causes DNA damage and lethality in unheated surrounding cells: active thermal bystander effect. *J. Invest. Dermatol.* 130, 86–92. doi:10.1038/jid.2009.205.

Radyuk, S. N., Michalak, K., Rebrin, I., Sohal, R. S., and Orr, W. C. (2006). Effects of ectopic expression of Drosophila DNA glycosylases dOgg1 and RpS3 in mitochondria. *Free Radic. Biol. Med.* 41, 757–764. doi:10.1016/j.freeradbiomed.2006.05.021.

Raposo, G., Nijman, H. W., Stoorvogel, W., Leijendekker, R., Harding, C. V., Melief, C. J. M., et al. (1996). B lymphocytes secrete antigen-presenting vesicles. *J. Exp. Med.* 183, 1161–1172. doi:10.1084/jem.183.3.1161.

Raposo, G., and Stoorvogel, W. (2013). Extracellular vesicles: Exosomes, microvesicles, and friends. *J. Cell Biol.* 200, 373–383. doi:10.1083/jcb.201211138.

Ratajczak, J., Miekus, K., Kucia, M., Zhang, J., Reca, R., Dvorak, P., et al. (2006). Embryonic stem cell-derived microvesicles reprogram hematopoietic progenitors: Evidence for horizontal transfer of mRNA and protein delivery. *Leukemia* 20, 847–856. doi:10.1038/sj.leu.2404132.

Raudvere, U., Kolberg, L., Kuzmin, I., Arak, T., Adler, P., Peterson, H., et al. (2019). G:Profiler: A web server for functional enrichment analysis and conversions of gene lists (2019 update). *Nucleic Acids Res.* 47, W191–W198. doi:10.1093/nar/gkz369.

Ray, D., Kazan, H., Cook, K. B., Weirauch, M. T., Najafabadi, H. S., Li, X., et al. (2013). A compendium of RNA-binding motifs for decoding gene regulation. *Nature* 499, 172–177. doi:10.1038/nature12311.

Reuter, S., Gupta, S. C., Chaturvedi, M. M., and Aggarwal, B. B. (2010). Oxidative stress, inflammation, and cancer: How are they linked? *Free Radic. Biol. Med.* 49, 1603–1616. doi:10.1016/j.freeradbiomed.2010.09.006.

Richard, G.-F., Kerrest, A., and Dujon, B. (2008). Comparative Genomics and Molecular Dynamics of DNA Repeats in Eukaryotes. *Microbiol. Mol. Biol. Rev.* 72, 686–727. doi:10.1128/mmbr.00011-08.

Ridder, K., Keller, S., Dams, M., Rupp, A. K., Schlaudraff, J., Del Turco, D., et al. (2014). Extracellular Vesicle-Mediated Transfer of Genetic Information between the Hematopoietic System and the Brain in Response to Inflammation. *PLoS Biol.* 12, e1001874. doi:10.1371/journal.pbio.1001874.

Ridder, K., Sevko, A., Heide, J., Dams, M., Rupp, A. K., Macas, J., et al. (2015). Extracellular vesicle-

mediated transfer of functional RNA in the tumor microenvironment. *Oncoimmunology* 4, e1008371. doi:10.1080/2162402X.2015.1008371.

Rimer, J. M., Lee, J., Holley, C. L., Crowder, R. J., Chen, D. L., Hanson, P. I., et al. (2018). Long-range function of secreted small nucleolar RNAs that direct 2-O-methylation. *J. Biol. Chem.* 293, 13284–13296. doi:10.1074/jbc.RA118.003410.

Ristow, M., and Zarse, K. (2010). How increased oxidative stress promotes longevity and metabolic health: The concept of mitochondrial hormesis (mitohormesis). *Exp. Gerontol.* 45, 410–418. doi:10.1016/j.exger.2010.03.014.

Roefs, M. T., Sluijter, J. P. G., and Vader, P. (2020). Extracellular Vesicle-Associated Proteins in Tissue Repair. *Trends Cell Biol.* 30, 990–1013. doi:10.1016/j.tcb.2020.09.009.

Routh, A., Domitrovic, T., and Johnson, J. E. (2012). Host RNAs, including transposons, are encapsidated by a eukaryotic single-stranded RNA virus. *Proc. Natl. Acad. Sci. U. S. A.* 109, 1907–1912. doi:10.1073/pnas.1116168109.

Russell, A. E., Jun, S., Sarkar, S., Geldenhuys, W. J., Lewis, S. E., Rellick, S. L., et al. (2019). Extracellular Vesicles Secreted in Response to Cytokine Exposure Increase Mitochondrial Oxygen Consumption in Recipient Cells. *Front. Cell. Neurosci.* 13, 51. doi:10.3389/fncel.2019.00051.

Rutter, B. D., and Innes, R. W. (2017). Extracellular vesicles isolated from the leaf apoplast carry stress-response proteins. *Plant Physiol.* 173, 728–741. doi:10.1104/pp.16.01253.

Salomon, C., Ryan, J., Sobrevia, L., Kobayashi, M., Ashman, K., Mitchell, M., et al. (2013). Exosomal Signaling during Hypoxia Mediates Microvascular Endothelial Cell Migration and Vasculogenesis. *PLoS One* 8, 68451. doi:10.1371/journal.pone.0068451.

Samuel, P., Mulcahy, L. A., Furlong, F., McCarthy, H. O., Brooks, S. A., Fabbri, M., et al. (2018). Cisplatin induces the release of extracellular vesicles from ovarian cancer cells that can induce invasiveness and drug resistance in bystander cells. *Philos. Trans. R. Soc. B Biol. Sci.* 373. doi:10.1098/rstb.2017.0065.

Sanchez-Fernandez, M. A., Sbacchi, S., Correa-Tapia, M., Naumann, R., Klemm, J., Chambon, P., et al. (2012). Transgenic Mice for a Tamoxifen-Induced, Conditional Expression of the Cre Recombinase in Osteoclasts. *PLoS One* 7, e37592. doi:10.1371/JOURNAL.PONE.0037592.

Santangelo, L., Giurato, G., Cicchini, C., Montaldo, C., Mancone, C., Tarallo, R., et al. (2016). The RNA-Binding Protein SYNCRIP Is a Component of the Hepatocyte Exosomal Machinery Controlling MicroRNA Sorting. *Cell Rep.* 17, 799–808. doi:10.1016/j.celrep.2016.09.031.

Schlienger, S., Campbell, S., and Claing, A. (2014). ARF1 regulates the Rho/MLC pathway to control EGF-dependent breast cancer cell invasion. *Mol. Biol. Cell* 25, 17–29. doi:10.1091/mbc.E13-06-0335.

Shelke, G. V., Yin, Y., Jang, S. C., Lässer, C., Wennmalm, S., Hoffmann, H. J., et al. (2019). Endosomal signalling via exosome surface TGFβ-1. *J. Extracell. Vesicles* 8, 1650458. doi:10.1080/20013078.2019.1650458.

Shuler, K. T., Wilson, B. E., Muñoz, E. R., Mitchell, A. D., Selsby, J. T., and Hudson, M. B. (2020). Muscle Stem Cell-Derived Extracellular Vesicles Reverse Hydrogen Peroxide-Induced Mitochondrial Dysfunction in Mouse Myotubes. *Cells* 9, 2544. doi:10.3390/cells9122544.

Shurtleff, M. J., Temoche-Diaz, M. M., Karfilis, K. V., Ri, S., and Schekman, R. (2016). Y-box protein 1 is required to sort microRNAs into exosomes in cells and in a cell-free reaction. *Elife* 5. doi:10.7554/eLife.19276.

Shurtleff, M. J., Yao, J., Qin, Y., Nottingham, R. M., Temoche-Diaz, M. M., Schekman, R., et al. (2017). Broad role for YBX1 in defining the small noncoding RNA composition of exosomes. *Proc. Natl. Acad. Sci. U. S. A.* 114, E8987–E8995. doi:10.1073/pnas.1712108114.

Sjöström, A. E., Sandblad, L., Uhlin, B. E., and Wai, S. N. (2015). Membrane vesicle-mediated release of bacterial RNA. *Sci. Rep.* 5, 15329. doi:10.1038/srep15329.

Skog, J., Würdinger, T., van Rijn, S., Meijer, D. H., Gainche, L., Curry, W. T., et al. (2008). Glioblastoma microvesicles transport RNA and proteins that promote tumour growth and provide diagnostic biomarkers. *Nat. Cell Biol.* 10, 1470–1476. doi:10.1038/ncb1800.

Söderberg, M., Raffalli-Mathieu, F., and Lang, M. A. (2007). Identification of a regulatory cis-element within the 3'-untranslated region of the murine inducible nitric oxide synthase (iNOS) mRNA; interaction with heterogeneous nuclear ribonucleoproteins I and L and role in the iNOS gene expression. *Mol. Immunol.* 44, 434–442. doi:10.1016/j.molimm.2006.02.019.

Sokolova, V., Ludwig, A. K., Hornung, S., Rotan, O., Horn, P. A., Epple, M., et al. (2011). Characterisation of exosomes derived from human cells by nanoparticle tracking analysis and scanning electron microscopy. *Colloids Surfaces B Biointerfaces* 87, 146–150. doi:10.1016/j.colsurfb.2011.05.013.

Sork, H., Conceicao, M., Corso, G., Nordin, J., Xin Fiona Lee, Y., Krjutskov, K., et al. (2020). Profiling of extracellular small RNAs highlights a strong bias towards non-vesicular secretion. *bioRxiv*, 2020.12.01.406207. doi:10.1101/2020.12.01.406207.

Squadrito, M. L., Baer, C., Burdet, F., Maderna, C., Gilfillan, G. D., Lyle, R., et al. (2014). Endogenous RNAs Modulate MicroRNA Sorting to Exosomes and Transfer to Acceptor Cells. *Cell Rep.* 8, 1432–1446. doi:10.1016/j.celrep.2014.07.035.

Stage, D. E., and Eickbush, T. H. (2007). Sequence variation within the rRNA gene loci of 12 Drosophila species. *Genome Res.* 17, 1888–1897. doi:10.1101/gr.6376807.

Statello, L., Maugeri, M., Garre, E., Nawaz, M., Wahlgren, J., Papadimitriou, A., et al. (2018). Identification of RNA-binding proteins in exosomes capable of interacting with different types of RNA: RBP-facilitated transport of RNAs into exosomes. *PLoS One* 13, e0195969. doi:10.1371/journal.pone.0195969.

Stepanov, G. A., Filippova, J. A., Komissarov, A. B., Kuligina, E. V., Richter, V. A., Semenov, D. V., et al. (2015). Regulatory role of Small nucleolar RNAs in human diseases. *Biomed Res. Int.* 2015. doi:10.1155/2015/206849.

Strauss, K., Goebel, C., Runz, H., Möbius, W., Weiss, S., Feussner, I., et al. (2010). Exosome secretion ameliorates lysosomal storage of cholesterol in Niemann-Pick type C disease. *J. Biol. Chem.* 285, 26279–26288. doi:10.1074/jbc.M110.134775.

Sudmant, P. H., Lee, H., Dominguez, D., Heiman, M., and Burge, C. B. (2018). Widespread Accumulation of Ribosome-Associated Isolated 3' UTRs in Neuronal Cell Populations of the Aging Brain. *Cell Rep.* 25, 2447-2456.e4. doi:10.1016/j.celrep.2018.10.094.

Sultan, M., Amstislavskiy, V., Risch, T., Schuette, M., Dökel, S., Ralser, M., et al. (2014). Influence of RNA extraction methods and library selection schemes on RNA-seq data. *BMC Genomics* 15, 1–13. doi:10.1186/1471-2164-15-675.

Sun, C., Liu, M., Chang, J., Yang, D., Zhao, B., Wang, H., et al. (2020). hnRNP L negatively regulates foot-and-mouth disease virus replication through inhibiting viral RNA 1 synthesis by interacting with IRES in 5′ untranslated region 2 Downloaded from. *J. Virol*. doi:10.1128/JVI.00282-20.

Szatmári, T., Kis, D., Bogdándi, E. N., Benedek, A., Bright, S., Bowler, D., et al. (2017). Extracellular vesicles mediate radiation-induced systemic bystander signals in the bone marrow and spleen. *Front. Immunol.* 8, 347. doi:10.3389/fimmu.2017.00347.

Szostak, N., Royo, F., Rybarczyk, A., Szachniuk, M., Blazewicz, J., Del Sol, A., et al. (2014). Sorting signal targeting mRNA into hepatic extracellular vesicles. *RNA Biol.* 11, 836–844. doi:10.4161/rna.29305.

Takahashi, A., Okada, R., Nagao, K., Kawamata, Y., Hanyu, A., Yoshimoto, S., et al. (2017). Exosomes maintain cellular homeostasis by excreting harmful DNA from cells. *Nat. Commun.* 8. doi:10.1038/ncomms15287.

Takahashi, K., Yan, I. K., Kogure, T., Haga, H., and Patel, T. (2014). Extracellular vesicle-mediated transfer of long non-coding RNA ROR modulates chemosensitivity in human hepatocellular cancer. *FEBS Open Bio* 4, 458–467. doi:10.1016/j.fob.2014.04.007.

Tavakkoli, S., Sotoodehnejadnematalahi, F., Fathollahi, A., Bandehpour, M., Hoseini, M. H. M., and Yeganeh, F. (2020). EL4-derived Exosomes Carry Functional TNF-related Apoptosisinducing Ligand that are Able to Induce Apoptosis and Necrosis in the Target Cells. *Int. J. Mol. Cell. Med.* 9, 207–214. doi:10.22088/IJMCM.BUMS.9.3.207.

Temoche-Diaz, M. M., Shurtleff, M. J., Nottingham, R. M., Yao, J., Fadadu, R. P., Lambowitz, A. M., et al. (2019). Distinct mechanisms of microrna sorting into cancer cell-derived extracellular vesicle subtypes. *Elife* 8. doi:10.7554/eLife.47544.

Ter-Ovanesyan, D. (2019). Investigation of RNA in Extracellular Vesicles. 1–156. Available at: https://dash.harvard.edu/bitstream/handle/1/41121318/TER-OVANESYAN-DISSERTATION-2019.pdf?sequence=1&isAllowed=y.

Théry, C., Duban, L., Segura, E., Véron, P., Lantz, O., and Amigorena, S. (2002). Indirect activation of naïve CD4+ T cells by dendritic cell-derived exosomes. *Nat. Immunol.* 3, 1156–1162. doi:10.1038/ni854.

Théry, C., Witwer, K. W., Aikawa, E., Alcaraz, M. J., Anderson, J. D., Andriantsitohaina, R., et al. (2018). Minimal information for studies of extracellular vesicles 2018 (MISEV2018): a position statement of the International Society for Extracellular Vesicles and update of the MISEV2014 guidelines. *J. Extracell. Vesicles* 7. doi:10.1080/20013078.2018.1535750.

Thomas, M. P., Liu, X., Whangbo, J., McCrossan, G., Sanborn, K. B., Basar, E., et al. (2015). Apoptosis Triggers Specific, Rapid, and Global mRNA Decay with 3′ Uridylated Intermediates Degraded by DIS3L2. *Cell Rep.* 11, 1079–1089. doi:10.1016/j.celrep.2015.04.026.

Thomas, R. E., Vincow, E. S., Merrihew, G. E., MacCoss, M. J., Davis, M. Y., and Pallanck, L. J. (2018). Glucocerebrosidase deficiency promotes protein aggregation through

dysregulation of extracellular vesicles. *PLOS Genet.* 14, e1007694. doi:10.1371/journal.pgen.1007694.

Thompson, A. G., Gray, E., Heman-Ackah, S. M., Mäger, I., Talbot, K., El Andaloussi, S., et al. (2016). Extracellular vesicles in neurodegenerative disease-pathogenesis to biomarkers. *Nat. Rev. Neurol.* 12, 346–357. doi:10.1038/nrneurol.2016.68.

Thompson, M. K., Kiourlappou, M., and Davis, I. (2020). Ribo-Pop: Simple, cost-effective, and widely applicable ribosomal RNA depletion. *RNA* 26, rna.076562.120. doi:10.1261/rna.076562.120.

Thorvaldsdottir, H., Robinson, J. T., and Mesirov, J. P. (2013). Integrative Genomics Viewer (IGV): high-performance genomics data visualization and exploration. *Brief. Bioinform.* 14, 178–192. doi:10.1093/bib/bbs017.

Tian, T., Zhu, Y. L., Zhou, Y. Y., Liang, G. F., Wang, Y. Y., Hu, F. H., et al. (2014). Exosome uptake through clathrin-mediated endocytosis and macropinocytosis and mediating miR-21 delivery. *J. Biol. Chem.* 289, 22258–22267. doi:10.1074/jbc.M114.588046.

Tkach, M., Kowal, J., Zucchetti, A. E., Enserink, L., Jouve, M., Lankar, D., et al. (2017). Qualitative differences in T-cell activation by dendritic cell-derived extracellular vesicle subtypes. *EMBO J.* 36, 3012–3028. doi:10.15252/embj.201696003.

Tosar, J. P., Gámbaro, F., Sanguinetti, J., Bonilla, B., Witwer, K. W., and Cayota, A. (2015). Assessment of small RNA sorting into different extracellular fractions revealed by high-throughput sequencing of breast cell lines. *Nucleic Acids Res.* 43, 5601–5616. doi:10.1093/nar/gkv432.

Tosar, J. P., Segovia, M., Castellano, M., Gámbaro, F., Akiyama, Y., Fagúndez, P., et al. (2020). Fragmentation of extracellular ribosomes and tRNAs shapes the extracellular RNAome. *Nucleic Acids Res.* 48, 12874–12888. doi:10.1093/nar/gkaa674.

Tosar, J. P., Witwer, K., and Cayota, A. (2021). Revisiting Extracellular RNA Release, Processing, and Function. *Trends Biochem. Sci.* 46, 438–445. doi:10.1016/j.tibs.2020.12.008.

Trajkovic, K., Hsu, C., Chiantia, S., Rajendran, L., Wenzel, D., Wieland, F., et al. (2008). Ceramide triggers budding of exosome vesicles into multivesicular endosomes. *Science (80-. ).* 319, 1244–1247. doi:10.1126/science.1153124.

Trams, E. G., Lauter, C. J., Norman Salem, J., and Heine, U. (1981). Exfoliation of membrane ecto-enzymes in the form of micro-vesicles. *Biochim. Biophys. Acta - Biomembr.* 645, 63–70. doi:10.1016/0005-2736(81)90512-5.

Trapnell, C., Williams, B. A., Pertea, G., Mortazavi, A., Kwan, G., Van Baren, M. J., et al. (2010). Transcript assembly and quantification by RNA-Seq reveals unannotated transcripts and isoform switching during cell differentiation. *Nat. Biotechnol.* 28, 511–515. doi:10.1038/nbt.1621.

Tsai, Y. W., Sung, H. H., Li, J. C., Yeh, C. Y., Chen, P. Y., Cheng, Y. J., et al. (2019). Glia-derived exosomal miR-274 targets Sprouty in trachea and synaptic boutons to modulate growth and responses to hypoxia. *Proc. Natl. Acad. Sci. U. S. A.* 116, 24651–24661. doi:10.1073/pnas.1902537116.

Turchinovich, A., Weiz, L., Langheinz, A., and Burwinkel, B. (2011). Characterization of

extracellular circulating microRNA. *Nucleic Acids Res.* 39, 7223–7233. doi:10.1093/nar/gkr254.

Valadi, H., Ekström, K., Bossios, A., Sjöstrand, M., Lee, J. J., and Lötvall, J. O. (2007). Exosome-mediated transfer of mRNAs and microRNAs is a novel mechanism of genetic exchange between cells. *Nat. Cell Biol.* 9, 654–659. doi:10.1038/ncb1596.

Vale-Costa, S., and Amorim, M. J. (2016). Recycling endosomes and viral infection. *Viruses* 8, 64. doi:10.3390/v8030064.

Van Balkom, B. W. M., Eisele, A. S., Michiel Pegtel, D., Bervoets, S., and Verhaar, M. C. (2015). Quantitative and qualitative analysis of small RNAs in human endothelial cells and exosomes provides insights into localized RNA processing, degradation and sorting. *J. Extracell. Vesicles* 4, 1–14. doi:10.3402/jev.v4.26760.

Van den Brande, S., Gijbels, M., Wynant, N., Santos, D., Mingels, L., Gansemans, Y., et al. (2018). The presence of extracellular microRNAs in the media of cultured Drosophila cells. *Sci. Rep.* 8. doi:10.1038/s41598-018-35531-z.

van der Pol, E., Coumans, F. A. W., Grootemaat, A. E., Gardiner, C., Sargent, I. L., Harrison, P., et al. (2014). Particle size distribution of exosomes and microvesicles determined by transmission electron microscopy, flow cytometry, nanoparticle tracking analysis, and resistive pulse sensing. *J. Thromb. Haemost.* 12, 1182–1192. doi:10.1111/jth.12602.

van Niel, G., Charrin, S., Simoes, S., Romao, M., Rochin, L., Saftig, P., et al. (2011). The Tetraspanin CD63 Regulates ESCRT-Independent and -Dependent Endosomal Sorting during Melanogenesis. *Dev. Cell* 21, 708–721. doi:10.1016/j.devcel.2011.08.019.

van Niel, G., D'Angelo, G., and Raposo, G. (2018). Shedding light on the cell biology of extracellular vesicles. *Nat. Rev. Mol. Cell Biol.* 19, 213–228. doi:10.1038/nrm.2017.125.

Venter, P. A., Marshall, D., and Schneemann, A. (2009). Dual Roles for an Arginine-Rich Motif in Specific Genome Recognition and Localization of Viral Coat Protein to RNA Replication Sites in Flock House Virus-Infected Cells. *J. Virol.* 83, 2872–2882. doi:10.1128/jvi.01780-08.

Vickers, K. C., Palmisano, B. T., Shoucri, B. M., Shamburek, R. D., and Remaley, A. T. (2011). MicroRNAs are transported in plasma and delivered to recipient cells by high-density lipoproteins. *Nat. Cell Biol.* 13, 423–435. doi:10.1038/ncb2210.

Vidal, M. (2019). Exosomes: Revisiting their role as "garbage bags." *Traffic* 20, 815–828. doi:10.1111/tra.12687.

Vietri, M., Radulovic, M., and Stenmark, H. (2020). The many functions of ESCRTs. *Nat. Rev. Mol. Cell Biol.* 21, 25–42. doi:10.1038/s41580-019-0177-4.

Villarroya-Beltri, C., Gutiérrez-Vázquez, C., Sánchez-Cabo, F., Pérez-Hernández, D., Vázquez, J., Martin-Cofreces, N., et al. (2013). Sumoylated hnRNPA2B1 controls the sorting of miRNAs into exosomes through binding to specific motifs. *Nat. Commun.* 4, 2980. doi:10.1038/ncomms3980.

Wang, L., Wang, S., and Li, W. (2012). RSeQC: Quality control of RNA-seq experiments. *Bioinformatics* 28, 2184–2185. doi:10.1093/bioinformatics/bts356.

Wang, Y., Li, H., Sun, Q., and Yao, Y. (2016). Characterization of small RNAs derived from tRNAs,

rRNAs and snoRNAs and their response to heat stress in wheat seedlings. *PLoS One* 11. doi:10.1371/journal.pone.0150933.

Wang, Y., Zhang, L., Li, Y., Chen, L., Wang, X., Guo, W., et al. (2015). Exosomes/microvesicles from induced pluripotent stem cells deliver cardioprotective miRNAs and prevent cardiomyocyte apoptosis in the ischemic myocardium. *Int. J. Cardiol.* 192, 61–69. doi:10.1016/j.ijcard.2015.05.020.

Wang, Z., Gerstein, M., and Snyder, M. (2009). RNA-Seq: A revolutionary tool for transcriptomics. *Nat. Rev. Genet.* 10, 57–63. doi:10.1038/nrg2484.

Warkocki, Z., Krawczyk, P. S., Adamska, D., Bijata, K., Garcia-Perez, J. L., and Dziembowski, A. (2018). Uridylation by TUT4/7 Restricts Retrotransposition of Human LINE-1s. *Cell* 174, 1537-1548.e29. doi:10.1016/j.cell.2018.07.022.

Webster, C. L., Longdon, B., Lewis, S. H., and Obbard, D. J. (2016). Twenty-Five New Viruses Associated with the Drosophilidae (Diptera). *Evol. Bioinforma.* 12s2, EBO.S39454. doi:10.4137/EBO.S39454.

Wei, Z., Batagov, A. O., Carter, D. R. F., and Krichevsky, A. M. (2016). Fetal Bovine Serum RNA Interferes with the Cell Culture derived Extracellular RNA. *Sci. Rep.* 6, 31175. doi:10.1038/srep31175.

Wei, Z., Batagov, A. O., Schinelli, S., Wang, J., Wang, Y., El Fatimy, R., et al. (2017). Coding and noncoding landscape of extracellular RNA released by human glioma stem cells. *Nat. Commun.* 8, 1145. doi:10.1038/s41467-017-01196-x.

Willms, E., Johansson, H. J., Mäger, I., Lee, Y., Blomberg, K. E. M., Sadik, M., et al. (2016). Cells release subpopulations of exosomes with distinct molecular and biological properties. *Sci. Rep.* 6. doi:10.1038/srep22519.

Witwer, K. W., Buzás, E. I., Bemis, L. T., Bora, A., Lässer, C., Lötvall, J., et al. (2013). Standardization of sample collection, isolation and analysis methods in extracellular vesicle research. *J. Extracell. Vesicles* 2. doi:10.3402/jev.v2i0.20360.

Wolf, P. (1967). The nature and significance of platelet products in human plasma. *Br. J. Haematol.* 13, 269–288. doi:10.1111/j.1365-2141.1967.tb08741.x.

Wolozin, B., and Ivanov, P. (2019). Stress granules and neurodegeneration. *Nat. Rev. Neurosci.* 20, 649–666. doi:10.1038/s41583-019-0222-5.

Wong, S., Pomatto, L., Davies, K. J. A., and Tower, J. (2016). Aging and Sex-Dependent Adaptive Homeostasis in Response to Oxidative Stress. *Free Radic. Biol. Med.* 100, S48. doi:10.1016/j.freeradbiomed.2016.10.128.

Wood, D. E., and Salzberg, S. L. (2014). Kraken: Ultrafast metagenomic sequence classification using exact alignments. *Genome Biol.* 15, R46. doi:10.1186/gb-2014-15-3-r46.

Wozniak, A. L., Adams, A., King, K. E., Dunn, W., Christenson, L. K., Hung, W. T., et al. (2020). The RNA binding protein FMR1 controls selective exosomal miRNA cargo loading during inflammation. *J. Cell Biol.* 219. doi:10.1083/jcb.201912074.

Wu, Q., Luo, Y., Lu, R., Lau, N., Lai, E. C., Li, W. X., et al. (2010). Virus discovery by deep sequencing and assembly of virus-derived small silencing RNAs. *Proc. Natl. Acad. Sci. U. S. A.* 107, 1606–

1611. doi:10.1073/pnas.0911353107.

Xu, R., Rai, A., Chen, M., Suwakulsiri, W., Greening, D. W., and Simpson, R. J. (2018). Extracellular vesicles in cancer — implications for future improvements in cancer care. *Nat. Rev. Clin. Oncol.* doi:10.1038/s41571-018-0036-9.

Xu, S., Wang, J., Ding, N., Hu, W., Zhang, X., Wang, B., et al. (2015). Exosome-mediated microRNA transfer plays a role in radiation-induced bystander effect. *RNA Biol.* 12, 1355–1363. doi:10.1080/15476286.2015.1100795.

Yang, J., Hagen, J., Guntur, K. V, Allette, K., Schuyler, S., Ranjan, J., et al. (2017). A next generation sequencing based approach to identify extracellular vesicle mediated mRNA transfers between cells. *BMC Genomics* 18. doi:10.1186/s12864-017-4359-1.

Yang, Y., Wang, L., Han, X., Yang, W. L., Zhang, M., Ma, H. L., et al. (2019). RNA 5-Methylcytosine Facilitates the Maternal-to-Zygotic Transition by Preventing Maternal mRNA Decay. *Mol. Cell* 75, 1188-1202.e11. doi:10.1016/j.molcel.2019.06.033.

Yates, A. D., Achuthan, P., Akanni, W., Allen, J., Allen, J., Alvarez-Jarreta, J., et al. (2020). Ensembl 2020. *Nucleic Acids Res.* 48, D682–D688. doi:10.1093/nar/gkz966.

Yuyama, K., Sun, H., Mitsutake, S., and Igarashi, Y. (2012). Sphingolipid-modulated exosome secretion promotes clearance of amyloid-β by microglia. *J. Biol. Chem.* 287, 10977–10989. doi:10.1074/jbc.M111.324616.

Zhang, H., Freitas, D., Kim, H. S., Fabijanic, K., Li, Z., Chen, H., et al. (2018). Identification of distinct nanoparticles and subsets of extracellular vesicles by asymmetric flow field-flow fractionation. *Nat. Cell Biol.* 20, 332–343. doi:10.1038/s41556-018-0040-4.

Zhang, N., and Ashizawa, T. (2017). RNA toxicity and foci formation in microsatellite expansion diseases. *Curr. Opin. Genet. Dev.* 44, 17–29. doi:10.1016/j.gde.2017.01.005.

Zhang, Q., Higginbotham, J. N., Jeppesen, D. K., Yang, Y. P., Li, W., McKinley, E. T., et al. (2019). Transfer of Functional Cargo in Exomeres. *Cell Rep.* 27, 940-954.e6. doi:10.1016/j.celrep.2019.01.009.

Zhang, X., Abels, E. R., Redzic, J. S., Margulis, J., Finkbeiner, S., and Breakefield, X. O. (2016). Potential Transfer of Polyglutamine and CAG-Repeat RNA in Extracellular Vesicles in Huntington's Disease: Background and Evaluation in Cell Culture. *Cell. Mol. Neurobiol.* 36, 459–470. doi:10.1007/s10571-016-0350-7.

Zhou, Y., McNamara, R. P., and Dittmer, D. P. (2020). Purification Methods and the Presence of RNA in Virus Particles and Extracellular Vesicles. *Viruses* 12, 917. doi:10.3390/v12090917.

Zhu, C., Yan, Q., Weng, C., Hou, X., Mao, H., Liu, D., et al. (2018). Erroneous ribosomal RNAs promote the generation of antisense ribosomal siRNA. *Proc. Natl. Acad. Sci. U. S. A.* 115, 10082–10087. doi:10.1073/pnas.1800974115.

Zietzer, A., Hosen, M. R., Wang, H., Goody, P. R., Sylvester, M., Latz, E., et al. (2020). The RNA-binding protein hnRNPU regulates the sorting of microRNA-30c-5p into large extracellular vesicles. *J. Extracell. Vesicles* 9, 1786967. doi:10.1080/20013078.2020.1786967.

Zomer, A., Maynard, C., Verweij, F. J., Kamermans, A., Schäfer, R., Beerling, E., et al. (2015). In vivo imaging reveals extracellular vesicle-mediated phenocopying of metastatic behavior.

*Cell* 161, 1046–1057. doi:10.1016/j.cell.2015.04.042.

Zomer, A., Steenbeek, S. C., Maynard, C., and Van Rheenen, J. (2016). Studying extracellular vesicle transfer by a Cre-loxP method. *Nat. Protoc.* 11, 87–101. doi:10.1038/nprot.2015.138.

Zou, F., Tu, R., Duan, B., Yang, Z., Ping, Z., Song, X., et al. (2020). Drosophila YBX1 homolog YPS promotes ovarian germ line stem cell development by preferentially recognizing 5-methylcytosine RNAs. *Proc. Natl. Acad. Sci.* 117, 3603–3609. doi:10.1073/pnas.1910862117.

Zwaal, R. F. A., and Schroit, A. J. (1997). Pathophysiologic implications of membrane phospholipid asymmetry in blood cells. *Blood* 89, 1121–1132. doi:10.1182/blood.v89.4.1121.